Flow-Based Crystallization-Driven Self-Assembly: Advancements in Reproducibility, Scalability, and Functional Design

Laihui Xiao

UNIVERSITY OF BIRMINGHAM

A thesis submitted to the University of Birmingham for the degree of

DOCTOR OF PHILOSOPHY

Supervised by Prof. Rachel O'Reilly

School of Chemistry

College of Engineering and Physical Sciences

University of Birmingham

January 2025

Abstract

Crystallization-Driven Self-Assembly (CDSA) is a powerful technique for synthesizing anisotropic nanoparticles. However, CDSA often requires long aging times and low concentrations to maintain precise control over nanoparticle dimensions, leading to low throughput and limiting its potential for commercial applications. Furthermore, CDSA faces challenges in increasing structural complexity. This project aims to address these limitations by increasing the throughput of nanoparticle preparation through the transition from batch to flow reactors, and subsequently enhancing the structural complexity of the resulting nanoparticles. The entire process was divided into three key stages, demonstrated through the preparation of platelet nanostructures. First, living CDSA was conducted using pre-formed seed particles to investigate flow conditions, highlighting the potential for enhanced scalability and reproducibility of platelet preparation using flow. In the next stage, a flash-freezing method was employed to improve seed formation efficiency significantly. Subsequently, an integral flow system was developed, combining seed formation and living growth stages, enabling the high-throughput synthesis of platelets directly from the polymer in just three minutes. Finally, a temperature-responsive CDSA strategy was implemented to fabricate delicate platelets with controllable 3D surface patterns, leveraging the precise temperature regulation offered by flow reactors. Overall, this work presents a novel approach to nanoparticle preparation that combines enhanced throughput with increased structural complexity, paving the way for innovations in nanotechnology and advancing the development of functional nanoparticles.

This thesis is dedicated to my family, with special gratitude to my sister, Shaorong Liao, for their constant encouragement and support.

Acknowledgements

I would like to extend my sincere gratitude to my supervisor, Prof. Rachel O'Reilly, for providing me with the opportunity to conduct my PhD and for offering an interesting project that increased my passion for research. Your guidance and encouragement have been invaluable in helping me develop critical thinking, writing, and presentation skills. I am especially grateful for your career advice and the support she provided during my postdoc applications. I would also like to thank the University of Birmingham and the China Scholarship Council for their scholarship, which supported both my studies and life throughout this journey.

I would like to extend my sincere thanks to the CDSA team. First and foremost, I am deeply grateful to my lab buddy, Mr. Tianlai Xia. Thank you for sharing polymers, ideas, and for always being willing to help with lab tasks, from washing NMR tubes to refilling acetone wash bottles. Your positive energy has been a constant source of motivation, especially on those weekends when I saw you hard at work in the office. I will also miss your dishes with the taste of home and the wonderful times you cooked for us. I would also like to express my heartfelt appreciation to Dr. Sam Parkinson for helping me get into flow chemistry and self-assembly, as well as for organizing the CDSA meetings. Your support throughout my PhD journey—whether in lab work, presentations, or paperwork—has been incredibly encouraging. I would like to say that your guidance has always been helpful. A huge thanks to happy Dr. Jian Zhang, the idea generator, who provided scientific answers to my questions and always sparked engaging discussions. I truly enjoyed working on collaborative projects with you. You are one of the

hardest-working researchers I have ever met, and I sincerely hope that your efforts will be paid, and your ideas published in N/S journals one day. Many thanks to Miss Phillippa Edge for all the help during the early stages of my PhD. Your detailed answers to my many questions were invaluable as I navigated the initial challenges in the UK. Additionally, thank you to Dr. Simon Dale for helping me start my PhD and demonstrating every step associated with CDSA, making the beginning of this journey much smoother. Thanks to Dr. Liangliang Shen, the CDSA successor, for providing guidance on my academic career and for bringing great joy throughout our interactions.

I would also like to thank my super colleagues and friends. Special thanks to Dr. Calum Ferguson and Dr. Julia Rho for their guidance, insightful discussions on my projects, and support during my postdoc position search. Thanks to Dr. Kaixiang Yang for bringing so much joy since joining the group; I will always cherish our food and travel adventures. Many thanks to Mr. Yu Lu for your assistance with organic synthesis—your skills in organic operations have often astonished me. I am also grateful to my neighbors, Dr. Josh Tibbetts and Dr. Peng Sun, for their kind help and for always answering my random questions. Thanks to my fume hood buddy, Miss Rachel Stracey, for allowing me enough space to lay out my flow setup in the fume hood, and for impressive moments when vial caps suddenly popped off from your samples. Thanks also to Dr. Daniel Smith and Miss Tessa Kintail for your assistance with lab technicalities and administration. Great thanks to Dr. Siriporn Chaimueangchuen, Dr. Lukmanul Samada, Dr. Ana Cubillo, Dr. Irem Akar, Dr. Marjolaine Thomas, Mr. David

Londono, Miss Bethany Crow, Mr. Jack Baker, and all Dove-O'Reilly group members for all your help within the group and in life. Thanks to my friends, Dr. Yifeng Ma, Dr. Bo Dong, Dr Song Yang, Dr. Chong Shen, Miss La Zhuo, Mr. Xinlie Jiang, Miss Yuanyu Huang, Miss Liyan Huang-you guys made my time abroad much more enjoyable.

Finally, I would like to express my heartfelt gratitude to my family. Your constant support and encouragement gave me the confidence to step out of my home country and explore the world. Your care, transcending time and distance, has been a source of strength, helping me overcome challenges and continue progressing in this foreign land. A special thanks to my girlfriend, Huan—your companionship, across countries, has been an incredible support that inspires me to keep going.

Table of Contents

List of Figures

List of Symbols and Abbreviations

1D	One-dimensional
2D	Two-dimensional
AIBN	2,2'-Azobis(2-methylpropionitrile)
CDSA	Crystallization-driven self-assembly
CTA	Chain transfer agents
$Đ$	Dispersity
DMF	Dimethylformamide
DP	Degree of polymerization
DPP	Diphenyl phosphate
HPLC	High-performance liquid chromatography
N_{agg}	Aggregation number
p	Packing parameter
P2VP	Poly(2-vinylpyridine)
P4VP	Poly(4-vinylpyridine)
PAA	Poly (acrylic acid)
PAIC	Poly(aryl isocyanide)
PCholMA	Poly(cholesteryl methacryloyoxy ethyl carbonate)
PCL	Polycaprolactone
PDMA	Polydimethylacrylamide
PDMAEMA	Poly(2-(dimethylamino)ethyl methacrylate)

PDHF	Poly(di-n-hexylfluorene)
PEO	Poly(ethylene oxide)
PEG	Poly(ethylene glycol)
PF	Poly(1-*O*-acryloyl-*β*-D-fructopyranose)
PFA	Perfluoroalkoxy alkane
PFS	Polyferrocenylsilane
PFTMC	Poly(fluorenetrimethylenecarbonate)
PI	Polyisoprene
PI-CDSA	Polymerization-induced crystallization-driven self-assembly
PISA	Polymerization-induced self-assembly
PLA	Polylactide
PMMA	Poly(methyl methacrylate)
PtBA	Poly(tert-butyl acrylate)
QPT	Quaternized polythiophene
RAFT	Reversible addition-fragmentation chain transfer
R_e	Reynolds number
ROP	Ring-opening polymerization
RTD	Residence time distribution
SAXS	Small-angle X-ray scattering
THF	Tetrahydrofuran

List of Publications

(1) **Xiao, L.**; Parkinson, S. J.; Xia, T.; Edge, P.; O'Reilly, R. K. Enhancing the Scalability of Crystallization-Driven Self-Assembly Using Flow Reactors. ACS Macro Letters 2023, 12 (12), 1636-1641. DOI: 10.1021/acsmacrolett.3c00600.

(2) **Xiao, L.**; Xia, T.; Zhang, J.; Parkinson, S. J.; Rho, J. Y.; Dove, A. P.; O'Reilly, R. K. Direct Preparation of 2D Platelets from Polymer Enabled by Accelerated Seed Formation. Nature Synthesis 2025, DOI: 10.1038/s44160-025-00767-x.

(3) **Xiao, L.**; Xia, T.; Ferguson, C. T. J.; Dove, A. P.; O'Reilly, R. K. 3D Nanopatterning of Platelets via Temperature-Controlled Self-Sorting. (Paper in preparation)

(4) **Xiao, L.**; Xia, T.; O'Reilly, R. K. Self-Assembled Poly(L-lactide)-Based Platelets Prepared via Seeded Growth. (Paper in preparation)

(5) Xia, T.; **Xiao, L.**; Xie, Y.; Dove, A. P.; O'Reilly, R. K. Deciphering Evolution, Function, and Observation of Crystallization-Driven Self-Assembly. (Paper in preparation)

(6) Guo, Y.; Xia, T.; Walter, V.; Xie, Y.; Rho, J. Y.; **Xiao, L.**; O'Reilly, R. K.; Wallace, M. I. Real-time label-free imaging of living crystallization-driven self-assembly. Nature Communications 2025, 16 (1), 2672. DOI: 10.1038/s41467-025-57776-9.

(7) Xia, T.; **Xiao, L.**; Sun, K.; Rho, J. Y.; Xie, Y.; Parkinson, S. J.; Sangroniz, L.; Zhang, J.; Lin, J.; Müller, A. J.; et al. Control over Aspect Ratio and Polymer Spatial Distribution of 2D

Platelets via Living Crystallization-Driven Self-Assembly. Macromolecules 2024, 57 (23), 11210–11220. DOI: 10.1021/acs.macromol.4c02496.

(8) Xia, T.; Tong, Z.; Xie, Y.; Arno, M. C.; Lei, S.; **Xiao, L.**; Rho, J. Y.; Ferguson, C. T. J.; Manners, I.; Dove, A. P.; et al. Tuning the Functionality of Self-Assembled 2D Platelets in the Third Dimension. Journal of the American Chemical Society 2023, 145 (46), 25274-25282. DOI: 10.1021/jacs.3c08770.

Declaration of Authorship

This thesis is submitted to the University of Birmingham in support of my application for the degree of Doctor of Philosophy. None of the material included herein has been submitted for any other degree or to any other institution.

Parts of this thesis have been published by the author as open-access articles in peer-reviewed scientific journals, as detailed below. The research presented, including project design, experimental execution, materials characterization, data collection and analysis, as well as figure and manuscript preparation, was conducted by myself, except where contributions from colleagues are specifically acknowledged and described in detail below:

Fluorescent dye-modified samples were imaged, and the theoretical calculation of rate constants in Chapter 4 was conducted by Mr. Tianlai Xia.

Chapter 1 - Introduction

1.1 Introduction to Polymers

Since the formal establishment of the polymer concept a century ago,[1] these materials have garnered significant attention and continue to enhance our lives. The versatility and wide-ranging properties of polymers enable their use across diverse fields, including industry,[2, 3] biomedicine,[4] energy transfer,[5] catalysis,[6] opto-electronics,[7] and agriculture,[8] with applications spanning from the nanoscale to the macroscopic level.[9, 10]

The properties of polymers are influenced by a range of factors, from the one-dimensional single-chain structure to complex three-dimensional stacking configurations. Among these, the chain structure is the most fundamental and significant. In addition to the chemical structure of the repeating unit (monomer), critical factors include the polymer chain length (degree of polymerization, DP), molecular weight distribution (dispersity, $Đ$), topology, and sequence.[11] These physical parameters, in turn, are intrinsically linked to the preparation method used.

1.1.1 Polymerization Mechanisms

Polymerization can be categorized into two main mechanisms (Figure 1.1): step-growth polymerization (condensation polymerization) and chain-growth polymerization (addition polymerization). In step-growth polymerization, initiation is not required; instead, monomers with functional groups react through a series of steps, often producing small molecules such as water or alcohol as byproducts. In contrast, chain-growth polymerization involves distinct phases of initiation, propagation, and termination. Here, monomers react with active species

(radical, anion, and cation) to form polymers, and the molecular weight of the resulting polymer is directly related to the amounts of initiator and monomer used.

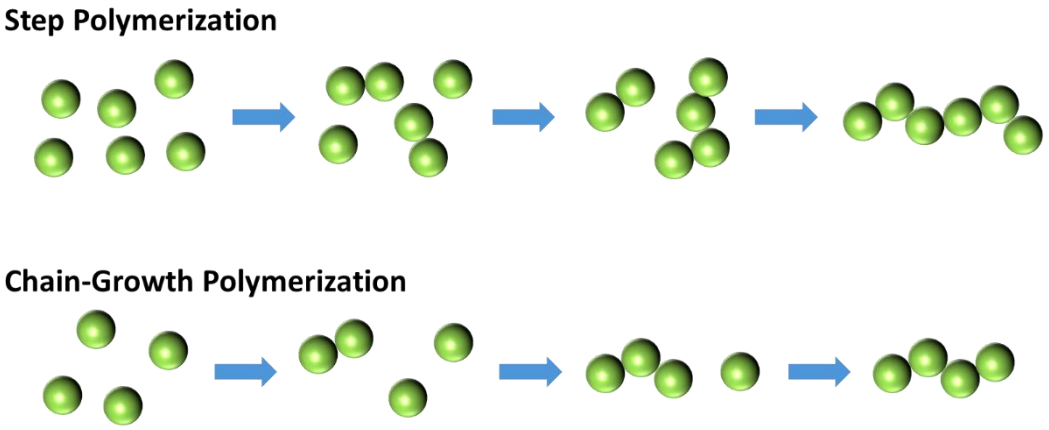

Figure 1.1. Schematic diagram of step-growth polymerization and chain-growth polymerization.

1.1.2 Controlled Polymerization Techniques

Radical polymerization is a widely used method for synthesizing polymers from vinyl monomers, typically initiated by free-radical generators (e.g., 2,2'-Azobis(2-methylpropionitrile) (AIBN)) and proceeding via a chain-growth mechanism.[12] However, conventional radical polymerization suffers from limited control over molecular weight, broad dispersity, and structural defects due to uncontrolled propagation and termination.[13] To address these limitations, controlled polymerization techniques have been developed, allowing the synthesis of polymers with tailored properties for diverse applications.

Reversible addition-fragmentation chain transfer (RAFT) polymerization is a widely used radical polymerization technique due to its applicability to a broad range of vinyl monomers.[14] Unlike conventional free radical polymerization, where radicals are active species that initiate chain-growth, RAFT polymerization employs chain transfer agents (CTAs), such as dithioesters, trithiocarbonates, xanthates, and dithiocarbamates. As the mechanism shows (Figure 1.2), CTA facilitates the rapid equilibrium between the propagating radical and its dormant state, minimizing bi-radical termination and ensuring uniform chain growth.[14-16] The target degree of DP is determined by the ratio of monomer to CTA ([M]/[CTA]). Once the monomers are consumed, all chains remain in the dormant state, allowing for the sequential addition of a second monomer to re-initiate polymerization and form block copolymers.

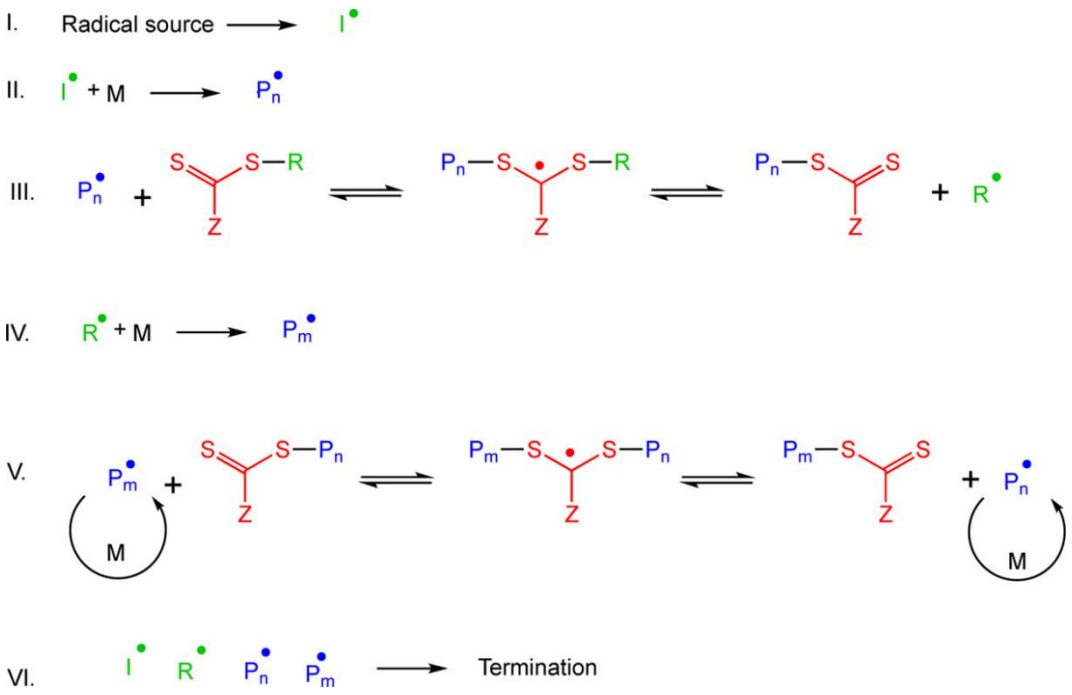

Figure 1.2. Mechanism of RAFT polymerization (reproduced from Ref.[14]).

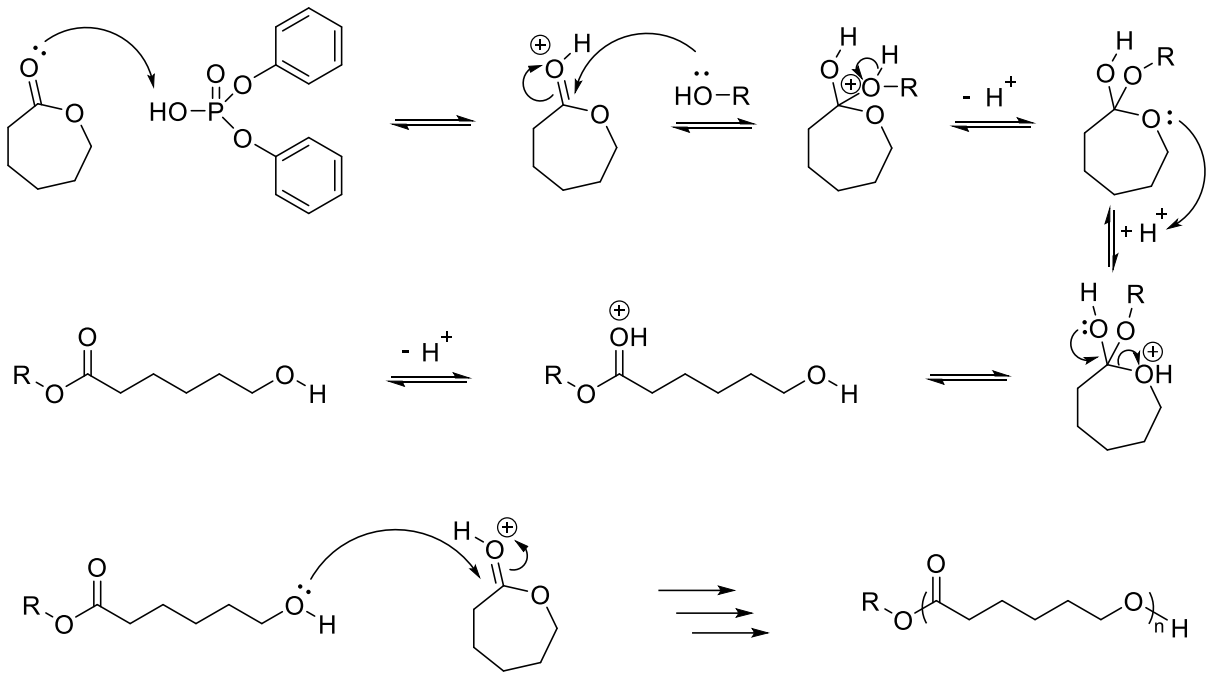

Figure 1.3. Proposed mechanism of ROP catalyzed by DPP.

In addition to vinyl monomers, a wide variety of cyclic monomers can be controllably polymerized through ring-opening polymerization (ROP). ROP can be catalyzed by enzymes,[17-19] acids,[20-22] or bases,[23-25] with the choice of catalyst and polymerization strategy tailored to the desired application and properties of the resulting polymers. For instance, polymers intended for biomedical applications must be non-toxic and biocompatible, which can be achieved using enzymatic ROP, as any residual catalyst will be non-toxic.[19] In contrast, when rapid polymerization is required, acid or base-catalyzed ROP is often employed.[23] [24] The development of ROP has greatly advanced the production of biocompatible and biodegradable polymers such as polycaprolactone (PCL) and polylactide (PLA). An example mechanism is shown in the polymerization of caprolactone (Figure 1.3), where diphenyl phosphate (DPP) acts as a catalyst by activating the monomer's carbonyl group, leading to continuous

nucleophilic reactions.[26] After polymerization, catalysts are typically removed to prevent undesired transesterification.

1.2 Polymer Self-Assembly

Polymeric nanostructures are gaining great attention due to their potential applications in electronic and optical devices,[27-29] biomedical treatments,[10, 30] templated synthesis,[31, 32] and catalysis.[33-35] Typically, these nanostructures refer to spherical micelles, cylinders, platelets, and vesicles.[36] Compared to their bio-based counterparts like liposomes, synthetic polymeric nanostructures offer enhanced long-term stability and tunable properties, including thickness, surface functionality, and permeability, making them more versatile for various applications.[37]

Most polymeric nanostructures are currently fabricated through the self-assembly of block copolymers, typically diblock copolymers, using the solvent-switching method.[36, 38, 39] In this approach, the diblock copolymers are first dissolved in a solvent that is good for both blocks. A second solvent, selective for one of the blocks, is then introduced. The disparity in solubility induces the selective block to form the solvophobic core of the nanostructure, while the solvophilic block forms a stabilizing corona. The formation of nanostructures is driven by the balance of solvophobic and solvophilic interactions between the polymer blocks and the selective solvent. The equilibrium nanostructure formed by the solvent-switching method can be predicted based on the packing parameter (p), $p = v/a_0 l_c$, where v is the volume of the

hydrophobic segment, a_0 is the contact area of the head group, and l_c is the length of the hydrophobic segment (Figure 1.4).[11, 36] Among these, anisotropic nanostructures, such as cylinders and platelets, characterized by their direction-dependent dimensions, exhibit superior performance in applications like targeted cargo delivery and catalysis due to their unique structural properties.[10, 40] However, their preparation is challenging, as they form only within a narrow range of block copolymer compositions and self-assembly conditions.

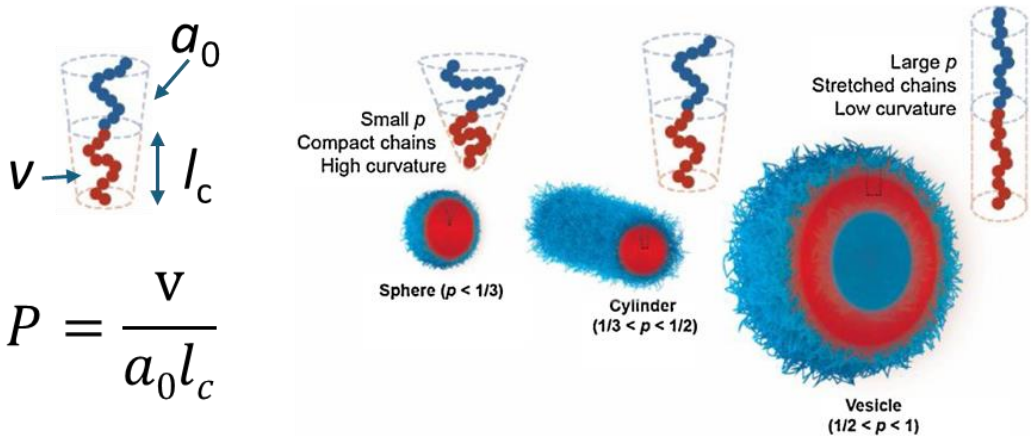

Figure 1.4. Self-assembled nanostructures predicted using packing parameter (reproduced from Ref.[36]).

1.3 Crystallization-Driven Self-Assembly (CDSA)

Crystallization is a process where dissolved molecules transition from a liquid or solution phase into a well-ordered solid crystalline phase. In solution, this occurs when the solution becomes supersaturated, meaning the solute concentration exceeds its equilibrium solubility at a given temperature (Figure 1.5). If one of the blocks is crystallizable, such as PCL, PLA, and

polyferrocenylsilane (PFS), crystallization can serve as a driving force that supersedes solvophilic and solvophobic interactions during self-assembly. This process is known as crystallization-driven self-assembly (CDSA).[41-44] Through CDSA, cylinders and platelets can be obtained in an easy manner as crystallization favors structures of low curvature.

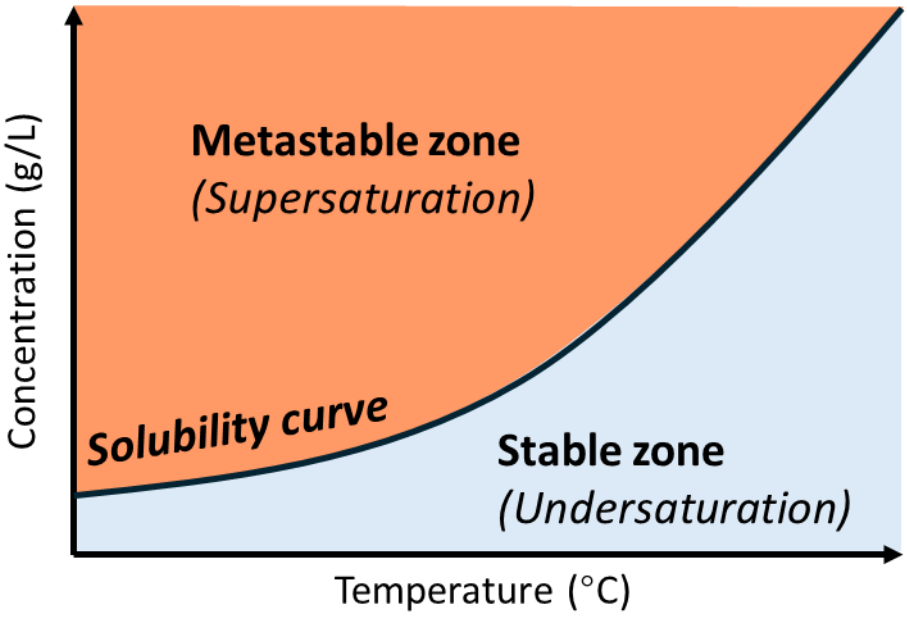

Figure 1.5. Schematic illustration of solubility curve.

1.3.1 Direct CDSA

CDSA can be categorized into two types based on the method and control over nanostructure size: direct CDSA and living CDSA.[41, 42] In direct CDSA, unimers — fully dissolved polymer — first form and then undergo crystallization. A common approach involves heating a supersaturated polymer solution until all polymers dissolve, forming a unimer solution. Upon cooling, polymers aggregate, and CDSA occurs simultaneously (Figure 1.6a). Another method

is solvent switching, where the polymer is dissolved in a good solvent, followed by the addition of a poor solvent to trigger CDSA. The Chen[45-48] and Xu[49-52] groups conducted a lot of solvent-switching work on PCL-based block copolymers of various corona chemistries (PEO (poly(ethylene oxide)), PDMAEMA (poly(2-(dimethylamino)ethyl methacrylate)), PAA (poly (acrylic acid)), PtBA (poly (*tert*-butyl acrylate))), typically using tetrahydrofuran (THF) or dimethylformamide (DMF) to dissolve the polymers, followed by the addition of methanol or water as a poor solvent to induce CDSA.(Figure 1.6b).

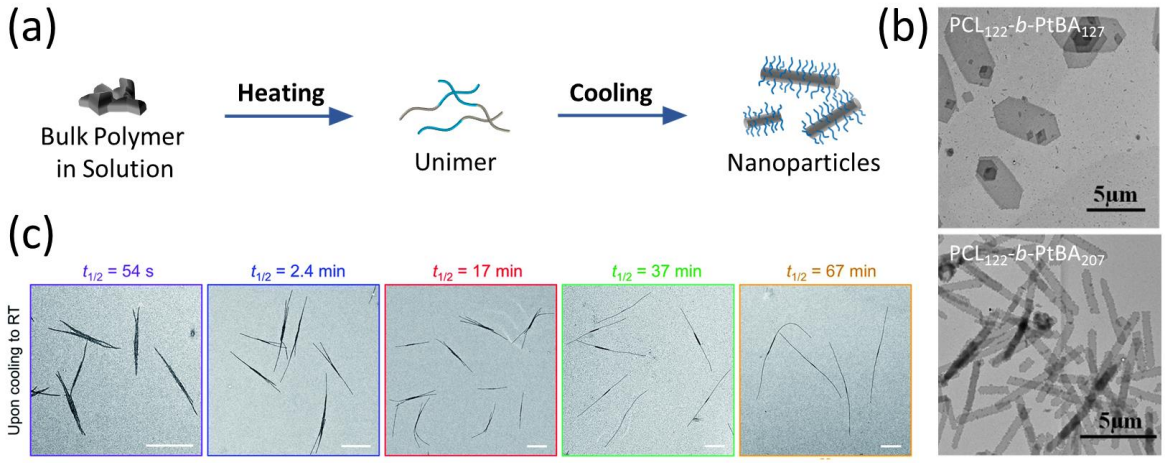

Figure 1.6. Direct CDSA: (a) Scheme of the temperature-regulated direct CDSA, (b) Nanostructures prepared by solvent-switched direct CDSA (reproduced from Ref.[48]), and (c) Nanostructures prepared by direct CDSA under controlled cooling rates (reproduced from Ref.[53]).

However, controlling the size and morphology of nanostructures using direct CDSA is challenging, as nucleation and epitaxial growth occur simultaneously, making it difficult to regulate both processes.[41] Previous studies have shown that polymer precipitation rate, influenced by cooling rate or the solvophobic strength of the poor solvent, significantly impact

the resulting nanostructures.[53, 54] For instance, Song et al. demonstrated that in PFS-*b*-PI (poly(ferrocenyldimethylsilane)-*b*-polyisoprene) block polymers, rapid cooling led to short, branched cylinders, while slower cooling produced long, well-defined cylinders (Figure 1.6c).[53] Excessively fast cooling can cause rapid precipitation, even hindering crystallization and resulting in an amorphous core with reduced structural stability.[55]

1.3.2 Living CDSA

To achieve precise control over the morphology and size of the nanostructures, living CDSA was developed to separate the phases of nucleation and epitaxial growth.[41, 42] To prepare nuclei seed particles, diblock copolymers are initially used to prepare dispersed cylinders through direct CDSA, which are then fragmented via sonication to generate uniform seeds (Figure 1.7a).[40, 56, 57]. The increased solubility and steric hindrance from the corona block reduce the crystallinity of the diblock polymers, making the formation of these cylinders a time-consuming process, often requiring more than a week. In addition, the quality and state of seed particles significantly influence epitaxial growth and, consequently, the morphology of the resulting nanostructures. For instance, Tong and co-workers found that seed particles can become deactivated when combined with metal ions, which inhibit the initiation of epitaxial growth.[58] Moreover, Qiu and co-workers demonstrated that immobilizing seeds on a surface can lead to asymmetric growth, yielding unilateral platelets.[59]

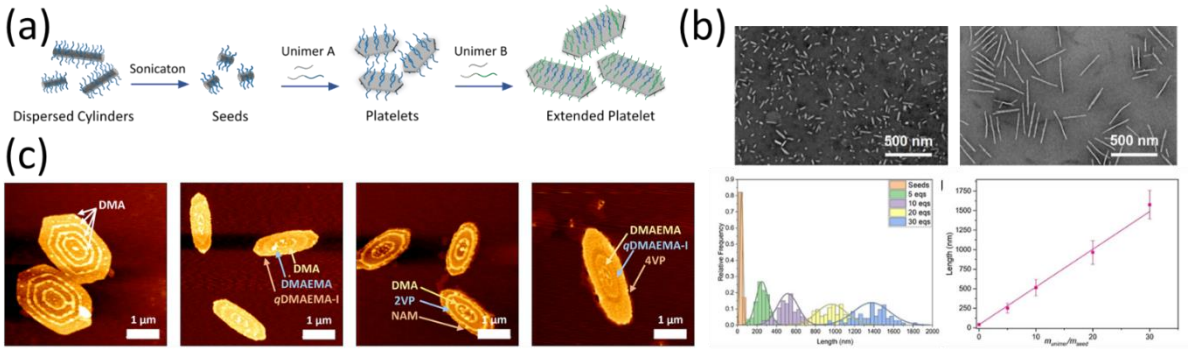

Figure 1.7. Seeded growth: (a) Preparation scheme, (b) Cylinders prepared by seeded growth CDSA showing linear relationship between length and unimer amount (reproduced from Ref.[60]), and (c) PCL-based platelets with various coronas (reproduced from Ref.[61]).

Following the preparation of seeds, the growth process can be initiated through two primary methods: seeded growth and self-seeding. In the seeded growth approach, an additional unimer solution (polymer dissolved in a good solvent) is added to the seed solution to drive epitaxial growth. This method allows for the production of uniform nanostructures, with their size exhibiting a linear relationship with the amount of added unimer, making it practical to control size by adjusting the unimer-to-seed ratio. Besides, the final morphology of the nanostructures can be tuned according to the composition of the unimer solution. Reports indicate that one-dimensional (1D) cylinders are formed when only diblock polymers are added to the seeds, while the synthesis of two-dimensional (2D) platelets necessitates a mixture of homopolymers and diblock polymers. Eisenberg and colleagues conducted a detailed study on the effects of homopolymer additives and found that increasing the ratio of homopolymer leads to a morphological transition from cylinders to platelets.[62] In addition, seeded growth enables linear control of nanostructure size with the amount of added unimer, providing a basis for size

regulation during epitaxial growth (Figure 1.7b).[60] Furthermore, unimers with the same core block but different coronas or end groups can be used to prepare hybrid structures.[61, 63] For example, Xia et al. synthesized PCL-based platelets by sequentially adding unimers with varying corona chemistries (PDMA (polydimethylacrylamide), P2VP (poly(2-vinylpyridine)), P4VP (poly(4-vinylpyridine)), PDMAEMA) to seed solutions, resulting in diverse surface patterns on the platelets (Figure 1.7c).

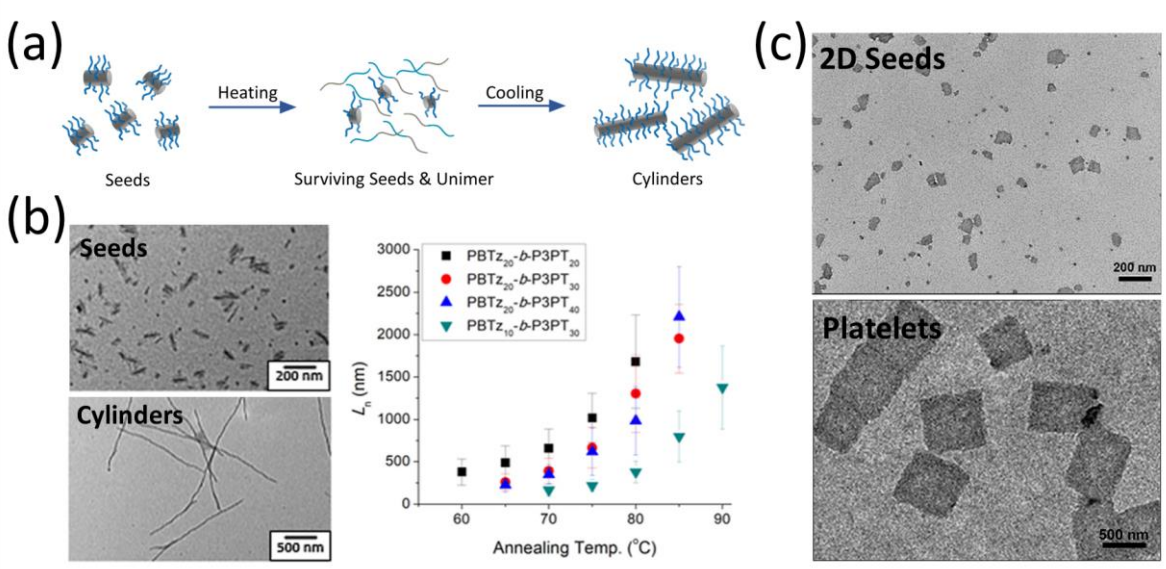

Figure 1.8. Self-seeding CDSA: (a) Preparation scheme, (b) Cylinders prepared by self-seeding (reproduced from Ref.[64]), and (c) Platelets prepared by self-seeding (reproduced from Ref.[65]).

Another living CDSA strategy is self-seeding (Figure 1.8a). In this process, a seed solution is first annealed at an elevated temperature, where low-crystallinity, defective seeds melt to form unimers, while high-crystallinity seeds remain stable and survive.[66-70] During subsequent cooling, the newly formed unimers epitaxially grow on the remaining seeds, leading to uniform extended nanostructures. A variation of this method, solvent-induced self-seeding, involves

partially dissolving the seeds by adding a volatile good solvent. Upon solvent evaporation, the remaining seeds undergo regrowth, producing well-defined nanostructures.[66] Although self-seeding is a practical method for producing uniform particles, its size control is less precise than seeded growth. This is due to the many factors affecting seed survival after annealing, such as temperature, annealing time, and concentration, making it difficult to establish a linear relationship between the final size of the nanomaterials and any single factor. For example, Choi and co-workers used a π-conjugated polymer to prepare uniform nanofibers via self-seeding, observing that while nanofiber length increased with temperature, the relationship was not linear (Figure 1.8b).[64] While self-seeding is commonly used to prepare uniform cylinders, reports also demonstrate the preparation of uniform platelets using this method (Figure 1.8c).[65]

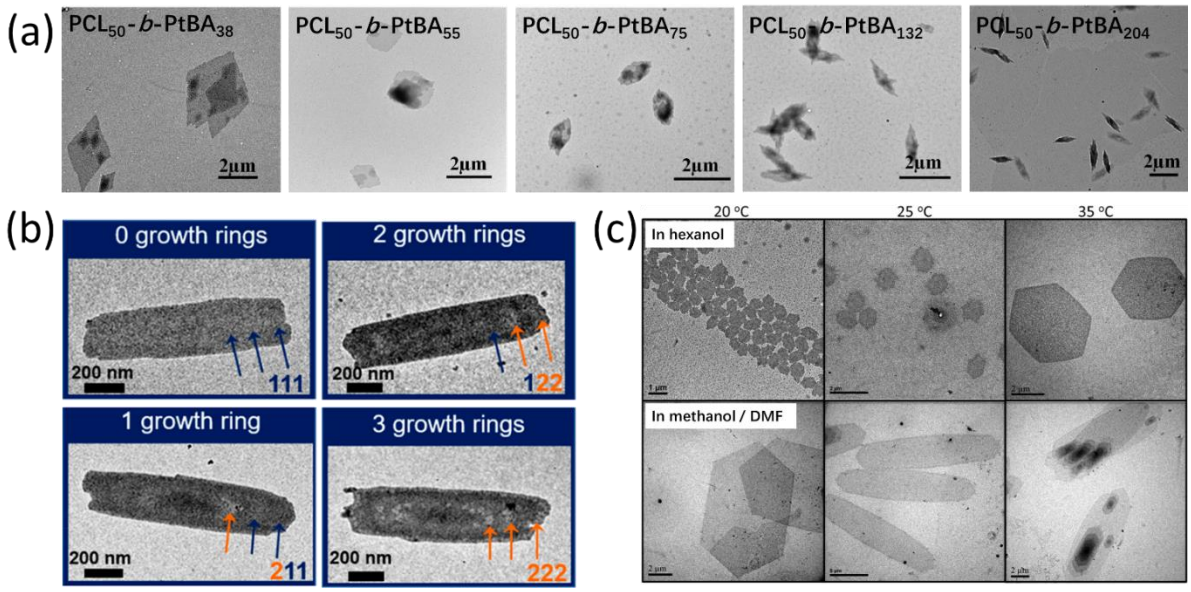

Figure 1.9. Factors influencing CDSA: (a) Effect of corona length (reproduced from Ref.[48]), (b) Surface patterns tuned by unimer composition (reproduced from Ref.[71]), and (c) Platelet morphology influenced by temperature (reproduced from Ref.[72]).

1.3.3 Factors Affecting CDSA

Factors influencing crystallization affect the CDSA process, impacting kinetics, morphology, stability, and uniformity of the resulting nanostructures. Current studies primarily examine the effects of polymer composition, temperature, solvent conditions, and external additives.

The composition of polymers is a fundamental factor in CDSA. The chemistry and chain length of the core block, as well as the ratio of homopolymer to block copolymer (when used as unimers for platelet growth), dictate crystallization behavior.[73-77] Similarly, the corona block composition influences the uniformity and stability of the resulting nanoparticles.[47, 48, 78] For example, Shen et al. observed that increasing the core block length shifted the morphology from low-dimensional structures (spheres) to higher-dimensional ones (cylinders and platelets) across different CDSA systems.[73] Furthermore, modifying the core block chemistry via copolymerization further adjusted crystallization properties, producing distinct morphologies. Similarly, the morphology evolution of PCL-*b*-PtBA CDSA nanoparticles was investigated, revealing that as the length of the corona block increased, the morphology transitioned from lozenges to spindle micelles with high aspect ratios (Figure 1.9a).[48] This transition was influenced by the relative lengths of the polymer blocks.

For CDSA systems involving mixed polymers (typically using a mixture of homo and block polymers as unimer), not only has a morphology evolution from 1D to 2D been observed, but more complex hierarchical structures and intricate patterning can also be achieved.[71, 75, 79-82] For instance, in a PFS/PFS-*b*-PI CDSA system, Winnik and co-workers introduced PFS

homopolymers to create crystal defects within the self-assembled structures.[75] By precisely controlling these defects, they were able to produce hierarchical 3D spherulites. In another example, the Manners group adjusted the ratio of PFS/PFS-*b*-P2VP to control their respective crystallization rates, leading to distinct polymer distributions and various surface patterns on 2D platelets (Figure 1.9b).[71] These findings demonstrate the potential for tailoring polymer blends to create sophisticated nanostructures with unique functional properties.

Temperature is a critical factor in CDSA, as it directly influences crystallization kinetics.[83, 84] Lower crystallization temperatures often result in faster kinetics, limiting the time available for proper chain folding and inhibiting epitaxial growth, leading to the formation of small, low-crystallinity, or even amorphous spherical particles.[54, 55] Conversely, Zhuo et al. demonstrated that controlling CDSA temperature offers a way to fine-tune nucleation efficiency, allowing selective control over the polymer involved in nucleation and epitaxial growth, and enabling the production of nanoparticles with adjustable sizes (Figure 1.9c).[72] Furthermore, temperature is particularly crucial in self-seeding strategies, where small changes in temperature can significantly affect the ratio of surviving seeds that are able to grow, leading to nanostructures with vastly different sizes.[64, 65, 85]

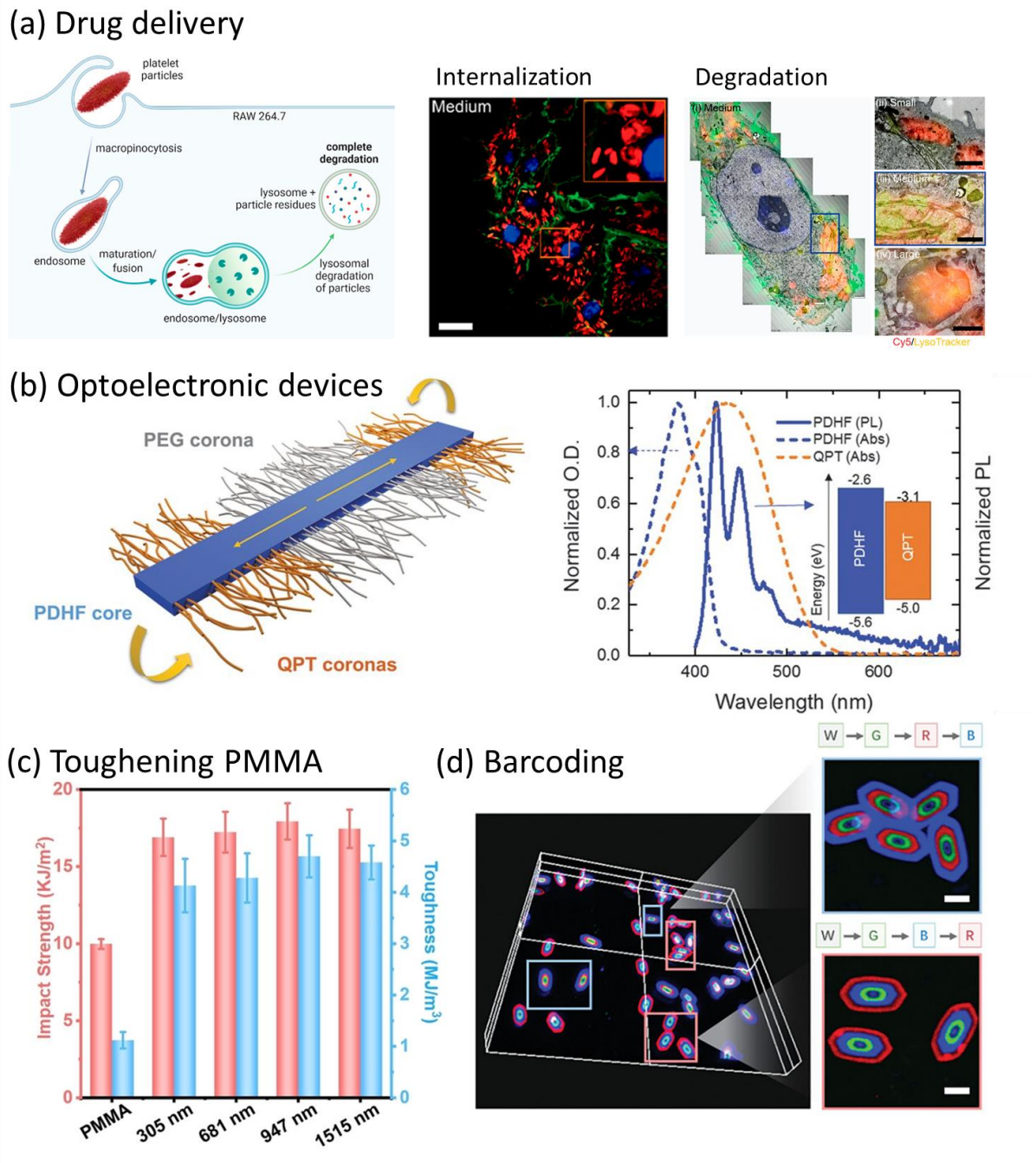

Figure 1.10. Applications of nanoparticles prepared by CDSA: (a) Biodegradable PCL-*b*-PF platelets for drug delivery (reproduced from Ref.[86]), (b) Conjugated polymer cylinders for optoelectronic devices (reproduced from Ref.[35]), (c) Toughening of commercial PMMA using liquid crystalline block copolymer cylinders (reproduced from Ref.[87]), and (d) Fluorescent platelets for information encryption (reproduced from Ref.[56]).

1.3.4 Application of CDSA Nanoparticles

The precise control over the nanoparticles prepared by CDSA is a potent tool to design materials according to a specific application. These assembled nanoparticles have demonstrated their applications in terms of biomedicine, catalysis, additives, and optical devices.

Biomedical applications account for the majority of these applications. The Manners group focused on the application of 1D cylinders, where they prepared a series of PFTMC-*b*-PEG (poly(fluorenetrimethylenecarbonate)-*b*-poly(ethylene glycol)) and PFTMC-*b*-PDMAEMA cylinders and conducted detailed study on antibacterial effect,[88] and cargo delivery effect based on different loading strategies.[60, 89-92] In the meantime, there are also reports using 2D platelets as carrier for drug delivery.[45, 86, 93] For example, Stenzel and co-workers synthesized PCL-*b*-PF (poly(ε-caprolactone)-*b*-poly(1-*O*-acryloyl-*β*-D-fructopyranose)) platelets, and conducted detailed study on the uptake mechanism and downstream intracellular processing (Figure 1.10a).[86]

In addition, researchers functionally designed core and corona blocks to equip CDSA nanoparticles with catalytic and optical applications. Conjugated polymers have excellent electronic and optical properties, and they are used as core blocks to prepare nanostructures for applications in optoelectronics. [35, 94, 95] Friend and co-workers prepared block cylinders using PDHF-*b*-QPT (poly(di-n-hexylfluorene)-*b*-quaternized polythiophene) and PDHF-*b*-PEG, whose long-range exciton transport on the critical length scale comparable to the optical

absorption length in conjugated polymers, and can be used as light-harvesting devices with photon absorption efficiency of 98% (Figure 1.10b).[35]

The use of CDSA nanoparticles as additives is another important application. Recently, Li and co-workers enhanced the mechanical properties of commercial poly(methyl methacrylate) PMMA resin using PCholMA-*b*-PMMA (poly(cholesteryl methacryloyoxy ethyl carbonate)-*b*-poly(methyl methacrylate)) cylinders, investigating the influence of cylinder length on the toughening effect (Figure 1.10c).[87] The results showed that an optimal cylinder length of 947 nm maximizes the toughening effect by bridging cracks and increasing the chain flexibility of the matrix. Furthermore, several studies have reported that these cylinders improve the mechanical strength of hydrogels.[96-98] In addition to cylinders, 2D platelets have also been utilized to modify hydrogels, indicating that the shape of nanoparticles significantly influences properties such as adhesive strength and self-healing.[99]

Spatial control over CDSA nanostructures allows programmable design, enabling applications such as information storage. Research has shown that adjusting the distribution of dye-labeled polymers on both 1D cylinders and 2D platelets can create intricate fluorescent patterns for use as barcoding materials.[56, 63, 100-102] For example, Xie et al. fabricated PCL/PCL-*b*-PDMA platelets with layered fluorescent patterns, where the color sequence was programmed as an encryption method that can be decrypted using microscopy and spectroscopy techniques (Figure 1.10d).[56]

1.3.5 Scale up

To enable the commercial application of nanoparticles prepared via CDSA, scalable production is crucial. However, the process requires extended aging times and dilute conditions (typically less than 0.1 wt%) to achieve monodisperse nanoparticles through living CDSA, which limits throughput significantly (Figure 1.11). Additionally, sonication used for seed particle preparation is restricted to small-scale production due to the limited propagation of ultrasonic energy. These factors make scaling up CDSA nanoparticle production a significant challenge.

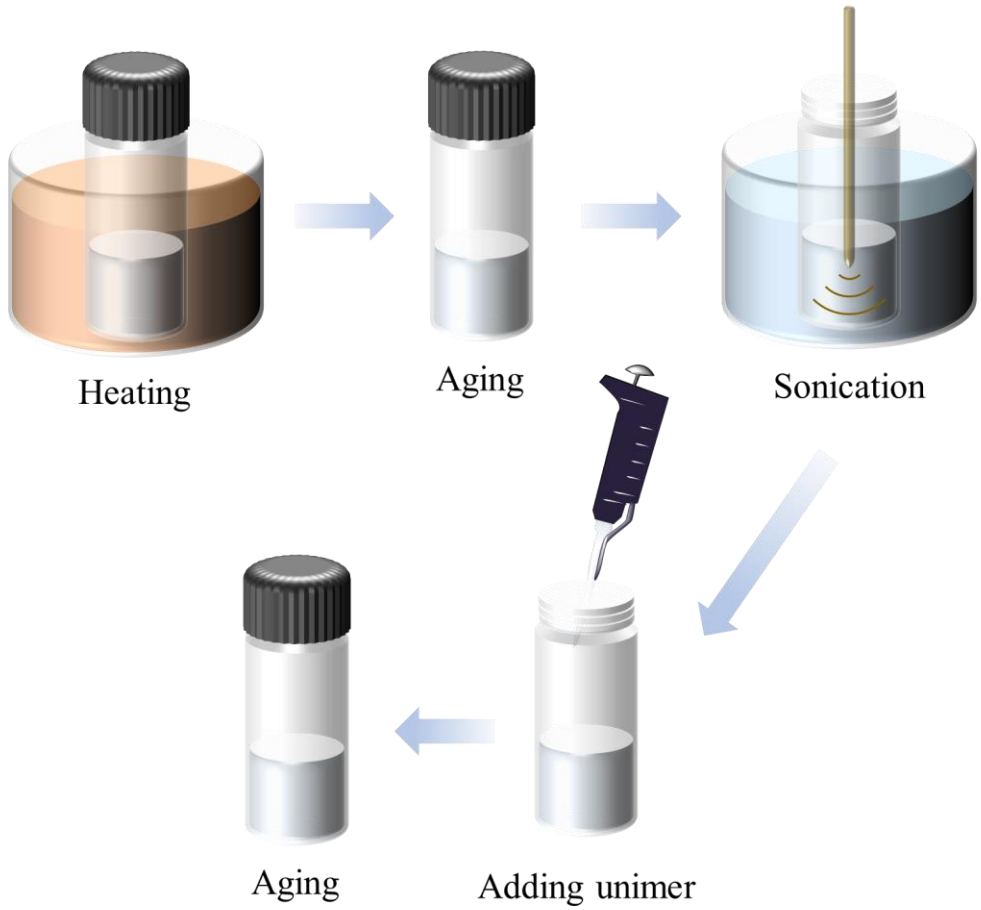

Figure 1.11. Schematic illustration of procedures to conduct CDSA in batch.

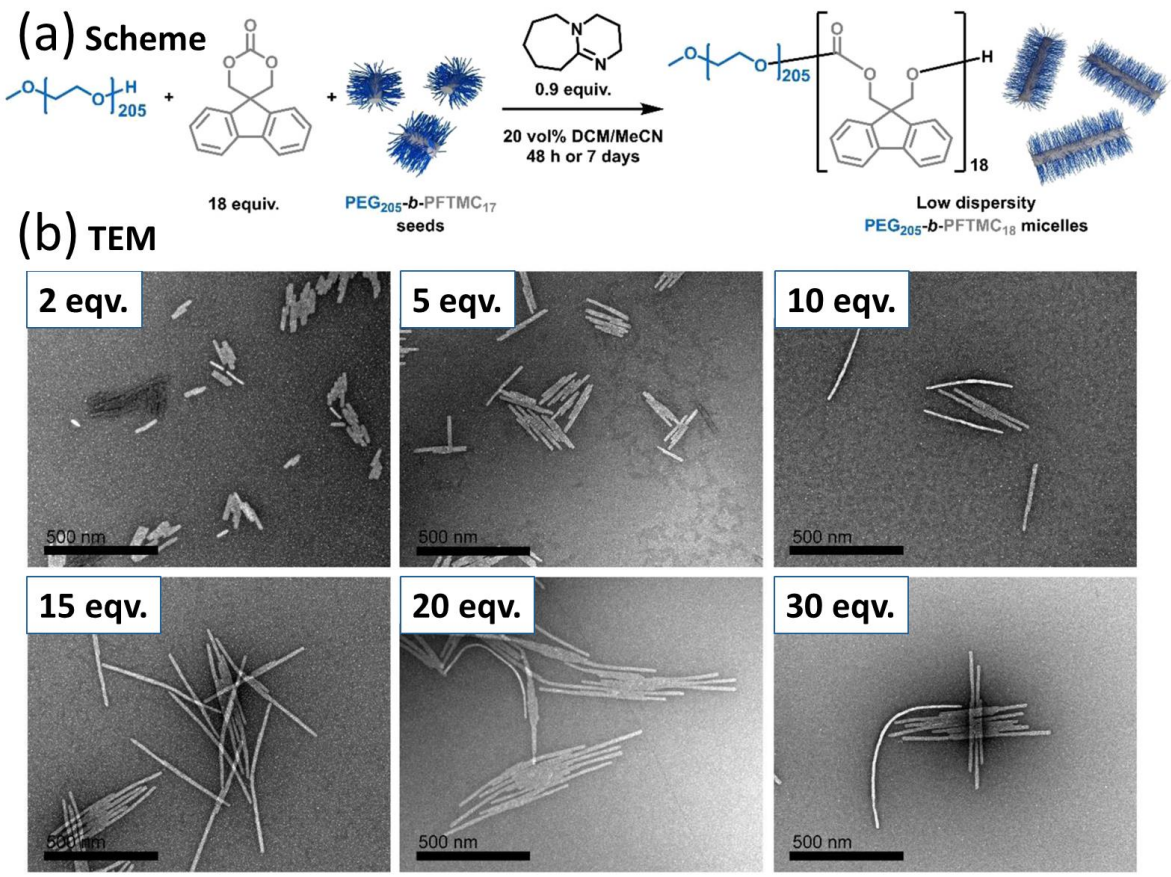

Figure 1.12. Preparation of low-dispersity length-controlled nanofibers by living PI-CDSA from seeds: (a) Preparation scheme, and (b) Representative TEM images of low-dispersity length-controlled nanofibers with various amount of unimer (reproduced from Ref.[103]).

Inspired by polymerization-induced self-assembly (PISA), where polymerization and self-assembly occur simultaneously at high concentrations, researchers developed polymerization-induced crystallization-driven self-assembly (PI-CDSA) to improve throughput. While some studies have increased production, they often compromised nanoparticle size control, leading to high dispersity.[73, 78, 104] To address this, Manners group introduced preformed seed particles into the PEG-*b*-PFTMC PI-CDSA system (living PI-CDSA), separating nucleation from epitaxial growth to better control cylinder size (Figure 1.12).[103] However, there are few reports

of uniform 2D structures, possibly because 2D platelet formation typically requires mixtures of homopolymers and block copolymers, which adds complexity to the already fast PI-CDSA process. To date, to the best of our knowledge, only Reuther and colleagues have successfully produced uniform platelets using poly(aryl isocyanide) (PAIC) in PI-CDSA, though size control was inferior to traditional methods.[105] Consequently, scaling up CDSA remains challenging, and new, more efficient techniques are needed.

1.4 Flow Chemistry

Flow chemistry is where reactions are carried out in a continuous stream. [106] As opposed to traditional batch methods, flow chemistry is typically conducted within microreactors or tubular systems. The reaction stoichiometry for flow chemistry is controlled by the concentration of chemicals and their corresponding flow rates, and the reaction time, which is also called retention time, is determined by the flow rate and the volume of the flow reactor. Nowadays, flow reactors have received more interest because of their superiorities in safety, controllability, and scalability.[107, 108]

1.4.1 Components and Key Parameters

A flow system consists of various modules, typically including a sample injector, mixing device, and reactor (Figure 1.13).[106, 109] In more complex setups, modules for analysis and purification

are integrated, enabling automated production.[110-113] The modular design allows for flexible configuration, adding or removing modules as needed, and reusing the same module type in more advanced systems.

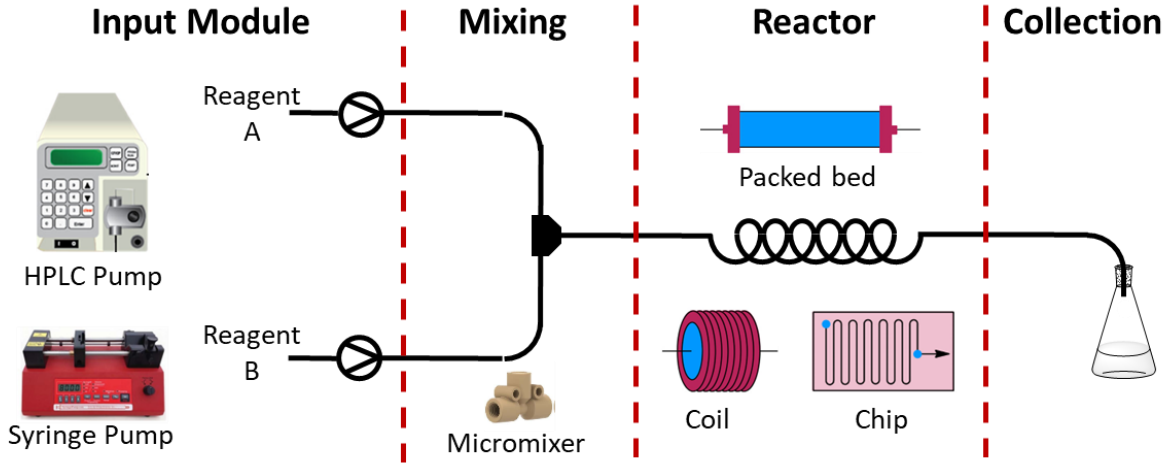

Figure 1.13. Essential components of a flow reactor (reproduced from Ref.[106]).

Input Module

In flow chemistry, pumps serve as delivery modules that not only inject reactants into the system but also drive mass transfer throughout the process. The most commonly used pumps are high-performance liquid chromatography (HPLC) pumps, syringe pumps, and peristaltic pumps.[106, 114, 115] Syringe pumps are ideal for small-scale experiments and low flow rates but generate low pressure, making them unsuitable for systems with long tubing. HPLC pumps, on the other hand, can generate high pressure but are typically limited to flow rates above 0.1 mL/min. Peristaltic pumps are particularly useful for delivering highly concentrated solutions or suspensions, minimizing fouling and blockages.[106]

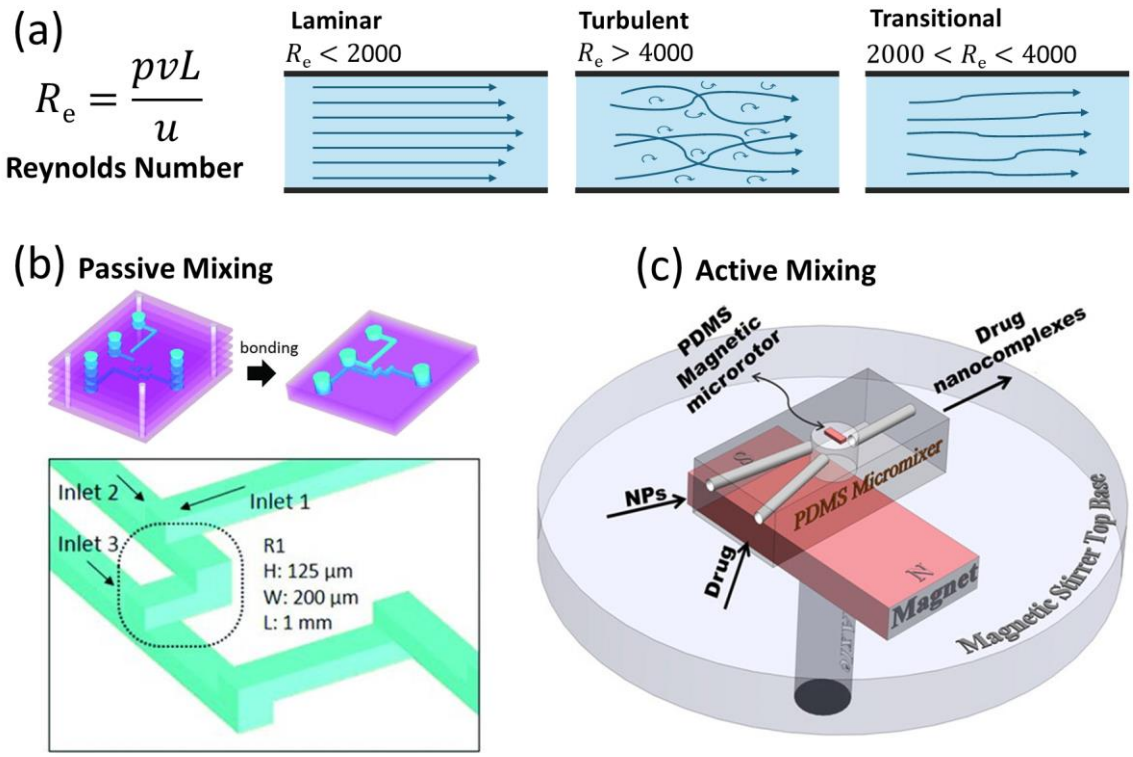

Figure 1.14. (a) Reynolds number (R_e) and flow regimes, where p, u, v, and L represent density, velocity, velocity, and channel length respectively, (b) Passive mixing via optimized geometry (reproduced from Ref.[116]), and (c) Active mixing with magnetic stirring (reproduced from Ref.[117]).

Mixer

Mixers are essential for merging multiple reactant streams, and their mixing efficiency is critical in flow chemistry.[106] The mixing efficiency is closely tied to the flow regime, typically indicated by the Reynolds number (R_e, $R_e = pvL/u$, Figure 1.14a), which can be adjusted by fluid density (p), velocity (v), viscosity (u), and channel length (L). In laboratory-based flow systems, laminar flow dominates ($R_e < 2000$), where mixing occurs through passive diffusion. This process takes time to achieve uniformity, which can lead to premature reactions if the reaction kinetics are fast. In such cases, reactants may react before reaching even concentrations,

resulting in incomplete conversions or the formation of undesired byproducts.[106] To address this, efficient micromixers have been designed.[109, 116, 118-120] For instance, Kim et al. developed a serpentine mixer with a volume of 25 nanoliters that enables rapid mixing, making it suitable for flash reactions completed in sub-millisecond timescales (Figure 1.14b).[116] Additionally, external energy sources, such as sonication and magnetic stirring, are used to enhance mixing, a process known as active mixing (Figure 1.14c).[109, 117, 121]

Reactor

Various types of reactors can be integrated into a flow system based on the reaction requirements (Figure 1.13).[106, 122] Tubular reactors, which can be easily assembled by coiling tubes of specific lengths, are widely used for their simplicity and versatility. Different tubing materials can be selected based on reaction conditions. For high-temperature reactions, stainless steel tubing is preferred,[123] while transparent perfluoroalkoxy alkane (PFA) tubing is more suitable for photochemical reactions.[124] Tubing can also be reshaped into various geometries to enhance mixing and improve reaction efficiency.[107, 125, 126] For example, Wang et al. demonstrated that screw patterns created in commercial polymer tubing through thermoforming significantly improved mixing compared to coiled or straight tubes.[125] Chip reactors, with channel widths of 10 to 500 μm, are widely used in microfluidic systems for small-scale reactions due to their high accuracy and controllability.[106, 115, 127] However, they are more susceptible to blockages and tend to be more expensive.[106] Packed-bed reactors are ideal for heterogeneous reactions. For example, catalysts used in heterogeneous catalytic reactions can

be housed within these reactors, where the high surface area ensures efficient contact between reactants and catalysts, driving the reaction efficiently.[128, 129]

1.4.2 Benefits of Flow

Flow chemistry offers several key advantages over traditional batch processes, particularly in terms of reproducibility, heat transfer, efficiency, and scalability (Figure 1.15).[108] Under a set of pre-defined parameters, reactants continuously flow through the system, ensuring consistent product formation. This contrasts with batch systems, where conditions can vary between runs, leading to inconsistencies in product quality.[108, 109] Another significant benefit of flow reactors is their high surface area-to-volume ratio, which dramatically improves heat transfer.[109, 130] This feature is particularly valuable for reactions with significant thermal effects, as it allows the reaction environment to remain isothermal even at elevated temperatures, promoting reaction homogeneity and increased reaction speed.[131-134] Flow chemistry also excels in terms of scalability and high throughput. The continuous nature of flow systems reduces downtime, allowing even milliliter-scale reactors to produce hundreds of grams of product per day.[130] Moreover, scaling up in flow systems is straightforward as the reactor volume (V, $V = \pi NLD^2/4$) can be increased by adjusting parameters such as channel number (N), length (L), and diameter (D).[109] In addition, due to the modularity of the flow system, in situ monitoring and self-automation can be easily achieved by integrating characterization equipment, which promotes synthesis towards greater refinement, efficiency, and automation.[110-113]

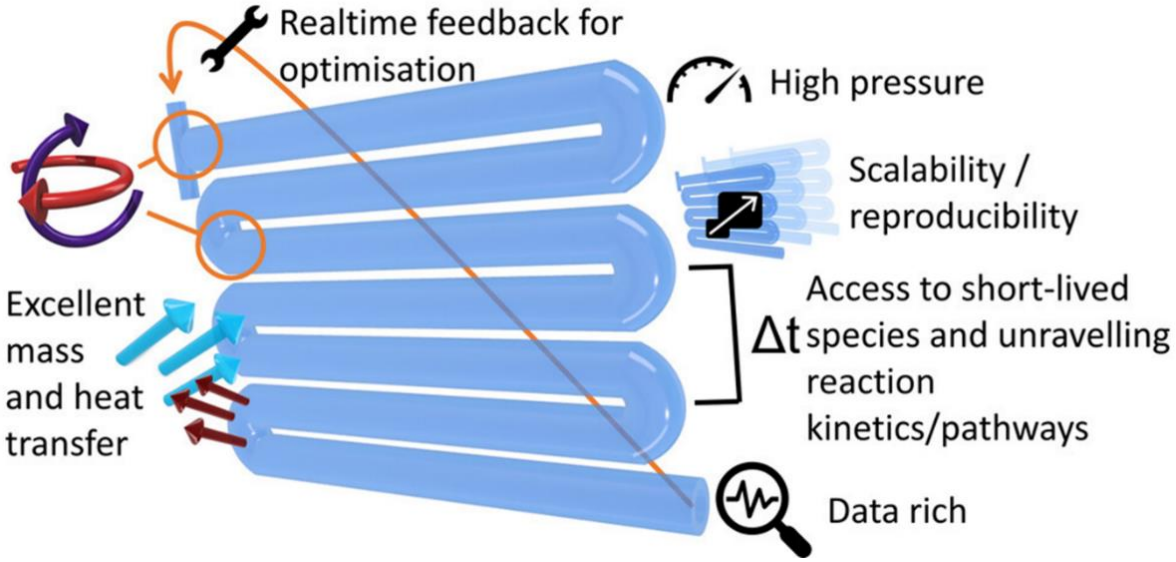

Figure 1.15. Potential benefits of flow (reproduced from Ref.[108]).

Based on the advantages mentioned above, a wide range of synthesis processes can be achieved in flow, including small organic synthesis, polymerization, and nanoparticle fabrication.[112, 135-138]

1.4.3 Organic Synthesis in Flow

The rising demand for efficient, scalable, and sustainable manufacturing processes has established flow chemistry as a transformative tool in pharmaceutical synthesis. By addressing challenges in throughput and efficiency, Kulkarni and co-workers developed a screw reactor for the continuous flow synthesis of amides, where both high throughput (50 g/h) and conversion (90%) can be achieved simultaneously.[139] Furthermore, given the complexity of organic synthesis, which often involves multiple reaction and purification steps, achieving end-

to-end production has become a critical objective. Collaborative efforts between chemists and engineers have led to integrated flow systems, exemplified by the compact, refrigerator-sized platform developed by the Behnam and Zhang groups that seamlessly combines synthesis, purification, and characterization processes (Figure 1.16).[113] These systems have demonstrated continuous large-scale production of pharmaceutical ingredients, including diphenhydramine hydrochloride and fluoxetine hydrochloride. As demonstrated, commercial pharmaceutical ingredients such as diphenhydramine hydrochloride and fluoxetine hydrochloride can be produced continuously with enlarged scale. In addition, flow systems significantly enhance mass transfer in multiphase reactions compared to batch methods, improving efficiency and kinetics, as demonstrated by the Noël group's accelerated gas–liquid C(sp3)–H carbonylation.[140]

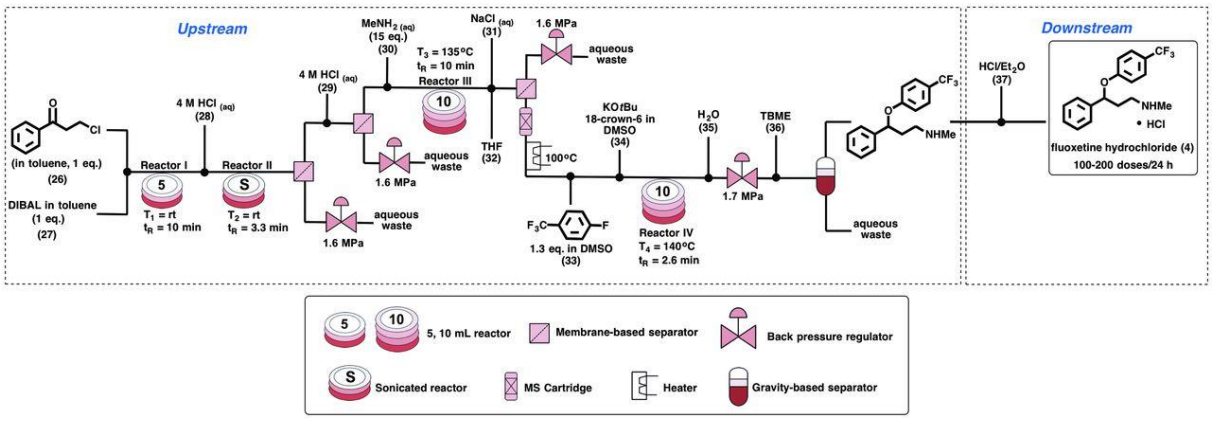

Figure 1.16. Schematic diagram of an integrated flow system for organic synthesis (reproduced from Ref.[113]).

1.4.4 Polymerization in Flow

Flow reactors have been applied to scale up polymerization since 1960s, and polymers synthesized in flow exhibit high reproducibility and precision.[141, 142] As most polymerization is highly exothermic and sensitive to localized hotspots, scaling up in batch would result in local overheating, which could lead to safety issue and increase termination that contributes to wide molecular distribution.[130, 143, 144] However, this can be effectively avoided in flow, since the high surface-to-volume ratio of flow reactors contributes to the excellent thermal management. For instance, Hornung et al. showed that high conversion RAFT polymerization of various monomers including acrylamides, acrylates, and vinyl acetate could be achieved in flow within 2 hours, and the obtained polymers exhibited low molecular weight dispersities (1.15-1.20) and similar molecular weights to those prepared in batch.[145] Even though the increased molecular weight dispersity could be observed due to the normally observed laminar property of flow polymerization leading to the variation in residence time distribution (RTD), especially within a system of wide tubing, high viscosity, and high flow rate,[122, 146] this can be circumvented by an alternative droplet flow module (Figure 1.17a),[146, 147] and flow reactor re-configuring (Figure 1.17b).[126, 146, 148] In addition, Yeo et al. demonstrated that performing RAFT copolymerization in a flow reactor increased the apparent propagation rate constant by tenfold compared to batch processing.[133] In such systems, light is distributed more evenly, which reduces the heterogeneity of light intensity according to the Beer-Lambert-Bouguer law, improving the efficiency of reaction like photo-initiated polymerization.[122, 149-151]

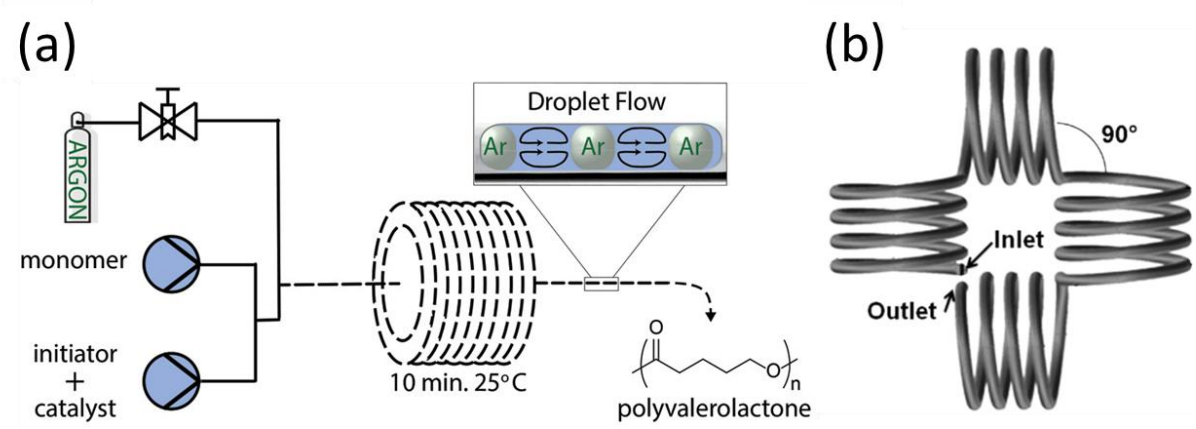

Figure 1.17. (a) Schematic diagram of polymerization using droplet flow (reproduced from Ref.[146]) and (b) Re-configured flow reactor (reproduced from Ref.[126]).

1.4.5 Self-Assembly in Flow

While flow reactors are traditionally used for synthesis and polymerization, they have also been effectively applied to polymer self-assembly, offering distinct advantages over batch processes.[127, 137, 152-155] For instance, Buckinx et al. demonstrated that a standard flow reactor setup enabled the self-assembly of diblock polymers to form uniform micelles within just 1 minute, compared to 12 hours in a batch reactor, which produced micelles with higher dispersity.[152] Additionally, the Stenzel group developed a general flow-based strategy to produce polymersomes at a high throughput of over 3 g/h, achieving size control through thermal annealing and/or secondary micromixing.[137] Besides, PISA has also been adapted to flow systems, and often equipped with in-line monitor to realize precise control over morphology and size.[110, 111, 123, 135, 156-158] For instance, the Warren group conducted an in-depth study on aqueous-based flow PISA, utilizing in-line small-angle X-ray scattering (SAXS) to

analyze rapid particle formation (Figure 1.18).[110] Their findings revealed that the aggregation number (N_{agg}) increased as polymerization progressed, with final N_{agg} value decreasing when longer solvophilic blocks were used for chain extension. These examples underscore how flow reactors can significantly enhance both the efficiency and precision of polymer self-assembly.

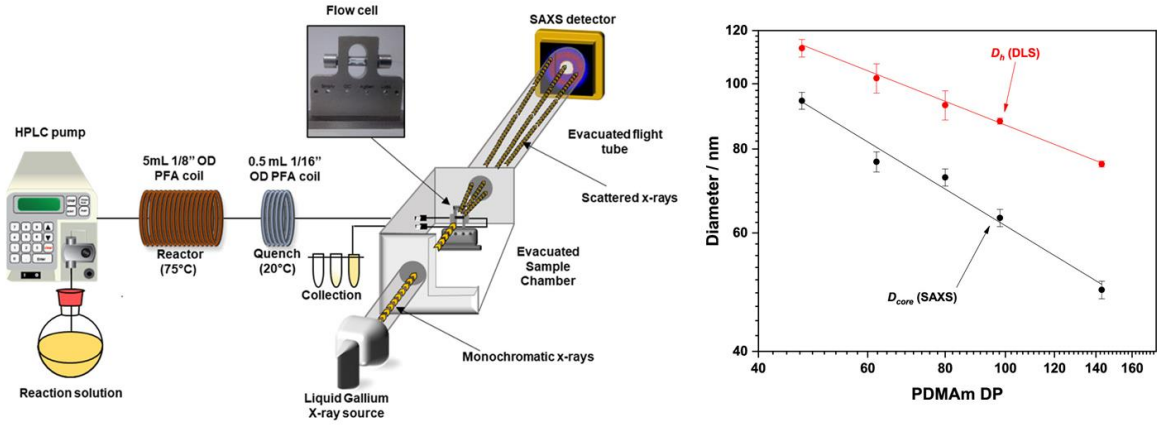

Figure 1.18. Schematic PISA flow system equipped with SAXS for in situ determination (reproduced from Ref.[110]).

1.5 Summary

This chapter introduces the key concepts of polymers, self-assembly, and flow chemistry in relation to this work. It begins by outlining the fundamental properties of polymers and their preparation mechanisms, followed by a detailed discussion of the controlled polymerization techniques RAFT and ROP, which are central to obtaining the polymers used in this study. Next, the concept of polymer self-assembly is briefly introduced, leading into an in-depth discussion of CDSA. The distinctions between general self-assembly and CDSA are clarified, and the key

steps for preparing nanoparticles via CDSA are explained, along with strategies for achieving size control, particularly through living CDSA. Important parameters influencing CDSA behavior are reviewed, and the applications of nanoparticles produced by CDSA are highlighted. The chapter then shifts focus to the challenge of scaling CDSA, introducing flow chemistry as an effective solution. Essential components of a flow reactor and key parameters relevant to this work are discussed, emphasizing the benefits of flow chemistry over traditional batch processes. The section concludes with an overview of polymer self-assembly in flow systems and the potential advantages it offers for nanoparticle production.

The objective of this thesis is to scale up CDSA using flow reactors and the preparation of fine nanostructures by leveraging the excellent controllability of flow reactors. Given the complexity of morphology transitions and the challenges of process integration, the study was conducted in three phases: (1) scaling up living CDSA to prepare platelets from seeds, (2) exploring efficient seed preparation in flow and integrating it with living CDSA sections to establish an all-flow process, and (3) fabricating fine nanostructures on platelets by precisely controlling flow parameters. These phases correspond to the work detailed in chapter 2-4 respectively.

1.6 Reference

1. H. Staudinger, *Berichte der deutschen chemischen Gesellschaft (A and B Series)*, 1920, **53**, 1073-1085.

2. A. Shundo, S. Yamamoto and K. Tanaka, *JACS Au*, 2022, **2**, 1522-1542.

3. O. Zabihi, M. Ahmadi, S. Nikafshar, K. Chandrakumar Preyeswary and M. Naebe, *Compos. B Eng.*, 2018, **135**, 1-24.

4. S. Chen, Y. Wang, L. Yang, C. Chu, S. Cao, Z. Wang, J. Xue and Z. You, *Prog. Polym. Sci.*, 2023, **147**, 101763.

5. G. Li, R. Zhu and Y. Yang, *Nat. Photonics*, 2012, **6**, 153-161.

6. C. T. J. Ferguson and K. A. I. Zhang, *ACS Catal.*, 2021, **11**, 9547-9560.

7. T. Wang, Y. Cheng and C. Yang, *Prog. Polym. Sci.*, 2024, **158**, 101892.

8. A. Sikder, A. K. Pearce, S. J. Parkinson, R. Napier and R. K. O'Reilly, *ACS Appl. Polym. Mater.*, 2021, **3**, 1203-1217.

9. M. Zhang, M. Kim, W. Choi, J. Choi, D. H. Kim, Y. Liu and Z. Lin, *Prog. Polym. Sci.*, 2024, **151**, 101800.

10. A. K. Pearce, T. R. Wilks, M. C. Arno and R. K. O'Reilly, *Nat. Rev. Chem.*, 2020, **5**, 21-45.

11. K. E. B. Doncom, L. D. Blackman, D. B. Wright, M. I. Gibson and R. K. O'Reilly, *Chem. Soc. Rev.*, 2017, **46**, 4119-4134.

12. T. Fukuda, K. Kubo and Y.-D. Ma, *Prog. Polym. Sci.*, 1992, **17**, 875-916.

13. D. Colombani, *Prog. Polym. Sci.*, 1997, **22**, 1649-1720.

14. S. Perrier, *Macromolecules*, 2017, **50**, 7433-7447.

15. J. Skey and R. K. O'Reilly, *Chem. Commun.*, 2008, 4183-4185.

16. G. Moad, E. Rizzardo and S. H. Thang, *Aust. J. Chem.*, 2005, **58**, 379-410.

17. A.-C. Albertsson and R. K. Srivastava, *Adv. Drug Deliv. Rev.*, 2008, **60**, 1077-1093.

18. E. Champagne, S. Strandman and X.-X. Zhu, *Macromol. Rapid Commun.*, 2016, **37**, 1986-2004.

19. K. Wang, C. Li, L. Man, M. Zhang, Y.-G. Jia and X. X. Zhu, *Chem. Commun.*, 2023, **59**, 9182-9194.

20. I. A. Barker and A. P. Dove, *Chem. Commun.*, 2013, **49**, 1205-1207.

21. D. Delcroix, B. Martín-Vaca, D. Bourissou and C. Navarro, *Macromolecules*, 2010, **43**, 8828-8835.

22. K. Makiguchi, Y. Ogasawara, S. Kikuchi, T. Satoh and T. Kakuchi, *Macromolecules*, 2013, **46**, 1772-1782.

23. Y. Chen, J. Zhang, W. Xiao, A. Chen, Z. Dong, J. Xu, W. Xu and C. Lei, *Eur. Polym. J.*, 2021, **161**, 110861.

24. T. F. Burton, J. Pinaud, N. Pétry, F. Lamaty and O. Giani, *ACS Macro Lett.*, 2021, **10**, 1454-1459.

25. P. Olsén, K. Odelius, H. Keul and A.-C. Albertsson, *Macromolecules*, 2015, **48**, 1703-1710.

26. K. Makiguchi, T. Satoh and T. Kakuchi, *Macromolecules*, 2011, **44**, 1999-2005.

27. M. Stefik, S. Guldin, S. Vignolini, U. Wiesner and U. Steiner, *Chem. Soc. Rev.*, 2015, **44**, 5076-5091.

28. S. Ji, L. Wan, C.-C. Liu and P. F. Nealey, *Prog. Polym. Sci.*, 2016, **54-55**, 76-127.

29. R. Dehmel, J. A. Dolan, Y. B. Gu, U. Wiesner, T. D. Wilkinson, J. J. Baumberg, U. Steiner, B. D. Wilts and I. Gunkel, *Macromolecules*, 2017, **50**, 6255-6262.

30. H. G. Börner, *Prog. Polym. Sci.*, 2009, **34**, 811-851.

31. J. K. Kim, S. Y. Yang, Y. Lee and Y. Kim, *Prog. Polym. Sci.*, 2010, **35**, 1325-1349.

32. P. S. Chinthamanipeta, Q. Lou and D. A. Shipp, *ACS Nano*, 2011, **5**, 450-456.

33. J. Cai, C. Li, N. Kong, Y. Lu, G. Lin, X. Wang, Y. Yao, I. Manners and H. Qiu, *Science*, 2019, **366**, 1095-1098.

34. J. Tian, Y. Zhang, L. Du, Y. He, X.-H. Jin, S. Pearce, J.-C. Eloi, R. L. Harniman, D. Alibhai, R. Ye, D. L. Phillips and I. Manners, *Nat. Chem.*, 2020, **12**, 1150-1156.

35. X.-H. Jin, M. B. Price, J. R. Finnegan, C. E. Boott, J. M. Richter, A. Rao, S. M. Menke, R. H. Friend, G. R. Whittell and I. Manners, *Science*, 2018, **360**, 897-900.

36. S. Varlas, S. B. Lawrenson, L. A. Arkinstall, R. K. O'Reilly and J. C. Foster, *Prog. Polym. Sci.*, 2020, **107**, 101278.

37. J. d. A. Pachioni-Vasconcelos, A. M. Lopes, A. C. Apolinário, J. K. Valenzuela-Oses, J. S. R. Costa, L. d. O. Nascimento, A. Pessoa, L. R. S. Barbosa and C. d. O. Rangel-Yagui, *Biomater. Sci.*, 2016, **4**, 205-218.

38. J. C. Foster, S. Varlas, B. Couturaud, Z. Coe and R. K. O'Reilly, *J. Am. Chem. Soc.*, 2019, **141**, 2742-2753.

39. M. Karayianni and S. Pispas, *J. Polym. Sci.*, 2021, **59**, 1874-1898.

40. M. C. Arno, M. Inam, Z. Coe, G. Cambridge, L. J. Macdougall, R. Keogh, A. P. Dove and R. K. O'Reilly, *J. Am. Chem. Soc.*, 2017, **139**, 16980-16985.

41. L. MacFarlane, C. Zhao, J. Cai, H. Qiu and I. Manners, *Chem. Sci.*, 2021, **12**, 4661-4682.

42. S. Ganda and M. H. Stenzel, *Prog. Polym. Sci.*, 2020, **101**, 101195.

43. E. R. L. Brisson, M. J. H. Worthington, S. Kerai and M. Müllner, *Chem. Soc. Rev.*, 2024, **53**, 1984-2021.

44. C. Yang, Z.-X. Li and J.-T. Xu, *J. Polym. Sci.*, 2022, **60**, 2153-2174.

45. W. Zhu, B. Peng, J. Wang, K. Zhang, L. Liu and Y. Chen, *Macromol. Biosci.*, 2014, **14**, 1764-1770.

46. J. Wang, W. Zhu, B. Peng and Y. Chen, *Polymer*, 2013, **54**, 6760-6767.

47. J. Wang, Y. Lu and Y. Chen, *Polymer*, 2019, **160**, 196-203.

48. J. Wang, J. Si, J. Zhu, Y. Nie, Y. Lu and Y. Chen, *Polymer*, 2023, **284**, 126292.

49. Z.-X. Du, J.-T. Xu and Z.-Q. Fan, *Macromolecules*, 2007, **40**, 7633-7637.

50. Z.-X. Du, J.-T. Xu and Z.-Q. Fan, *Macromol. Rapid Commun.*, 2008, **29**, 467-471.

51. W.-N. He, J.-T. Xu, B.-Y. Du, Z.-Q. Fan and F.-L. Sun, *Macromol. Chem. Phys.*, 2012, **213**, 952-964.

52. X.-Y. Wang, R.-Y. Wang, B. Fan, J.-T. Xu, B.-Y. Du and Z.-Q. Fan, *Macromolecules*, 2018, **51**, 2138-2144.

53. S. Song, J. Jiang, E. Nikbin, J. Y. Howe, I. Manners and M. A. Winnik, *Chem. Sci.*, 2022, **13**, 396-409.

54. A. M. Mihut, M. Drechsler, M. Möller and M. Ballauff, *Macromol. Rapid Commun.*, 2010, **31**, 449-453.

55. M.-S. Hsiao, S. F. M. Yusoff, M. A. Winnik and I. Manners, *Macromolecules*, 2014, **47**, 2361-2372.

56. Y. Xie, Z. Tong, T. Xia, J. C. Worch, J. Y. Rho, A. P. Dove and R. K. O'Reilly, *Adv. Mater.*, 2023, **36**, 2308154.

57. Z. Tong, Y. Xie, M. C. Arno, Y. Zhang, I. Manners, R. K. O'Reilly and A. P. Dove, *Nat. Chem.*, 2023, **15**, 824-831.

58. L. Zhu, B. Xiang, Y. Su and Z. Tong, *Polymer*, 2023, **272**, 125831.

59. G. Lin, J. Tao, Y. Sun, Y. Cui, I. Manners and H. Qiu, *J. Am. Chem. Soc.*, 2024, **146**, 14734-14744.

60. C. Zhao, Q. Chen, J. D. Garcia-Hernandez, L. K. Watanabe, J. M. Rawson, J. Rao and I. Manners, *Macromolecules*, 2022, **56**, 263-270.

61. T. Xia, Z. Tong, Y. Xie, M. C. Arno, S. Lei, L. Xiao, J. Y. Rho, C. T. J. Ferguson, I. Manners, A. P. Dove and R. K. O'Reilly, *J. Am. Chem. Soc.*, 2023, **145**, 25274-25282.

62. G. Rizis, T. G. M. van de Ven and A. Eisenberg, *Angew. Chem. Int. Ed.*, 2014, **53**, 9000-9003.

63. H. Qiu, Y. Gao, C. E. Boott, O. E. C. Gould, R. L. Harniman, M. J. Miles, S. E. D. Webb, M. A. Winnik and I. Manners, *Science*, 2016, **352**, 697-701.

64. H. Kim, J. Lee, S.-H. Hwang, N. Yun, S. Park and T.-L. Choi, *J. Am. Chem. Soc.*, 2024, **146**, 20750-20757.

65. X. Zhang, G. Chen, L. Liu, L. Zhu and Z. Tong, *Macromolecules*, 2022, **55**, 8250-8261.

66. J. Qian, Y. Lu, A. Chia, M. Zhang, P. A. Rupar, N. Gunari, G. C. Walker, G. Cambridge, F. He, G. Guerin, I. Manners and M. A. Winnik, *ACS Nano*, 2013, **7**, 3754-3766.

67. J. Qian, G. Guerin, Y. Lu, G. Cambridge, I. Manners and M. A. Winnik, *Angew. Chem. Int. Ed.*, 2011, **50**, 1622-1625.

68. J. Qian, X. Li, D. J. Lunn, J. Gwyther, Z. M. Hudson, E. Kynaston, P. A. Rupar, M. A. Winnik and I. Manners, *J. Am. Chem. Soc.*, 2014, **136**, 4121-4124.

69. D. L. Tao, C. Feng, Y. J. Lu, Y. N. Cui, X. Yang, I. Manners, M. A. Winnik and X. Y. Huang, *Macromolecules*, 2018, **51**, 2065-2075.

70. W. Yu, J. C. Foster, A. P. Dove and R. K. O'Reilly, *Macromolecules*, 2020, **53**, 1514-1521.

71. R. Deng, X. Mao, S. Pearce, J. Tian, Y. Zhang and I. Manners, *J. Am. Chem. Soc.*, 2022, **144**, 19051-19059.

72. W. Q. Zhuo, Y. M. Li, R. K. Zhang, R. S. Huang, J. Zhou, Z. Z. Tong and G. H. Jiang, *J. Appl. Polym. Sci.*, 2017, **134**, 45089.

73. D. Shen, B. Shi, P. Zhou, D. Li and G. Wang, *Macromolecules*, 2023, **56**, 4814-4822.

74. B. Jin, Q. Li, L. Hu, Q. Liu, Y. Chen, Y. Luo, S. Chi and X. Li, *Angew. Chem. Int. Ed.*, 2023, **62**, e202219067.

75. J. Jiang, E. Nikbin, Y. Liu, S. Lei, G. Ye, J. Y. Howe, I. Manners and M. A. Winnik, *J. Am. Chem. Soc.*, 2023, **145**, 28096-28110.

76. W. Hu, M. Safari, Y. Zhou, R. A. Pérez-Camargo, G. Liu, A. J. Müller and D. Wang, *Macromolecules*, 2023, **56**, 5058-5067.

77. Y. Yao, L. Gao, C. Cai, J. Lin, S. Wang and S. Song, *Macromolecules*, 2023, **56**, 10254-10263.

78. L. Yu, Y. Cui, M. Xing, Y. Sun, Z. Li, Y. Liu, X. Qu and S. Chen, *Macromol. Rapid Commun.*, 2024, **45**, 2400549.

79. H. Qiu, G. Cambridge, M. A. Winnik and I. Manners, *J. Am. Chem. Soc.*, 2013, **135**, 12180-12183.

80. J. R. Finnegan, D. J. Lunn, O. E. C. Gould, Z. M. Hudson, G. R. Whittell, M. A. Winnik and I. Manners, *J. Am. Chem. Soc.*, 2014, **136**, 13835-13844.

81. H. Qiu, Z. M. Hudson, M. A. Winnik and I. Manners, *Science*, 2015, **347**, 1329-1332.

82. J. Kim, W. Chung, D. Kim, J. Kang, C. F. Grandes Reyes, J. Jeong and K. T. Kim, *Chem. Commun.*, 2023, **59**, 3578-3581.

83. M. R. Caputo, A. Olmos, B. Li, J. L. Olmedo-Martínez, A. Malafronte, C. De Rosa, H. Sardon, R. K. O'Reilly, A. P. Dove and A. J. Müller, *Biomacromolecules*, 2023, **24**, 3256-3267.

84. A. Fernández-Tena, R. A. Pérez-Camargo, O. Coulembier, L. Sangroniz, N. Aranburu, G. Guerrica-Echevarria, G. Liu, D. Wang, D. Cavallo and A. J. Müller, *Macromolecules*, 2023, **56**, 4602-4620.

85. I. Choi, S.-Y. Kang, S. Yang, N. Yun and T.-L. Choi, *Macromolecules*, 2022, **55**, 3484-3492.

86. S. Ganda, C. K. Wong, J. Biazik, R. Raveendran, L. Zhang, F. Chen, N. Ariotti and M. H. Stenzel, *ACS Appl. Mater. Interfaces*, 2022, **14**, 35333-35343.

87. L. Hu, Q. Li, Y. Luo, B. Jin, S. Chi and X. Li, *Angew. Chem. Int. Ed.*, 2023, **62**, e202310022.

88. H. C. Parkin, J. D. Garcia-Hernandez, S. T. G. Street, R. Hof and I. Manners, *Polym. Chem.*, 2022, **13**, 2941-2949.

89. J. D. Garcia-Hernandez, S. T. G. Street, Y. Kang, Y. Zhang and I. Manners, *Macromolecules*, 2021, **54**, 5784-5796.

90. J. D. Garcia-Hernandez, H. C. Parkin, Y. Ren, Y. Zhang and I. Manners, *Polym. Chem.*, 2022, **13**, 4100-4110.

91. S. T. G. Street, J. Chrenek, R. L. Harniman, K. Letwin, J. M. Mantell, U. Borucu, S. M. Willerth and I. Manners, *J. Am. Chem. Soc.*, 2022, **144**, 19799-19812.

92. S. T. G. Street, Y. He, R. L. Harniman, J. D. Garcia-Hernandez and I. Manners, *Polym. Chem.*, 2022, **13**, 3009-3025.

93. X. Zhang, G. Chen, B. Zheng, Z. Wan, L. Liu, L. Zhu, Y. Xie and Z. Tong, *Biomacromolecules*, 2023, **24**, 1032–1041.

94. J. Ma, B. Hao, S. Zhang, X. Huang, G. Lu and C. Feng, *Adv. Mater. Interfaces*, 2022, **9**, 2201823.

95. H. Shaikh, X.-H. Jin, R. L. Harniman, R. M. Richardson, G. R. Whittell and I. Manners, *J. Am. Chem. Soc.*, 2020, **142**, 13469-13480.

96. Z. Li, A. K. Pearce, J. Du, A. P. Dove and R. K. O'Reilly, *J. Polym. Sci.*, 2022, **61**, 44.

97. J. Yu, J. Liu, C. Li, J. Huang, Y. Zhu and H. You, *Chem. Commun.*, 2024, **60**, 3217-3225.

98. Z. Li, A. Pearce, A. Dove and R. O'Reilly, *Polymers*, 2021, **13**, 2202.

99. M. C. Arno, M. Inam, A. C. Weems, Z. Li, A. L. A. Binch, C. I. Platt, S. M. Richardson, J. A. Hoyland, A. P. Dove and R. K. O'Reilly, *Nat. Commun.*, 2020, **11**, 1420.

100. M. Li, J. Guo, C. Zhang, Y. Che, Y. Yi and B. Liu, *Angew. Chem. Int. Ed.*, 2023, **62**, e202309914.

101. A. Rajak and A. Das, *Angew. Chem. Int. Ed.*, 2022, **61**, e202116572.

102. A. Rajak and A. Das, *Angew. Chem. Int. Ed.*, 2023, **62**, e202314290.

103. C. E. Ellis, J. D. Garcia-Hernandez and I. Manners, *J. Am. Chem. Soc.*, 2022, **144**, 20525-20538.

104. P. J. Hurst, A. A. Graham and J. P. Patterson, *ACS Polym. Au*, 2022, **2**, 501-509.

105. R. A. Scanga, A. Shahrokhinia, J. Borges, S. H. Sarault, M. B. Ross and J. F. Reuther, *J. Am. Chem. Soc.*, 2023, **145**, 6319–6329.

106. M. B. Plutschack, B. Pieber, K. Gilmore and P. H. Seeberger, *Chem. Rev.*, 2017, **117**, 11796-11893.

107. M. H. Reis, F. A. Leibfarth and L. M. Pitet, *ACS Macro Lett.*, 2020, **9**, 123-133.

108. A. Laybourn, K. Robertson and A. G. Slater, *J. Am. Chem. Soc.*, 2023, **145**, 4355-4365.

109. L. Capaldo, Z. Wen and T. Noël, *Chem. Sci.*, 2023, **14**, 4230-4247.

110. J. D. Guild, S. T. Knox, S. B. Burholt, E. M. Hilton, N. J. Terrill, S. L. M. Schroeder and N. J. Warren, *Macromolecules*, 2023, **56**, 6426-6435.

111. S. T. Knox, S. Parkinson, R. Stone and N. J. Warren, *Polym. Chem.*, 2019, **10**, 4774-4778.

112. A. Slattery, Z. Wen, P. Tenblad, J. Sanjosé-Orduna, D. Pintossi, T. den Hartog and T. Noël, *Science*, 2024, **383**, eadj1817.

113. A. Adamo, R. L. Beingessner, M. Behnam, J. Chen, T. F. Jamison, K. F. Jensen, J.-C. M. Monbaliu, A. S. Myerson, E. M. Revalor, D. R. Snead, T. Stelzer, N. Weeranoppanant, S. Y. Wong and P. Zhang, *Science*, 2016, **352**, 61-67.

114. L. Akh, D. Jung, W. Frantz, C. Bowman, A. C. Neu and X. Ding, *Biomicrofluidics*, 2023, **17**.

115. A. Mudugamuwa, U. Roshan, S. Hettiarachchi, H. Cha, H. Musharaf, X. Kang, Q. T. Trinh, H. M. Xia, N.-T. Nguyen and J. Zhang, *Small*, 2024, **20**, 2404685.

116. H. Kim, K.-I. Min, K. Inoue, D. J. Im, D.-P. Kim and J.-i. Yoshida, *Science*, 2016, **352**, 691-694.

117. N. Veldurthi, P. Ghoderao, S. Sahare, V. Kumar, D. Bodas, A. Kulkarni and T. Bhave, *Mater. Sci. Eng. C*, 2016, **68**, 455-464.

118. M. Bayareh, M. N. Ashani and A. Usefian, *Chem. Eng. Process.*, 2020, **147**, 107771.

119. A. D. Stroock, S. K. W. Dertinger, A. Ajdari, I. Mezić, H. A. Stone and G. M. Whitesides, *Science*, 2002, **295**, 647-651.

120. Y. Liao, Y. Mechulam and B. Lassalle-Kaiser, *Sci. Rep.*, 2021, **11**, 20119.

121. Z. Dong, S. D. A. Zondag, M. Schmid, Z. Wen and T. Noël, *Chem. Eng. J.*, 2022, **428**, 130968.

122. S. T. Knox and N. J. Warren, *Reac. Chem. Eng.*, 2020, **5**, 405-423.

123. S. Parkinson, N. S. Hondow, J. S. Conteh, R. A. Bourne and N. J. Warren, *Reac. Chem. Eng.*, 2019, **4**, 852-861.

124. O. Eckardt, B. Wenn, P. Biehl, T. Junkers and F. H. Schacher, *Reac. Chem. Eng.*, 2017, **2**, 479-486.

125. K. Wang, H. Zhang, Y. Shen, A. Adamo and K. F. Jensen, *Reac. Chem. Eng.*, 2018, **3**, 707-713.

126. D. Parida, C. A. Serra, D. K. Garg, Y. Hoarau, F. Bally, R. Muller and M. Bouquey, *Macromolecules*, 2014, **47**, 3282-3287.

127. W. Li, L. Zhang, X. Ge, B. Xu, W. Zhang, L. Qu, C.-H. Choi, J. Xu, A. Zhang, H. Lee and D. A. Weitz, *Chem. Soc. Rev.*, 2018, **47**, 5646-5683.

128. J. Britton and C. L. Raston, *Chem. Soc. Rev.*, 2017, **46**, 1250-1271.

129. M. G. Russell and T. F. Jamison, *Angew. Chem. Int. Ed.*, 2019, **58**, 7678-7681.

130. N. Zaquen, M. Rubens, N. Corrigan, J. Xu, P. B. Zetterlund, C. Boyer and T. Junkers, *Prog. Polym. Sci.*, 2020, **107**, 101256.

131. C. Diehl, P. Laurino, N. Azzouz and P. H. Seeberger, *Macromolecules*, 2010, **43**, 10311-10314.

132. F. Lauterbach, M. Rubens, V. Abetz and T. Junkers, *Angew. Chem. Int. Ed.*, 2018, **57**, 14260-14264.

133. J. Yeo, J. Woo, S. Choi, K. Kwon, J.-K. Lee and M. Kim, *Polym. Chem.*, 2022, **13**, 4535-4546.

134. N. K. Vishwakarma, Y.-H. Hwang, A. K. Mishra, J. K. Kim and D.-P. Kim, *Reac. Chem. Eng.*, 2019, **4**, 1854-1860.

135. J. Peng, C. Tian, L. Zhang, Z. Cheng and X. Zhu, *Polym. Chem.*, 2017, **8**, 1495-1506.

136. C. J. Richmond, H. N. Miras, A. R. de la Oliva, H. Zang, V. Sans, L. Paramonov, C. Makatsoris, R. Inglis, E. K. Brechin, D.-L. Long and L. Cronin, *Nat. Chem.*, 2012, **4**, 1037-1043.

137. C. K. Wong, R. Y. Lai and M. H. Stenzel, *Nat. Commun.*, 2023, **14**, 6237.

138. N. Corrigan, L. Zhernakov, M. H. Hashim, J. Xu and C. Boyer, *Reac. Chem. Eng.*, 2019, **4**, 1216-1228.

139. R. S. Atapalkar and A. A. Kulkarni, *Chem. Commun.*, 2023, **59**, 9231-9234.

140. F. Raymenants, T. M. Masson, J. Sanjosé-Orduna and T. Noël, *Angew. Chem. Int. Ed.*, 2023, **62**, e202308563.

141. C. Geacintov, J. Smid and M. Szwarc, *J. Am. Chem. Soc.*, 1962, **84**, 2508-2514.

142. D. N. Bhattacharyya, C. L. Lee, J. Smid and M. Szwarc, *J. Am. Chem. Soc.*, 1963, **85**, 533-539.

143. X. Hu, N. Zhu, Z. Fang and K. Guo, *Reac. Chem. Eng.*, 2017, **2**, 20-26.

144. T. Junkers, *Macromol. Chem. Phys.*, 2017, **218**, 1600421.

145. C. H. Hornung, C. Guerrero-Sanchez, M. Brasholz, S. Saubern, J. Chiefari, G. Moad, E. Rizzardo and S. H. Thang, *Organic Process Research & Development*, 2011, **15**, 593-601.

146. M. H. Reis, T. P. Varner and F. A. Leibfarth, *Macromolecules*, 2019, **52**, 3551-3557.

147. N. Corrigan, R. Manahan, Z. T. Lew, J. Yeow, J. Xu and C. Boyer, *Macromolecules*, 2018, **51**, 4553-4563.

148. F. Zhong, Y. Zhou and M. Chen, *Polym. Chem.*, 2019, **10**, 4879-4886.

149. J. Wang, X. Hu, N. Zhu and K. Guo, *Chem. Eng. J.*, 2021, **420**, 127663.

150. D. Cambié, C. Bottecchia, N. J. W. Straathof, V. Hessel and T. Noël, *Chem. Rev.*, 2016, **116**, 10276-10341.

151. N. Zaquen, H. Zu, A. M. N. B. P. H. A. Kadir, T. Junkers, P. B. Zetterlund and C. Boyer, *ACS Appl. Polym. Mater.*, 2019, **1**, 1251-1256.

152. A.-L. Buckinx, K. Verstraete, E. Baeten, R. F. Tabor, A. Sokolova, N. Zaquen and T. Junkers, *Angew. Chem. Int. Ed.*, 2019, **58**, 13799-13802.

153. C.-W. Wang, D. Sinton and M. G. Moffitt, *ACS Nano*, 2013, **7**, 1424-1436.

154. Y. Huang, A. Moini Jazani, E. P. Howell, J. K. Oh and M. G. Moffitt, *ACS Appl. Mater. Interfaces*, 2020, **12**, 177-190.

155. J. Liu, Y. Lan, Z. Yu, C. S. Y. Tan, R. M. Parker, C. Abell and O. A. Scherman, *Acc. Chem. Res.*, 2017, **50**, 208-217.

156. L. Hou, M. Dueñas-Díez, R. Srivastava and J. Pérez-Mercader, *Commun. Chem.*, 2019, **2**, 139.

157. S. Parkinson, S. T. Knox, R. A. Bourne and N. J. Warren, *Polym. Chem.*, 2020, **11**, 3465-3474.

158. N. Zaquen, J. Yeow, T. Junkers, C. Boyer and P. B. Zetterlund, *Macromolecules*, 2018, **51**, 5165-5172.

Chapter 2 - Enhancing the Scalability of Crystallization-Driven Self-Assembly Using Flow Reactors

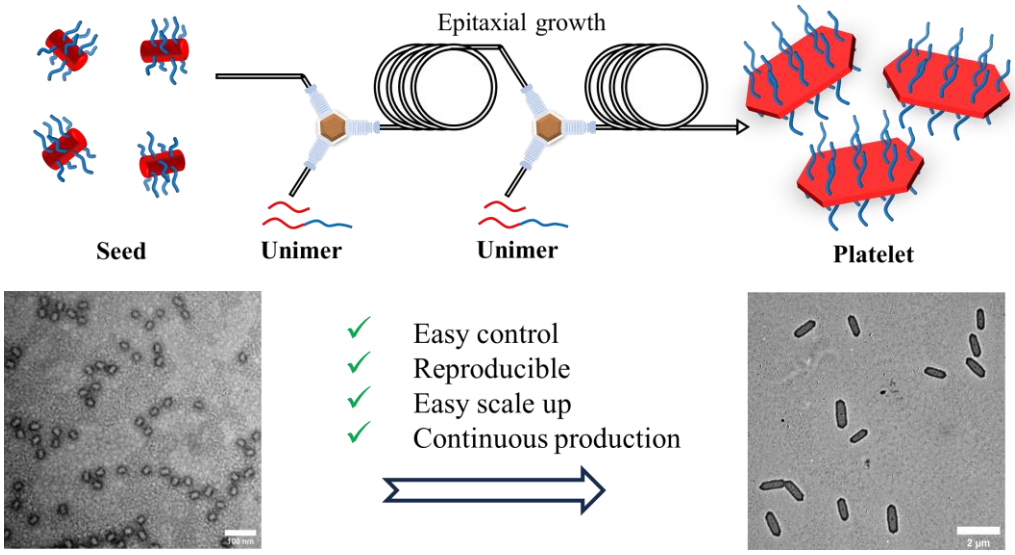

2.1 Publication Details and Overview

Title: Enhancing the Scalability of Crystallization-Driven Self-Assembly Using Flow Reactors

Authors: Laihui Xiao,[†] Sam J. Parkinson,[†] Tianlai Xia,[†] Phillippa Edge,[†] and Rachel K. O'Reilly[†,*]

Affiliation: [†]School of Chemistry, University of Birmingham, Edgbaston, Birmingham B15 2TT, United Kingdom

Journal: ACS Macro Letters

Year: 2023

Volume: 12

Page Number: 1636–1641.

DOI: 10.1021/acsmacrolett.3c00600

Submitted: 12 October 2023

Publishes: 16 November 2023

Permission: This article and its supporting information are available on the ACS Publications website at https://pubs.acs.org/doi/10.1021/acsmacrolett.3c00600. Further permissions related to the material excerpted should be directed to the ACS Publications Support.

Coauthor Contributions: Dr. Sam J. Parkinson advised on flow setups and proofread the manuscript. Mr. Tianlai Xia assisted with batch CDSA and confocal microscopy. Ms. Phillippa Edge helped with synthesis. Prof. Rachel K. O'Reilly supervised the project and reviewed the manuscript.

Overview:

This work investigates the living CDSA of PCL-based polymers to create anisotropic nanoparticles using continuous flow processing. Living CDSA provides an efficient method for producing well-defined nanostructures, such as platelets and cylinders, which have diverse applications. However, the scalability of this method has remained a challenge. To overcome this, we developed the first continuous-flow system for living CDSA of PCL-based polymers.

The process began by transferring the epitaxial growth of platelets from batch-based living CDSA to a flow reactor, where optimal conditions were identified. Temperature was found to play a critical role in maintaining platelet uniformity by enhancing the mixing of seeds and unimers while controlling crystallization rates. Building on this, we implemented a series flow system that enabled the production of platelets directly from seeds, with precise size control achieved by adjusting flow rates.

This novel approach significantly improves reproducibility by eliminating batch-to-batch variation, a common issue in traditional methods. Furthermore, it minimizes the high size dispersity typically seen in large-volume batch systems, while ensuring consistent particle quality and uniformity over time.

ACS Macro Letters

pubs.acs.org/macroletters
Letter

Enhancing the Scalability of Crystallization-Driven Self-Assembly Using Flow Reactors

Laihui Xiao, Sam J. Parkinson, Tianlai Xia, Phillippa Edge, and Rachel K. O'Reilly*

Cite This: ACS Macro Lett. 2023, 12, 1636−1641
Read Online

ABSTRACT: Anisotropic materials have garnered significant attention due to their potential applications in cargo delivery, surface modification, and composite reinforcement. Crystallization-driven self-assembly (CDSA) is a practical way to access anisotropic structures, such as 2D platelets. Living CDSA, where platelets are formed by using seed particles, allows the platelet size to be well controlled. Nonetheless, the current method of platelet preparation is restricted to low concentrations and small scales, resulting in inefficient production, which hampers its potential for commercial applications. To address this limitation, continuous flow reactors were employed to improve the production efficiency. Flow platforms ensure consistent product quality by maintaining the same parameters throughout the process, circumventing batch-to-batch variations and discrepancies observed during scale-up. In this study, we present the first demonstration of living CDSA performed within flow reactors. A continuous flow system was established, and the epitaxial growth of platelets was initially conducted to study the influence of flow parameters such as temperature, residence time, and flow rate on the morphology of platelets. Comparison of different epitaxial growth manners of seeds and platelets was made when using seeds to perform living CDSA. Size-controllable platelets from seeds can be obtained from a series flow system by easily tuning flow rates. Additionally, uniform platelets were continuously collected, exhibiting improved size and dispersity compared to those obtained in batch reactions.

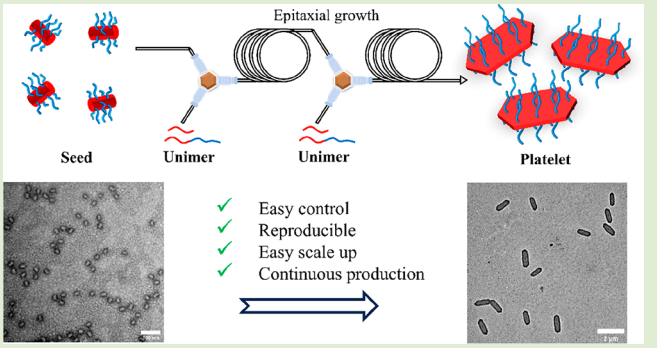

Two-Dimensional (2D) polymeric platelets are gaining great attention because of their diverse range of applications.[1−3] Specifically, 2D platelets with high aspect ratios have attracted significant interest due to their exceptional properties in cargo delivery,[4,5] surface modification[6] and composite reinforcement.[7] Compared to traditional self-assembly, by which pure platelets cannot be generally obtained, crystallization-driven self-assembly (CDSA) can easily access this morphology. Furthermore, using a seeded growth method, known as living CDSA, precise control over the size of the platelets can be achieved by adjusting the amount of unimer added to the seed solution. Several studies have reported successful preparation of platelets using semicrystalline block copolymers such as polyferrocenylsilane (PFS),[8−10] polycaprolactone (PCL),[5,11,12] and polylactide (PLLA).[6,7,13] While these advancements have made platelet synthesis more accessible, scaling up the production remains challenging, as increasing the scale means slower diffusion of unimer and due to the rapid rate of crystallization this leads to an increase in size dispersity. Thus, the rapid crystallization rate associated with living CDSA limits its application to small-scale and dilute solutions (<1 wt % solids).[14,15] Undoubtedly, this limitation hinders its potential for widespread commercial use.

Flow chemistry, where reactions are carried out in a continuous stream, is seeing significant uptake because of its universality for chemistry.[16,17] Flow reactors provide advantages in terms of efficiency, safety, and scalability.[18,19] Batch scale-up often suffers from poor reproducibility due to inadequate heat transfer and mixing profiles, leading to reaction inhomogeneity, lack of control, and potential hazards.[17,18] In contrast, flow reactors, with their high surface area to volume ratio offer improved heat transfer, maintaining an isothermal reaction environment even at high temperatures, thus promoting homogeneous and rapid reactions in a safe manner.[18,20−23]

A variety of polymer self-assembly techniques has been transferred to flow platforms. For instance, Junkers and co-workers conducted solvent-driven self-assembly of amphiphilic block copolymers in flow. They found that using turbulent

Received: October 12, 2023
Revised: November 9, 2023
Accepted: November 14, 2023

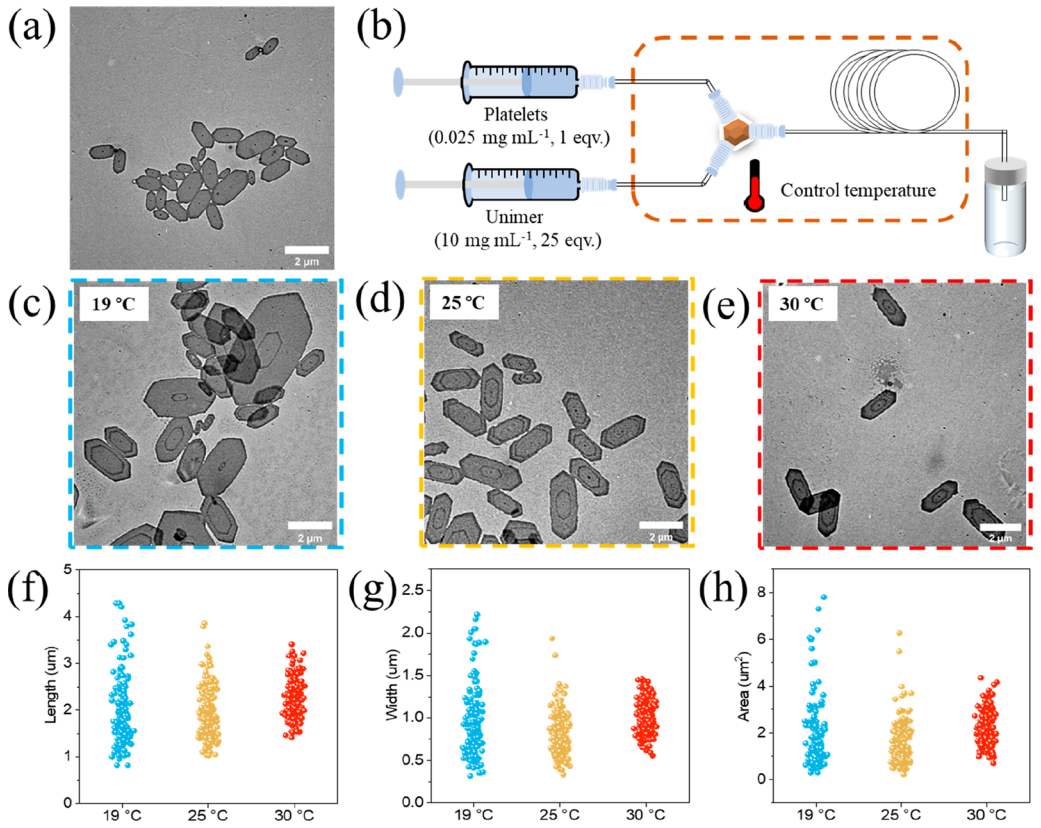

Figure 1. (a) TEM image of original platelets. (b) Illustration of flow setup for epitaxial growth of platelets. TEM images of platelets epitaxially grow at (c) 19 °C, (d) 25 °C, and (e) 30 °C. Platelet samples were not stained. Scale bars = 2 μm. Statistical value distribution of (f) length, (g) width, and (h) area.

mixing to homogenize the solution yielded more uniform and reproducible flow micelles compared to batch production. Furthermore, the aspect ratio of micelles was highly influenced by the flow rate.[24] Wang et al. illustrated that the shear forces in flow altered the morphologies of nanoparticles from those observed in batch, allowing more complex kinetically trapped structures to be formed.[25,26] Polymerization-induced self-assembly (PISA) emerged as an efficient way to prepare polymeric nanostructures by simultaneous polymerization and self-assembly, and it has also been conducted in flow for scale-up purposes.[27−30] Benefiting from short optical path lengths in flow reactors, photo-PISA in flow was applied to access nanoparticles of various morphologies in the collaboration of Boyer, Zetterlund, and Junkers.[29,31] By taking advantage of the high heat transfer rates in flow reactors, Warren and co-workers conducted all-aqueous PISA to realize rapid production of nanoparticles, where full conversion of monomer can be achieved in a short time and the morphologies can be tuned by the feed ratio.[28,30] These studies highlight the suitability of flow chemistry for providing an efficient pathway to scale up living CDSA.

Herein, we present the first-ever transfer of living CDSA of PCL-based polymers from batch to flow reactors. The primary focus was to scale up production and investigate the influence of multiple mixing parameters on the morphology of nanoparticles. Continuous flow systems were developed, and the effect of temperature, flow rate, and residence time on the morphology of extended platelets was explored during epitaxial growth in flow (Tables S1−S5). Subsequently, the epitaxial growth of seeds in flow was performed, revealing distinct growth behaviors between seeds and platelets. Following this, a combination of two flow systems was utilized to prepare platelets with controllable sizes by easily adjusting the flow rates. Most importantly, platelets could be continuously collected under the predetermined mixing parameters, and the uniformity of flow platelets was significantly improved compared with the scaled-up batch counterparts.

Initially batch controls were established; living CDSA was conducted in 1 mL batch scale according to our previous report (Figures S1−S8).[11,12] As expected, the incremental addition of the unimer corresponded to a proportional increase in the size of the platelets (Figure S8 and Table S7). After that, epitaxial growth of seeds was scaled up to 10 mL at a 1:10 seed/unimer ratio to investigate the reproducibility and scalability of batch living CDSA. The platelets prepared were similar in size to those made on a small scale (Figure S9 and Table S7, A_n = 0.65 μm^2 for 10 mL and A_n = 0.69 μm^2 for 1 mL). However, they exhibited a greater dispersity (A_w/A_n = 1.27 for 10 mL and A_w/A_n = 1.06 for 1 mL), which was attributed to the poor mixing conditions encountered at larger scales. At larger solution volumes, it takes longer to obtain a mixed homogeneous solution upon unimer addition. Due to the rapid rate of crystallization, these concentration gradients lead to platelets with a greater size dispersity. On the other hand, we attempted to scale up living CDSA by increasing the concentration of reactants to 10 times. However, the obtained platelets were of higher dispersity, and many extremely large platelets were observed (Figure S10). This was likely due to higher concentrations leading to a faster crystallization rate.[32−34]

https://doi.org/10.1021/acsmacrolett.3c00600
ACS Macro Lett. 2023, 12, 1636−1641

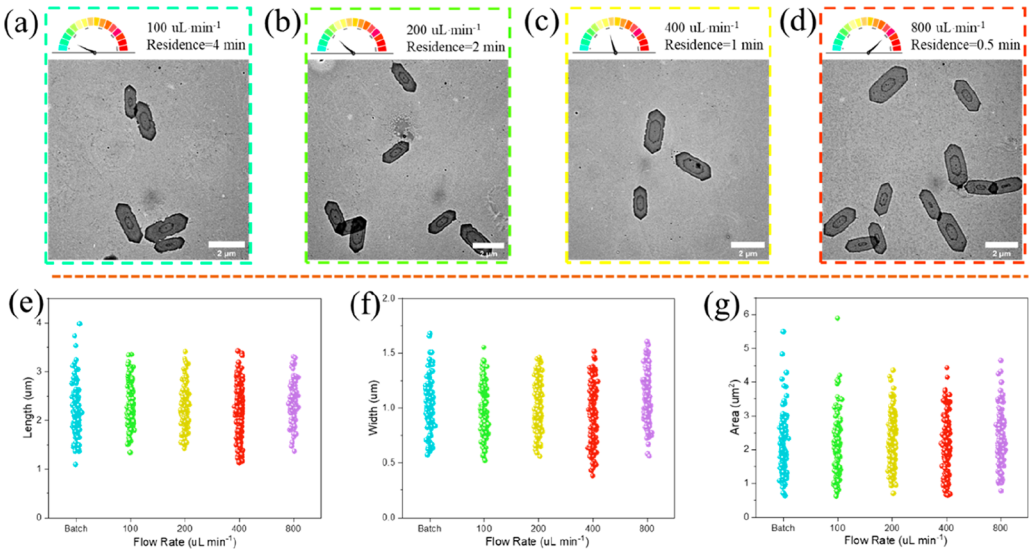

Figure 2. TEM images of platelets epitaxially grow at (a) 100 μL·min^{-1}, (b) 200 μL·min^{-1}, (c) 400 μL·min^{-1}, and (d) 800 μL·min^{-1}. Statistical value distributions of (e) length, (f) width, and (g) area.

Next, we transferred this living CDSA process to continuous flow platforms. The ultimate objective of this research was to develop a flow reactor system for the preparation of controllable platelets directly from seeds. However, it is important to acknowledge that living CDSA involves seeded growth followed by epitaxial growth; directly transferring both steps to the flow system without a comprehensive understanding of the underlying processes may result in uncontrollable outcomes. To simplify this process, the latter stage, the direct epitaxial growth of platelets, was initially conducted in our flow reactor to optimize conditions. These preprepared platelets are mentioned as original platelets to differentiate them from subsequent platelets after epitaxial growth in flow.

In the flow setup (Figure 1b), the original platelets (Figure 1a) and unimer solution were injected using syringe pumps, with the mass ratio of the original platelet/unimer controlled by their respective flow rates. To investigate the effect of temperature on the morphology of platelets, epitaxial growth of the original platelets was conducted at 19 °C (room temperature), 25 °C, and 30 °C. The total flow rate and the added amount of unimer was kept constant at 200 μL·min^{-1} and 25 equiv. Transmission electron microscopy (TEM) analysis of the platelets (Figure 1c–h, Table S8) clearly indicated that the size distribution of the platelets narrowed, indicating improved uniformity as temperature increased. There are two possible explanations for this observation: First, higher temperatures decreased the rate of crystallization,[35] allowing for slightly longer mixing times, thereby increasing the uniformity of the extended platelets. Second, the laminar flow model exhibits a parabolic distribution of flow velocity, leading to significant layering of the fluid. Consequently, reactants between different layers experience limited diffusion, resulting in regional variations in the reactant concentration. However, higher temperatures promote the Brownian motion of molecules and enhance interlayer diffusion, leading to improved mixing and the generation of more uniform platelets. This speculation was further confirmed when repeating the experiment in a flow reactor with wider tubing (I.D. = 0.75 mm) at the same flow rate. Due to reduced laminar mixing in a wider tube, platelets with high size dispersity were observed even at 30 °C (Figure S12a). Therefore, to achieve highly uniform platelets, the following living CDSA work was performed at 30 °C in a narrow tube reactor (I.D. = 0.3 mm).

Next the influence of the flow rate on the platelet size distribution was investigated. We expected that higher flow rates would lead to better mixing in the mixer as there is an increase in turbulence in the micromixer, and thus the dispersity would decrease.[36] However, over the range of flow rates tested (100–800 μL·min^{-1}), the shape and size of the extended platelets remained almost the same (Figure 2 and Table S9). This consistency suggests that adequate mixing was achieved across all of the flow rates. It can be substantiated by the rapid growth rate, with epitaxial growth completing within just 0.5 min at a flow rate of 800 μL·min^{-1}. Inadequate mixing during this rapid growth phase could lead to concentration gradients, ultimately manifested as increased dispersity. However, it is worth considering that higher flow rates require higher pressure to counteract the resistance in the flow system, especially at elevated flow rates, which can increase the burden on the equipment. Therefore, for the subsequent experiments, the flow rate was maintained at 200 μL·min^{-1} to strike a balance between efficient production and manageable pressure requirements.

After optimizing reactor conditions, the next step was to control the size of extended platelets. Different amounts of unimer ranging from 12.5 to 100 equiv of seeds were added by adjusting the flow rates of the original platelet and unimer solutions. Additionally, batch epitaxial growth experiments were conducted for comparison. As anticipated, the length, width, and area of the extended platelets in the flow reactor increased with increasing unimer equivalents (Figure 3, Figure S11, and Table S10). Notably, the area of the extended platelets exhibited a linear relationship with the unimer equivalents. These results were found to be comparable to those obtained from the batch reactor with a slightly narrower size dispersity seen for the flow system. This further validated the effectiveness of the continuous flow approach to control platelet size and dispersity compared to batch. To enhance clarity, all studied flow conditions and the size of corresponding platelets were summarized in Table S11.

https://doi.org/10.1021/acsmacrolett.3c00600
ACS Macro Lett. 2023, 12, 1636–1641

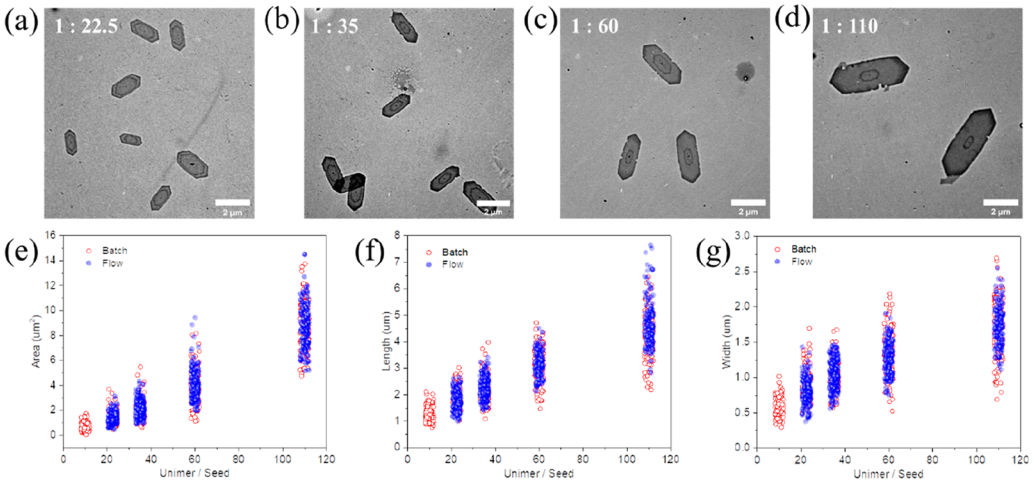

Figure 3. TEM images of flow extended platelets prepared at seed/unimer ratios of (a) 1:22.5, (b) 1:35, (c) 1:60, and (d) 1:110. Statistical comparison of platelets from flow and batch: (e) area, (f) length, and (g) width.

After optimizing the conditions, living CDSA was attempted using seed particles (Figure 4a). Initial attempts using seeds in the flow reactor differed significantly compared to the batch (Figure S12b). The presence of large, disperse platelets indicated the occurrence of self-nucleation of PCL homopolymer.[37,38] These findings suggest there are different growth behaviors between seeds and platelets. Previous studies from our group demonstrated that the 1D seeds grow primarily from their ends,[12] while 2D platelets can epitaxially grow in all directions, thus greater availability ensures unimer can be consumed quickly. Additionally, reduced corona density of the platelets, resulting from the addition of 50 wt % PCL homopolymer during the preparation of the original platelets, minimizes steric hindrance during crystallization, and thus epitaxial growth can be fast. Both reasons are conducive to reducing the occurrence of self-nucleation. If the unimer is not consumed quickly, then self-nucleation can occur, leading to rapid growth of undesired structures.

Given these potential causes of self-nucleation during the epitaxial growth of seeds, we proposed two possible solutions: (a) sonication of platelets to generate 2D seeds with a low corona density, which would consume unimer more efficiently, and (b) reducing the unimer/seed ratio to decrease the concentration of unimer, which was based on the observation that the rate of crystallization is highly influenced by the concentration.[32−34] Even though large self-nucleation platelets were avoided when using platelet fragments as seeds, poor platelet uniformity (Figure S12d) was observed due to these 2D seeds (Figure S12c) being more disperse than those from 1D cylinders. However, when conducting living CDSA using seed particles at a lower unimer/seed ratio (5:1), where the rate of crystallization should be slower, no self-nucleated platelets were observed, and uniform platelets were obtained (Figure 4c).

After optimizing living CDSA from both seed and platelet particles, we then developed a flow reactor cascade (Figure 4b) capable of making multilayered platelets. Besides the epitaxial growth of seeds at the fixed unimer/seed ratio of 5:1, an additional living CDSA section was incorporated to control the size of the platelets. This combined approach involved the epitaxial growth of both seeds and platelets. Final platelet size was controlled by varying the amount of unimer added to the second living CDSA section, resulting in total unimer/seed ratios of 10:1, 20:1, and 30:1 (Figure 4d−f and Table S12). The size of the flow platelets increased as more unimer was added, and the area values showed a good fit to the batch controls (Figure 4g). For a more distinct presentation of the layered structure, fluorescence labeling was employed to highlight the second layer of platelets. As anticipated, this revealed hollow platelets (Figure S13), confirming the sequential execution of two distinct living CDSA processes in achieving size-controllable platelets. The advantages of flow reactors in terms of reproducibility and scalability were evident when comparing platelets prepared by using different methods. To illustrate it more intuitively, quality measurements were employed instead of volume. Although platelets prepared through different methods were of similar size, they differed significantly in uniformity (Figure 4h and Figure S14). When batch living CDSA was scaled up from 1 to 10 mL, although 1.1 mg platelets were obtained, the uniformity decreased considerably, with the standard deviation of area doubling (0.167 μm^2 to 0.344 μm^2), as well as for length and width. Comparatively, the uniformity of the 2.2 mg flow platelets, while slightly lower than the 0.11 mg platelets from the 1 mL batch scale, still surpassed that of the 10 mL batch scale despite being double the quantity. Furthermore, in terms of preparing platelets in large quantities, the flow reactor allowed for the continuous production of platelets of the same size and uniformity. In theory, even with higher output, the size and uniformity of flow platelets should remain consistent. This capability circumvented the sacrifice of uniformity that occurs in the scale-up of the batch counterpart. Attempts were made to further augment platelet yield by increasing concentration 10-fold. While 11 mg of platelets were successfully produced, the results closely resembled those obtained from the batch concentration increase, resulting in platelets with greater size dispersity (Figure S15). Nevertheless, the flow reactor demonstrated advantages in terms of reproducibility, scalability, and maintaining uniformity compared to the batch reactor for the preparation of platelets.

In conclusion, living CDSA was conducted in the flow reactors for the first time to prepare platelets continuously. Initially, the epitaxial growth of platelets, which were prepared using batch living CDSA, was transferred to the flow reactor to optimize conditions. The results revealed that the uniformity of extended platelets was highly influenced by temperature.

https://doi.org/10.1021/acsmacrolett.3c00600
ACS Macro Lett. 2023, 12, 1636−1641

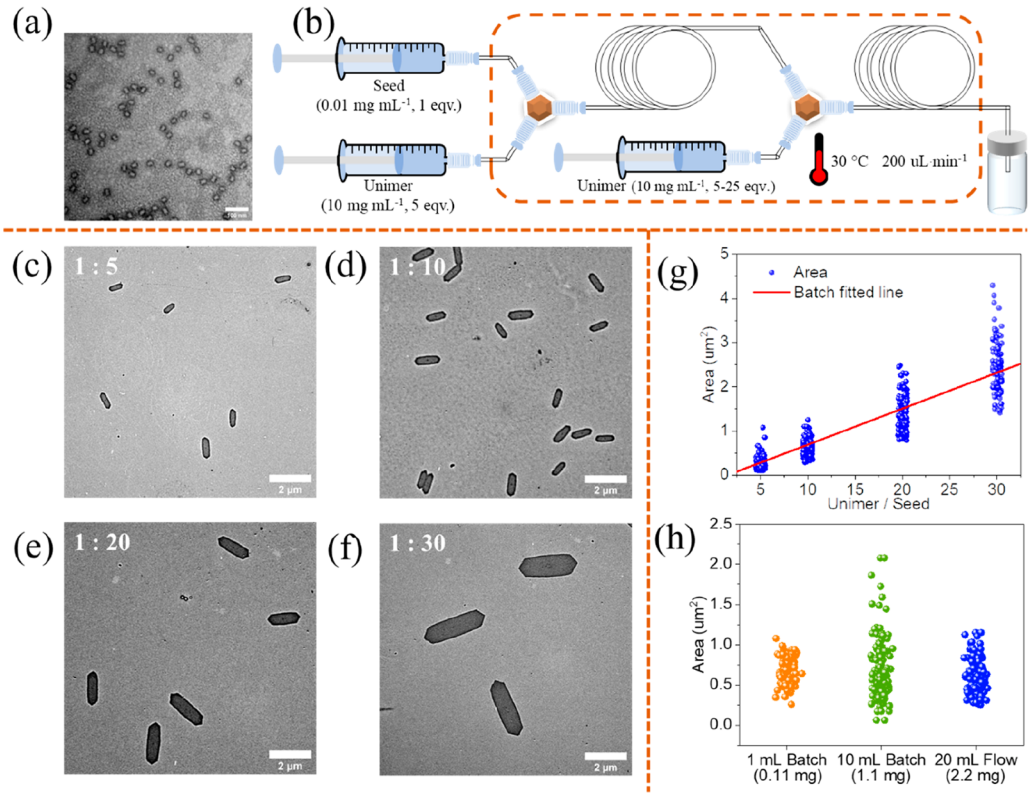

Figure 4. (a) TEM image of seeds. Sample was stained by uranyl acetate solution (1 wt %). (b) Illustration of flow setup for epitaxial growth of platelets. TEM images of flow platelets grown from seeds prepared at seed/unimer ratio of (c) 1:5, (d) 1:10, (e) 1:20, and (f) 1:30. (g) Area of flow platelets in comparison to the batch standards (red line). (h) Comparison of statistical size parameters of platelets prepared in different methods. Seed/unimer ratio is 1:10.

Higher temperatures facilitated the mixing of seeds and the unimer while reducing the crystallization rate. The epitaxial growth of platelets could be completed within 30 s, and their size could be easily controlled in flow reactors by adjusting the reagent flow rates. When using seeds to conduct living CDSA in flow, high size dispersity platelets, as a consequence of PCL homopolymer self-nucleation, were observed until the unimer/seed ratio was decreased to 5:1. Size-controllable flow platelets grown from seeds could be obtained by connecting another living CDSA stage in series. These flow platelets exhibited superior uniformity compared to upscaled batch platelets, although the dispersity was slightly higher than that of 1 mL batch reactions. Through flow living CDSA, we successfully achieved the continuous production of uniform platelets in large quantities. We firmly believe that this technology will play a crucial role in realizing the commercial application potential of nanomaterials.

■ ASSOCIATED CONTENT

Supporting Information

The Supporting Information is available free of charge at https://pubs.acs.org/doi/10.1021/acsmacrolett.3c00600.

Materials, characterization techniques, experimental procedures, and additional data (NMR, SEC, TEM images) (PDF)

■ AUTHOR INFORMATION

Corresponding Author

Rachel K. O'Reilly − *School of Chemistry, University of Birmingham, Edgbaston, Birmingham B15 2TT, U.K.;* orcid.org/0000-0002-1043-7172; Email: r.oreilly@bham.ac.uk

Authors

Laihui Xiao − *School of Chemistry, University of Birmingham, Edgbaston, Birmingham B15 2TT, U.K.;* orcid.org/0000-0002-3412-0954

Sam J. Parkinson − *School of Chemistry, University of Birmingham, Edgbaston, Birmingham B15 2TT, U.K.*

Tianlai Xia − *School of Chemistry, University of Birmingham, Edgbaston, Birmingham B15 2TT, U.K.;* orcid.org/0000-0002-4391-0296

Phillippa Edge − *School of Chemistry, University of Birmingham, Edgbaston, Birmingham B15 2TT, U.K.*

Complete contact information is available at: https://pubs.acs.org/10.1021/acsmacrolett.3c00600

Author Contributions

The manuscript was written through contributions of all authors.

Notes

The authors declare no competing financial interest.

■ ACKNOWLEDGMENTS

The authors would like to thank the University of Birmingham and China Scholarship Council for funding and support.

■ REFERENCES

(1) Liu, Y.; Genzer, J.; Dickey, M. D. 2D or not 2D": Shape-programming polymer sheets. *Prog. Polym. Sci.* **2016**, *52*, 79−106.

(2) Boott, C. E.; Nazemi, A.; Manners, I. Synthetic Covalent and Non-Covalent 2D Materials. *Angew. Chem., Int. Ed.* **2015**, *54* (47), 13876−13894.
(3) Yang, C.; Li, Z.-X.; Xu, J.-T. Single crystals and two-dimensional crystalline assemblies of block copolymers. *J. Polym. Sci.* **2022**, *60* (15), 2153−2174.
(4) Ganda, S.; Wong, C. K.; Stenzel, M. H. Corona-Loading Strategies for Crystalline Particles Made by Living Crystallization-Driven Self-Assembly. *Macromolecules* **2021**, *54* (14), 6662−6669.
(5) Zhang, X.; Chen, G.; Zheng, B.; Wan, Z.; Liu, L.; Zhu, L.; Xie, Y.; Tong, Z. Uniform Two-Dimensional Crystalline Platelets with Tailored Compositions for pH Stimulus-Responsive Drug Release. *Biomacromolecules* **2023**, *24* (2), 1032−1041.
(6) Inam, M.; Jones, J. R.; Pérez-Madrigal, M. M.; Arno, M. C.; Dove, A. P.; O'Reilly, R. K. Controlling the Size of Two-Dimensional Polymer Platelets for Water-in-Water Emulsifiers. *ACS Central Sci.* **2018**, *4* (1), 63−70.
(7) Arno, M. C.; Inam, M.; Weems, A. C.; Li, Z.; Binch, A. L. A.; Platt, C. I.; Richardson, S. M.; Hoyland, J. A.; Dove, A. P.; O'Reilly, R. K. Exploiting the role of nanoparticle shape in enhancing hydrogel adhesive and mechanical properties. *Nat. Commun.* **2020**, *11* (1), 1420.
(8) Cao, L.; Manners, I.; Winnik, M. A. Influence of the Interplay of Crystallization and Chain Stretching on Micellar Morphologies: Solution Self-Assembly of Coil−Crystalline Poly(isoprene-block-ferrocenylsilane). *Macromolecules* **2002**, *35* (22), 8258−8260.
(9) Tian, J.; Xie, S.-H.; Borucu, U.; Lei, S.; Zhang, Y.; Manners, I. High-resolution cryo-electron microscopy structure of block copolymer nanofibres with a crystalline core. *Nat. Mater.* **2023**, *22* (6), 786−792.
(10) Wang, X.; Guerin, G.; Wang, H.; Wang, Y.; Manners, I.; Winnik, M. A. Cylindrical Block Copolymer Micelles and Co-Micelles of Controlled Length and Architecture. *Science* **2007**, *317* (5838), 644−647.
(11) Tong, Z.; Xie, Y.; Arno, M. C.; Zhang, Y.; Manners, I.; O'Reilly, R. K.; Dove, A. P. Uniform segmented platelet micelles with compositionally distinct and selectively degradable cores. *Nat. Chem.* **2023**, *15* (6), 824−831.
(12) Arno, M. C.; Inam, M.; Coe, Z.; Cambridge, G.; Macdougall, L. J.; Keogh, R.; Dove, A. P.; O'Reilly, R. K. Precision Epitaxy for Aqueous 1D and 2D Poly(epsilon-caprolactone) Assemblies. *J. Am. Chem. Soc.* **2017**, *139* (46), 16980−16985.
(13) Yu, W.; Inam, M.; Jones, J. R.; Dove, A. P.; O'Reilly, R. K. Understanding the CDSA of poly(lactide) containing triblock copolymers. *Polym. Chem.* **2017**, *8* (36), 5504−5512.
(14) Oliver, A. M.; Gwyther, J.; Boott, C. E.; Davis, S.; Pearce, S.; Manners, I. Scalable Fiber-like Micelles and Block Co-micelles by Polymerization-Induced Crystallization-Driven Self-Assembly. *J. Am. Chem. Soc.* **2018**, *140* (51), 18104−18114.
(15) Boott, C. E.; Gwyther, J.; Harniman, R. L.; Hayward, D. W.; Manners, I. Scalable and uniform 1D nanoparticles by synchronous polymerization, crystallization and self-assembly. *Nat. Chem.* **2017**, *9* (8), 785−792.
(16) Plutschack, M. B.; Pieber, B.; Gilmore, K.; Seeberger, P. H. The Hitchhiker's Guide to Flow Chemistry. *Chem. Rev.* **2017**, *117* (18), 11796−11893.
(17) Reis, M. H.; Leibfarth, F. A.; Pitet, L. M. Polymerizations in Continuous Flow: Recent Advances in the Synthesis of Diverse Polymeric Materials. *ACS Macro Lett.* **2020**, *9* (1), 123−133.
(18) Zaquen, N.; Rubens, M.; Corrigan, N.; Xu, J.; Zetterlund, P. B.; Boyer, C.; Junkers, T. Polymer Synthesis in Continuous Flow Reactors. *Prog. Polym. Sci.* **2020**, *107*, No. 101256.
(19) Knox, S. T.; Warren, N. J. Enabling technologies in polymer synthesis: accessing a new design space for advanced polymer materials. *Reac. Chem. Eng.* **2020**, *5* (3), 405−423.
(20) Diehl, C.; Laurino, P.; Azzouz, N.; Seeberger, P. H. Accelerated Continuous Flow RAFT Polymerization. *Macromolecules* **2010**, *43* (24), 10311−10314.
(21) Lauterbach, F.; Rubens, M.; Abetz, V.; Junkers, T. Ultrafast PhotoRAFT Block Copolymerization of Isoprene and Styrene Facilitated through Continuous-Flow Operation. *Angew. Chem., Int. Ed.* **2018**, *57* (43), 14260−14264.
(22) Yeo, J.; Woo, J.; Choi, S.; Kwon, K.; Lee, J.-K.; Kim, M. Comprehensive studies of continuous flow reversible addition−fragmentation chain transfer copolymerization and its application for photoimaging materials. *Polym. Chem.* **2022**, *13* (31), 4535−4546.
(23) Vishwakarma, N. K.; Hwang, Y.-H.; Mishra, A. K.; Kim, J. K.; Kim, D.-P. A platform for accelerated continuous-flow radical polymerization of acrylates and styrene with copper-wire threads. *Reac. Chem. Eng.* **2019**, *4* (10), 1854−1860.
(24) Buckinx, A.-L.; Verstraete, K.; Baeten, E.; Tabor, R. F.; Sokolova, A.; Zaquen, N.; Junkers, T. Kinetic Control of Aggregation Shape in Micellar Self-Assembly. *Angew. Chem., Int. Ed.* **2019**, *58* (39), 13799−13802.
(25) Wang, C.-W.; Sinton, D.; Moffitt, M. G. Morphological Control via Chemical and Shear Forces in Block Copolymer Self-Assembly in the Lab-on-Chip. *ACS Nano* **2013**, *7* (2), 1424−1436.
(26) Wang, C.-W.; Sinton, D.; Moffitt, M. G. Flow-Directed Block Copolymer Micelle Morphologies via Microfluidic Self-Assembly. *J. Am. Chem. Soc.* **2011**, *133* (46), 18853−18864.
(27) Peng, J.; Tian, C.; Zhang, L.; Cheng, Z.; Zhu, X. The in situ formation of nanoparticles via RAFT polymerization-induced self-assembly in a continuous tubular reactor. *Polym. Chem.* **2017**, *8* (9), 1495−1506.
(28) Parkinson, S.; Hondow, N. S.; Conteh, J. S.; Bourne, R. A.; Warren, N. J. All-aqueous continuous-flow RAFT dispersion polymerisation for efficient preparation of diblock copolymer spheres, worms and vesicles. *Reac. Chem. Eng.* **2019**, *4* (5), 852−861.
(29) Zaquen, N.; Yeow, J.; Junkers, T.; Boyer, C.; Zetterlund, P. B. Visible Light-Mediated Polymerization-Induced Self-Assembly Using Continuous Flow Reactors. *Macromolecules* **2018**, *51* (14), 5165−5172.
(30) Parkinson, S.; Knox, S. T.; Bourne, R. A.; Warren, N. J. Rapid production of block copolymer nano-objects via continuous-flow ultrafast RAFT dispersion polymerisation. *Polym. Chem.* **2020**, *11* (20), 3465−3474.
(31) Zaquen, N.; Zu, H.; Kadir, A. M. N. B. P. H. A.; Junkers, T.; Zetterlund, P. B.; Boyer, C. Scalable Aqueous Reversible Addition−Fragmentation Chain Transfer Photopolymerization-Induced Self-Assembly of Acrylamides for Direct Synthesis of Polymer Nanoparticles for Potential Drug Delivery Applications. *ACS Appl. Polym. Mater.* **2019**, *1* (6), 1251−1256.
(32) Deng, R.; Mao, X.; Pearce, S.; Tian, J.; Zhang, Y.; Manners, I. Role of Competitive Crystallization Kinetics in the Formation of 2D Platelets with Distinct Coronal Surface Patterns via Seeded Growth. *J. Am. Chem. Soc.* **2022**, *144* (41), 19051−19059.
(33) Keller, A.; Pedemonte, E. A study of growth rates of polyethylene single crystals. *J. Cryst. Growth* **1973**, *18* (2), 111−123.
(34) Zhou, Y.; Hu, W. Kinetic Analysis of Quasi-One-Dimensional Growth of Polymer Lamellar Crystals in Dilute Solutions. *J. Phys. Chem. B* **2013**, *117* (10), 3047−3053.
(35) Zhuravlev, E.; Schmelzer, J. W. P.; Wunderlich, B.; Schick, C. Kinetics of nucleation and crystallization in poly(ε-caprolactone) (PCL). *Polymer* **2011**, *52* (9), 1983−1997.
(36) Broeren, S.; Pereira, I. F.; Wang, T.; den Toonder, J.; Wang, Y. On-demand microfluidic mixing by actuating integrated magnetic microwalls. *Lab Chip* **2023**, *23* (6), 1524−1530.
(37) Qiu, H.; Gao, Y.; Boott, C. E.; Gould, O. E. C.; Harniman, R. L.; Miles, M. J.; Webb, S. E. D.; Winnik, M. A.; Manners, I. Uniform patchy and hollow rectangular platelet micelles from crystallizable polymer blends. *Science* **2016**, *352* (6286), 697−701.
(38) He, X.; Hsiao, M.-S.; Boott, C. E.; Harniman, R. L.; Nazemi, A.; Li, X.; Winnik, M. A.; Manners, I. Two-dimensional assemblies from crystallizable homopolymers with charged termini. *Nat. Mater.* **2017**, *16* (4), 481−488.

https://doi.org/10.1021/acsmacrolett.3c00600
ACS Macro Lett. 2023, 12, 1636−1641

2.2 Supporting Information

Supporting Information

Enhancing the scalability of crystallization-driven self-assembly using flow reactors

Laihui Xiao, Sam J. Parkinson, Tianlai Xia, Phillippa Edge, Rachel K. O'Reilly*

[a]School of Chemistry, University of Birmingham, Edgbaston, Birmingham B15 2TT, UK

*Corresponding Author: r.oreilly@bham.ac.uk (ROR)

Summary of Content:

Number of pages: 24

Number of tables: 12

Number of figures: 15

Number of schemes: 2

Materials

Sodium ethanethiolate (80%, Sigma Aldrich), carbon disulfide (≥99.9%, Sigma Aldrich), solid iodine (≥99.99%, Sigma Aldrich), 4,4'-azobis(4-cyanovaleric acid) (ACVA, ≥98%, Sigma Aldrich), borane tetrahydrofuran complex solution (1.0 M in THF, Sigma Aldrich), ethanol (anhydrous, ≥99.5%, Fisher Scientific), diethyl ether (anhydrous, ≥99.0%, Fisher Scientific), and chloroform ($CHCl_3$, anhydrous, ≥99%, Sigma Aldrich) were used as received. Dry tetrahydrofuran (THF, ≥99.9%, inhibitor-free, Sigma Aldrich) was purified through a solvent tower. ε-caprolactone (99%, ACROS Organics) was stored in the glovebox filled with N_2 after being dried with CaH_2 and then distilled. Diphenylphosphate (DPP, 99%, Sigma Aldrich) was dried using P_2O_5 before being kept in the glove box. 2,2'-azobis(2-methylpropionitrile) (AIBN, 98%, Sigma Aldrich) was recrystallized in methanol and stored at 4 °C in the dark before use. 1,4-dioxane (anhydrous, 99.8%, Fisher Scientific) and N, N-dimethyl acrylamide (DMA, 99%, Sigma Aldrich contains 500 ppm monomethyl ether hydroquinone as inhibitor) was purified with basic alumina every time before use.

Instrumentation

NMR spectra were recorded with a Bruker DPX-400 (400 MHz) spectrometer, and deuterated chloroform ($CDCl_3$) was used as the solvent. The obtained results were analysed and exported with MestReNova x64 software. SEC was conducted on Agilent 390-MDS equipment coupled with PLgel Mixed-D type columns, and the signals were detected by refractive index (RI) and ultraviolet (UV) detectors. Chloroform with 0.5% NEt_3 was used as eluent and the flow rate is 1 $mL \cdot min^{-1}$. Number-average (M_n) and weight-average (M_w) molecular weights and dispersity ($Đ_M$) were calibrated against polystyrene (PS) standards using Agilent SEC software. DSC was conducted using a Mettler Toledo HP DSC827 instrument. Samples of 5-10 mg in weight were placed in aluminium pans and heated and cooled between the temperature of -100 °C and 100 °C at 10 $°C \cdot min^{-1}$ under the N_2 atmosphere. Three cycles were carried out for each sample, and the data from the second cycle was analysed and collected. TEM images were captured on a Jeol 1400 Bio TEM microscope with an acceleration voltage of 80 kV. Samples were prepared by

drop cast 8 μL of solution on formvar-coated copper grids and then blotting away with filter paper. Another 8 μL of aqueous uranyl acetate solution (1 wt%) was dropped on the grid to stain the sample, and the excess was removed by filter paper. Samples were dried overnight in a desiccator box before testing. The obtained images were analysed by ImageJ, and at least 100 particles were analysed to calculate the average size. The number average length (L_n) and weight average length (L_w) were calculated according to equations (1) and (2), and the distribution was the value of L_w/L_n.

$$L_n = \frac{\sum_{i=1}^{n} N_i L_i}{\sum_{i=1}^{n} N_i} \quad (1) \qquad L_n = \frac{\sum_{i=1}^{n} N_i {L_i}^2}{\sum_{i=1}^{n} N_i L_i} \quad (2)$$

Similarly, the number average width (W_n), weight average width (W_w), number average area (A_n), and weight average area (A_w) were calculated according to equations (3) to (6), and their distributions were defined as W_w/W_n and A_w/A_n.

$$W_n = \frac{\sum_{i=1}^{n} N_i W_i}{\sum_{i=1}^{n} N_i} \quad (3) \qquad W_w = \frac{\sum_{i=1}^{n} N_i {W_i}^2}{\sum_{i=1}^{n} N_i W_i} \quad (4)$$

$$A_n = \frac{\sum_{i=1}^{n} N_i A_i}{\sum_{i=1}^{n} N_i} \quad (5) \qquad A_w = \frac{\sum_{i=1}^{n} N_i {A_i}^2}{\sum_{i=1}^{n} N_i A_i} \quad (6)$$

Flow reactors were set up by connecting several syringes with PTFE tubing (Figure 1a). Seeds and unimer (PCL / PCL-PDMA=1:1, 10 mg·mL^{-1} in $CHCl_3$) were stored in different syringes, and the weight ratios of seeds and unimer were tuned by their flow rates. To make sure seeds and unimer were well mixed, a Y-mixer was equipped at their intersection, where living CDSA started. Before entering the Y-mixer, seed solution was pre-heated to the setting temperature in a tubing coil (inner diameter: 0.8 mm, residence: 2 minutes), and then a cycle of living CDSA was completed once the mixture flowed through another tubing coil (inner diameter: 0.3 mm, residence: 2 minutes) after the Y-mixer. Both the mixer and the tubing coil were buried in the pre-heated sand bath. To conduct more living CDSA sessions, more mixers and tubing coils could be connected in series, as illustrated in Figure 4b.

Synthesis

Synthesis of dual-headed chain transfer agent (CTA)

Synthesis of bis-(ethylsulfanylthiocarbonyl) disulfide

Carbon disulfide (7.74 mL) was added to a solution of sodium ethanethiolate (10 g) in diethyl ether (500 mL), which is immersed in an ice bath with a constant stir. After stirring for another 2 hours, excess iodine was added to the flask until the colour of the reaction system became dark brown. The solution was kept stirred overnight, and then it was washed with a solution of sodium thiosulfate (1M, 3 × 100 mL) followed by brine (3 × 100 mL) after it was transferred into a separation funnel. The solvent was removed by rotary evaporation after the organic layer was dried with anhydrous magnesium sulfate. 15.27 g (yield: 93.7%) of an orange liquid was obtained.

^{1}H NMR (400 MHz, Chloroform-d, δ (ppm)): 3.32 (q, J = 7.5 Hz, 2H, SC***H***$_2$CH$_3$), 1.36 (t, J = 7.5 Hz, 3H, SCH$_2$C***H***$_3$).

Synthesis of 4-cyano-4-[(ethylsulfanylthiocarbonyl)sulfanyl] pentanoic acid (CEPA)

Bis-(ethylsulfanylthiocarbonyl) disulfide (9.0265 g, 32.88 mmol), ACVA (13.8245 g, 49.32 mmol), and ethyl acetate (500 mL) were charged into a 1-L round bottle flask equipped with a condenser, and the reaction was heated to reflux overnight in an N_2 atmosphere. After being concentrated by rotary evaporation, the crude product was purified through silica gel column chromatography (EtOAc / DCM = 1:3). Finally, 21.58 g (yield: 73.7%) of an orange solid was obtained.

^{1}H NMR (400 MHz, Chloroform-d, δ (ppm)): 3.35 (q, J = 7.4 Hz, 2H, SC***H***$_2$CH$_3$), 2.73 – 2.62 (m, 2H, C***H***$_2$COOH), 2.62 – 2.48 (m, 1H, C***H***$_2$CH$_2$COOH), 2.40 (m, 1H, C***H***$_2$CH$_2$COOH), 1.89 (s, 3H, C***H***$_3$C), 1.36 (t, J = 7.4 Hz, 3H, SCH$_2$C***H***$_3$).

Synthesis of 2-cyano-5-hydroxypentan-2-yl-ethyl carbonotrithioate (CHPET)

CEPA (3 g, 11.4 mmol) was charged into a two-neck flask coupled with a dropping flask, and then the reaction apparatus was kept in the nitrogen flow and cooled to -78 °C with a dry ice –

acetone bath. Dry tetrahydrofuran was used as the solvent and added to the flask with a syringe, and borane tetrahydrofuran (12 mL, 0.12 mmol) was dropped into the solution subsequently. After an hour of reaction at -78 °C, the solvent was left at room temperature and kept stirred overnight. 2-propanol was added to react with the extra borane. After the reaction, the solvent was removed by rotary evaporation, and diethyl ether (200 mL) was added to dissolve the crude product. The solution was washed with saturated $NaHCO_3$ (3 × 200 mL) and then with brine (1 × 200 mL). The organic layer was concentrated by rotary evaporation after it was dried by anhydrous $MgSO_4$. Silica gel column chromatography (n-hexane / EtOAc = 1:1) was used to purify the product further, and 2.13 g (yield: 74.9%) of orange oil was finally obtained. The synthesis route to access CTA was illustrated in Scheme S1.

^{1}H NMR (400 MHz, Chloroform-d, δ (ppm)): 3.72 (t, J = 6.1 Hz, 1H, C***H***$_2$OH), 3.35 (q, J = 7.4 Hz, 2H, SC***H***$_2$CH$_3$), 2.34 – 2.22 (m, 1H, C(CN)(CH$_3$)C***H***$_2$CH$_2$), 2.16 – 2.06 (m, 1H, C(CN)(CH$_3$)C***H***$_2$CH$_2$), 1.90 (s, 3H, C(CN)(C***H***$_3$)CH$_2$CH$_2$), 1.89 – 1.79 (m, 2H, C(CN)(CH$_3$)CH$_2$C***H***$_2$), 1.36 (t, J = 7.4 Hz, 3H, SCH$_2$C***H***$_3$).

^{13}C NMR (101 MHz, Chloroform-d, δ (ppm)): 217.39 (***C***=S), 119.57 (C(***C***N)(CH$_3$)CH$_2$CH$_2$), 61.80 (***C***H$_2$OH), 46.99 (***C***(CN)(CH$_3$)CH$_2$CH$_2$), 35.76 (C(CN)(CH$_3$)***C***H$_2$CH$_2$), 31.31 (S***C***H$_2$CH$_3$), 27.91 (C(CN)(CH$_3$)CH2***C***H$_2$), 24.93 (C(CN)(***C***H$_3$)CH$_2$CH$_2$), 12.80 (SCH$_2$***C***H$_3$).

Synthesis of polymers

Polycaprolactone (PCL_{50}) synthesized by ring-opening polymerization

Ring-opening polymerization was conducted in a glove box filled with N_2. Briefly, caprolactone (2.246g, 19.68 mmol), diphenylphosphate (DPP, 70.33 mg, 0.28 mmol), and CHPET (70 mg, 0.28 mmol) were weighed accurately in vials and then transferred to a 50-mL round bottle flask. Toluene (19.726 mL) was used as the solvent for the reaction. Polymerization was conducted at room temperature, and ^{1}H NMR was used to monitor the process. After about 6.5 h, the reaction was quenched by the Amberlyst agent, and the solution was removed from the glove box. The crude product was precipitated into cold diethyl ether 3 times and collected after

centrifugation. 1.34 g (monomer conversion: 71%) of light-yellow solid was obtained before it was dry in a vacuum oven.

^{1}H NMR (400 MHz, Chloroform-d, δ (ppm)): 4.06 (t, J = 6.7 Hz, 2H, COOC***H***$_2$), 2.30 (t, J = 7.5 Hz, 2H, C***H***$_2$COO), 1.65 (dtt, J = 13.4, 6.7, 3.7 Hz, 4H, COOCH$_2$C***H***$_2$CH$_2$C***H***$_2$CH$_2$OH), 1.44 – 1.32 (m, 2H, (CH2)$_2$C***H***$_2$(CH$_2$)$_2$).

Polycaprolactone-b-polydimethylacetamide (PCL_{50}-$PDMA_{196}$) synthesized by RAFT polymerization

Macro-CTA (PCL_{50}, 100 mg, 0.0168 mmol), DMA (399.7 mg, 4.032 mmol), and AIBN (0.276 mg, 0.00168 mmol, 10 mg mL^{-1} in dioxane) were dissolved in dioxane (1 mL) and then transferred into an ampoule. The solution was freeze-pump-thawed three times before the ampoule was immersed in an oil bath set at 70 °C. After 2 hours, polymerization was quenched by immersing the ampoule in the liquid N_2. The crude product was precipitated into the cold diethyl ether once it reached room temperature and then collected by centrifugation, and this process was repeated three times. After drying in a vacuum oven for 3 days, 458.5 mg (monomer conversion: 80%) of a solid product was obtained.

^{1}H NMR (400 MHz, Chloroform-d, δ (ppm)): 4.06 (t, J = 6.7 Hz, 2H, COOC***H***$_2$), 3.21 – 2.75 (m, 6H, CON(C***H***$_3$)$_2$), 2.30 (t, J = 7.5 Hz, 1H, C***H***$_2$COO), 1.71 – 1.58 (m, 4H, COOCH$_2$C***H***$_2$CH$_2$C***H***$_2$CH$_2$OH), 1.44 – 1.32 (m, 2H, (CH2)$_2$C***H***$_2$(CH$_2$)$_2$).

PCL modified by bodipy 630/650

Bodipy 630/650 was grafted to PCL50 by esterification reaction, which was catalyzed by N,N′-dicyclohexylcarbodiimide (DCC) and 4-(dimethylamino)pyridine (DMAP). In brief, PCL_{50} (100 mg, 0.0168 mmol), bodipy 630/650 (3.78 mg, 0.0084 mmol), DCC (34.64 mg, 0.168 mmol), DMAP (2.05 mg, 0.0168 mmol), and DCM (2 mL) were added into a vial and stirred at room temperature for 2 days. After the reaction, the undissolved substance was removed by filtration, and the filtrate was precipitated into the cold diethyl ether and then the precipitated

PCL polymer was collected after centrifugation. Two other precipitation and centrifugation processes were conducted, and the final product was dried in a vacuum oven overnight.

General procedure for CDSA

Cylinders prepared by direct crystallisation-driven self-assembly (CDSA)

PCL_{50}-b-$PDMA_{196}$ (10 mg) and ethanol (2 mL) were measured accurately and added into a 7-mL vial. The mixture was heated at 70 °C for 3 hours without stirring and then left to cool down naturally. After ageing for 7 days at room temperature, a cloudy cylinder solution was obtained.

Seeds prepared by sonicating cylinders

The original solution of cylinders was diluted to 0.5 $mg \cdot mL^{-1}$, and then 3 mL of the diluted solution was transferred into a quartz tube and immersed in the dry ice-acetone bath during the whole sonication process. A total of 20 min sonication was applied by a sonic probe with the model of 60 cycles of a 20-second sonication followed by a 100-second pause. The obtained solution of seeds was transferred to a vial for storage and imaged through TEM to determine the average size.

General procedure of living CDSA to prepare platelets in batch

The solution of seeds was diluted to 0.01, and then in the 1-mL scale, the unimer solution (10 $mg \cdot mL^{-1}$ of the 1:1 mixture in weight of homo and diblock polymers in $CHCl_3$) of a pre-calculated amount was added. After a 5-second handshake followed by 2-minute ageing at room temperature, samples were prepared for TEM or AFM, and the average size of platelets was measured according to the obtained images. For the batch scale-up, a 10-mL scale living CDSA was conducted using the same procedure.

General procedure of living CDSA to prepare platelets in the flow reactor

Seeds (or original platelets) and unimer were loaded into syringes, and then the mixer and coil were buried in the sand bath at a pre-set temperature and equilibrated for 30 minutes before the

flow started. The flow rates of seeds and unimer were set up according to Table 1-5. Every time flow rates, seeds, or unimer were changed, samples were collected after passing 3 reactor volumes to make sure they reached the steady state. TEM samples were prepared instantly once platelets were collected. The detailed flow setups for different experiments were listed in Table S1-5.

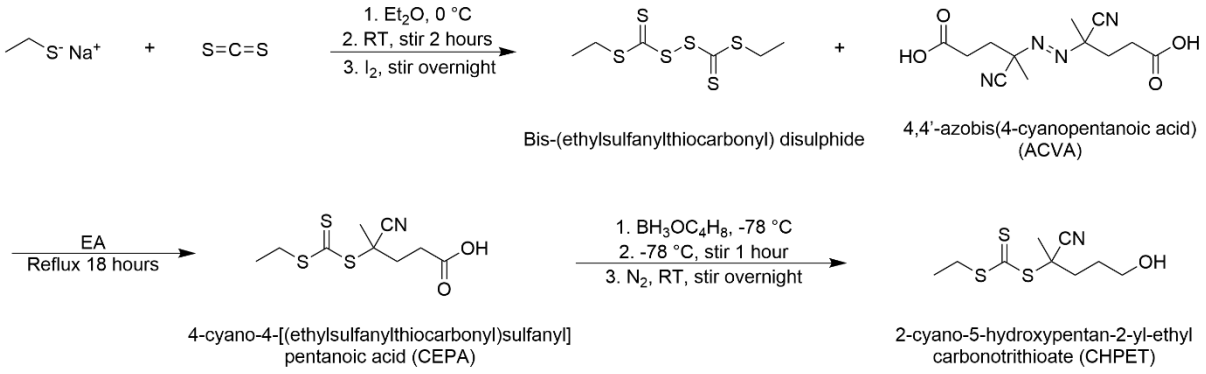

Scheme S1. The synthetic route of CHPET.

Table S1. Setup of flow reactor for epitaxial growth of platelets at various temperatures.

Sample	Temperature (°C)	Unimer (eqv. of seed)	R_p [a] (μL·min^{-1})	R_u [a] (μL·min^{-1})	Time [b] (min)
1	19	25	198	2	2
2	25	25	198	2	2
3	30	25	198	2	2

[a] R_p and R_u are abbreviations of the flow rate of original platelets and unimer, and [b] T is the time solution flows through the coil. The concentrations of original and unimer are fixed at 0.04 and 10 mg·mL^{-1} respectively in this work.

Table S2. Setup of flow reactor for epitaxial growth of platelets at various flow rates.

Sample	R_p (μL·min^{-1})	R_u (μL·min^{-1})	Unimer (eqv. of seed)	Temperature (°C)	Time (min)	*Re**
1	99	1	25	30	4	5.8
2	198	2	25	30	2	11.5
3	396	4	25	30	1	23.0
4	792	8	25	30	0.5	46.0

*Re is the abbreviation of Reynolds number, which is calculated by $Re = \rho v d/\mu$. ρ, v, d, and μ are density, flow rate, diameter of tubing, and viscosity respectively.

Table S3. Setup of flow reactor for epitaxial growth of platelets with various amounts of unimer.

Sample	Unimer (eqv. of seed)	R_p (μL·min^{-1})	R_u (μL·min^{-1})	Temperature (°C)	T (min)
1	12.5	198	2	30	2
2	25	198	2	30	2
3	50	198	2	30	2
4	100	198	2	30	2

Table S4. Setup of flow reactor for epitaxial growth of seeds with various amounts of unimer.

Sample	Unimer (eqv. of seed)	R_s [a] (μL·min^{-1})	R_u (μL·min^{-1})	Temperature (°C)	Time (min)
1	10	198	2	30	2
2	5	199	1	30	2
3*	10	198	2	30	2

[a] R_s is the abbreviation of the flow rate of seeds, and " * " indicates the seeds were prepared by sonicating platelets.

Table S5. Setup of flow reactor to prepare size-controllable platelets from seeds

Sample	Total unimer (eqv. of seed)	1st section			2nd section		Time (min)
		Unimer (eqv. of seed)	R_s (μL·min^{-1})	R_u (μL·min^{-1})	Unimer (eqv. of seed)	R_u (μL·min^{-1})	
1	5	5	199	1			2
2	10	5	199	1	5	1	4
3	20	5	199	1	15	3	4
4	30	5	199	1	25	5	4

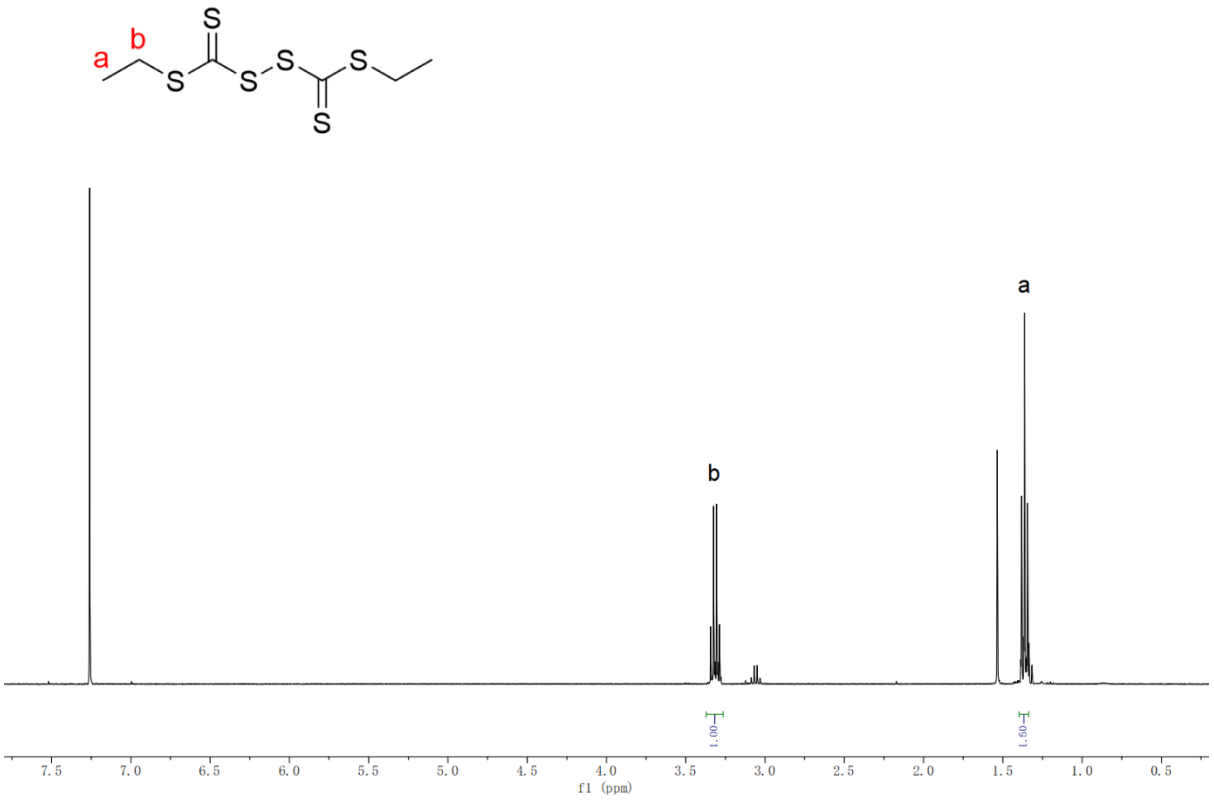

Figure S1. ^{1}H NMR spectrum of bis-(ethylsulfanylthiocarbonyl) disulfide (400 MHz, in $CDCl_3$).

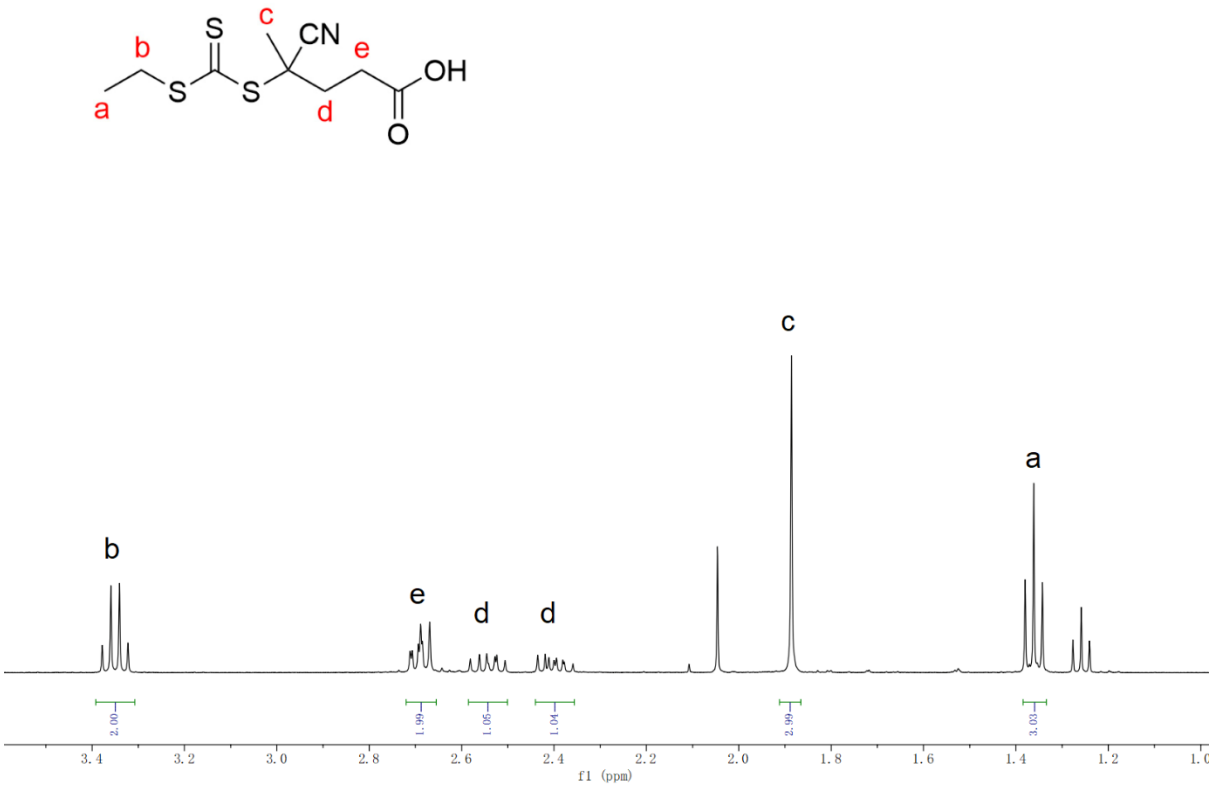

Figure S2. ^{1}H NMR spectrum of CEPA (400 MHz, in $CDCl_3$).

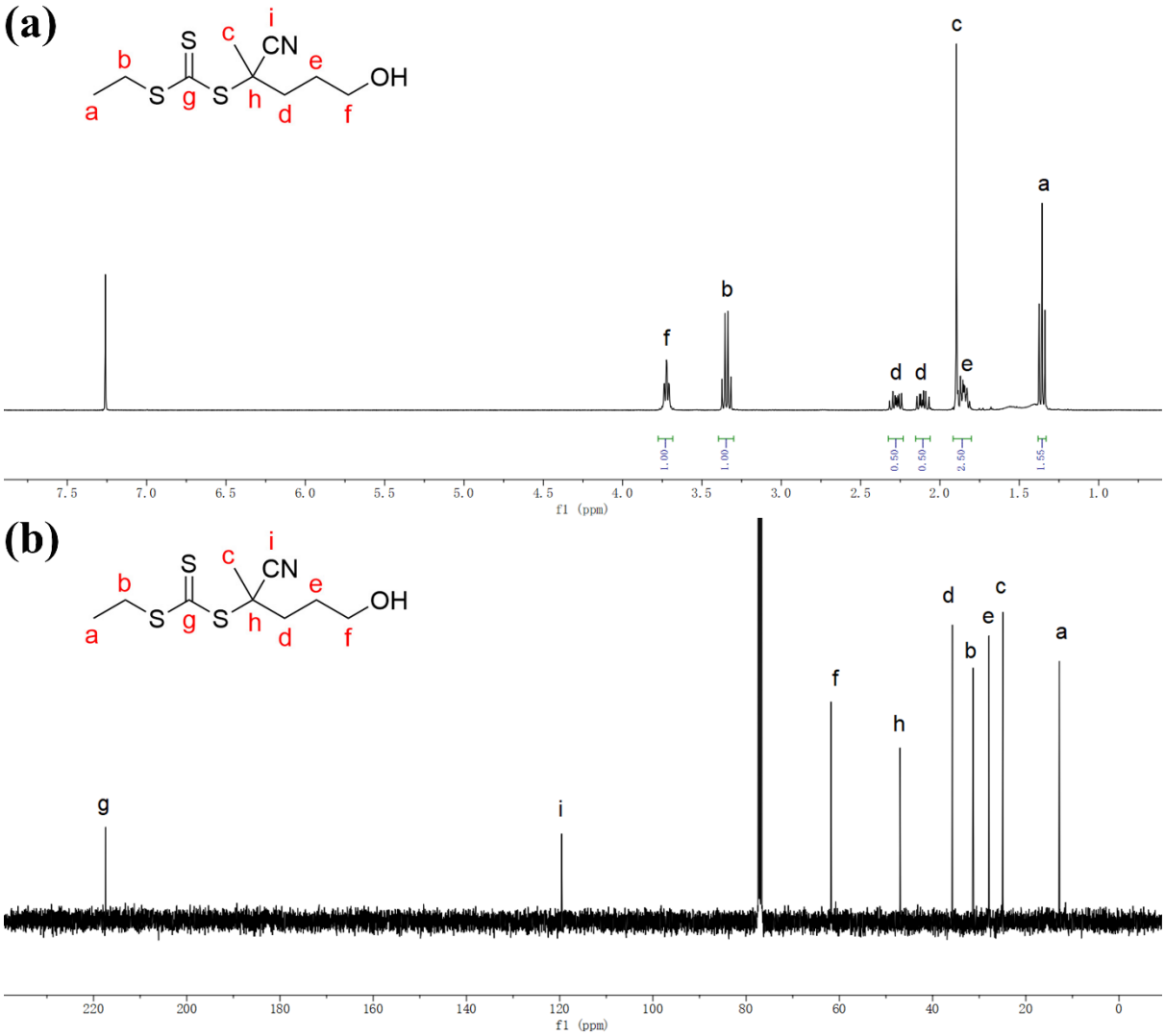

Figure S3. ^{1}H (a) and ^{13}C (b) NMR spectrum of CEPET (400 MHz, in $CDCl_3$).

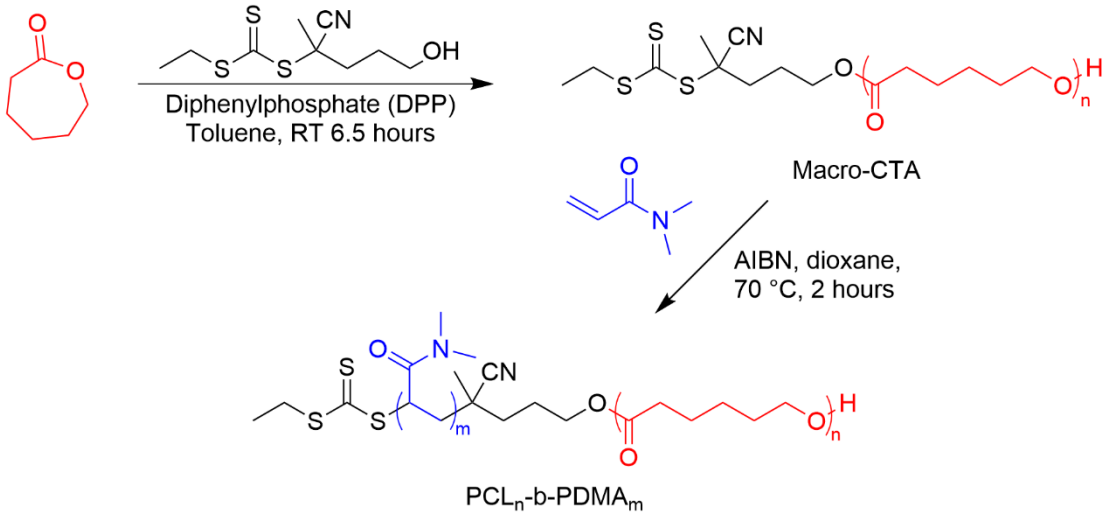

Scheme S2. Synthetic route of PCL-b-PDMA.

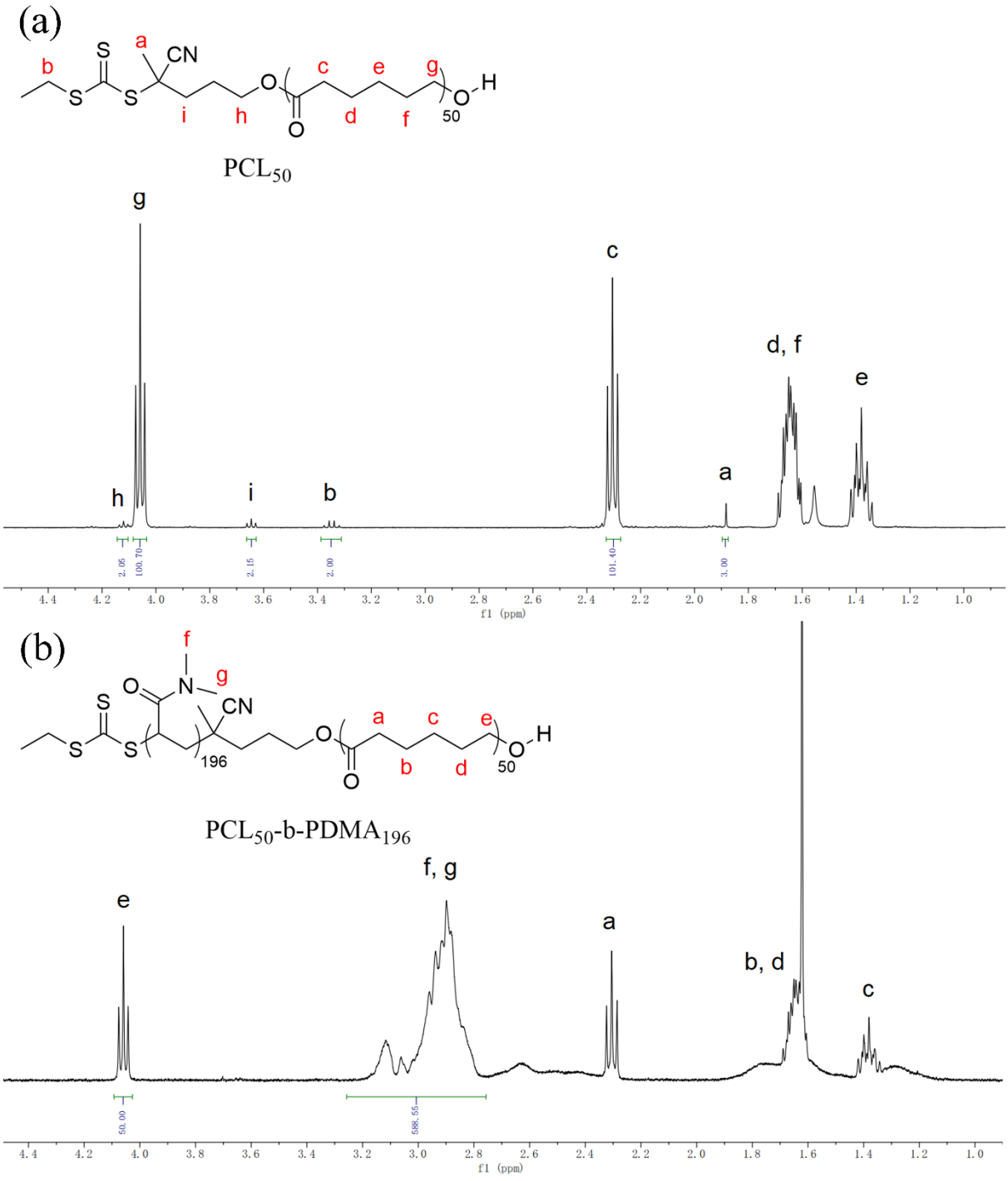

Figure S4. ^{1}H NMR spectra of (a) PCL_{50} and (b) PCL_{50}-b-$PDMA_{196}$ (400 MHz, in $CDCl_3$).

Table S6. SEC results of polymers detected by RI.

Polymer	M_n (kg·mol^{-1})	M_w (kg·mol^{-1})	$Đ$
PCL_{50}	13.3	14.2	1.06
PCL_{50}-b-$PDMA_{196}$	33.0	37.5	1.14

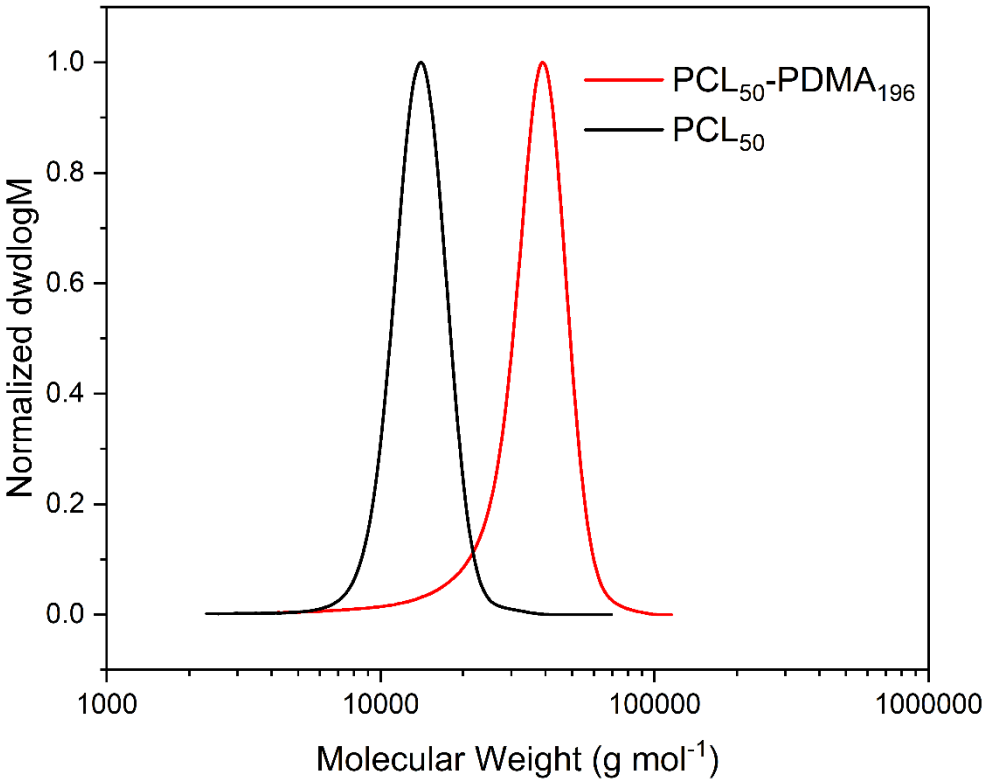

Figure S5. Normalized SEC curves of PCL_{50} and PCL_{50}-b-$PDMA_{196}$.

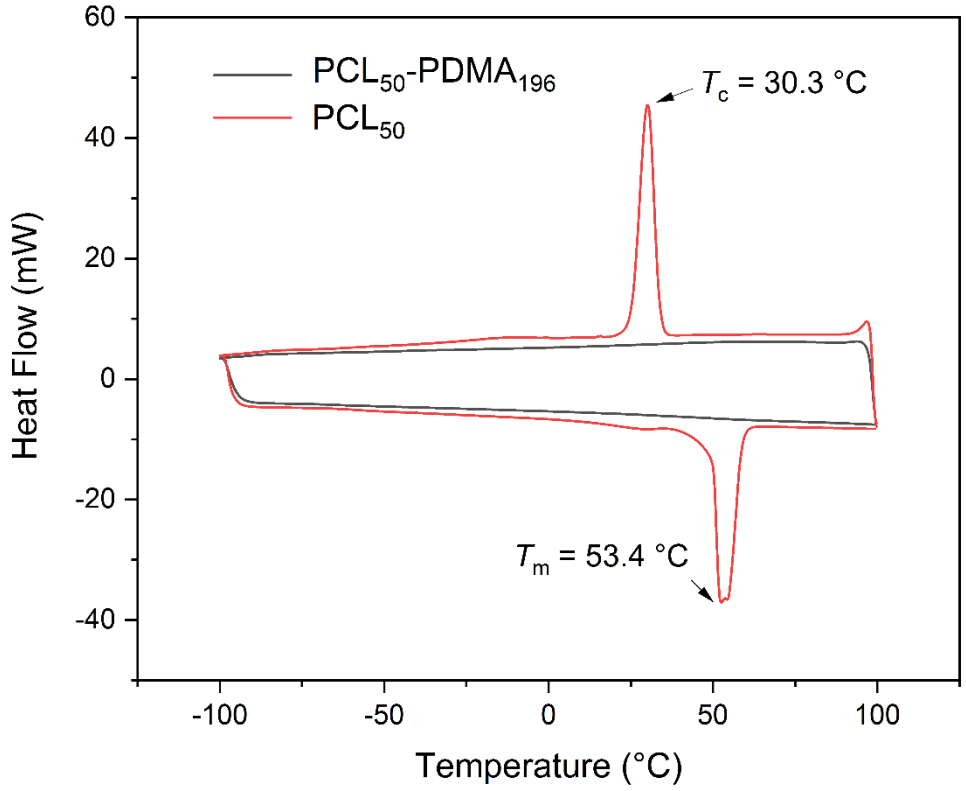

Figure S6. DSC thermogram of PCL_{50} and PCL_{50}-$PDMA_{196}$.

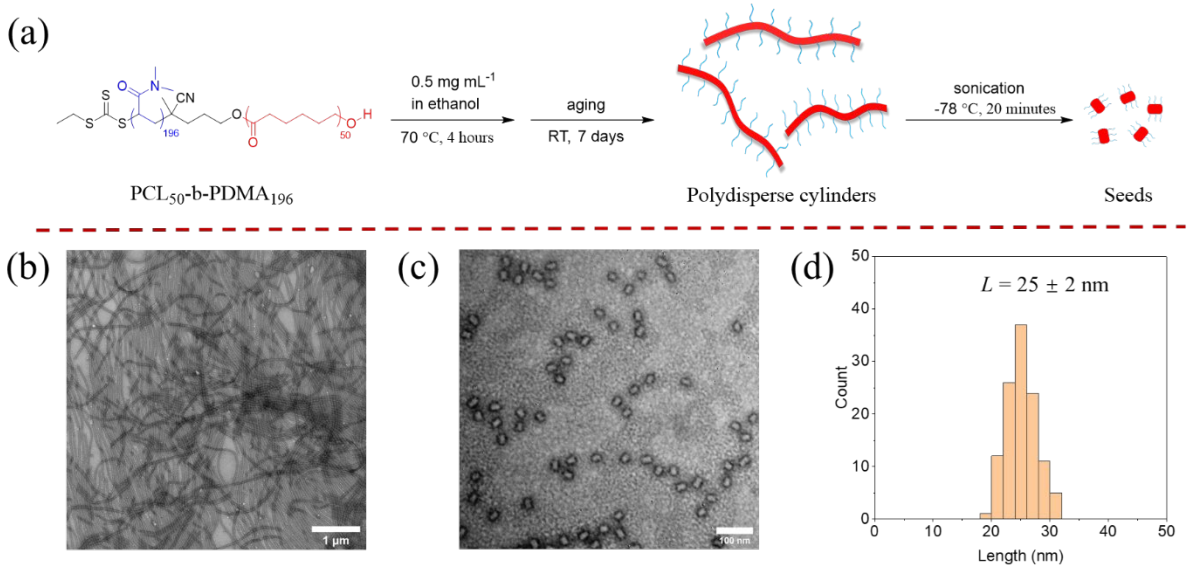

Figure S7. (a) Scheme to prepare seeds from PCL-PDMA. TEM images of (b) polydisperse cylinders and (c) seeds. Uranyl acetate aqueous solution (1%) was used for stain. (d) Length distribution of seeds. At least 100 particles were analysed to obtain statistical results.

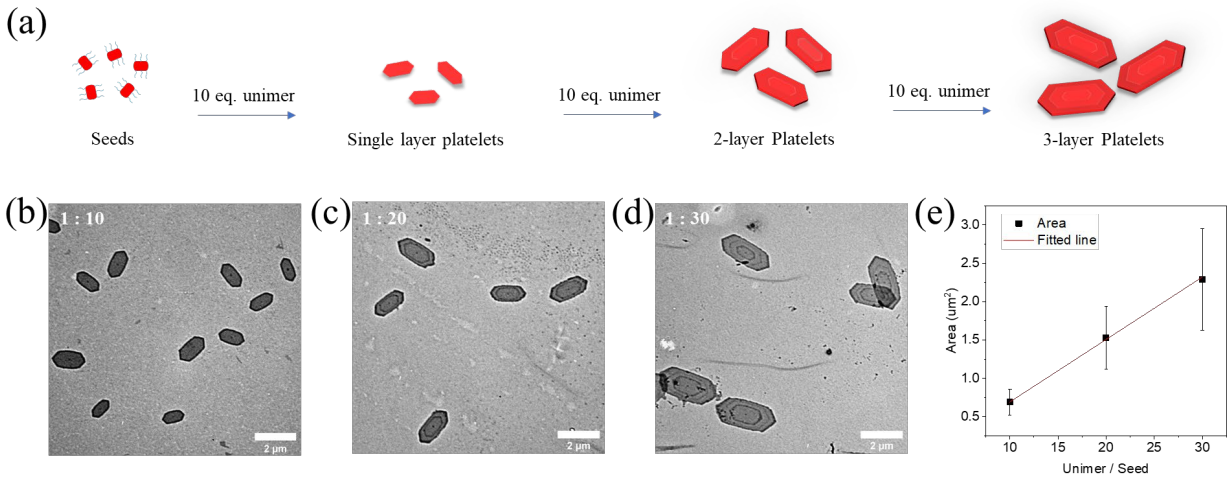

Figure S8. (a) Scheme of living CDSA. TEM images of platelets prepared at seed/unimer ratio of (b) 1:10, (c) 1:20, and (d) 1:30. (e) Linear fit of area upon different unimer/seed ratios. Error bars represent the standard deviation of the area distribution.

Table S7. Batch platelets prepared using various amount of unimer.

Unimer	Area (um^2)			Length (um)			Width (um)			
(eqv. of seed)	A_n	A_w	A_w/A_n	L_n	L_w	L_w/L_n	W_n	W_w	W_w/W_n	L/W
10	0.69	0.73	1.06	1.25	1.28	1.02	0.60	0.62	1.03	2.09
20	1.53	1.64	1.07	1.96	1.99	1.02	0.87	0.89	1.02	2.24
30	2.29	2.48	1.08	2.32	2.37	1.02	1.01	1.04	1.03	2.30
10*	0.65	0.83	1.27	1.24	1.31	1.04	0.58	0.62	1.05	2.14

*Platelets were prepared at 10 mL scale.

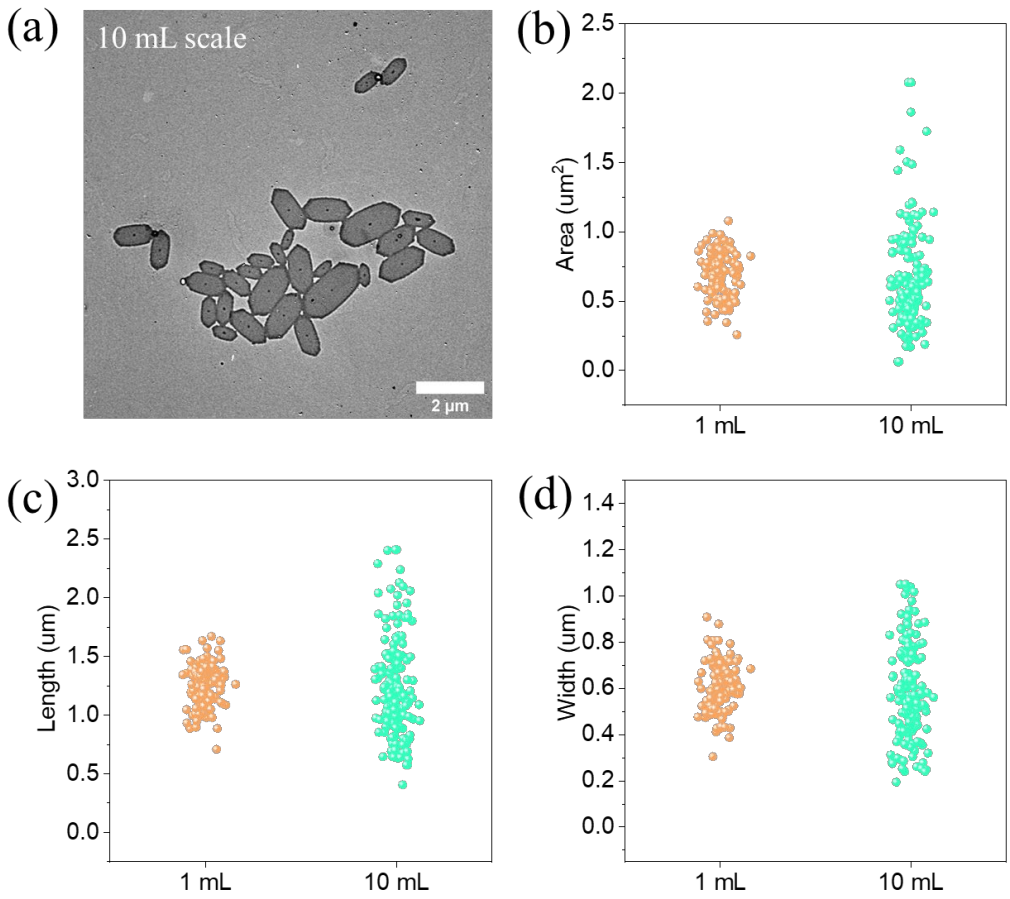

Figure S9. Size comparison of platelets from 1-mL and 10-mL scales: (a) TEM image of platelets prepared from the 10 mL scale, (b) area, (c) length, and (d) width.

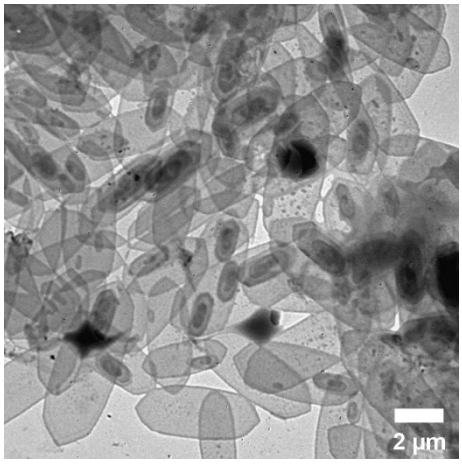

Figure S10. TEM image of platelets prepared at 1 mg mL^{-1} in 1 mL batch scale.

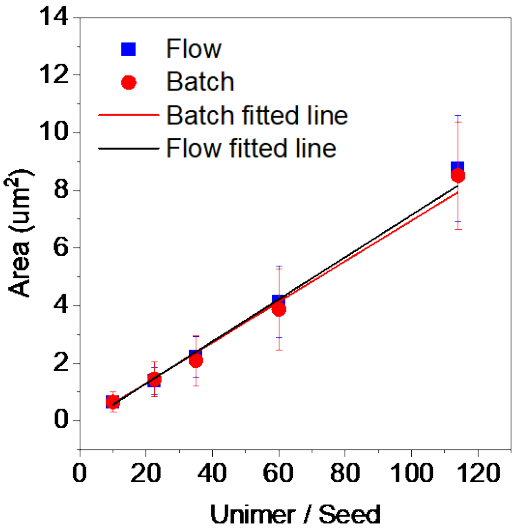

Figure S11. Linear fitting of area and unimer/seed ratio. The error bar represents the standard deviation.

Table S8. Extended flow platelets prepared using original platelets as seeds at various temperature.

Temperature	Area (um^2)			Length (um)			Width (um)			
(°C)	A_n	A_w	A_w/A_n	L_n	L_w	L_w/L_n	W_n	W_w	W_w/W_n	L/W
19	1.88	2.97	1.58	2.00	2.27	1.13	0.97	1.14	1.17	2.06
25	1.51	2.01	1.33	1.91	2.06	1.08	0.82	0.89	1.09	2.33
30	2.21	2.44	1.10	2.27	2.33	1.03	1.02	1.06	1.04	2.23

Table S9. Extended flow platelets prepared using original platelets as seeds at various flow rates.

Flow rate ($\mu L \cdot min^{-1}$)	Time spent (min)	Area (um^2)			Length (um)			Width (um)			
		A_n	A_w	A_w/A_n	L_n	L_w	L_w/L_n	W_n	W_w	W_w/W_n	L/W
100	4	2.05	2.39	1.16	2.26	2.34	1.04	0.98	1.03	1.05	2.30
200	2	2.21	2.44	1.10	2.27	2.33	1.03	1.02	1.06	1.04	2.23
400	1	2.11	2.44	1.15	2.24	2.37	1.06	0.96	1.04	1.08	2.33
800	0.5	2.33	2.56	1.10	2.40	2.47	1.03	1.10	1.14	1.04	2.19

Table S10. Extended platelets prepared using original platelets as seeds with various amount of unimer both in flow and batch reactors.

	Unimer	Area (um^2)			Length (um)			Width (um)			
	(eqv. of seed)	A_n	A_w	A_w/A_n	L_n	L_w	L_w/L_n	W_n	W_w	W_w/W_n	L/W
Flow	12.5	1.38	1.53	1.11	1.77	1.85	1.04	0.80	0.85	1.06	2.21
	25	2.21	2.44	1.10	2.27	2.33	1.03	1.02	1.06	1.04	2.23
	50	4.13	4.51	1.09	3.13	3.21	1.03	1.27	1.32	1.03	2.46
	100	8.76	9.14	1.04	4.78	4.99	1.04	1.73	1.78	1.03	2.76
Batch	12.5	1.45	1.69	1.17	1.89	1.99	1.05	0.93	0.98	1.06	2.05
	25	2.09	2.45	1.17	2.19	2.30	1.05	1.02	1.07	1.05	2.16
	50	3.87	4.38	1.13	3.08	3.21	1.04	1.38	1.45	1.05	2.23
	100	8.51	8.91	1.05	4.31	4.48	1.04	1.70	1.79	1.05	2.54

Table S11. Summary table of all condition studied for flow living CDSA and the size of the corresponding platelets.

	R_t	Time	Temperature	Unimer	Area (um^2)			Length (um)			Width (um)			
	($\mu L \cdot min^{-1}$)	(min)	(°C)	(eqv. of seed)	A_n	A_w	A_w/A_n	L_n	L_w	L_w/L_n	W_n	W_w	W_w/W_n	L/W
Flow	200	2	19	25	1.88	2.97	1.58	2.00	2.27	1.13	0.97	1.14	1.17	2.06
	200	2	25	25	1.51	2.01	1.33	1.91	2.06	1.08	0.82	0.89	1.09	2.33
	200	2	30	25	2.21	2.44	1.10	2.27	2.33	1.03	1.02	1.06	1.04	2.23
	100	4	30	25	2.05	2.39	1.16	2.26	2.34	1.04	0.98	1.03	1.05	2.30
	400	1	30	25	2.11	2.44	1.15	2.24	2.37	1.06	0.96	1.04	1.08	2.33
	800	0.5	30	25	2.33	2.56	1.10	2.40	2.47	1.03	1.10	1.14	1.04	2.19
	200	2	30	12.5	1.38	1.53	1.11	1.77	1.85	1.04	0.80	0.85	1.06	2.21
	200	2	30	50	4.13	4.51	1.09	3.13	3.21	1.03	1.27	1.32	1.03	2.46
	200	2	30	100	8.76	9.14	1.04	4.78	4.99	1.04	1.73	1.78	1.03	2.76
Batch				12.5	1.45	1.69	1.17	1.89	1.99	1.05	0.93	0.98	1.06	2.05
				25	2.09	2.45	1.17	2.19	2.30	1.05	1.02	1.07	1.05	2.16
				50	3.87	4.38	1.13	3.08	3.21	1.04	1.38	1.45	1.05	2.23
				100	8.51	8.91	1.05	4.31	4.48	1.04	1.70	1.79	1.05	2.54

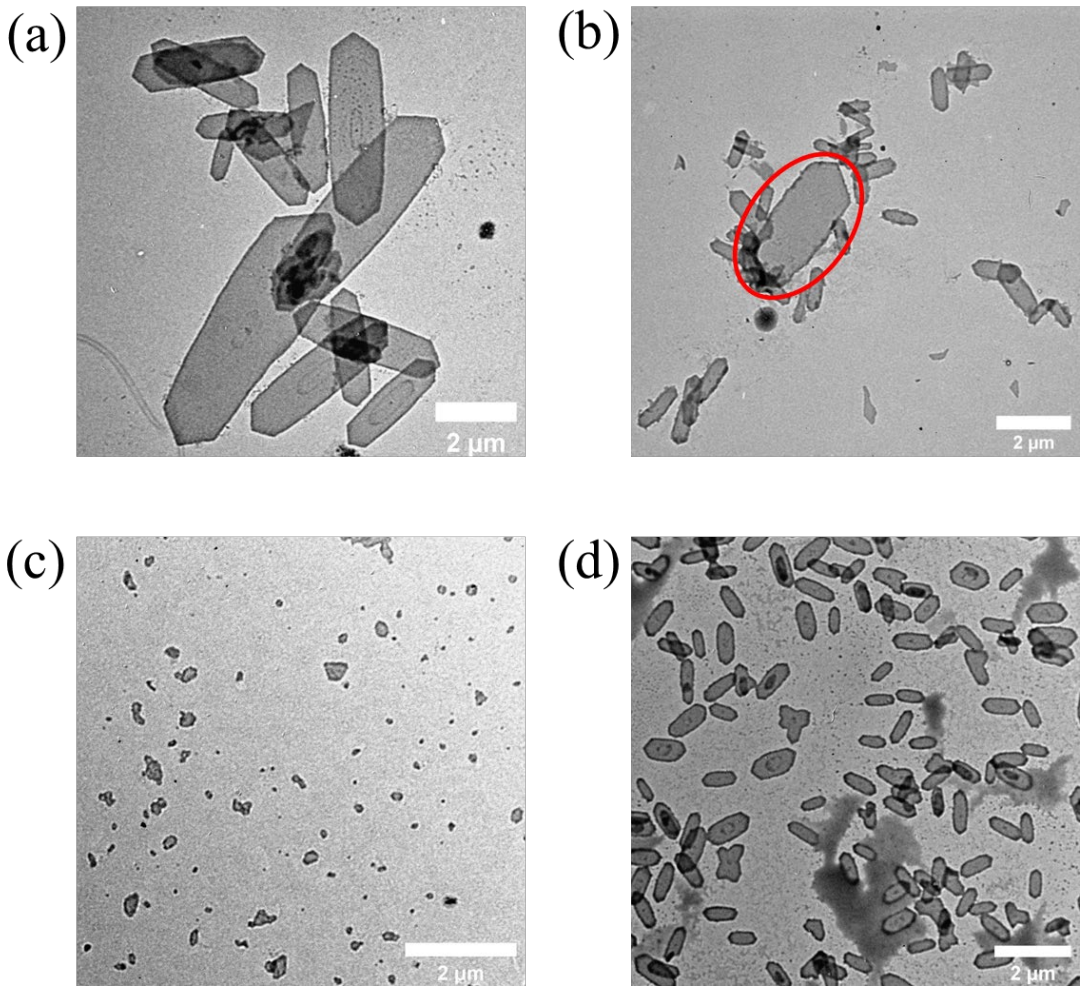

Figure S12. (a) TEM images of extended flow platelets obtained from wider tubing, (b) flow platelets from seeds at the unimer/seed ratio of 10, (c) fragments of platelets, and (d) flow platelets from platelet fragments at the unimer/seed ratio of 10.

Table S12. Flow platelets from seeds with various amount of unimer.

Unimer	Area (um^2)			Length (um)			Width (um)			
(eqv. of seed)	A_n	A_w	A_w/A_n	L_n	L_w	L_w/L_n	W_n	W_w	W_w/W_n	L/W
5	0.27	0.35	1.31	0.84	0.87	1.05	0.32	0.33	1.05	2.63
10	0.59	0.66	1.11	1.22	1.27	1.04	0.43	0.45	1.04	2.80
20	1.35	1.48	1.09	1.95	2.00	1.03	0.68	0.70	1.04	2.88
30	2.41	2.55	1.06	2.87	2.91	1.01	0.96	0.99	1.02	2.98

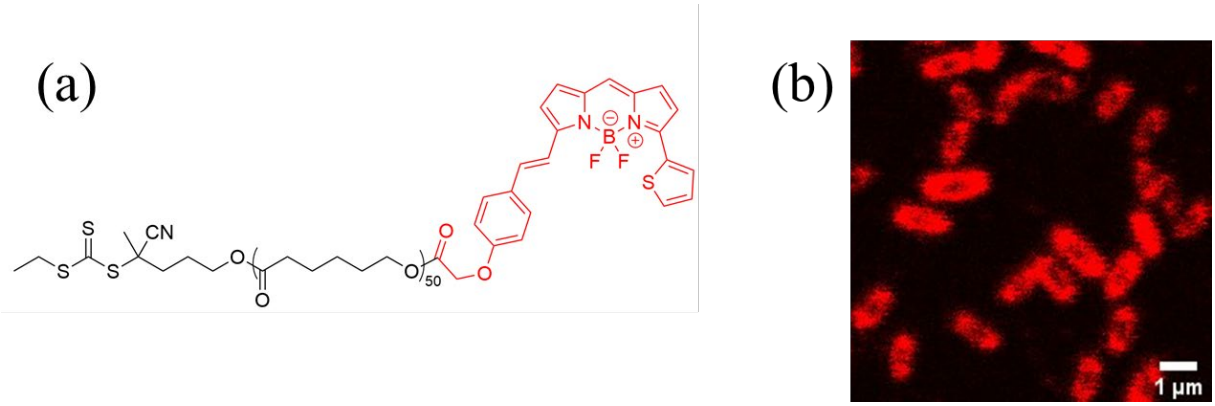

Figure S13. (a) molecular structure of bodipy 630/650 modified PCL and (b) confocal microscopy image (scale bar = 20 μm) of fluorescently labelled platelets.

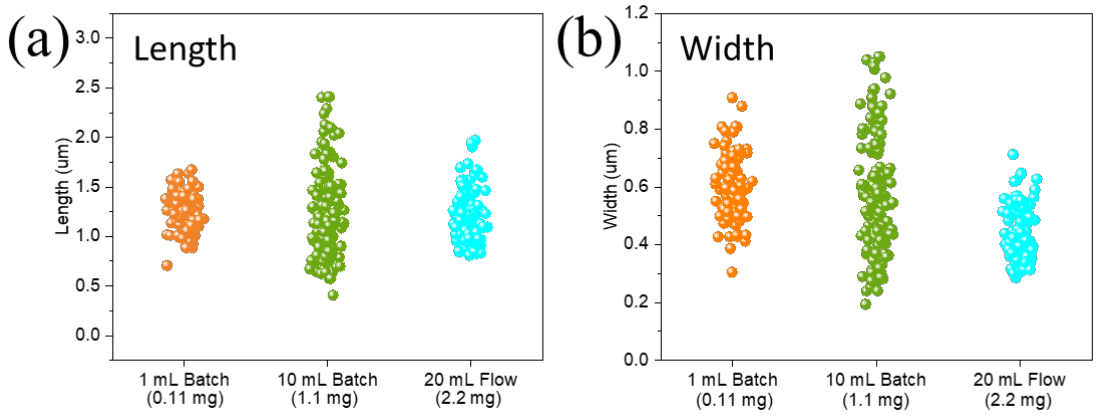

Figure S14. Size comparison of platelets from 1-mL and 10-mL batch scales and 20-mL flow: (a) length and (b) width.

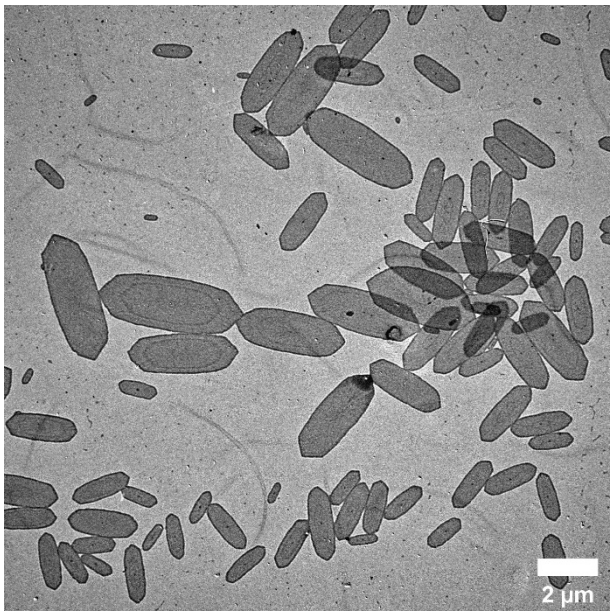

Figure S15. TEM image of platelets prepared at 1 mg mL^{-1} in flow reactors.

Chapter 3 - Direct Preparation of 2D Platelets from Polymer Enabled by Accelerated Seed Formation

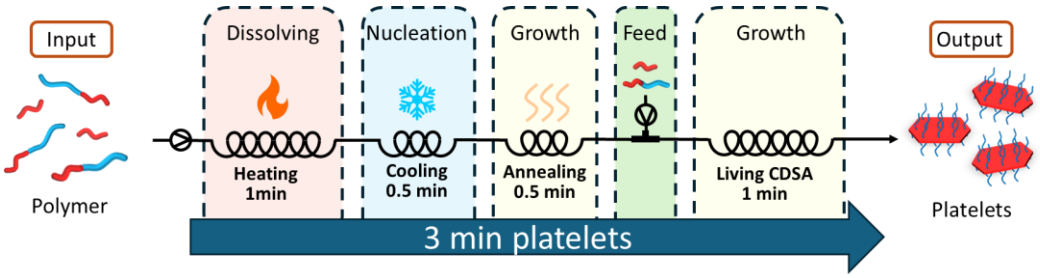

3.1 Publication Details and Overview

Title: Direct Preparation of 2D Platelets from Polymer Enabled by Accelerated Seed Formation

Authors: Laihui Xiao,[†] Tianlai Xia,[†] Jian Zhang,[†] Sam J. Parkinson,[†] Julia Y. Rho,[†] Andrew P. Dove,[†,*] and Rachel K. O'Reilly[†,*]

Affiliation: [†]School of Chemistry, University of Birmingham, Edgbaston, Birmingham B15 2TT, United Kingdom

Journal: Nature Synthesis

Year: 2025

Page Number: 1–8.

DOI: 10.1038/s44160-025-00767-x

Submitted: 11 October 2024

Publishes: 10 February 2025

Coauthor Contributions: Mr. Tianlai Xia assisted with batch CDSA and confocal microscopy. Dr. Jian Zhang contributed to polymer synthesis. Dr. Sam J. Parkinson advised on flow setups and proofread the manuscript. Dr. Julia Y. Rho helped with proofreading and correction. Prof. Andrew P. Dove assisted in proofreading and guidance. Prof. Rachel K. O'Reilly supervised the project and reviewed the manuscript.

Overview:

This chapter presents a universal strategy to significantly reduce the processing time for the preparation of 2D platelets through crystallization-driven self-assembly (CDSA), which substantially enhances the throughput of uniform platelets across a range of crystallizable polymers.

To achieve this, a rapid seed preparation method was developed that leverages polymer supersaturation to initiate nucleation. This process reduces the processing time from a week to 3 minutes, while maintain great control of the size and morphology of our nanostructures. Moreover, flash-frozen seeds generated using this method exhibit epitaxial growth behavior equivalent to seed prepared using typically method that require long ageing and sonication. This work also highlights the importance of heat transfer and concentration during the seed preparation process. Furthermore, it was shown that this process can be translated into flow to successfully scale up seed preparation while further decreasing processing time. Extensive characterization demonstrated that the properties of the seeds remained unchanged when scaling up small batch reactions (0.2 mg) by a factor of 100 (20 mg) using flow reactors.

An integrated flow cascade was subsequently devised for the direct preparation of 2D nanoplatelets from polymer. The integrated flow cascade, which encompasses both seed preparation and controlled epitaxial seed growth (living CDSA), enables end-to-end production from polymer to platelet in one continuous reactor setup. Remarkably, uniform platelets were produced directly from polymers in just 3 minutes, substantially boosting throughput and significantly surpassing all other CDSA methods. Furthermore, by modularly designing the flow system, platelets with tunable core and corona chemistries were efficiently produced.

Overall, this advancement opens new possibilities for programmable material design by enabling precise control over nanostructure properties. It represents a significant step forward

in high-throughput polymer nanomaterial synthesis, with the potential to greatly enhance the commercialization of precision nanomaterials.

nature synthesis

Article

https://doi.org/10.1038/s44160-025-00767-x

Direct preparation of two-dimensional platelets from polymers enabled by accelerated seed formation

Received: 11 October 2024

Accepted: 10 February 2025

Published online: 14 March 2025

Check for updates

Laihui Xiao, Tianlai Xia, Jian Zhang, Sam J. Parkinson, Julia Y. Rho, Andrew P. Dove & Rachel K. O' Reilly

Crystallization-driven self-assembly (CDSA) presents a facile method to access well-defined nanostructures. However, nanostructure preparation via CDSA has been constrained by prolonged processing time and limited throughput, primarily due to seed preparation and confinement to small batch scales. In turn, this limits the potential to scale up CDSA to enable application of the resultant particles. Here we report a rapid seed preparation method that drives uniform seed micelle formation by supersaturating polymer solutions in a flow system. This leads to a large reduction in processing time, from a week down to minutes. Importantly, the modular flow cascade applied can integrate both seed preparation and living CDSA, enabling end-to-end production of nanostructures directly from polymers in 3 min. The attained throughput of 132 mg h^{-1} surpasses that of other reported methods by orders of magnitude and, in turn, provides a step forward for the scaling-up of precision nanomaterials.

Crystallization-driven self-assembly (CDSA) has emerged as a powerful method to fabricate anisotropic nanostructures, such as one-dimensional (1D) cylinders and two-dimensional (2D) platelets[1,2]. The vast array of stable, uniform nanostructures formed through this method has led to their diverse range of applications, including catalysis[3,4], biomedical engineering[5,6] and energy transfer[7]. Through 'living CDSA', these self-assembled systems can adopt high levels of precision, uniformity and complexity. Notably, living CDSA enables precise epitaxial growth of nanostructures upon the addition of further unimers. This method allows the size and shape of the self-assembled nanostructures to be tuned by adjusting the quantity and composition of the unimers added to the nucleated seeds in solution[8,9].

Despite the application potential of CDSA-formed particles, the complex and time-intensive nature of seed preparation, which involves heating polymer solutions, extended ageing and sonication, presents substantial synthetic challenges that hinder their application at scale[8,9]. Poly(ε-caprolactone) (PCL)-based polymers, valued for their biodegradability and biocompatibility, have been effectively utilized in living CDSA to prepare 1D and 2D nanoparticles[10–14]. Typically, in this method, the initial transformation of bulk polymers into unimers is achieved through heating, followed by spontaneous nucleation during cooling. Due to the spontaneous formation of nucleation sites, the resulting 1D cylinders form over an extended ageing period, typically 1 week, and have a high dispersity (that is, a large distribution of cylinder lengths) and no size control. Subsequently, sonication is commonly used to fragment these cylinders to achieve uniform seeds[10,12,14]. Inconsistency in seed sizes upon increasing the volumes of dispersed cylinders that are subjected to sonication limits the synthesis of these uniform seeds to small-scale batches. Moreover, the transition from polymers to platelets involves multiple morphological changes and batch-to-batch processes. To achieve good size control and uniformity, living CDSA requires a dilute solution (typically less than 0.1 wt%), which in turn leads to a notable reduction in throughput[2,8,15]. Unsurprisingly, given the multiple steps required to transform polymers to platelets, scale-up is challenging. Although efforts have been made to scale CDSA, the obtained structures were predominantly 1D cylinders, with limited control over size and morphology. For example, the Manners

School of Chemistry, University of Birmingham, Birmingham, UK. e-mail: a.dove@bham.ac.uk; r.oreilly@bham.ac.uk

https://doi.org/10.1038/s44160-025-00767-x

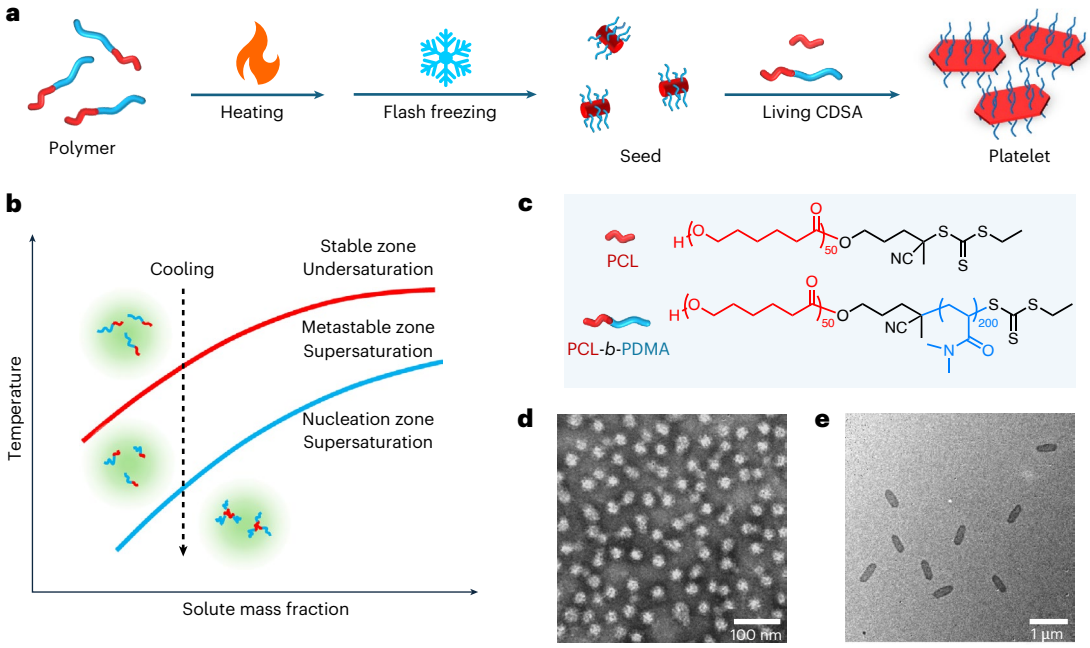

Fig. 1 | Preparation and living CDSA of flash-frozen seeds in batch. a, Scheme to prepare platelets from polymers via flash-frozen seeds. **b**, A phase diagram illustrating diblock polymer crystallization using the flash-freezing strategy. **c**, Chemical structures of PCL-based homo and diblock polymers. **d**, A TEM image of flash-frozen seeds prepared at 0.1 mg ml^{-1} with 2 min heating at 75 °C and 1 min cooling in a dry-ice–acetone bath. The seed sample was stained by 1 wt% uranyl acetate aqueous solution. **e**, A TEM image of platelets prepared by living CDSA using flash-frozen seeds.

and Patterson groups introduced polymerization-induced CDSA (PI-CDSA) to perform polymerization and CDSA simultaneously[16–18], whereas the Winnik group conducted CDSA by co-self-assembly of block copolymers with trace amounts of homopolymer, leveraging controlled annealing and cooling conditions to produce uniform micelles at high polymer concentrations[19].

We hypothesized that a transition from a batch process to a flow process would be a key enabler for efficient and reproducible preparation of high-quality seeds, while still maintaining excellent size control (uniformity throughout seed solution). Continuous-flow reactors, where reactants flow steadily through the reactor while chemical reactions occur concurrently, have been demonstrated to be an ideal way to scale up reactions[20,21]. We anticipated that minimization of the processing time would be essential to enable transition of the seed formation process into continuous flow. Therefore, we sought to favour spontaneous self-nucleation in a short window, so that we could develop a more efficient and, hence, more reproducible and scalable method to obtain uniform seeds.

While studying the formation of polydisperse cylinders, we noticed that self-nucleation could be favoured when the solution was cooled from a supersaturated state[13,22]. Inspired by reports of flash nanoprecipitation for polymer and peptide nanoparticles[23–25], we anticipated that, if a highly supersaturated solution could be achieved, it would rapidly favour instantaneous nucleation to potentially provide a process that could be used in situ for the creation of complex multilayered 1D and 2D polymer particles, dramatically reducing the time it takes to make uniform platelets from polymers (from a week down to a few minutes) and allowing a leap forward in the scalable synthesis of precision nanoparticles. Here, we introduce a flash-freezing strategy to prepare seeds, leveraging excellent temperature control for seamless scale-up in flow. Building on this, an integrated flow cascade, combining seed formation and living CDSA, was established, enabling end-to-end production of platelets directly from polymers, significantly reducing processing time and increasing throughput.

Results and discussion

We used the established PCL homo (PCL_{50}) and poly(ε-caprolactone)-*block*-polydimethylacrylamide diblock (PCL_{50}-*b*-$PDMA_{200}$) polymers, based on their demonstrated effectiveness in both seed and platelet preparation using conventional CDSA methods (Fig. 1c, Supplementary Figs. 1–6 and Supplementary Table 1)[10,12,13]. Initially, we focused on creating seeds in a rapid manner in a batch process. Unlike previous methods that formed seeds through the sonication of polydisperse cylinders, here we studied an in situ flash-freezing method to produce seeds in minutes by removing the time-consuming ageing process (Fig. 1a). To achieve this, the diblock polymer was initially dissolved in ethanol at elevated temperature, to generate an undersaturated solution. The solution was subsequently cooled rapidly (flash freezing) to induce spontaneous nucleation and generate uniform seeds. Conditions such as heating and cooling times and polymer concentration were studied in batch to explore the best conditions for preparing flash-frozen seeds (Supplementary Table 2). Optimal conditions were found when the diblock polymer solution was prepared by heating at 75 °C and then quenched using a dry-ice–acetone bath, with the production of uniform seeds, as shown by transmission electron microscopy (TEM) analysis (Fig. 1d). Other methods, namely ice and air cooling, resulted in long cylinders and large aggregates (Supplementary Figs. 7 and 8). While these particles exhibit higher melting points due to slow crystallization kinetics (Supplementary Fig. 9), their irregular structures and low crystallization rate during air cooling make them unsuitable as seeds because of low preparation efficiency. Further optimization towards smaller and more uniform seeds was achieved by heating the diblock polymer solution for longer time periods, with the size of the flash-frozen seeds constant at 50 nm (characterized by dynamic light scattering (DLS)) for all time periods >2 min (Supplementary Figs. 10 and 11). This suggests that, if the solution is not thoroughly heated, regional chain entanglement or aggregation can induce large particle formation during cooling. Seed particle sizes were also influenced by the concentration of diblock polymer solution such that the size of the seeds decreased with increasing concentration but reached a plateau at

https://doi.org/10.1038/s44160-025-00767-x

50 nm when the concentration exceeded 0.05 mg ml^{-1} (Supplementary Figs. 12 and 13). This is consistent with a lower polymer concentration leading to lower supersaturation levels upon flash-freezing, thereby reducing self-nucleation and forming large seeds.

Further exploration of the cooling conditions demonstrated that a 1 min cooling period is necessary to achieve consistent seed size (Supplementary Figs. 14 and 15). This duration is considered the minimum time required to reach the temperature at which uniform seeds form when immersed in a dry-ice–acetone bath (−78 °C). To test the temperature threshold, samples were cooled to various temperatures (from −10 °C to −50 °C) for 5 min. Decreasing seed size with decreasing temperature was observed, which indicated that there was an increased nucleation efficiency at lower temperatures (Supplementary Figs. 16 and 17). The threshold for obtaining uniform seeds was found to be −50 °C, close to the glass transition temperature (T_g) of PCL. At this temperature, chain movement is extremely limited, causing neighbouring PCL blocks to nucleate rather than grow on preformed nuclei through chain movement. We suggest that sufficient cooling time is required to enable the solution to reach a supersaturated state in the nucleation zone. If not, only partial nucleation to seeds will be achieved, where remaining polymers may epitaxially grow on these seeds to form cylinders. These studies show that the formation of well-defined, uniform seeds requires heating followed by rapid cooling of the solution, to take it from an undersaturated state to a supersaturated state within the nucleation zone (Fig. 1b)[26–28], resulting in fast spontaneous nucleation to uniform seeds. Based on the above results, flash-frozen seeds were optimally prepared at 0.1 mg ml^{-1} by heating the solution to 75 °C for 2 min followed by cooling for 1 min using a dry-ice–acetone bath.

To confirm that the flash-frozen seeds remained efficient for living CDSA, unimer addition was conducted according to our previous procedure (Fig. 1a)[10,12,13]. Similar results to the living CDSA using seeds prepared in a classical manner through sonication (Supplementary Figs. 18 and 19 and Supplementary Table 3) were obtained, with all seeds converting to platelets and the size of platelet increasing with the addition of more unimers (area, length and width increased from 0.11 μm^2, 0.57 μm and 0.21 μm to 1.47 μm^2, 2.46 μm and 0.66 μm respectively; Fig. 1e, Supplementary Figs. 20 and 21 and Supplementary Table 4). The linear relationship between the mass of the unimers and the area of the platelets (Supplementary Fig. 20d) indicates the controllable living behaviour was retained. This was further confirmed using fluorescent-dye-modified unimers in different aliquots, revealing platelets with layered structures, indicated using confocal laser scanning microscopy (CLSM; Supplementary Fig. 22).

We further sought to quantify the nucleation efficiency of the flash-freezing approach; however, as DLS provides only particle size information, comparing the number of flash-frozen seeds was not feasible. Consequently, we hypothesized that using living CDSA using flash-frozen seeds prepared under different conditions, with the addition of unimers at a constant unimer-to-seed ratio of 10, would allow correlation between platelet size and seed number, such that a lower number of seeds results in larger platelets, while a higher seed content leads to smaller platelet sizes (Supplementary Figs. 23–30 and Supplementary Tables 5 and 6). As anticipated, there was no evidence of remaining seeds after seeded growth, and the size of platelets decreased with an increasing heating time to prepare flash-frozen seeds and then reached a plateau (Supplementary Fig. 25), aligning with the observed trend in the size of flash-frozen seeds. In addition, smaller platelets were produced from flash-frozen seeds compared with those produced from classical seeds, indicating that flash-freezing is a more effective method for seed formation, a conclusion also supported by living CDSA with flash-frozen seeds prepared under different conditions (Supplementary Figs. 24–30).

To increase the scale of seed preparation, we attempted to increase the volume by fivefold in batch. However, owing to insufficient heat transfer at a larger scale (total mass of 1 mg) in batch, the obtained seeds exhibited high dispersity (Supplementary Figs. 31 and 32). Although uniform seeds were obtained after increasing the heating time, their size did not match that of the 0.2 mg control batch, which was previously prepared on a small scale, and the size of the platelets obtained after living CDSA was substantially larger (Supplementary Figs. 33 and 34).

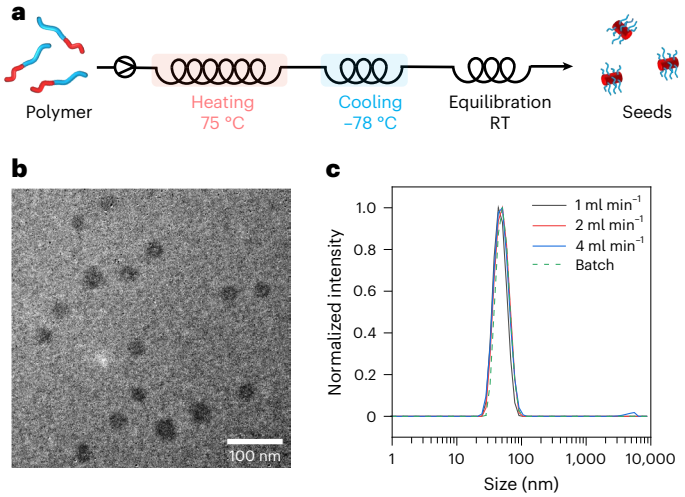

Fig. 2 | Flash-frozen seeds prepared in flow using diblock polymers only. a, Preparation scheme. RT, room temperature. **b**, A TEM image of seeds prepared in flow at flow rate of 1 ml min^{-1}. **c**, The DLS size distribution of flow seeds prepared at various flow rates and in batch. Samples were stained using 1 wt% uranyl acetate aqueous solution.

Critically, seed preparation provides the biggest challenge to the scalability and reproducibility of precision nanoparticles by CDSA, due to the arduous process of preparing uniform seeds. Our previous work demonstrated the potential of flow reactors in CDSA living growth[29] and therefore directed our attention to exploring the synthesis of seeds in a flow reactor, as reaction conditions can be kept constant and greater scale is achieved by scaling-out or through continuous production. The modularity of flow reactors allows flexible reactor design, connecting components with specific functions to the flow cascade as needed[30,31]. Importantly, the high surface area-to-volume ratio in these flow reactors facilitates excellent heat transfer and, therefore, enhances temperature control[32,33], ensuring isothermal conditions and rapid, controllable cooling to achieve supersaturation, which is crucial for seed formation. Furthermore, we envisaged that integration of seed preparation with living CDSA, in a single continuous flow set-up will allow the direct preparation of platelets from polymers to streamline the end-to-end process, facilitating the direct transformation from polymers to platelets while retaining uniformity and circumventing potential issues of batch-to-batch variability.

A flow reactor was established (Fig. 2a and Supplementary Fig. 35) with the in-series connection of a heating channel (2 ml) in an oil bath set at 75 °C, a cooling channel (1 ml) in a dry-ice–acetone bath and an equilibration channel at room temperature. The polymer solution was initially pumped through the flow reactor at 1 mg ml^{-1}, with heating (2 min), cooling (1 min) and annealing (1 min) times optimized on the basis of batch conditions. The resulting seeds (20 mg, 46 nm; Fig. 2b,c and Supplementary Table 7) prepared in this manner closely resembled those prepared in the batch control (0.2 mg, 50 nm). Owing to the increased heat transfer in flow, we hypothesized that we could shorten the heating and cooling times to obtain more rapid seed synthesis while retaining the high quality. Thus, the flow rate was increased from 1 ml min^{-1} to 2 and 4 ml min^{-1} to give total residence times of 2 min and 1 min, respectively. TEM and DLS confirmed that the flash-frozen seeds prepared in flow maintained a consistent size and morphology with increasing flow rates, although some aggregates were observed

https://doi.org/10.1038/s44160-025-00767-x

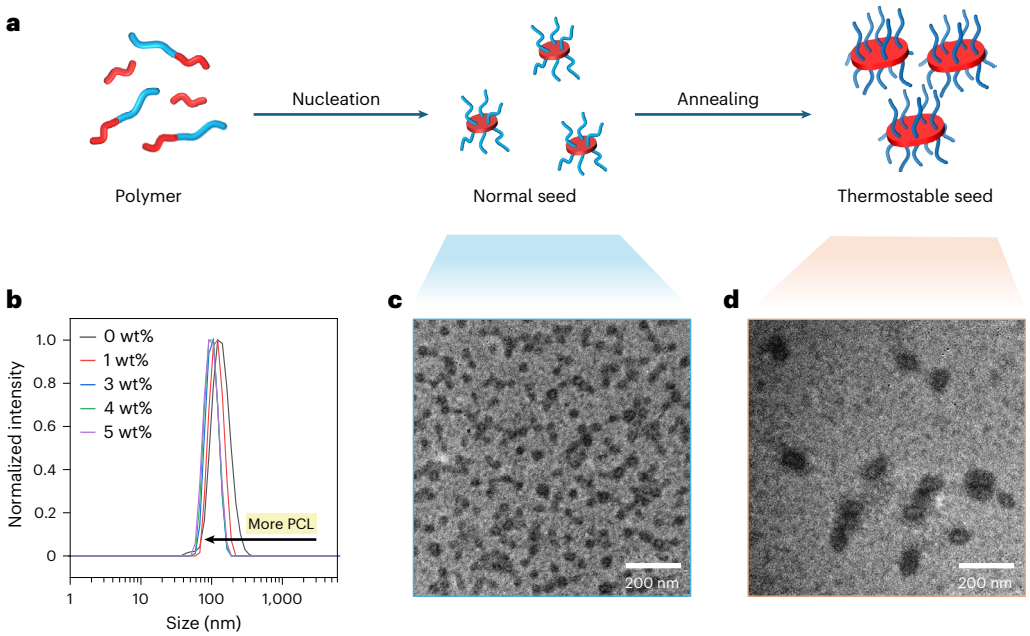

Fig. 3 | Preparation of flash-frozen seeds in the flow reactor. a, Mechanism of preparing robust seeds. **b**, DLS size distribution of robust seeds with various PCL contents. **c**, A TEM image of seeds prepared by the mixture of PCL (3 wt%) and diblock copolymer (PCL-*b*-PDMA) before annealing. **d**, A TEM image of robust seeds prepared by the mixture of PCL (3 wt%) and diblock copolymer (PCL-*b*-PDMA) after annealing. Samples were stained using 1 wt% uranyl acetate aqueous solution.

at a flow rate of 4 ml min^{-1} (Fig. 2c, Supplementary Fig. 36 and Supplementary Table 7). Nevertheless, the throughput could be increased to 0.2 mg min^{-1} at the flow rate of 2 ml min^{-1}, equivalent to the uninterrupted production efficiency of three batch reactors (0.067 mg min^{-1}), irrespective of loading and unloading.

Living CDSA using flow flash-frozen seeds was initially investigated in a detached flow reactor. In this flow reactor (Supplementary Fig. 37a), to achieve good mixing, flash-frozen seeds were preheated to 30 °C, and epitaxial growth occurred after mixing with unimers[29]. Unexpected unimer self-nucleation was observed, which resulted in the formation of extremely large platelets (length >10 µm; Supplementary Fig. 37b). In addition, a notable number of the platelets were much larger than those prepared in batch that were grown from the same seeds. We suggest that this is a consequence of the combined influence of elevated temperature and shear force in flow, which causes some of the seeds to dissolve due to their low crystallinity. To avoid self-nucleation, the crystallization rate was decreased by halving the concentration in our previous work; however, this also decreases the throughput. Alternatively, to stabilize the seeds made from diblock polymer, a small amount of PCL homopolymer was introduced as an additive during the seed preparation process. PCL homopolymer was chosen due to its higher crystallization ability and melting point than the diblock copolymer, as well as its ability to cocrystallize with the diblock polymer.

Flash-frozen seeds generated in flow containing various amounts of PCL (1–5 wt%) were prepared using an identical flow set-up (Supplementary Figs. 35 and 38a). All seed samples containing PCL were found to be of a similar size (Fig. 3c, Supplementary Fig. 38 and Supplementary Table 8). We propose that these seeds have a 2D structure, in line with previous work that has shown that adding PCL homopolymer to diblock copolymers during self-assembly induces a morphological transition from 1D to 2D (ref. 34). The temperature of the equilibration channel was then increased to 30 °C to anneal the seeds (Supplementary Fig. 39a), enhancing their thermal stability and initiation efficiency by promoting higher crystallinity, as shown in previous work[35]. This adjustment enables a more detailed analysis of seed morphologies immediately before mixing with unimers during living CDSA. As observed in TEM images (Supplementary Fig. 39b), all annealed samples showed similar morphology, and the sizes of the thermostable seeds measured by DLS decreased as more homopolymers were added (Fig. 3b). To demonstrate that some seeds were dissolved as they passed through the annealing channel, these seed samples aged for 3 days, and the sizes of the seeds were measured using DLS (Supplementary Fig. 40 and Supplementary Table 9). The size of the seeds without PCL increased gradually with the extension of ageing time (Supplementary Fig. 40f), and a short cylindrical morphology was obtained after 3 days of ageing (Supplementary Fig. 40a), on account of the redissolved unimers growing on the surviving seeds[36,37]. A similar trend occurred in the sample with 1 wt% PCL (Supplementary Fig. 40b); however, with a PCL content increased to 3 wt% or higher, the seed samples were stable, and similar morphologies before and after ageing were observed, as shown by TEM images (Supplementary Fig. 40c–e).

Flow flash-frozen seeds with various PCL contents were used to conduct living CDSA with 10 equiv. unimers to show how PCL content influences the behaviour of epitaxial growth of the flash-frozen seeds (Supplementary Fig. 37). The results indicated that self-nucleation can be avoided once PCL was involved in the seed preparation, and the size of the obtained platelets decreased as more PCL was used to prepare flash-frozen seeds (Supplementary Fig. 37 and Supplementary Table 10). The results were in line with the stability trend of flash-frozen seeds (Supplementary Fig. 41). As PCL increased the stability of seeds, more seeds survived after preheating; thus, each seed shared fewer unimers, resulting in smaller platelets.

After optimizing seed preparation and living CDSA in flow, a flow reactor cascade was developed to prepare size-controllable platelets directly from polymers (Fig. 4a and Supplementary Fig. 42). It should be noted that, to combine the two sections and push the productivity as high as possible, the flow rate in the flow cascade was conducted at 1 ml min^{-1}, which is faster than that applied for the separate living CDSA process. In addition, the throughput was further enhanced by increasing concentration. Typically, flash-frozen seeds are prepared at 0.1 mg ml^{-1} in flow, while traditional batch living CDSA is performed at a seed concentration of 0.01 mg ml^{-1}. Challenges arise as a higher

https://doi.org/10.1038/s44160-025-00767-x

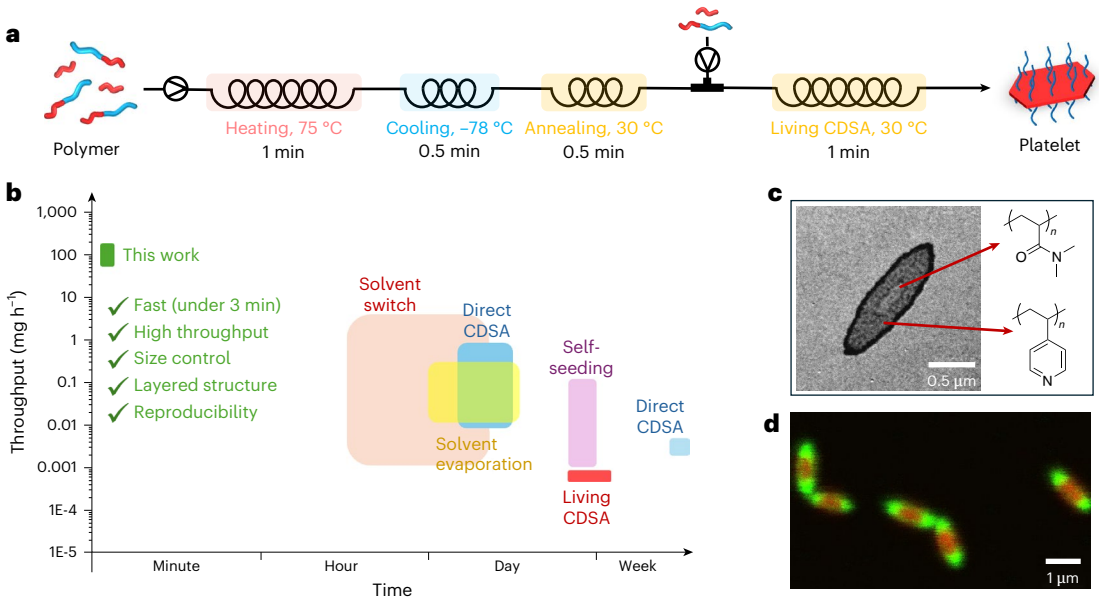

Fig. 4 | End-to-end production of platelets from polymers using an integral flow reactor. a, Preparation scheme of platelets prepared in 3 min. **b**, A comparison of processing time and throughput of reported 2D PCL-based platelets in the literature[10–14,34,47–72]. **c**, Double-layered platelets with heterogeneous coronas. **d**, CLSM image of layered platelets with tunable core chemistry.

concentration contributes to a faster crystallization rate, which increases the burden on the short mixing time to achieve a homogeneous system to grow uniform platelets. To solve this problem, a reverse T micromixer and folding tubing were applied to increase mixing by creating turbulence in flow (Supplementary Figs. 35 and 42). The practicality of both strategies has been demonstrated in the literature[20,38,39].

Fast preparation and high throughput can be achieved simultaneously using this integral flow cascade. By controlling the flow rates, platelets of controllable size can be prepared in 6 min through a continuous end-to-end manner (Supplementary Table 11). The platelets obtained through this flow process are uniform (Supplementary Fig. 43 and Supplementary Table 12), and the area of platelets exhibits a linear relationship with the mass of the unimers (Supplementary Fig. 43d). Alternatively, the dimensions of the platelets can be adjusted using the self-seeding strategy by fixing the unimer-to-seed ratio and varying the annealing temperature (Supplementary Tables 13 and 14 and Supplementary Fig. 44). However, the size control achieved with this method is not as precise as that in the seeded growth approach, which adjusts the amount of added unimers. To demonstrate the facile nature of expanding this reactor cascade, another reactor was added to allow the production of multilayered fluorescent platelets (Supplementary Fig. 45). To further increase the throughput, the total flow rate was increased to 2 ml min^{-1}, which is based on the successful seed preparation at this flow rate. As we expected, uniform platelets can still be obtained at the increased flow rate (Supplementary Fig. 46), and these platelets are of an even higher uniformity owing to better mixing at higher flow rates. Therefore, the timescale to prepare platelets from polymers was reduced to 3 min, and the throughput increased to 2.2 mg min^{-1} (132 mg h^{-1}).

For comparison, we summarized the timescale and throughput of the production of the reported PCL-based platelets and platelets of other core chemistries (poly(ferrocenyldimethylsilane)[2,40], poly(L-lactide) (PLLA)[41] and conjugated polymers[42,43]) prepared by living CDSA (Fig. 4b and Supplementary Fig. 47). Our work demonstrates an efficient method for preparing size-controllable platelets through CDSA, with a significant reduction in processing timescale (>240 times) and improvement in throughput (>60 times) compared with previous works. Compared with PI-CDSA, another scale-up strategy for CDSA, our flow method offers superior size control and reproducibility[16–18]. The high efficiency was achieved through excellent heat transfer in the flow cascade for seed preparation, combined with ideal mixing and the fast crystallization rate induced by high concentration.

To demonstrate the scope and potential of the flow cascade technique, we used PCL-based polymers with various chemistries to synthesize functional and complex platelets. Double-layered platelets with different corona chemistries were prepared using the integrated flow cascade, with two living CDSA modules connected in series (Supplementary Table 15). Due to the different stain adsorption capacities of coronas, platelets with heterogeneous coronas exhibited different patterns after staining (Supplementary Fig. 48). In addition to tuning the corona chemistry, the core chemistry was also modified using fluorescent-dye-labelled PCLs. By leveraging the differences in crystallization rates of PCLs with different molecular weights, various fluorescent patterns were prepared (Supplementary Table 16 and Supplementary Fig. 49). These patterns can be further tuned by easily adjusting the relative flow rates in a four-way flow cascade (Supplementary Fig. 49a).

Building on this, we extended our method to PLLA-based polymers (Supplementary Figs. 50–53 and Supplementary Tables 17 and 18), which are also biocompatible and biodegradable, but it has proven challenging to obtain dimensional control over them in CDSA[6,41,44–46]. Using the same flow set-up, we synthesized PLLA-based rhombic platelets with tunable sizes through living CDSA (Supplementary Fig. 54 and Supplementary Table 19). This method's ability to control the platelet size in PLLA block polymers via seeded growth showcases its versatility, precision and scalability. The ability to fine-tune platelet dimensions highlights the broad applicability of our approach and its potential for advancing precision polymer self-assembly. Overall, these results underscore the unique advantages of our technique, offering a powerful, scalable and precise method for developing diverse and complex nanostructures.

Conclusions

This study presents an advance in polymer nanoparticle preparation via CDSA by integrating seed formation and living growth within a flow cascade reactor. This integration reduces the processing time from a week to 3 min and improves the throughput to 132 mg h^{-1}, surpassing

other methods by orders of magnitude. The use of flash-freezing for seed preparation shortens batch processing times, with potential benefits for other CDSA systems to enhance efficiency. By optimizing experimental parameters and utilizing a modular reactor design, this study seamlessly integrates CDSA and flow synthesis, enabling the rapid, controlled production of uniform anisotropic polymer nanoparticles. Overall, this advance opens possibilities for programmable material design, allowing precise control over nanostructure properties and marking a meaningful step forward in high-throughput polymer nanomaterial synthesis.

Methods

Preparation of homopolymer

Homopolymers were prepared by ring-opening polymerization in a glovebox filled with N_2. ε-Caprolactone (2.246 g, 19.68 mmol), diphenylphosphate (70.33 mg, 0.28 mmol), 2-cyano-5-hydroxypentan -2-yl-ethyl carbonotrithioate (70 mg, 0.28 mmol) and toluene (19.726 ml) were charged into a 50 ml round-bottom flask. The mixture was stirred at room temperature, and ^{1}H NMR spectroscopy was used for monitoring. After approximately 6.5 h, the reaction was quenched using AmberLyst agent, and the solution was removed from the glovebox. The product was purified by precipitation three times in cold diethyl ether and collected through centrifugation. A yield of 1.42 g (monomer conversion 71%) of light-yellow solid was obtained after thorough drying in a vacuum oven.

Preparation of diblock polymer

PCL-*b*-PDMA was prepared by chain extension of PCL homopolymer. Here, PCL_{50} (100 mg, 0.0168 mmol), *N,N*-dimethyl acrylamide (400 mg, 4.03 mmol), 2,2'-azobis(2-methylpropionitrile) (0.276 mg, 0.00168 mmol, 10 mg ml^{-1} in dioxane) and dioxane (1 ml) were added into an ampoule. Before immersion in an oil bath set at 70 °C, the solution was freeze-pump-thawed three times. After 2 h, polymerization was quenched by immersing the ampoule in the liquid N_2. Once it reached room temperature, the crude product was precipitated three times into the cold diethyl ether and collected by centrifugation. Then, 428 mg (monomer conversion 88%) of a solid was obtained after thoroughly drying in the vacuum oven.

Flash-frozen seeds prepared in batch reactors

Typically, batch preparation of flash-frozen seeds was carried out in a 7 ml vial with the polymer concentration maintained at 0.1 mg ml^{-1}. Specifically, 4 µl of PCL-*b*-PDMA stock solution (50 mg ml^{-1} in tetrahydrofuran) was introduced into 2 ml of ethanol. The mixture was heated to 75 °C for a specified duration (1–60 min) and then rapidly cooled by immersion into a dry-ice–acetone bath (or ice bath and natural cooling) for several minutes (1–5 min). The resulting seed micelles were obtained after equilibration to room temperature. Seed samples of different concentrations were prepared by tuning the addition of PCL-*b*-PDMA stock solution.

Flash-frozen seeds prepared in flow reactors

The flow reactor was set up as shown in Supplementary Fig. 35. A high-performance liquid chromatography pump (Jasco PU-980) was connected to a steel coil (inner diameter 0.75 mm, 2 ml), which was immersed in an oil bath set at 75 °C. A polytetrafluoroethylene tubing (inner diameter 0.5 mm, 2 ml) was connected downstream of the heating component, of which a winding component (0.5 ml) and a coil (0.5 ml) was controlled at −78 °C using a dry-ice–acetone bath, and the following equilibration coil (1 ml) was set at room temperature. The winding tubing, designed to enhance mixing in flow, was created by winding polytetrafluoroethylene tubing in an S shape around the tip holder (SureOne Pipet Tips, Fisher).The diblock polymer solution (PCL-*b*-PDMA, 0.1 mg ml^{-1} in ethanol), prepared as described, was injected by the high-performance liquid chromatography pump at various flow rates (1, 2 and 4 ml min^{-1}), and steady samples were collected after passing 12 ml polymer solution (three times the reactor volumes).

Continuous end-to-end preparation of platelets in flow

The integral flow cascade to prepare platelets from polymers directly is shown in Supplementary Fig. 42. The polymer solution (PCL/PCL-*b*-PDMA = 3/97 (wt%), 0.1 mg ml^{-1} in ethanol) was initially pumped into a steel coil (inner diameter 0.75 mm, 2 ml) set at 75 °C and then passed through the cooling channel set at −78 °C, which included winding (inner diameter 0.5 mm, 0.5 ml) and coil (inner diameter 0.5 mm, 0.5 ml) parts. After passing through the annealing channel at 30 °C (inner diameter 0.5 mm, 1 ml), the seed solution was mixed with unimers in a reverse T micromixer. An ageing channel was set downstream, which included a winding tubing (inner diameter 0.5 mm, 0.5 ml) followed by a coil (inner diameter 0.5 mm, 1.5 ml). Platelets were collected from the outlet. The self-seeding strategy was conducted to tune the size of platelets by setting the annealing channel at various temperatures (28, 30, 32 and 34 °C) and fixing a unimer-to-seed ratio of 10 (Supplementary Fig. 44a). To prepare layered platelets, another reverse T mixer and ageing channel was connected downstream. To prepare platelets with tunable core chemistry, the reverse T micromixer was replaced by a four-way cross micromixer (Supplementary Fig. 49a).

Data availability

The data supporting the findings of this study are available within this Article and its Supplementary Information.

References

1. Wang, X. et al. Cylindrical block copolymer micelles and co-micelles of controlled length and architecture. *Science* **317**, 644–647 (2007).
2. Qiu, H. et al. Uniform patchy and hollow rectangular platelet micelles from crystallizable polymer blends. *Science* **352**, 697–701 (2016).
3. Cai, J. et al. Tailored multifunctional micellar brushes via crystallization-driven growth from a surface. *Science* **366**, 1095–1098 (2019).
4. Tian, J. et al. Tailored self-assembled photocatalytic nanofibres for visible-light-driven hydrogen production. *Nat. Chem.* **12**, 1150–1156 (2020).
5. Pearce, A. K., Wilks, T. R., Arno, M. C. & O'Reilly, R. K. Synthesis and applications of anisotropic nanoparticles with precisely defined dimensions. *Nat. Rev. Chem.* **5**, 21–45 (2020).
6. Arno, M. C. et al. Exploiting the role of nanoparticle shape in enhancing hydrogel adhesive and mechanical properties. *Nat. Commun.* **11**, 1420 (2020).
7. Jin, X.-H. et al. Long-range exciton transport in conjugated polymer nanofibers prepared by seeded growth. *Science* **360**, 897–900 (2018).
8. MacFarlane, L., Zhao, C., Cai, J., Qiu, H. & Manners, I. Emerging applications for living crystallization-driven self-assembly. *Chem. Sci.* **12**, 4661–4682 (2021).
9. Ganda, S. & Stenzel, M. H. Concepts, fabrication methods and applications of living crystallization-driven self-assembly of block copolymers. *Prog. Polym. Sci.* **101**, 101195 (2020).
10. Tong, Z. et al. Uniform segmented platelet micelles with compositionally distinct and selectively degradable cores. *Nat. Chem.* **15**, 824–831 (2023).
11. Liu, L. et al. Synthesis of hollow platelet polymer particles by spontaneous precision fragmentation. *Nat. Synth.* **3**, 903–912 (2024).
12. Xie, Y. et al. 2D hierarchical microbarcodes with expanded storage capacity for optical multiplex and information encryption. *Adv. Mater.* **36**, 2308154 (2023).

13. Xia, T. et al. Tuning the functionality of self-assembled 2D platelets in the third dimension. *J. Am. Chem. Soc.* **145**, 25274–25282 (2023).
14. Arno, M. C. et al. Precision epitaxy for aqueous 1D and 2D poly(ε-caprolactone) assemblies. *J. Am. Chem. Soc.* **139**, 16980–16985 (2017).
15. Jiang, J. et al. Polyferrocenylsilane block copolymer spherulites in dilute solution. *J. Am. Chem. Soc.* **145**, 1247–1261 (2023).
16. Ellis, C. E., Garcia-Hernandez, J. D. & Manners, I. Scalable and uniform length-tunable biodegradable block copolymer nanofibers with a polycarbonate core via living polymerization-induced crystallization-driven self-assembly. *J. Am. Chem. Soc.* **144**, 20525–20538 (2022).
17. Boott, C. E., Gwyther, J., Harniman, R. L., Hayward, D. W. & Manners, I. Scalable and uniform 1D nanoparticles by synchronous polymerization, crystallization and self-assembly. *Nat. Chem.* **9**, 785–792 (2017).
18. Hurst, P. J., Rakowski, A. M. & Patterson, J. P. Ring-opening polymerization-induced crystallization-driven self-assembly of poly-L-lactide-block-polyethylene glycol block copolymers (ROPI-CDSA). *Nat. Commun.* **11**, 4690 (2020).
19. Song, S. et al. Uniform 1D micelles and patchy & block comicelles via scalable, one-step crystallization-driven block copolymer self-assembly. *J. Am. Chem. Soc.* **143**, 6266–6280 (2021).
20. Wong, C. K., Lai, R. Y. & Stenzel, M. H. Dynamic metastable polymersomes enable continuous flow manufacturing. *Nat. Commun.* **14**, 6237 (2023).
21. Zhang, W. et al. Accelerated discovery of molecular nanojunction photocatalysts for hydrogen evolution by using automated screening and flow synthesis. *Nat. Synth.* **3**, 595–605 (2024).
22. He, Y. et al. Uniform biodegradable fiber-like micelles and block comicelles via 'living' crystallization-driven self-assembly of poly(L-lactide) block copolymers: the importance of reducing unimer self-nucleation via hydrogen bond disruption. *J. Am. Chem. Soc.* **141**, 19088–19098 (2019).
23. Mihut, A. M., Drechsler, M., Möller, M. & Ballauff, M. Sphere-to-rod transition of micelles formed by the semicrystalline polybutadiene-block-poly(ethylene oxide) block copolymer in a selective solvent. *Macromol. Rapid Commun.* **31**, 449–453 (2010).
24. Gerdts, C. J. et al. Time-controlled microfluidic seeding in nl-volume droplets to separate nucleation and growth stages of protein crystallization. *Angew. Chem. Int. Ed.* **45**, 8156–8160 (2006).
25. Zhang, Q. et al. Formation of protein nanoparticles in microdroplet flow reactors. *ACS Nano* **17**, 11335–11344 (2023).
26. Coquerel, G. Crystallization of molecular systems from solution: phase diagrams, supersaturation and other basic concepts. *Chem. Soc. Rev.* **43**, 2286–2300 (2014).
27. Threlfall, T. L. & Coles, S. J. A perspective on the growth-only zone, the secondary nucleation threshold and crystal size distribution in solution crystallisation. *CrystEngComm* **18**, 369–378 (2016).
28. Ming, H. et al. A review of solvent freeze-out technology for protein crystallization. *CrystEngComm* **23**, 2723–2732 (2021).
29. Xiao, L., Parkinson, S. J., Xia, T., Edge, P. & O'Reilly, R. K. Enhancing the scalability of crystallization-driven self-assembly using flow reactors. *ACS Macro Lett.* **12**, 1636–1641 (2023).
30. Adamo, A. et al. On-demand continuous-flow production of pharmaceuticals in a compact, reconfigurable system. *Science* **352**, 61–67 (2016).
31. Slattery, A. et al. Automated self-optimization, intensification, and scale-up of photocatalysis in flow. *Science* **383**, eadj1817 (2024).
32. Zaquen, N. et al. Polymer synthesis in continuous flow reactors. *Prog. Polym. Sci.* **107**, 101256 (2020).
33. Plutschack, M. B., Pieber, B., Gilmore, K. & Seeberger, P. H. The Hitchhiker's guide to flow chemistry. *Chem. Rev.* **117**, 11796–11893 (2017).
34. Rizis, G., van de Ven, T. G. M. & Eisenberg, A. 'Raft' formation by two-dimensional self-assembly of block copolymer rod micelles in aqueous solution. *Angew. Chem. Int. Ed.* **53**, 9000–9003 (2014).
35. Guerin, G. et al. Lateral growth of 1D core-crystalline micelles upon annealing in solution. *Macromolecules* **49**, 7004–7014 (2016).
36. Guerin, G., Rupar, P. A., Manners, I. & Winnik, M. A. Explosive dissolution and trapping of block copolymer seed crystallites. *Nat. Commun.* **9**, 1158 (2018).
37. Yu, W., Foster, J. C., Dove, A. P. & O'Reilly, R. K. Length control of biodegradable fiber-like micelles via tuning solubility: A self-seeding crystallization-driven self-assembly of poly(ε-caprolactone)-containing triblock copolymers. *Macromolecules* **53**, 1514–1521 (2020).
38. Wang, K., Zhang, H., Shen, Y., Adamo, A. & Jensen, K. F. Thermoformed fluoropolymer tubing for in-line mixing. *Reac. Chem. Eng.* **3**, 707–713 (2018).
39. Mehraji, S. & DeVoe, D. L. Microfluidic synthesis of lipid-based nanoparticles for drug delivery: recent advances and opportunities. *Lab Chip* **24**, 1154–1174 (2024).
40. Deng, R. et al. Role of competitive crystallization kinetics in the formation of 2D platelets with distinct coronal surface patterns via seeded growth. *J. Am. Chem. Soc.* **144**, 19051–19059 (2022).
41. He, X. et al. Two-dimensional assemblies from crystallizable homopolymers with charged termini. *Nat. Mater.* **16**, 481–488 (2017).
42. Yun, N. et al. Size-tunable semiconducting 2D nanorectangles from conjugated polyenyne homopolymer synthesized via cascade metathesis and metallotropy polymerization. *J. Am. Chem. Soc.* **145**, 9029–9038 (2023).
43. Yang, S., Kang, S.-Y. & Choi, T.-L. Semi-conducting 2D rectangles with tunable length via uniaxial living crystallization-driven self-assembly of homopolymer. *Nat. Commun.* **12**, 2602 (2021).
44. Chakraborty, C., Rajak, A. & Das, A. Shape-tunable two-dimensional assemblies from chromophore-conjugated crystallizable poly(l-lactides) with chain-length-dependent photophysical properties. *Nanoscale* **16**, 13019–13028 (2024).
45. Xie, Y., Yu, W., Xia, T., O'Reilly, R. K. & Dove, A. P. Stereocomplex-driven morphological transition of coil–rod–coil poly(lactic acid)-based cylindrical nanoparticles. *Macromolecules* **56**, 7689–7697 (2023).
46. Sun, L. et al. Structural reorganization of cylindrical nanoparticles triggered by polylactide stereocomplexation. *Nat. Commun.* **5**, 5746 (2014).
47. Dong, B., Zhou, T., Zhang, H. & Li, C. Y. Directed self-assembly of nanoparticles for nanomotors. *ACS Nano* **7**, 5192–5198 (2013).
48. Qi, H., Zhou, T., Mei, S., Chen, X. & Li, C. Y. Responsive shape change of sub-5 nm thin, janus polymer nanoplates. *ACS Macro Lett.* **5**, 651–655 (2016).
49. Qi, H., Wang, W. & Li, C. Y. Janus polymer single crystal nanosheet via evaporative crystallization. *ACS Macro Lett.* **3**, 675–678 (2014).
50. Zhou, T., Wang, B., Dong, B. & Li, C. Y. Thermoresponsive amphiphilic Janus silica nanoparticles via combining 'polymer single-crystal templating' and 'grafting-from' methods. *Macromolecules* **45**, 8780–8789 (2012).
51. Hu, W. et al. Comonomer inclusion in single crystals of isodimorphic random copolymers of butylene succinate and ε-caprolactone. *Macromolecules* **56**, 5058–5067 (2023).
52. Tong, Z. et al. Spatially restricted templated growth of poly(ε-caprolactone) from carbon nanotubes by crystallization-driven self-assembly. *Macromolecules* **54**, 2844–2851 (2021).

53. Xia, T. et al. Control over aspect ratio and polymer spatial distribution of 2D platelets via living crystallization-driven self-assembly. *Macromolecules* **57**, 11210–11220 (2024).
54. Su, Y. et al. Hydrogen-bond-regulated platelet micelles by crystallization-driven self-assembly and templated growth for poly(ε-caprolactone) block copolymers. *Macromolecules* **55**, 1067–1076 (2022).
55. Zhang, X. et al. Uniform two-dimensional crystalline platelets with tailored compositions for pH stimulus-responsive drug release. *Biomacromolecules* **24**, 1032–1041 (2023).
56. Xiang, B. et al. Regulation of two-dimensional platelet micelles by dynamic changing of polymer topological architectures upon light irradiation. *Macromolecules* **56**, 9685–9696 (2023).
57. Liu, L., Zhu, L., Chu, Z. & Tong, Z. Seeded epitaxial growth of crystallizable polymers governed by crystallization temperatures. *Macromolecules* **56**, 5984–5992 (2023).
58. Zhu, L., Xiang, B., Su, Y. & Tong, Z. Chemical shield effect of metal complexation on seeded growth of poly(ε-caprolactone) core-forming blends. *Polymer* **272**, 125831 (2023).
59. Wang, J., Zhu, W., Peng, B. & Chen, Y. A facile way to prepare crystalline platelets of block copolymers by crystallization-driven self-assembly. *Polymer* **54**, 6760–6767 (2013).
60. Wang, J., Lu, Y. & Chen, Y. Fabrication of 2D surface-functional polymer platelets via crystallization-driven self-assembly of poly(ε-caprolactone)-contained block copolymers. *Polymer* **160**, 196–203 (2019).
61. Zhu, W. et al. Bamboo leaf-like micro-nano sheets self-assembled by block copolymers as wafers for cells. *Macromol. Biosci.* **14**, 1764–1770 (2014).
62. Rizis, G., van de Ven, T. G. M. & Eisenberg, A. Homopolymers as structure-driving agents in semicrystalline block copolymer micelles. *ACS Nano* **9**, 3627–3640 (2015).
63. Du, Z.-X., Xu, J.-T. & Fan, Z.-Q. Micellar morphologies of pol y(ε-caprolactone)-*b*-poly(ethylene oxide) block copolymers in water with a crystalline core. *Macromolecules* **40**, 7633–7637 (2007).
64. Du, Z.-X., Xu, J.-T. & Fan, Z.-Q. Regulation of micellar morphology of PCL-*b*-PEO block copolymers by crystallization temperature. *Macromol. Rapid Commun.* **29**, 467–471 (2008).
65. He, W.-N., Xu, J.-T., Du, B.-Y., Fan, Z.-Q. & Wang, X. Inorganic-salt-induced morphological transformation of semicrystalline micelles of PCL-*b*-PEO block copolymer in aqueous solution. *Macromol. Chem. Phys.* **211**, 1909–1916 (2010).
66. He, W.-N., Xu, J.-T., Du, B.-Y., Fan, Z.-Q. & Sun, F.-L. Effect of pH on the micellar morphology of semicrystalline PCL-*b*-PEO block copolymers in aqueous solution. *Macromol. Chem. Phys.* **213**, 952–964 (2012).
67. Su, M., Huang, H., Ma, X., Wang, Q. & Su, Z. Poly(2-vinylpyridin e)-block-poly(ε-caprolactone) single crystals in micellar solution. *Macromol. Rapid Commun.* **34**, 1067–1071 (2013).
68. Wang, J. et al. Effect of block ratios on self-assembly morphologies of poly(ε-caprolactone)-block-poly(*tert*-butyl acrylate) block copolymer. *Polymer* **284**, 126292 (2023).
69. Ganda, S., Wong, C. K. & Stenzel, M. H. Corona-loading strategies for crystalline particles made by living crystallization-driven self-assembly. *Macromolecules* **54**, 6662–6669 (2021).
70. Ganda, S. et al. Two-dimensional self-assembled structures of highly ordered bioactive crystalline-based block copolymers. *Macromolecules* **50**, 8544–8553 (2017).
71. Ganda, S. et al. Macrophage-targeting and complete lysosomal degradation of self-assembled two-dimensional poly(ε-caprolactone) platelet particles. *ACS Appl. Mater. Interfaces* **14**, 35333–35343 (2022).
72. Cha, Y. et al. Crystallization-driven self-assembly of metallo-polyelectrolyte block copolymers with a polycaprolactone core-forming segment. *ACS Macro Lett.* **8**, 835–840 (2019).

Acknowledgements

We thank the University of Birmingham and China Scholarship Council for funding and support.

Author contributions

R.K.O., L.X. and A.P.D. conceived the work. L.X., T.X. and R.K.O. designed the experiments. L.X., T.X., J.Z., S.J.P. and J.Y.R. performed the experiments. All authors contributed to the analysis of the data. R.K.O. and A.P.D. directed the research. L.X., A.P.D. and R.K.O. prepared the manuscript, and all authors contributed to manuscript revisions.

Competing interests

The authors declare no competing interests.

Additional information

Supplementary information The online version contains supplementary material available at https://doi.org/10.1038/s44160-025-00767-x.

Correspondence and requests for materials should be addressed to Andrew P. Dove or Rachel K. O' Reilly.

Peer review information *Nature Synthesis* thanks Chun Feng and the other, anonymous, reviewer(s) for their contribution to the peer review of this work. Primary Handling Editor: Alexandra Groves, in collaboration with the *Nature Synthesis* team.

3.2 Supporting Information

nature synthesis

Supplementary information

https://doi.org/10.1038/s44160-025-00767-x

Direct preparation of two-dimensional platelets from polymers enabled by accelerated seed formation

In the format provided by the authors and unedited

Table of Contents

Materials

Diphenylphosphate (DPP, ≥99%, Sigma Aldrich) was dried using P_2O_5 before being kept in the glove box. ε-caprolactone (≥99%, ACROS Organics) was dried with CaH_2, distilled, and then stored in the glovebox filled with N_2. L-Lactide was purchased from Corbion-Purac, recrystallized once from dichloromethane and twice from toluene, and subsequently transferred to the glovebox. 1,8-Diazabicyclo[5.4.0]undec-7-ene (DBU) was distilled over CaH_2 and then stored in the glovebox. The dual-functional chain transfer agent (CTA), 2-cyano-5-hydroxypentan-2-yl-ethyl carbonotrithioate (CHPET) was prepared according to our previous work.[1, 2] 2,2'-Azobis(2-methylpropionitrile) (AIBN, ≥98%, Sigma Aldrich) was recrystallized in methanol and stored at 4 °C in the dark before use. 1,4-dioxane (anhydrous, ≥99.8%, Fisher Scientific) and *N,N*-dimethyl acrylamide (DMA, ≥99%, Sigma Aldrich contains 500 ppm monomethyl ether hydroquinone as inhibitor) was purified with basic alumina every time before use. Ethanol (anhydrous, ≥99.5%, Fisher Scientific), diethyl ether (anhydrous, ≥99.0%, Fisher Scientific), and chloroform ($CHCl_3$, anhydrous, ≥99%, Sigma Aldrich) were used as received.

Instrumentation

Nuclear magnetic resonance (NMR), using deuterated chloroform ($CDCl_3$) as the solvent, was performed using a Bruker DPX-400 (400 MHz) spectrometer. MestReNova x64 software was employed for spectra analysis. Size-exclusion chromatography (SEC) was conducted using an Agilent 390-MDS system coupled with PLgel Mixed-D type columns, and signals were detected by refractive index (RI) and ultraviolet (UV) detectors. Elution was performed using chloroform with 0.5% NEt_3, and the flow rate was set at 1 $mL \cdot min^{-1}$. Calibration against polystyrene (PS) standards using Agilent SEC software was employed to determine number-average (M_n) and weight-average (M_w) molecular weights as well as dispersity ($Đ_M$). Dynamic light scattering (DLS) was performed at 25 °C using a Malvern Zetasizer Nano ZS with a 4 mW He-Ne 633 nm laser module. Measurements were carried out at an angle of 173° (back scattering), and Malvern DTS v7.03 software was used to determine results, such as hydrodynamic diameters (D_h) and size dispersity. D_h values were calculated using the StokesEinstein equation where particles are assumed to be spherical. Z-average was taken as the value

for size, and reported size distribution was based on scattering intensity. Confocal Laser Scanning Microscopy (CLSM) was performed using a FV3000 (Olympus) confocal microscope coupled with a IX-81 inverted base (Olympus) and the 20x and 60x oil lens (Olympus). The FV3000 system was driven with the FV31S-SW Viewer software platform (Olympus) with scan rates of 1 μs pixel^{-1} at 515 by 512 pixel^{-1} to 1024 by 1024 pixel^{-1}. Nano differential scanning calorimetry (Nano DSC) was conducted on a TA NanoDSC with 300 μL samples (1 mg mL^{-1}), using a heating and cooling rate of 1 °C min^{-1} under a constant pressure of 3 atmospheres. Samples were degassed for 15 min prior to injection into the instrument and were corrected against a background of pure ethanol. Collected data were processed using NanoAnalyze Software.

Transmission electron microscope (TEM) images were captured on a Jeol 1400 Bio TEM microscope with an acceleration voltage of 80 kV. Samples were prepared by drop cast 8 μL of solution on formvar-coated copper grids and then blotting away with filter paper. For seed samples, another 8 μL of aqueous uranyl acetate solution (1 wt%) was dropped on the grid for staining, and the excess was removed by filter paper. Samples were dried overnight in a desiccator box before testing. Using ImageJ software, at least 100 particles were analyzed to calculate the average size.

The number average length (L_n) and weight average length (L_w) were calculated according to equations (1) and (2), and the distribution was determined by L_w/L_n.

$$L_n = \frac{\sum_{i=1}^{n} N_i L_i}{\sum_{i=1}^{n} N_i} \qquad (1)$$

$$L_n = \frac{\sum_{i=1}^{n} N_i {L_i}^2}{\sum_{i=1}^{n} N_i L_i} \qquad (2)$$

Similarly, the number average width (W_n), weight average width (W_w), number average area (A_n), and weight average area (A_w) were calculated according to equations (3) to (6), and their distributions were defined as W_w/W_n and A_w/A_n.

$$W_n = \frac{\sum_{i=1}^{n} N_i W_i}{\sum_{i=1}^{n} N_i} \quad (3)$$

$$W_w = \frac{\sum_{i=1}^{n} N_i {W_i}^2}{\sum_{i=1}^{n} N_i W_i} \quad (4)$$

$$A_n = \frac{\sum_{i=1}^{n} N_i A_i}{\sum_{i=1}^{n} N_i} \quad (5)$$

$$A_w = \frac{\sum_{i=1}^{n} N_i {A_i}^2}{\sum_{i=1}^{n} N_i A_i} \quad (6)$$

Methods

Polycaprolactone (PCL)-RAFT agent

PCL-RAFT agent (PCL-CHPET) was prepared by ring-opening polymerization in the glovebox filled with N_2. ε-Caprolactone (2.246 g, 19.68 mmol), diphenylphosphate (DPP, 70.33 mg, 0.28 mmol), CHPET (70 mg, 0.28 mmol), and toluene (19.726 mL) were charged into a 50 mL round-bottom flask. The mixture was stirred at room temperature, and ^{1}H NMR spectroscopy was used for monitoring. After approximately 6.5 h, the reaction was quenched using the Amberlyst agent, and the solution was removed from the glove box. The product was purified by precipitation three times in cold diethyl ether and collected through centrifugation. A yield of 1.42 g (monomer conversion: 71%) of light-yellow solid was obtained after thorough drying in a vacuum oven.

^{1}H NMR (400 MHz, Chloroform-d, δ (ppm)): 4.12 (t, J = 6.2 Hz, 2H), 4.06 (t, J = 6.7 Hz, 100H), 3.65 (t, J = 6.5 Hz, 2H), 3.35 (q, J = 7.4 Hz, 2H), 2.30 (t, J = 7.5 Hz, 100H), 1.88 (s, 3H), 1.71 – 1.59 (m, 200H), 1.44 – 1.31 (m, 100H).

Polycaprolactone-*b*-polydimethylacrylamide (PCL-*b*-PDMA)

DMA was polymerized from a PCL containing RAFT agent (PCL-CHPET) to form diblock polymer polycaprolactone-*b*-polydimethylacrylamide (PCL-*b*-PDMA). Herein, PCL_{50} (100 mg, 0.0168 mmol), DMA (400 mg, 4.03 mmol), AIBN (0.276 mg, 0.00168 mmol, 10 mg mL^{-1} in dioxane), and dioxane (1 mL) were added into an ampoule. Before immersed in an oil bath set at 70 °C, the solution was freeze-pump-thawed three times. After 2 hours, polymerization was quenched by immersing the ampoule in the liquid N_2. Once it reached room temperature, the crude product was precipitated three times into the cold diethyl ether and collected by centrifugation., 428 mg (monomer conversion: 88%) of a solid was obtained after fully dried in the vacuum oven.

^{1}H NMR (400 MHz, Chloroform-d, δ (ppm)): 4.05 (t, J = 6.7 Hz, 100H), 3.19 – 2.76 (m, 1290H), 2.30 (t, J = 7.5 Hz, 100H), 1.64 (m, 200H), 1.43 – 1.32 (m, 100H).

Naphthalene monoimide (NMI) functionalized polycaprolactone (NMI-PCL)

A hydroxy-functionalized naphthalene monoimide (NMI-OH) was synthesized following the literature.[3] NMI-PCL was prepared using NMI as the initiator for ROP. Specifically, NMI (78.2 mg, 0.24 mmol), ε-caprolactone (1.93 g, 16.87 mmol), DPP (60.3 mg, 0.24 mmol), and toluene (16.9 mL) were charged into a 50 mL round-bottom flask. Polymerization was conducted at room temperature for approximately 10 h. Subsequently, the same procedures were employed for product purification. Finally, 1 g (monomer conversion: 71%) of yellow solid was obtained after complete drying in a vacuum oven.

^{1}H NMR (400 MHz, Chloroform-d, δ (ppm)): 4.06 (t, J = 6.7 Hz, 106H), 3.24 (t, J = 5.3 Hz, 4H), 2.30 (t, J = 7.5 Hz, 106H), 1.89 (t, J = 5.6 Hz, 4H), 1.72 – 1.59 (m, 212H), 1.43 – 1.33 (m, 106H).

Poly(L-lactide) (PLLA)-RAFT agent

PLLA was prepared by ring-opening polymerization in the glovebox filled with N_2. L-Lactide (600 mg, 5.26 mmol), DBU (9.4 μL, 0.06 mmol), CHPET (52 mg, 0.21 mmol), and dichloromethane (9.75 mL) were charged into a 20-mL vial. The mixture was stirred at room temperature for 2 minutes. The product was purified by precipitation once in hexane and twice in methanol. After being dried in vacuo, 280 mg (monomer conversion: 50%) of a yellow solid was obtained.

^{1}H NMR (400 MHz, Chloroform-d, δ (ppm)): 5.27 – 5.05 (m, 24H), 3.35 (q, J = 7.5 Hz, 2H), 1.87 (d, J = 1.4 Hz, 3H), 1.65 – 1.45 (m, 72H).

Poly(L-lactide)-*b*-poly(2-(dimethylamino)ethyl methacrylate) (PLLA-*b*-PDMAEMA)

$PLLA_{45}$ (100 mg, 0.019 mmol), DMAEMA (1.05 g, 6.69 mmol), AIBN (0.61 mg, 0.0037 mmol, 10 mg mL^{-1} in dioxane), and dioxane (2 mL) were added into an ampoule. Before being immersed in an oil bath set at 70 °C, the solution was freeze-pump-thawed three times. After 7.5 hours, polymerization was quenched by immersing the ampoule in the liquid N_2. Once it reached room temperature, the crude product was precipitated three times into the cold diethyl ether and collected by centrifugation. 622 mg (monomer conversion: 52%) of a solid was obtained after fully dried in the vacuum oven.

^{1}H NMR (400 MHz, Chloroform-d, δ (ppm)): 5.16 (q, J = 7.1 Hz, 90H), 4.15 – 3.97 (m, 366H), 2.64 – 2.50 (m, 366H), 2.28 (s, 1098H), 1.98 – 1.78 (m, 366H), 1.61 – 1.54 (m, 270H), 1.12 – 0.82 (m, 549H).

Flash-frozen seeds prepared in batch reactors

Batch preparation of flash-frozen seeds was carried out in 7 mL vials. Specifically, for seed samples with the polymer concentration of 0.1 mg mL^{-1}, 4 μL of PCL-*b*-PDMA stock solution (50 mg mL^{-1} in THF) was introduced into 2 mL of ethanol. The mixture was heated to 75 °C for a specified duration (1-60 min) and then rapidly cooled by immersion into a dry ice-acetone bath (or ice bath and natural cooling) for several minutes (1-5 min). The resulting seed micelles were obtained after equilibration to room temperature. Seed samples of different concentrations were prepared by tuning the addition of PCL-*b*-PDMA stock solution.

Preparation of seeds by traditional CDSA and sonication

Normal seeds were prepared using the method previously reported.[1] In this procedure, 10 mg of PCL-*b*-PDMA was added to 2 mL of ethanol and heated at 75 °C for 3 h. After cooling to room temperature, the sample was aged for 7 days, resulting in long polydisperse cylindrical structures. Seeds were obtained by sonicating these cylinders in a dry ice-acetone bath for 20 min.

Living CDSA in batch reactors

Batch living CDSA was conducted at 1 mL scale, where 100 μL flash-frozen seeds (0.1 mg mL^{-1} in ethanol) were added to 900 μL ethanol, or 20 μL classical seeds (0.5 mg mL^{-1} in ethanol) prepared by sonicating cylinders were added to 980 μL ethanol. The solution was preheated at 30 °C for 2 min. Then, 10 μL unimer solution (10 mg mL^{-1} in $CHCl_3$, PCL/PCL-*b*-PDMA = 1:1 wt%) was added, and platelets were obtained after another 2-min aging.

Flash-frozen seeds prepared in flow reactors

The flow reactor was set up as shown in Figure S35. A High-Performance Liquid Chromatography (HPLC) pump (Jasco PU-980) was connected to a steel coil (inner diameter: 0.75 mm, 2 mL), which was immersed in an oil bath set at 75 °C. A PTFE tubing (inner diameter: 0.5 mm, 2 mL) was connected downstream of the heating component, of which a winding component (0.5 mL) and a coil (0.5 mL) was controlled at -78 °C using a dry ice-acetone bath, and the following equilibration coil (1 mL) was set at room temperature. The winding tubing, designed to enhance mixing in flow, was created by winding PTFE tubing in an S-shape around the tip holder (SureOne^{TM} Pipet Tips, Fisher brand). The diblock polymer solution (PCL-*b*-PDMA, 0.1 mg mL^{-1} in ethanol), prepared as described, was injected by the HPLC pump at various flow rates (1, 2, and 4 mL min^{-1}), and steady samples were collected after passing 12 mL polymer solution (3 times of the reactor volumes).

Detached living CDSA in flow reactors

The flow setup was modified according to our previous work (Figure S37a).[1] Flash-frozen seeds obtained from the flow reactor were dilute to 0.01 mg mL^{-1}, and then pumped into the flow reactor using the HPLC pump (Jasco PU-980) at 0.2 mL min^{-1}. After passing through the coil (inner diameter: 0.75 mm, 0.2 mL) set at 30 °C, flash-frozen seeds were mixed with unimer injected using a syringe pump at 0.002 mL min^{-1} in a Y mixer. After aging in the downstream coil (inner diameter: 0.3 mm, 0.4 mL) set at 30 °C, platelets were collected from the outlet.

Thermostable seeds with PCL homopolymer prepared in flow

PCL homopolymer was introduced as an additive for thermostable flash-frozen seed preparation in the flow reactor. Briefly, a mixture of PCL and PCL-*b*-PDMA stock solution (50 mg mL^{-1} in THF, PCL ratio: 1-5 wt%) was added into warm ethanol (30-40 °C) and agitated. The resulting solution was employed for seed preparation in the flow reactor using the setup depicted in Figure S35. The temperature for equilibration coil was enhanced to 30 °C for the purpose of annealing.

Continuous end-to-end preparation of platelets in flow

The integral flow cascade to prepare platelets from polymers directly was shown in Figures S42. The polymer solution (PCL/PCL-*b*-PDMA = 3 / 97 (wt%), 0.1 mg mL^{-1} in ethanol) was initially pumped into a steel coil (inner diameter: 0.75 mm, 2 mL) set at 75 °C, and then passed through the cooling channel set at -78 °C, which included a winding (inner diameter: 0.5 mm, 0.5 mL) and a coil (inner diameter: 0.5 mm, 0.5 mL) parts. After passing through the annealing channel at 30 °C (inner diameter: 0.5 mm, 1 mL), the seed solution was mixed with unimer in a reverse T micromixer. An aging channel was set downstream, which included a winding tubing (inner diameter: 0.5 mm, 0.5 mL) followed by a coil (inner diameter: 0.5 mm, 1.5 mL). Platelets were collected from the outlet. Self-seeding strategy was conducted to tune the size of platelets by setting annealing channel at various temperatures (28, 30, 32, 34 °C) and fixing the unimer-to-seed ratio of 10 (Figure S44a). To prepare layered platelets, another reverse T mixer and aging channel was connected downstream. To prepare platelets with tunable core chemistry, the reverse T micromixer was replaced by a four-way cross micromixer (Figures S49a).

PLLA-based platelets prepared by the integral flow cascade

The same flow cascade was used to prepare PLLA-based platelets (Figures S42). PLLA-*b*-PDMAEMA solution (0.01 mg mL^{-1} in ethanol, prepared by introducing 100 μL of PLLA-*b*-PDMAEMA stock solution (10 mg mL^{-1} in $CHCl_3$) into 100 mL of ethanol) was initially pumped into a steel coil (inner diameter: 0.75 mm, 2 mL) set at 75 °C, and then passed through the cooling channel set at -78 °C, which included a winding (inner diameter: 0.5 mm, 0.5 mL) and a coil (inner diameter: 0.5 mm, 0.5 mL) parts. After passing through the annealing channel at 30 °C (inner diameter: 0.5 mm, 1 mL), the seed solution was mixed with unimer (PLLA/PLLA-*b*-PDMAEMA = 1/1, 10 mg mL^{-1} in $CHCl_3$) in a reverse T micromixer. An aging channel was set downstream, which included a winding channel (inner diameter: 0.5 mm, 0.5 mL) followed by a coil (inner diameter: 0.5 mm, 1.5 mL). Platelets were collected from the outlet.

Supplementary Table

Table S1. Characterization of PCL-based polymers.

Polymer	$M_{n,\,NMR}$ [a] (kg·mol^{-1})	$M_{n,\,GPC}$ [b] (kg·mol^{-1})	$Đ_{GPC}$ [b]
PCL_{50}	6.0	13.0	1.06
PCL_{50}-*b*-$PDMA_{215}$	27.3	33.0	1.14
NMI-PCL_{53}	6.4	13.6	1.07
PCL_{22}-G [c]	3.1	7.4	1.09
PCL_{73}-R [c]	9.1	20.4	1.08
PCL_{45}-*b*-$PDMAEMA_{160}$ [c]	30.4	40.4	1.23
PCL_{45}-*b*-$PNAM_{100}$ [c]	19.5	34.3	1.27
PCL_{45}-*b*-$P4VP_{220}$ [c]	28.4	26.8	1.56

[a] Results were determined by ^{1}H NMR.

[b] Results were determined by SEC, where signals were detected by refractive index (RI).

[c] PCL_{22}-G, PCL_{73}-R, PCL_{45}-*b*-poly(2-(dimethylamino)ethyl methacrylate) $(PDMAEMA)_{160}$, PCL_{45}-*b*-poly(4-acryloylmorpholine) $(PNAM)_{100}$, and PCL_{45}-*b*-poly(4-vinylpyridine) $(P4VP)_{220}$ were reported in our previous work.[4, 5]

Table S2. Various condition to prepare flash-frozen seeds and their size obtained from DLS.

Sample	Temperature (°C)	Heating Time (min)	Cooling Method	Cooling Time (min)	Concentration (mg ml^{-1})	Scale (mL)	Size (Z-average) (nm)	Dispersity	Size (intensity-average) (nm)
1	75	1	dry ice-acetone	1	0.1	2	50.9 ± 0.4	0.105 ± 0.014	69.4 ± 30.1
2	75	2	dry ice-acetone	1	0.1	2	49.9 ± 1.2	0.079 ± 0.034	52.0 ± 1.2
3	75	10	dry ice-acetone	1	0.1	2	49.2 ± 0.4	0.081 ± 0.020	52.2 ± 1.0
4	75	30	dry ice-acetone	1	0.1	2	50.5 ± 0.5	0.110 ± 0.016	53.3 ± 2.0
5	75	60	dry ice-acetone	1	0.1	2	47.3 ± 0.2	0.085 ± 0.017	50.0 ± 1.2
6	RT	2	dry ice-acetone	1	0.1	2	632.3 ± 163.8	0.801 ± 0.117	426.8 ± 56.4
7	75	2	ice	1	0.1	2	1912.0 ± 446.3	0.225 ± 0.162	961.7 ± 173.7
8	75	2	air cooling	1	0.1	2	2333.0 ± 243.0	0.811 ± 0.174	720.0 ± 136.4
9	75	2	dry ice-acetone	0.5	0.1	2	73.0 ± 1.1	0.082 ± 0.018	81.2 ± 5.2
10	75	2	dry ice-acetone	2	0.1	2	48.1 ± 0.7	0.114 ± 0.013	50.4 ± 1.9
11	75	2	dry ice-acetone	5	0.1	2	47.9 ± 0.8	0.064 ± 0.030	49.5 ± 0.5
12	75	2	dry ice-acetone	1	0.01	2	74.2 ± 12.8	0.174 ± 0.051	106.1 ± 40.2
13	75	2	dry ice-acetone	1	0.05	2	53.7 ±1.3	0.169 ± 0.011	79.0 ± 33.7
14	75	2	dry ice-acetone	1	0.5	2	48.5 ± 0.2	0.057 ± 0.004	51.4 ± 0.4
15	75	2	dry ice-acetone	1	1	2	48.4 ± 0.5	0.081 ± 0.004	50.4 ± 0.9
16	75	2	dry ice-acetone	1	0.1	10	93.5 ± 16.2	0.202 ± 0.020	122.7 ± 25.5
17 [a]							66.7 ± 0.9	0.094 ± 0.022	81.5 ± 24.6

[a] This sample is classical seeds prepared by sonicating cylinders.

Table S3. Size of platelets prepared from classical seeds of various unimer-to-seed ratios by tuning the amount of unimer.

Unimer-to-seed ratio	Area (μm^2)			Length (μm)			Width (μm)			L/W
	A_n	A_w	A_w/A_n	L_n	L_w	L_w/L_n	W_n	W_w	W_w/W_n	
10	0.52	0.54	1.04	1.36	1.38	1.01	0.43	0.43	1.01	3.18
30	1.53	1.59	1.04	2.41	2.43	1.01	0.72	0.73	1.01	3.36
60	3.13	3.36	1.07	3.57	3.61	1.01	1.03	1.05	1.02	3.46

Table S4. Size of platelets prepared from flash-frozen seeds of various unimer-to-seed ratios.

Unimer-to-seed ratio	Area (μm^2)			Length (μm)			Width (μm)			L/W
	A_n	A_w	A_w/A_n	L_n	L_w	L_w/L_n	W_n	W_w	W_w/W_n	
10	0.11	0.11	1.03	0.57	0.57	1.01	0.21	0.21	1.01	2.68
30	0.36	0.38	1.07	1.16	1.18	1.02	0.38	0.38	1.02	3.06
60	0.67	0.69	1.03	1.59	1.60	1.01	0.49	0.50	1.01	3.21
120	1.47	1.50	1.02	2.46	2.47	1.01	0.66	0.67	1.01	3.70

Table S5. Size of platelets prepared from classical seeds of various unimer-to-seed ratios by tuning seed concentration and maintaining the same added unimer amount.

Seed concentration mg mL^{-1}	Unimer-to-seed ratio	Area (μm^2)			Length (μm)			Width (μm)			L/W
		A_n	A_w	A_w/A_n	L_n	L_w	L_w/L_n	W_n	W_w	W_w/W_n	
0.01	10	0.52	0.54	1.04	1.36	1.38	1.01	0.43	0.43	1.01	3.18
0.02	5	0.20	0.21	1.03	0.86	0.87	1.01	0.27	0.27	1.01	3.23
0.03	0.33	0.07	0.08	1.05	0.50	0.51	1.02	0.17	0.18	1.02	2.87

Table S6. Platelet area, length, width and aspect ratio obtained at the fixed unimer-to-seed mass ratio of 10 using seeds using different preparation methods.

Sample	Area (μm^2)			Length (μm)			Width (μm)			L/W
	A_n	A_w	A_w/A_n	L_n	L_w	L_w/L_n	W_n	W_w	W_w/W_n	
1	0.14	0.15	1.03	0.58	0.59	1.01	0.21	0.22	1.01	2.71
2	0.11	0.11	1.03	0.57	0.57	1.01	0.21	0.21	1.01	2.68
3	0.10	0.11	1.03	0.58	0.59	1.01	0.21	0.21	1.01	2.80
4	0.10	0.11	1.03	0.55	0.56	1.01	0.21	0.21	1.01	2.64
5	0.11	0.11	1.04	0.55	0.56	1.01	0.20	0.21	1.01	2.71
9	0.23	0.24	1.05	0.86	0.87	1.02	0.29	0.29	1.02	2.97
10	0.10	0.10	1.04	0.56	0.57	1.01	0.20	0.20	1.01	2.78
11	0.10	0.11	1.07	0.57	0.58	1.03	0.21	0.21	1.02	2.74
12	0.45	0.47	1.03	1.17	1.18	1.01	0.39	0.39	1.01	3.00
13	0.25	0.26	1.02	0.90	0.91	1.01	0.30	0.30	1.01	3.02
14	0.25	0.26	1.01	0.94	0.94	1.01	0.32	0.32	1.01	2.91
15	0.32	0.33	1.03	1.05	1.06	1.01	0.33	0.33	1.01	3.22
16	0.34	0.35	1.03	1.03	1.04	1.01	0.36	0.37	1.01	2.84

Table S7. DLS size of flow flash-frozen seeds prepared at various flow rate.

Flow rate ($\mu L \cdot min^{-1}$)	Heating time (min)	Cooling time (min)	Size (Z-average) (nm)	PDI	Mean Intensity (nm)
1	2	1	45.6 ± 0.7	0.093 ± 0.026	47.6 ± 0.7
2	1	0.5	47.9 ± 0.5	0.109 ± 0.029	50.7 ± 0.8
4	0.5	0.25	48.1 ± 0.8	0.14 ± 0.019	100.9 ± 64.4

Table S8. DLS size of flow flash-frozen seeds with various PCL content prepared without annealing.

PCL content (wt%)	Size (Z-average) (nm)	PDI	Mean Intensity (nm)
0	45.6 ± 0.7	0.093 ± 0.026	47.6 ± 0.7
1	50.0 ± 0.4	0.156 ± 0.006	52.3 ± 1.0
3	46.4 ± 0.5	0.06 ± 0.014	49.1 ± 1.0
4	49.5 ± 0.6	0.108 ± 0.022	53.9 ± 1.2
5	50.8 ± 1.0	0.112 ± 0.022	53.7 ± 0.7

Table S9. DLS size of flow flash-frozen seeds with various PCL content over aging time after annealing at 30 °C.

Time (day)	PCL content (Z-average size, nm)				
	0%	1%	3%	4%	5%
0	126.7 ± 4.8	112.8 ± 0.8	97.9 ± 0.6	96.4 ± 1.5	96.2 ± 1.4
1	139.7 ± 0.8	126.2 ± 0.5	106.0 ± 1.5	102.0 ± 0.9	96.8 ± 0.9
2	147.6 ± 2.7	132.6 ± 2.7	107.1 ± 1.4	103.7 ± 1.0	99.2 ± 0.5
3	151.0 ± 0.7	138.6 ± 0.7	105.9 ± 0.2	105.2 ± 0.5	98.4 ± 0.6

Table S10. Platelets obtained from detached flow living CDSA using flow seeds modified various amount of PCL at the fixed unimer-to-seed ratio of 10.

PCL in seeds (wt%)	Area (μm^2)			Length (μm)			Width (μm)			L/W
	A_n	A_w	A_w/A_n	L_n	L_w	L_w/L_n	W_n	W_w	W_w/W_n	
0	1.02	1.13	1.10	1.85	1.89	1.02	0.64	0.65	1.02	2.90
1	0.46	0.50	1.09	1.12	1.14	1.02	0.39	0.40	1.02	2.86
3	0.25	0.27	1.08	0.91	0.93	1.02	0.35	0.36	1.02	2.58
4	0.22	0.23	1.06	0.80	0.82	1.02	0.28	0.28	1.02	2.88
5	0.08	0.08	1.08	0.48	0.50	1.02	0.17	0.17	1.03	2.92

Table S11. Setup of flow reactors to continuously prepare size-controllable platelets from polymers.

Sample	Total unimer-to-seed ratio	Total time (min)	Seed preparation		1st living CDSA			2nd living CDSA		
			R_s (μL·min^{-1})	Time (min)	Unimer-to-seed ratio	R_u (μL·min^{-1})	Time (min)	Unimer-to-seed ratio	R_u (μL·min^{-1})	Time (min)
a	5	6	1000	4	5	10	2			
b	10	6	1000	4	10	20	2			
c	20	6	1000	4	20	40	2			
d	10	3	2000	2	10	40	1			
e	20	8	1000	4	10	20	2	10	20	2

Table S12. Size-controllable platelets prepared from polymers directly using flow reactors.

Sample	Total unimer-to-seed ratio	Area (μm^2)			Length (μm)			Width (μm)			L/W
		A_n	A_w	A_w/A_n	L_n	L_w	L_w/L_n	W_n	W_w	W_w/W_n	
a	5	0.08	0.09	1.17	0.51	0.53	1.05	0.18	0.19	1.03	2.74
b	10	0.21	0.22	1.09	0.90	0.92	1.03	0.26	0.26	1.02	3.46
c	20	0.48	0.54	1.13	1.45	1.51	1.04	0.38	0.39	1.03	3.83
d	10	0.18	0.18	1.05	0.81	0.82	1.01	0.25	0.25	1.01	3.26
e	20	0.62	0.67	1.07	1.69	1.72	1.02	0.44	0.45	1.02	3.83

Table S13. Setup of integral flow reactors for controlled preparation of platelets by self-seeding strategy.

Annealing temperature (°C)	Seed preparation		Living CDSA		
	R_s (μL·min^{-1})	Time (min)	Unimer-to-seed ratio	R_u (μL·min^{-1})	Time (min)
28	1000	4	10	20	2
30	1000	4	10	20	2
32	1000	4	10	20	2
34	1000	4	10	20	2

Table S14. Size-controllable platelets prepared by self-seeding strategy.

Annealing temperature (°C)	Area (μm^2)			Length (μm)			Width (μm)			L/W
	A_n	A_w	A_w/A_n	L_n	L_w	L_w/L_n	W_n	W_w	W_w/W_n	
28	0.14	0.14	1.07	0.67	0.68	1.02	0.27	0.27	1.02	2.50
30	0.21	0.22	1.04	0.84	0.84	1.01	0.35	0.36	1.02	2.37
32	0.88	0.91	1.03	1.78	1.80	1.01	0.64	0.65	1.01	2.78
34	18.49	19.19	1.04	7.71	7.80	1.01	3.01	3.04	1.01	2.57

Table S15. Setup of flow reactors to prepare double-layered platelets with tunable corona chemistry.

Chemistry 1st / 2nd	Total unimer-to-seed ratio	Total time (min)	Seed preparation		1st living CDSA			2nd living CDSA		
			R_s (μL·min^{-1})	Time (min)	Unimer-to-seed ratio	R_u (μL·min^{-1})	Time (min)	Unimer-to-seed ratio	R_u (μL·min^{-1})	Time (min)
PDMA / P4VP	15	8	1000	4	5	10	2	10	20	2
P4VP / PDMA	15	8	1000	4	5	10	2	10	20	2
PDMA / PNAM	15	8	1000	4	5	10	2	10	20	2
PDMA / PDMAEMA	15	8	1000	4	5	10	2	10	20	2

Table S16. Setup of flow reactors to prepare platelets with tunable core chemistry.

Chemistry PCL_{22}-G / PCL_{73}-R	Total unimer-to-seed ratio	Total time (min)	Seed preparation		PCL_{22}-G		PCL_{73}-R		Time for living CDSA (min)
			R_s (μL·min^{-1})	Time (min)	Unimer-to-seed ratio	R_u (μL·min^{-1})	Unimer-to-seed ratio	R_u (μL·min^{-1})	
100 / 0	10	6	1000	4	10	20	0	0	2
75 / 25	10	6	1000	4	7.5	15	2.5	5	2
50 / 50	10	6	1000	4	5	10	5	10	2
25 / 75	10	6	1000	4	2.5	5	7.5	15	2
0 / 100	10	6	1000	4	0	0	10	20	2

Table S17. Characterization of PLLA-based polymers.

Polymer	$M_{n,\ NMR}$ [a] (kg·mol^{-1})	$M_{n,\ GPC}$ [b] (kg·mol^{-1})	$Đ_{GPC}$ [b]
$PLLA_{12}$	1.6	2.8	1.07
$PLLA_{45}$-*b*-$PDMAEMA_{183}$	34.2	39.3	1.39

[a] Results were determined by ^{1}H NMR.

[b] Results were determined by SEC, where signals were detected by refractive index (RI).

Table S18. Setup of flow reactors to continuously prepare size-controllable platelets from polymers.

Unimer-to-seed ratio	Total time (min)	Seed preparation		Living CDSA	
		R_s (μL·min^{-1})	Time (min)	R_u (μL·min^{-1})	Time (min)
5	6	1000	4	5	2
10	6	1000	4	10	2
15	6	1000	4	15	2

Table S19. Size of PLLA platelets prepared prepared using the integral flow cascade.

Unimer-to-seed ratio	Area (μm^2)			Length (μm)			Width (μm)			L/W
	A_n	A_w	A_w/A_n	L_n	L_w	L_w/L_n	W_n	W_w	W_w/W_n	
5	0.10	0.10	1.02	0.52	0.52	1.01	0.30	0.31	1.01	1.71
10	0.31	0.32	1.05	1.00	1.02	1.02	0.54	0.55	1.01	1.84
15	0.51	0.53	1.06	1.26	1.28	1.02	0.69	0.70	1.02	1.81

Supplementary Figure

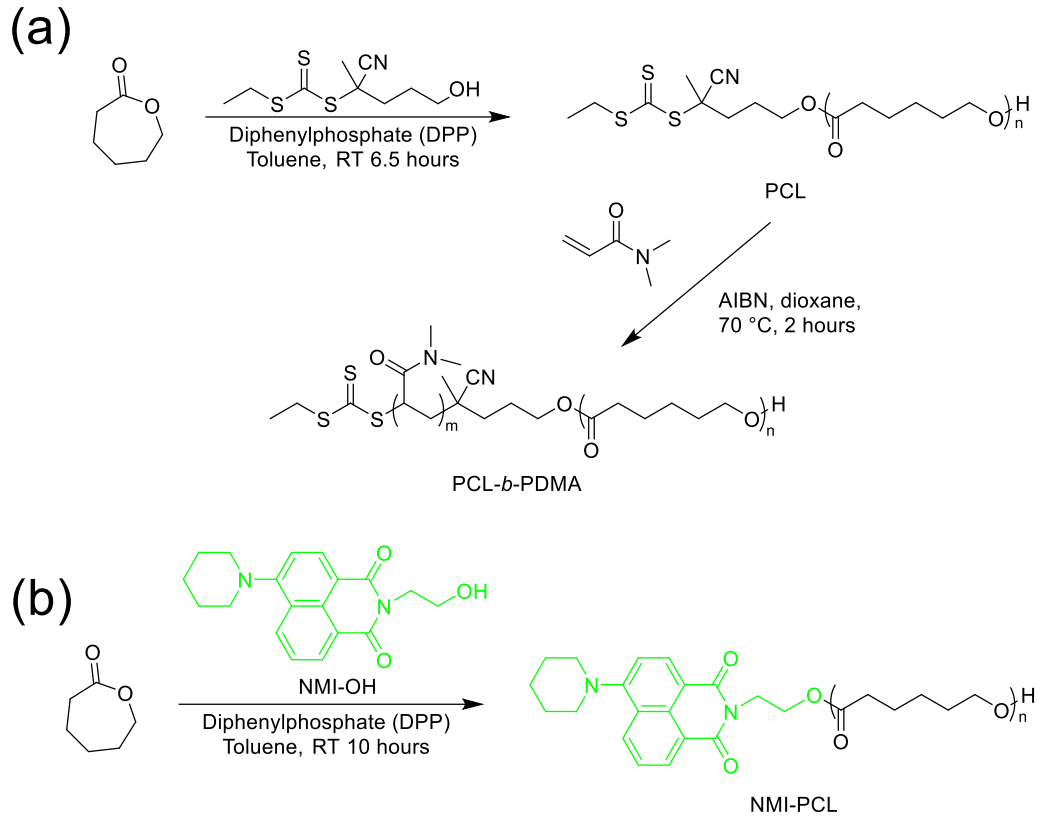

Figure S1. Synthetic routes of (a) PCL-*b*-PDMA and (b) NMI-PCL.

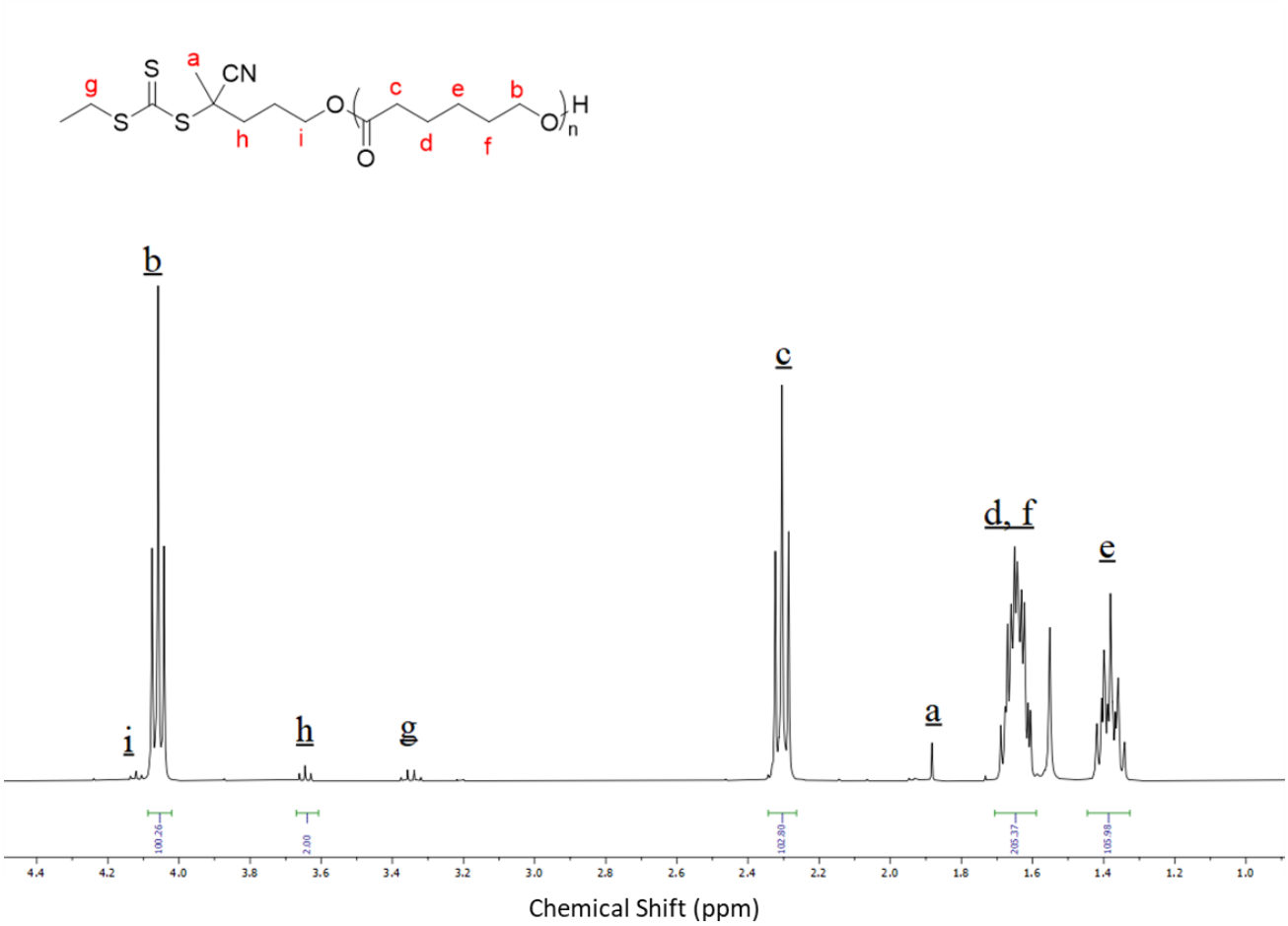

Figure S2. ^{1}H NMR spectra of PCL homopolymer.

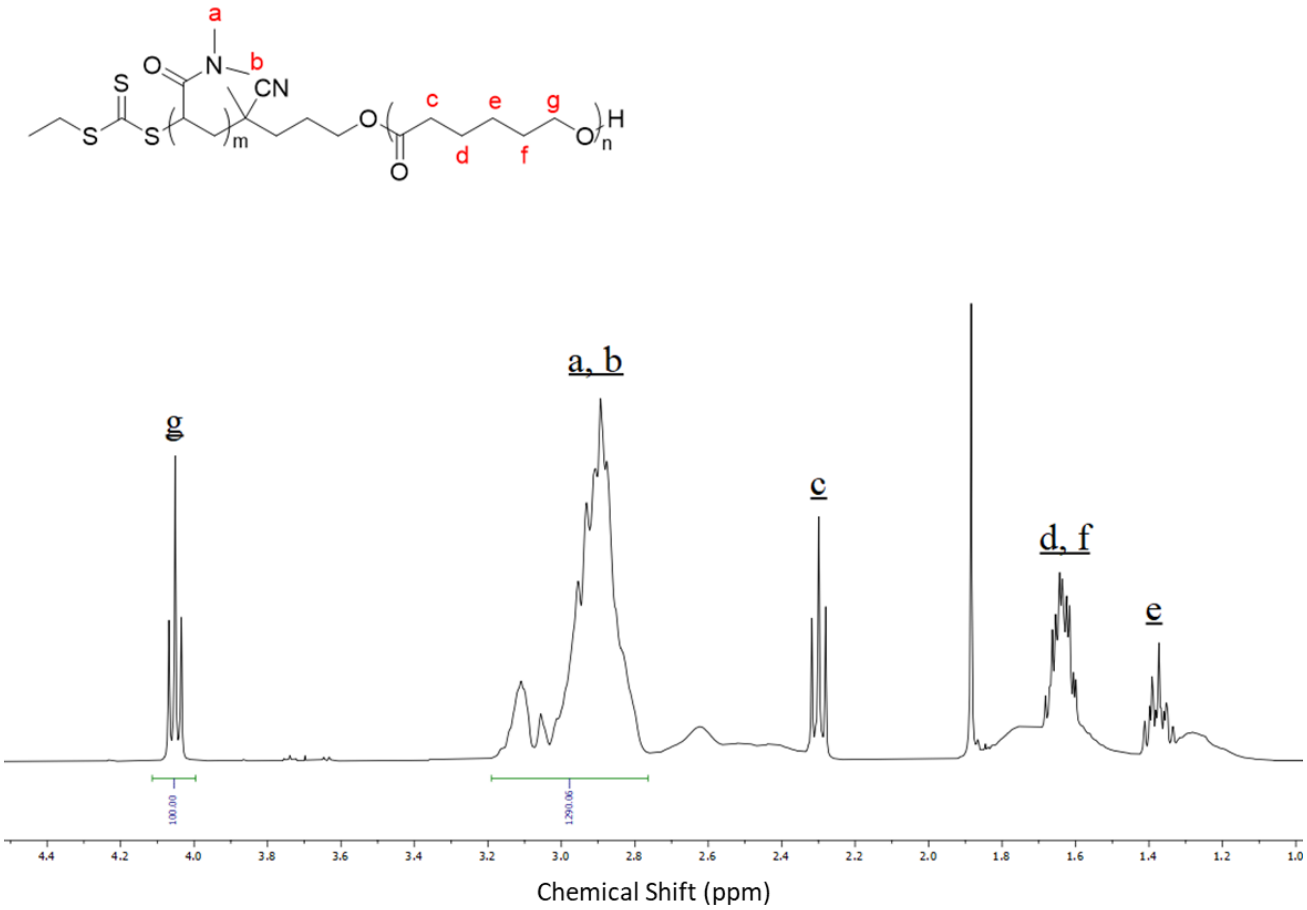

Figure S3. ^{1}H NMR spectra of PCL-*b*-PDMA.

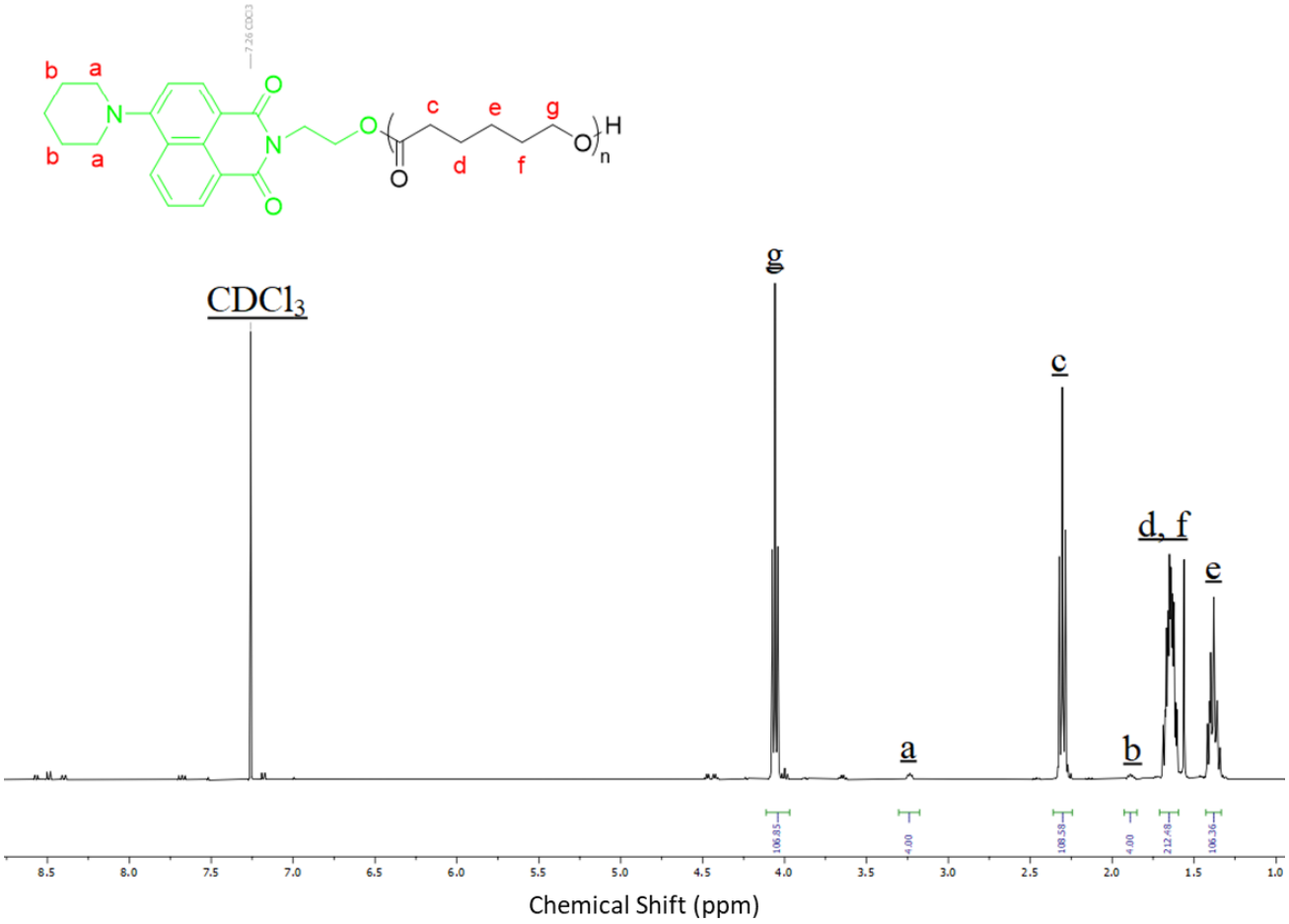

Figure S4. ^{1}H NMR spectra of NMI-PCL.

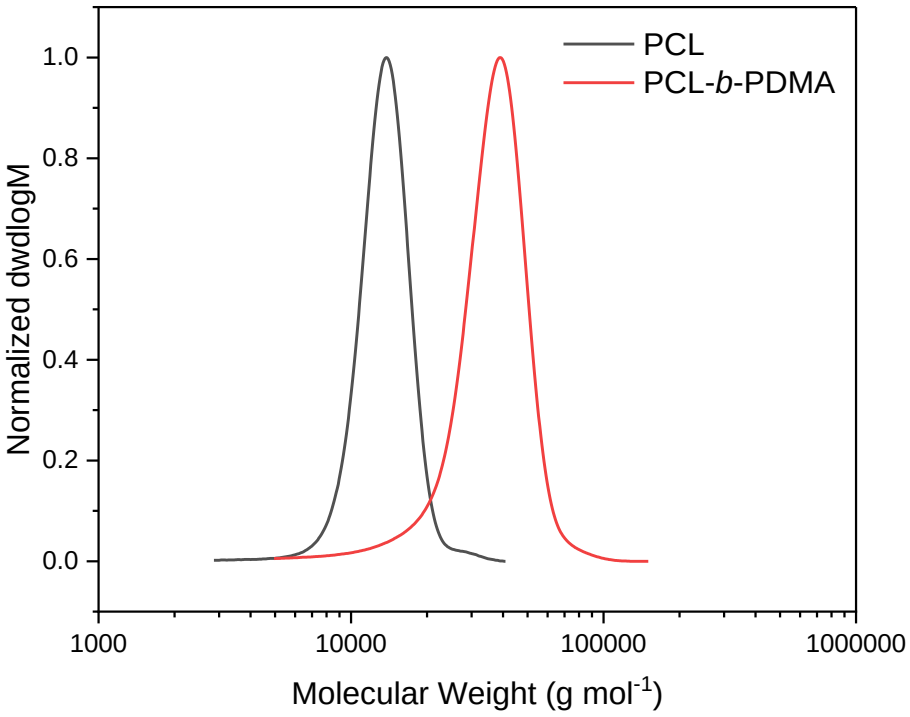

Figure S5. Normalized SEC curves of PCL and PCL-*b*-PDMA.

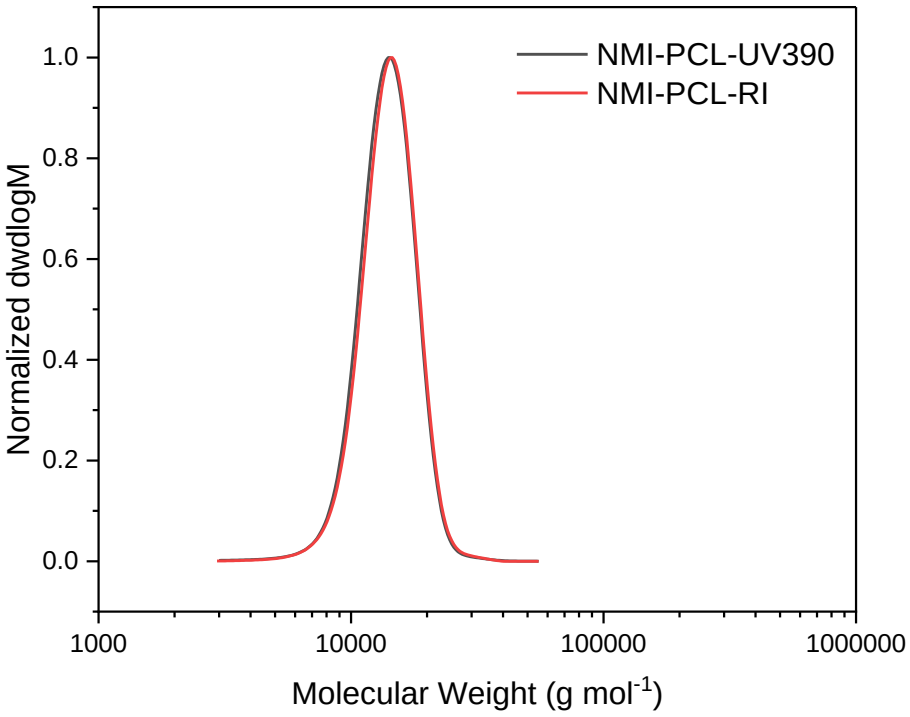

Figure S6. Normalized SEC curves of NMI-PCL detected by UV at 390 nm and the refractive index (RI).

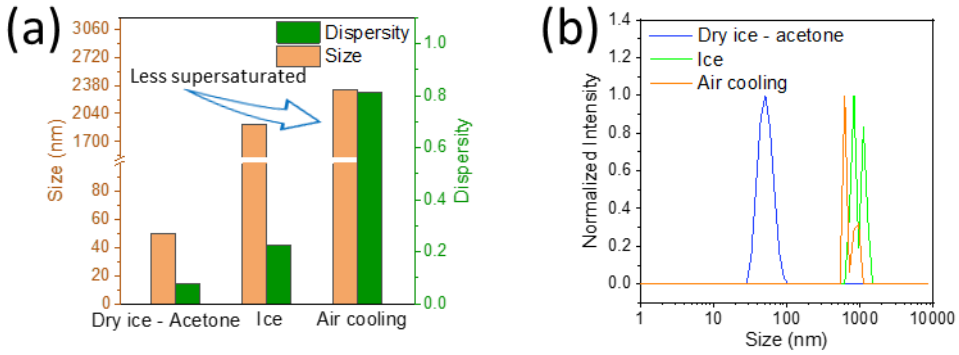

Figure S7. Flash-frozen seeds prepared using different cooling methods: (a) Size and dispersity, and (b) Size distribution based on scattering intensity.

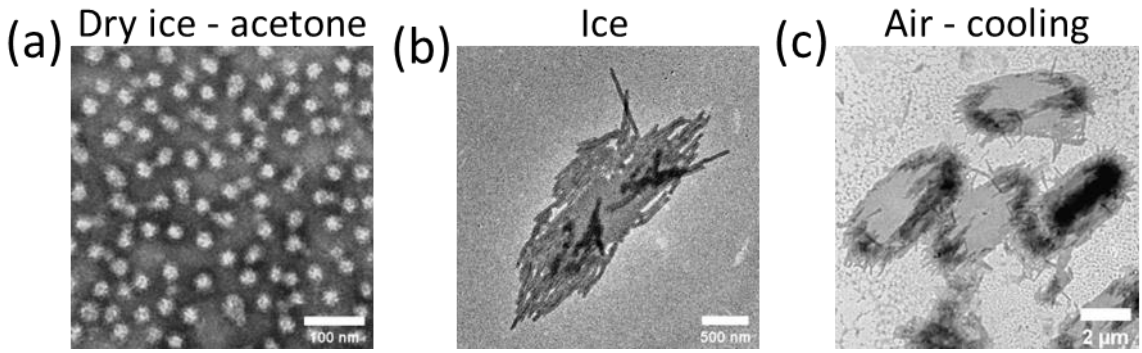

Figure S8. TEM images of flash-frozen seeds prepared by different cooling methods. Scale bar = 100 nm (a), 500 nm (b), and 2 μm (c). TEM samples were stained by uranyl acetate solution (1 wt%).

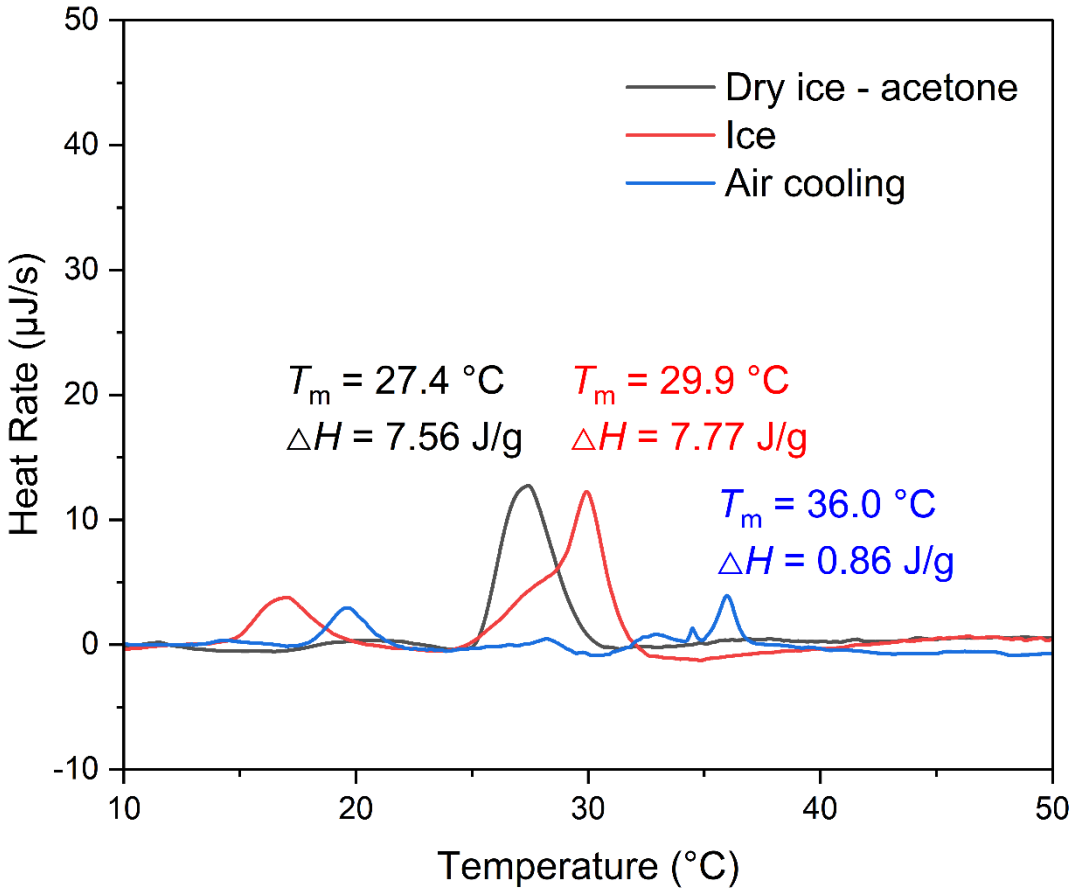

Figure S9. Nano DSC thermograms of seed samples prepared from different cooling methods.

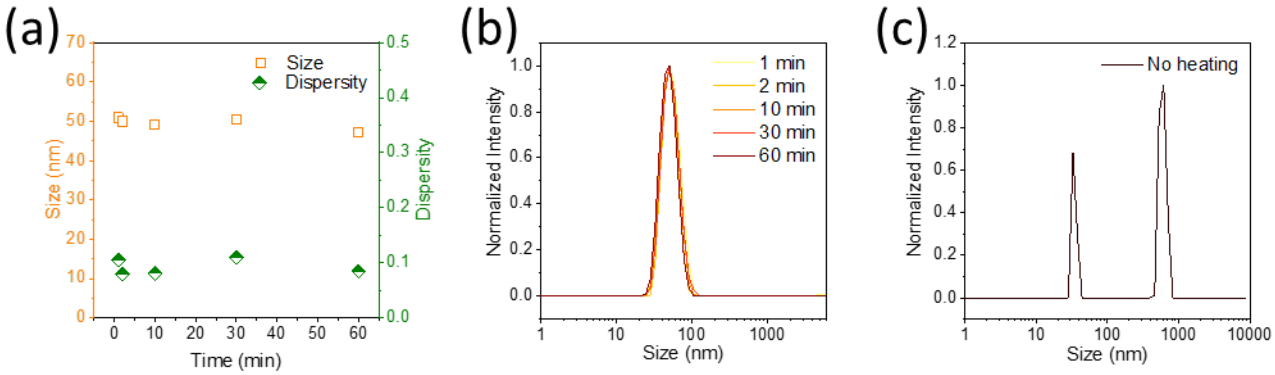

Figure S10. Flash-frozen seeds prepared with various heating time: (a) Variations of size and dispersity with heating time, (b) Size distribution based on scattering intensity, and (c) Size distribution of the control sample (sample 6) without heating.

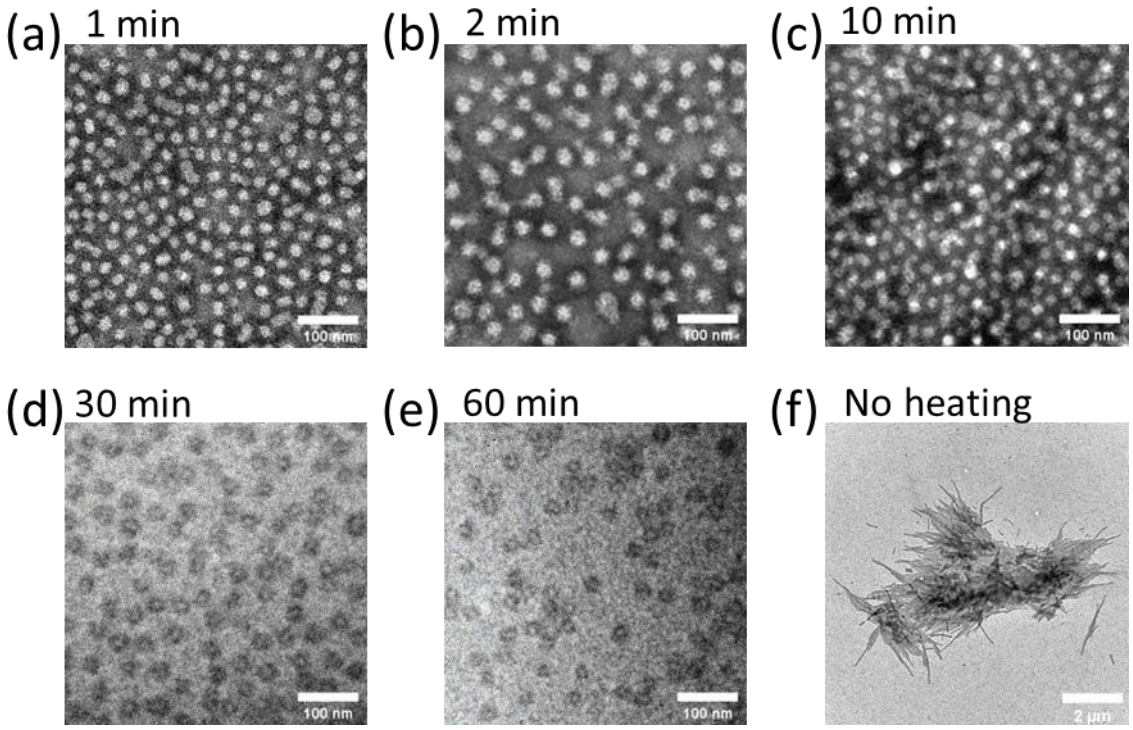

Figure S11. TEM images of flash-frozen seeds prepared by various heating time. Scale bar = 100 nm (a)-(e) and 2 μm (f). TEM samples were stained by uranyl acetate solution (1 wt%).

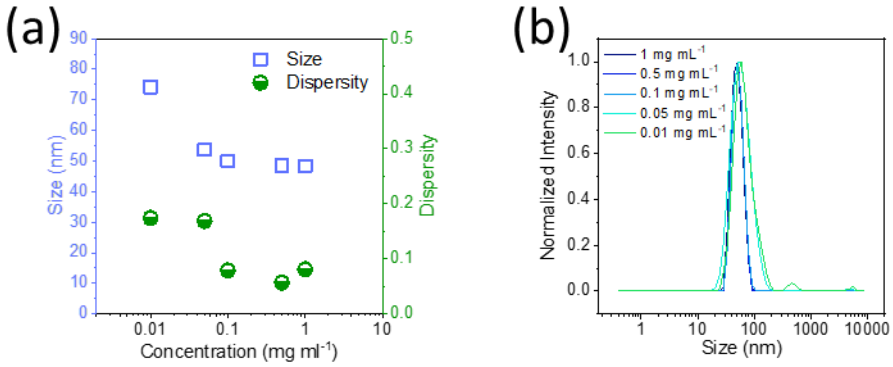

Figure S12. Flash-frozen seeds prepared with various concentrations: (a) Variations of size and dispersity with concentration, and (b) Size distribution based on scattering intensity.

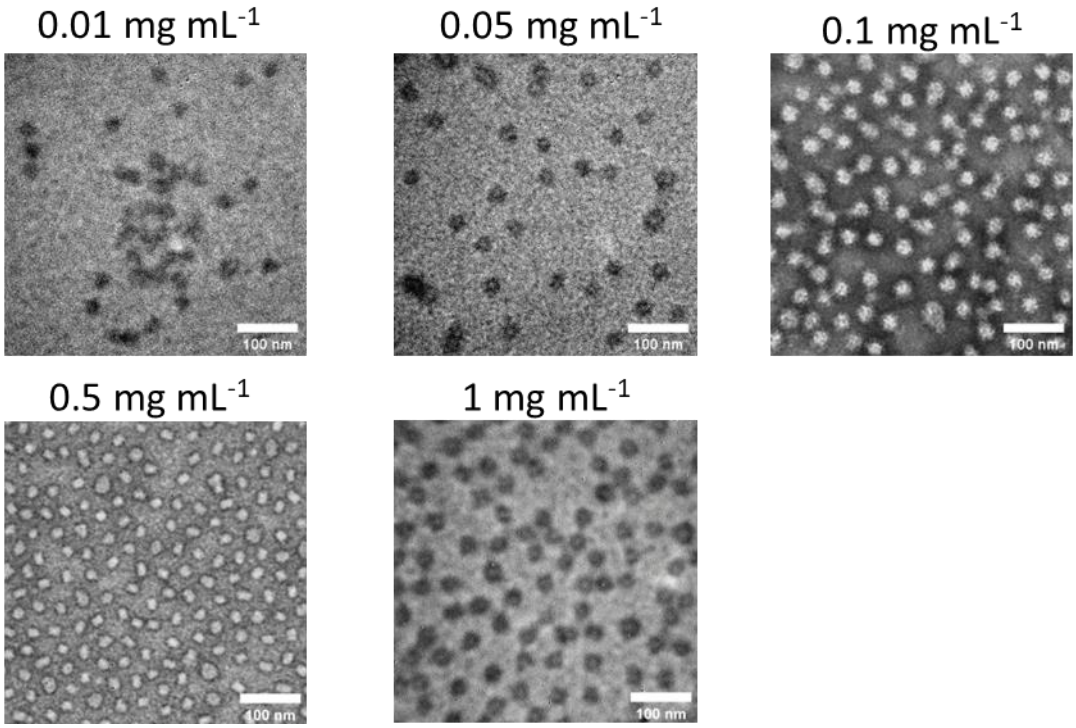

Figure S13. TEM images of flash-frozen seeds prepared at various concentrations. Scale bar = 100 nm. TEM samples were stained by uranyl acetate solution (1 wt%).

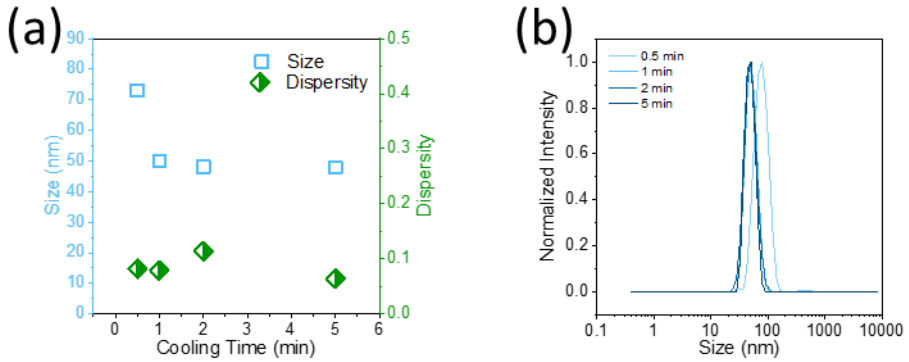

Figure S14. Flash-frozen seeds prepared with various cooling times: (a) Variations of size and dispersity with cooling time, and (b) Size distribution based on scattering intensity.

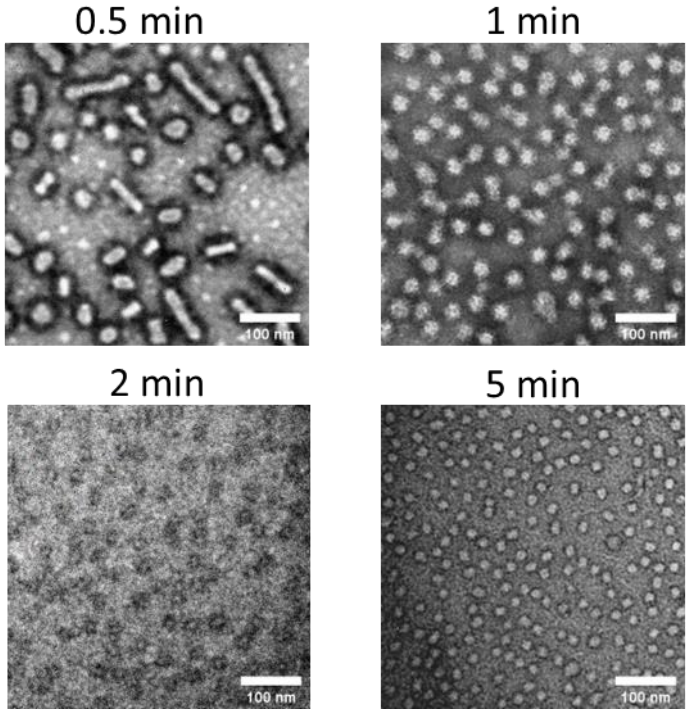

Figure S15. TEM images of flash-frozen seeds prepared by various cooling times. Scale bar = 100 nm. TEM samples were stained by uranyl acetate solution (1 wt%).

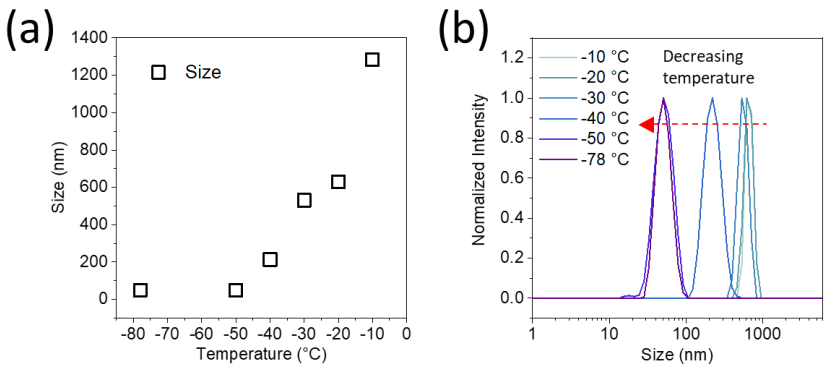

Figure S16. Flash-frozen seeds prepared at various cooling temperatures: (a) Variations of size with cooling temperature, and (b) Size distribution based on scattering intensity. Samples were heated at 75 °C for 2 min and then cooled for 5 min at various temperatures.

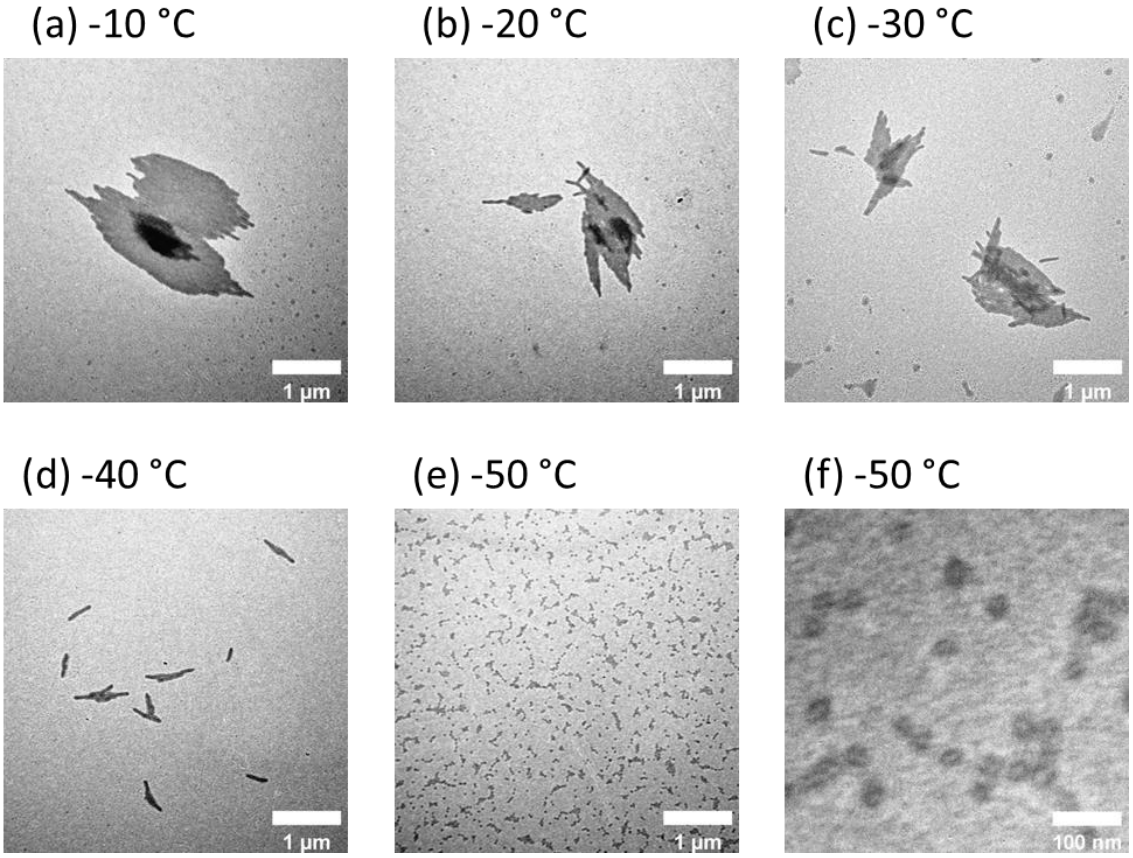

Figure S17. TEM images of flash-frozen seeds prepared by cooling at various temperatures. Scale bar = 1 µm (a)-(e) and 100 nm (f). Samples were stained by uranyl acetate solution (1wt%).

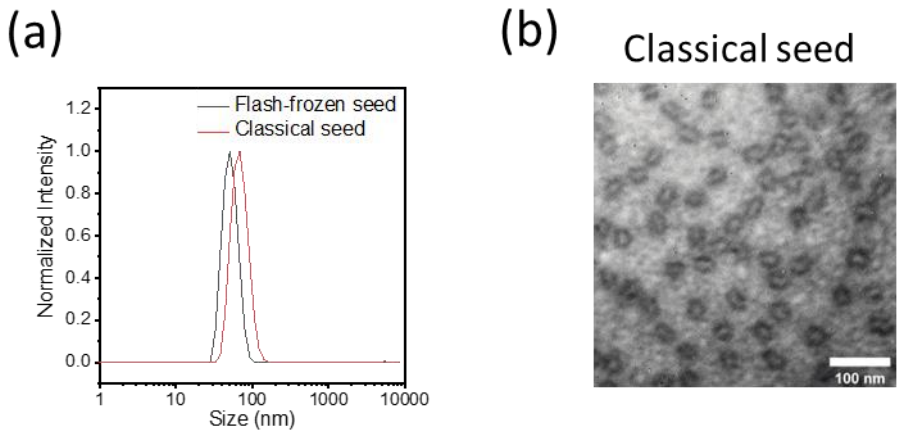

Figure S18. (a) Size distributions of flash-frozen and classical seeds based on scattering intensity, and (b) TEM image of classical seeds. Scale bar = 100 nm. TEM sample was stained by uranyl acetate solution (1wt%).

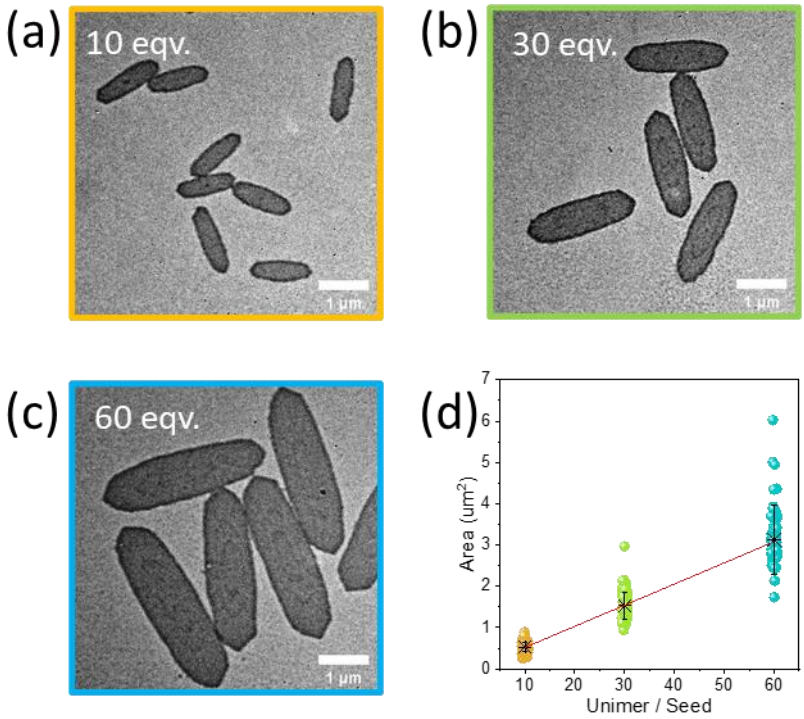

Figure S19. Living CDSA using classical seeds: (a), (b), and (c) are TEM images of platelets prepared at various unimer-to-seed ratios, and (d) Linear fit of area upon different unimer-to-seed ratios. 100 platelets were measured. Data are presented as mean values +/- standard deviation. Scale bar = 1 µm.

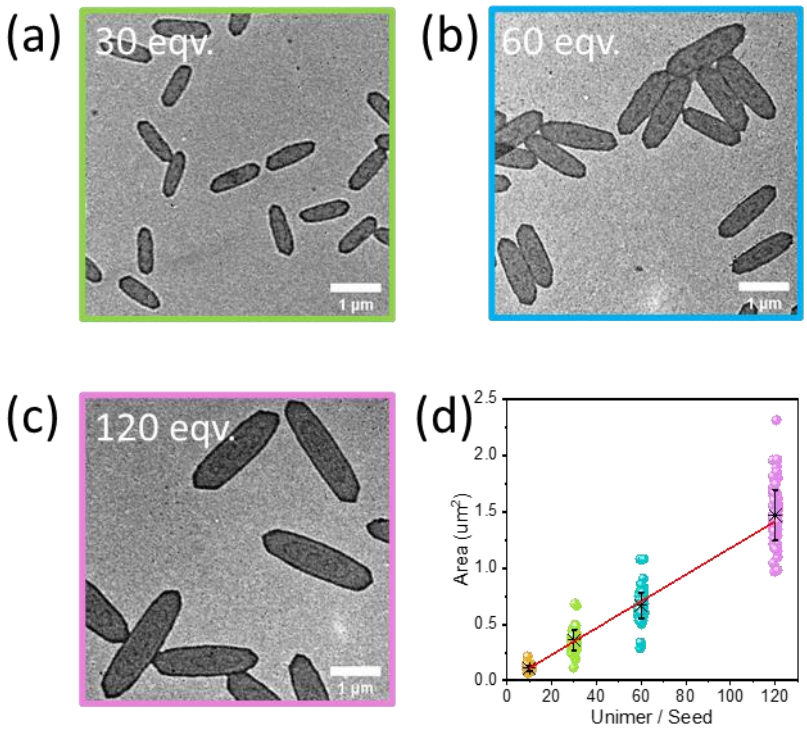

Figure S20. Living CDSA using flash-frozen seeds: (a), (b), and (c) are TEM images of platelets prepared at various unimer-to-seed ratios, and (d) Linear fit of area upon different unimer-to-seed ratios. 100 platelets were measured. Data are presented as mean values +/- standard deviation. Scale bar = 1 µm.

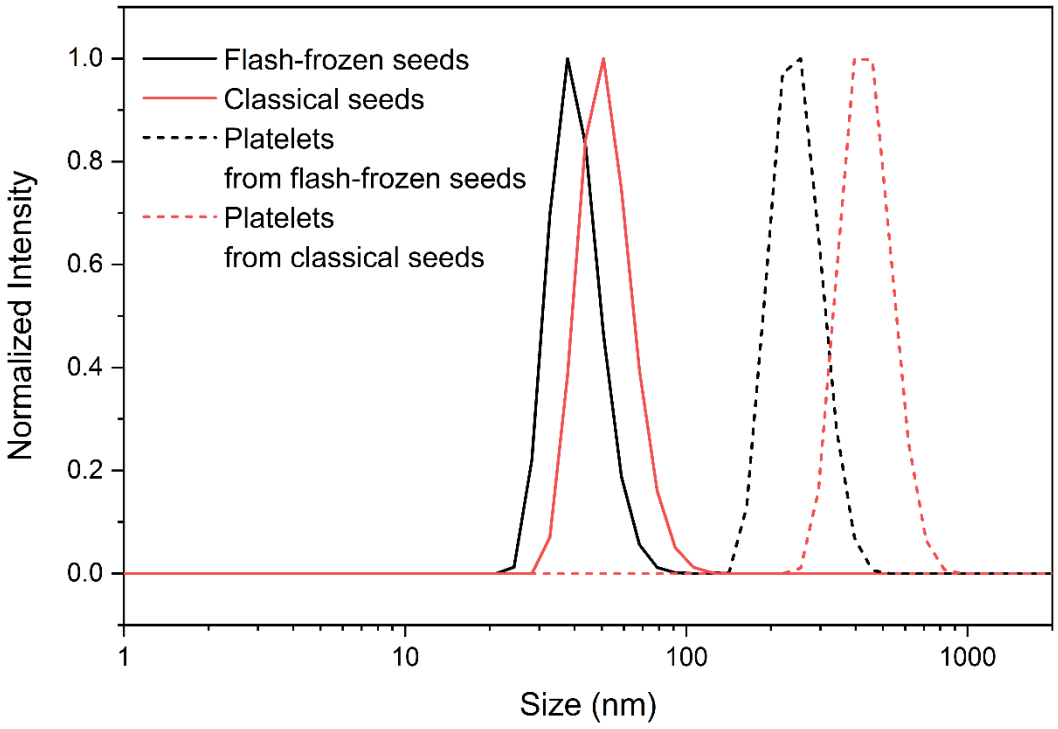

Figure S21. Comparison of DLS size distribution of flash-frozen and classical seeds with platelets prepared from these seed samples. The size is based on number distribution.

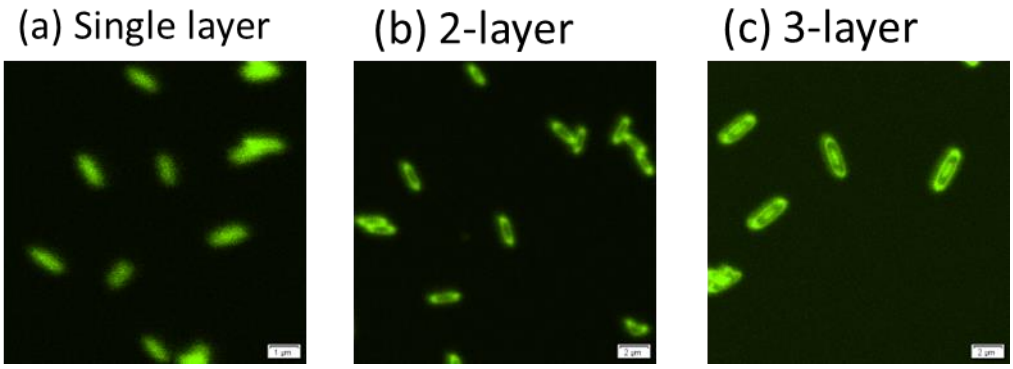

Figure S22. CLSM images of fluorescent layered platelets prepared using flash-frozen seeds. Scale bar = 1 μm (a) and 2 μm (b)-(c).

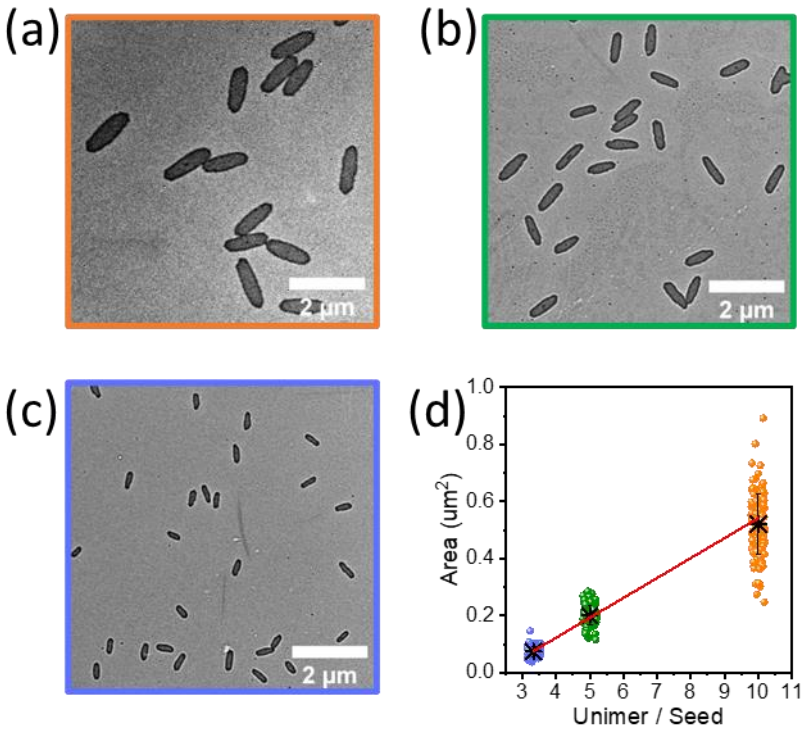

Figure S23. Living CDSA using classical seeds at various seed concentrations with a constant amount of unimer (10 µL, 10 mg mL^{-1} in $CHCl_3$): (a), (b), and (c) are TEM images of platelets prepared at seed concentrations of 0.01, 0.02, and 0.03 mg mL^{-1}, respectively correspond to unimer-to-seed ratios of 10, 5, and 3.3, and (d) Linear fit of area upon different unimer-to-seed ratios. 100 platelets were measured. Data are presented as mean values +/- standard deviation. Scale bar = 2 µm.

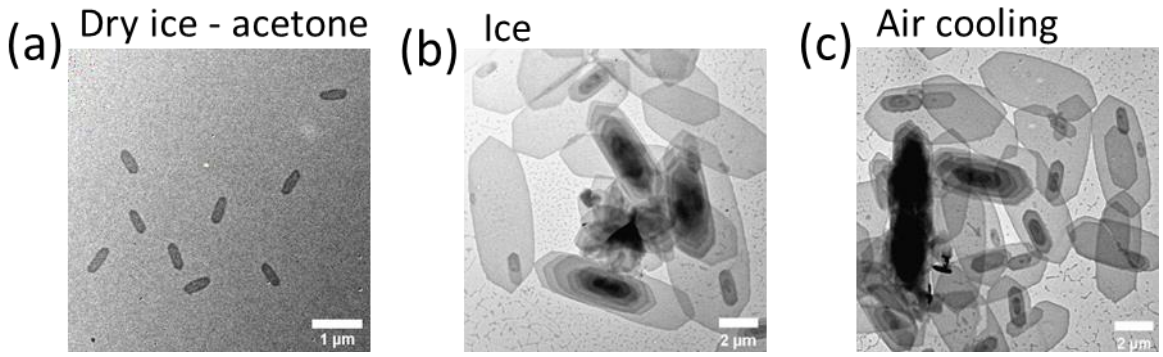

Figure S24. TEM images of platelets prepared using seeds prepared by various cooling methods. Scale bar = 1 µm (a) and 2 µm (b) and (c).

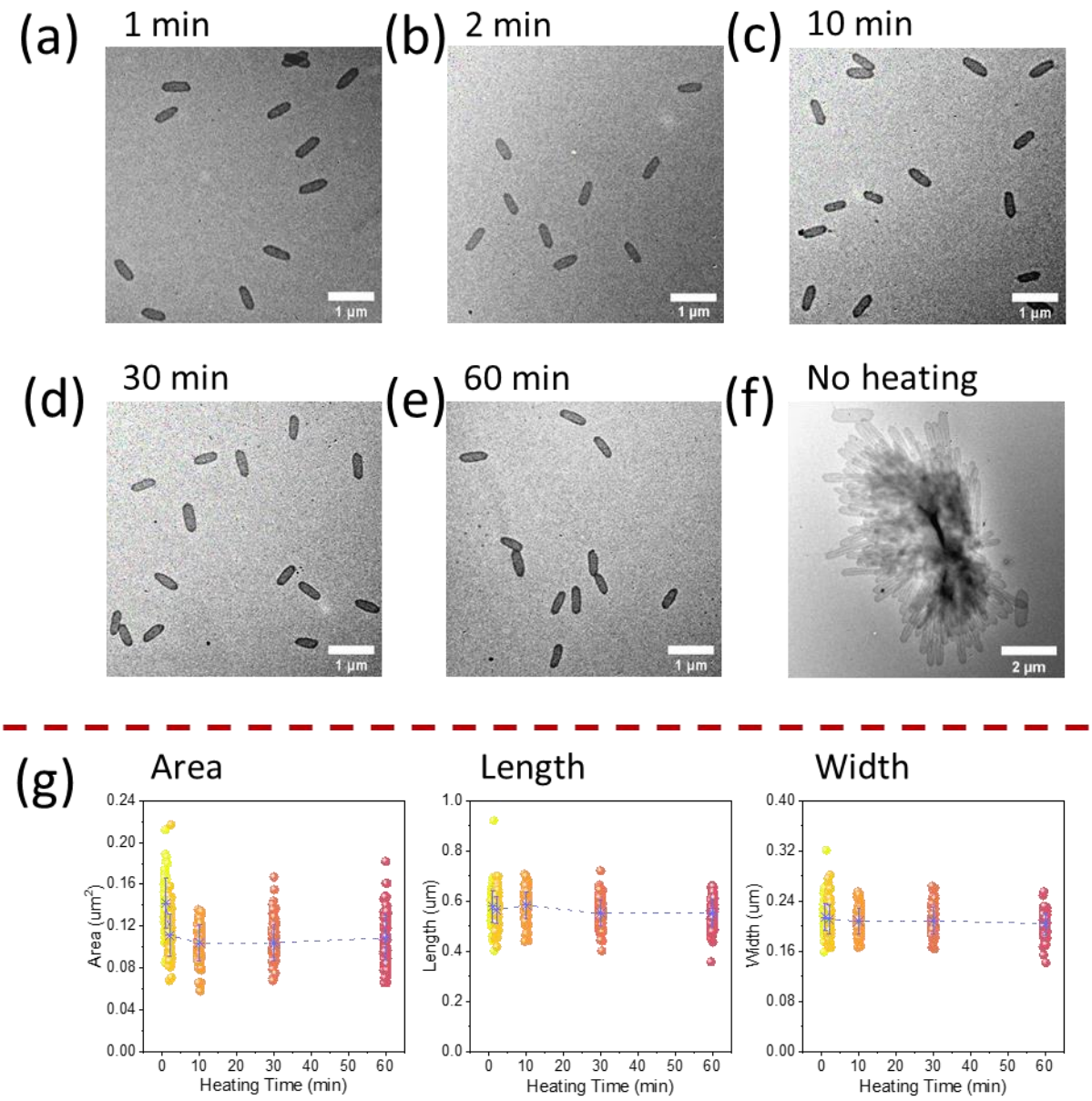

Figure S25. Living CDSA using flash-frozen seeds prepared with various heating times: (a)-(f)TEM images of platelets and (g) Statical sizes of obtained platelets. 100 platelets were measured. Data are presented as mean values +/- standard deviation. Scale bar = 1 µm (a)-(e) and 2 µm (f).

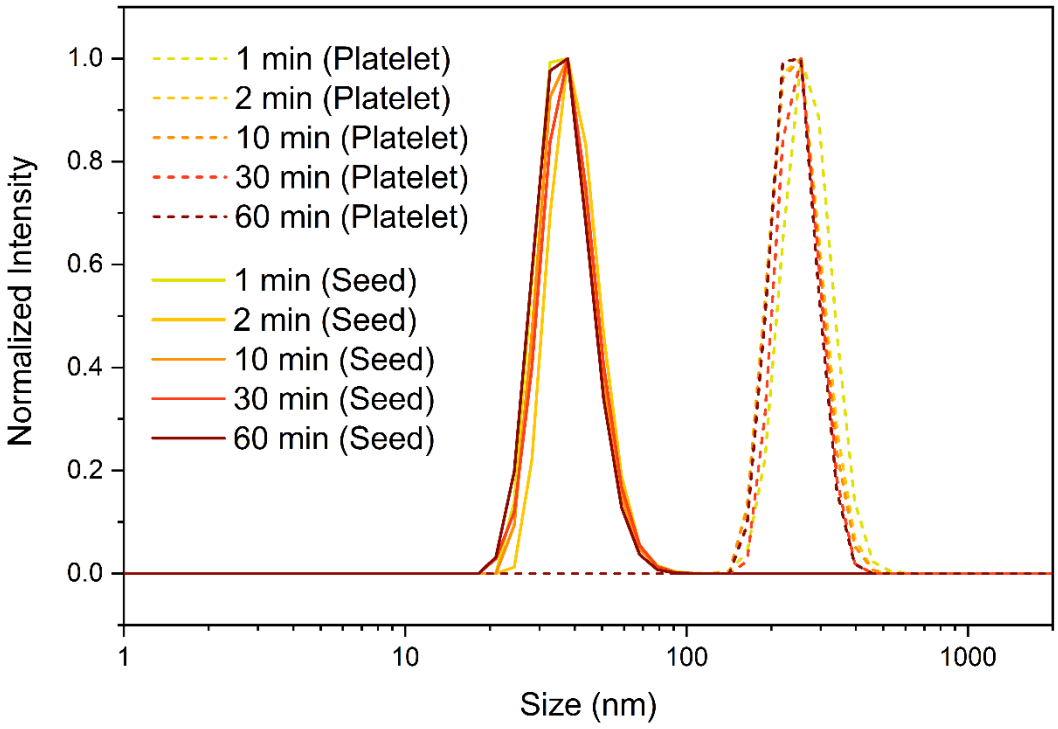

Figure S26. Comparison of DLS size distribution of flash-frozen seeds prepared with various heating times and platelets prepared from these seed samples. The size is based on number distribution.

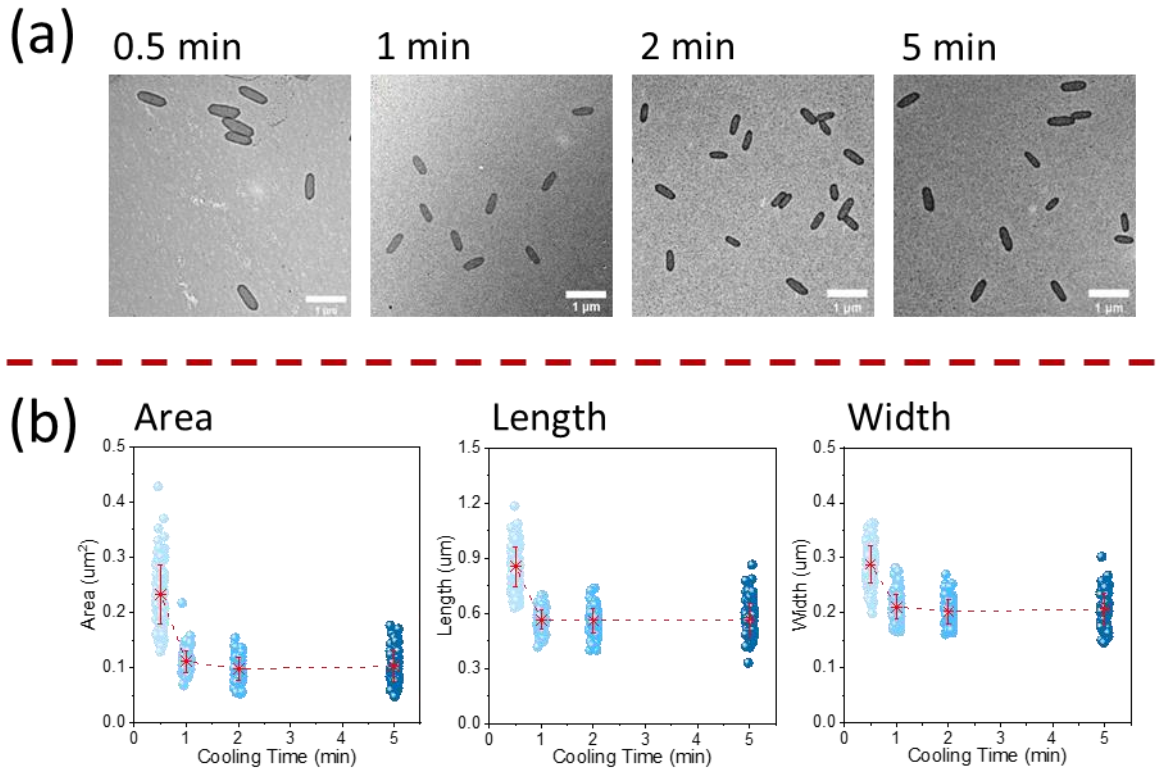

Figure S27. Living CDSA using flash-frozen seeds prepared with various cooling times: (a) TEM images of platelets and (b) Statical sizes of obtained platelets. 100 platelets were measured. Data are presented as mean values +/- standard deviation. Scale bar = 1 μm.

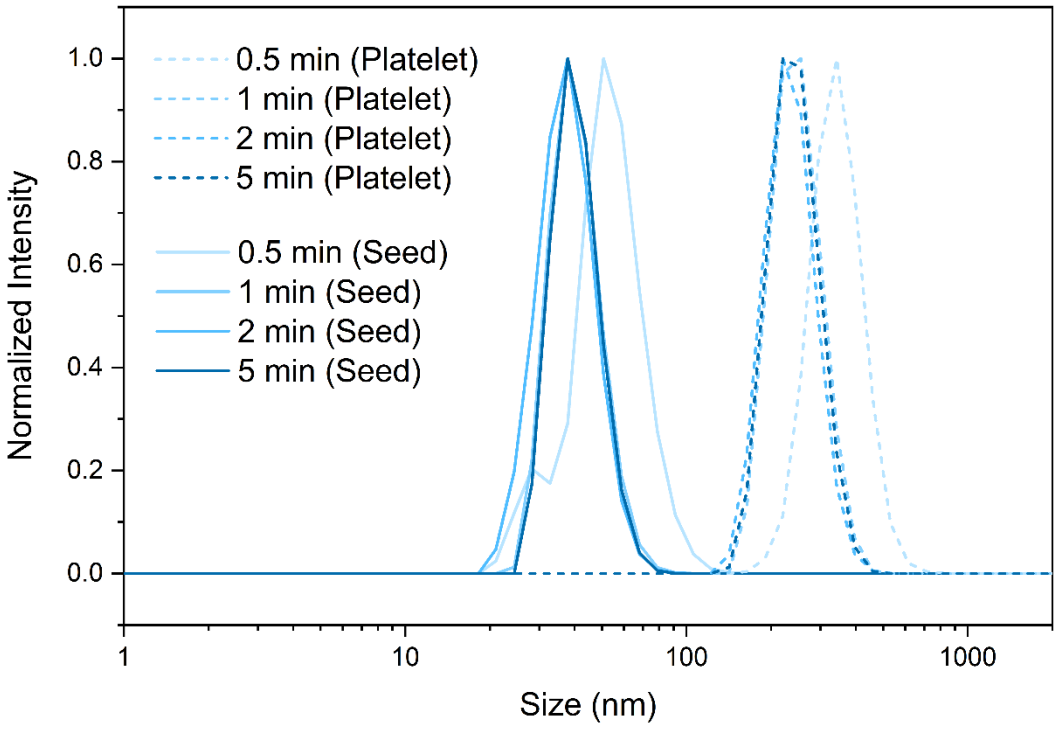

Figure S28. Comparison of DLS size distribution of flash-frozen seeds prepared with various cooling times and platelets prepared from these seed samples. The size is based on number distribution.

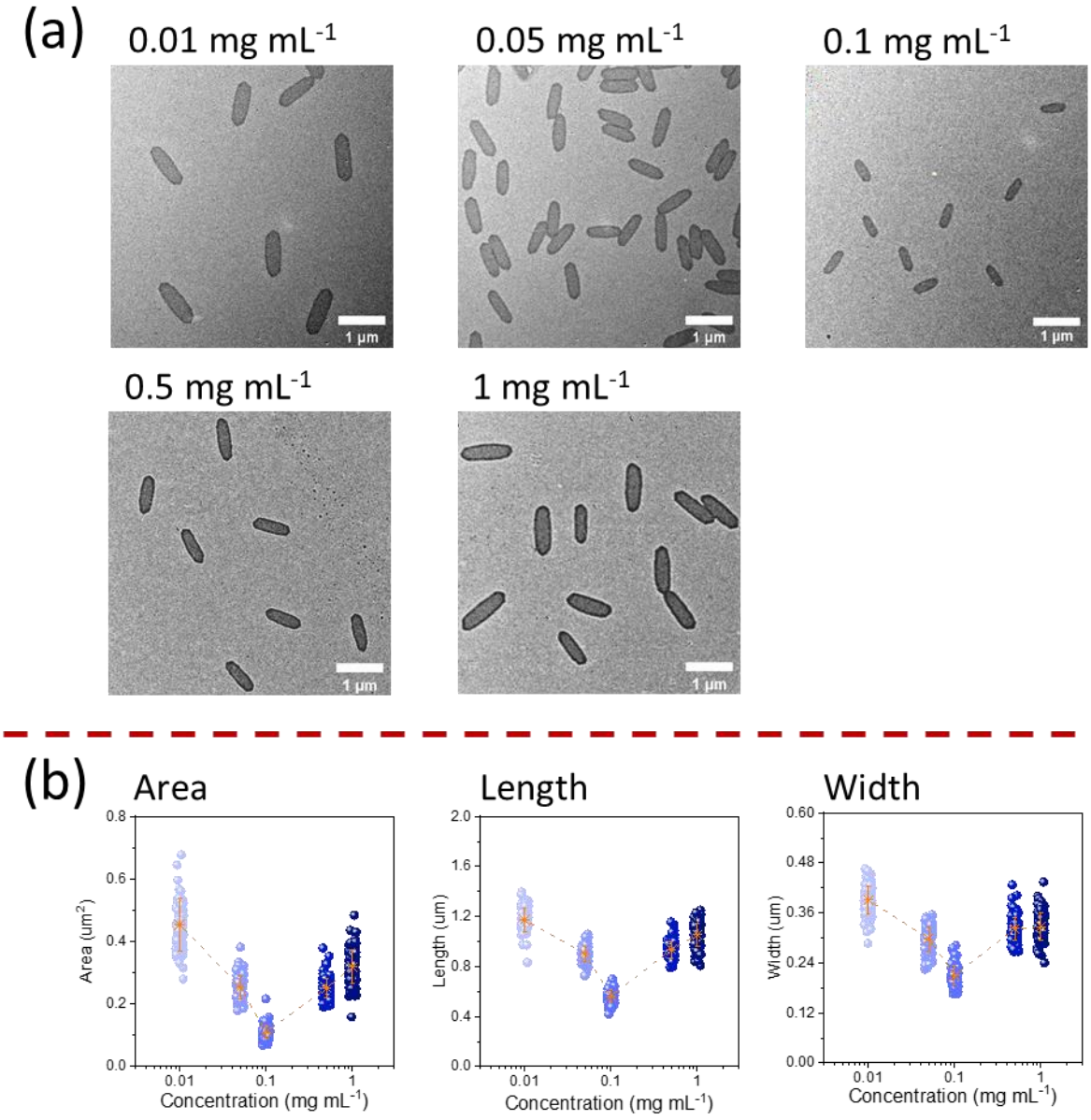

Figure S29. Living CDSA using flash-frozen seeds prepared at various concentrations: (a)TEM images of platelets and (b) Statical sizes of obtained platelets. 100 platelets were measured. Data are presented as mean values +/- standard deviation. Scale bar = 1 µm.

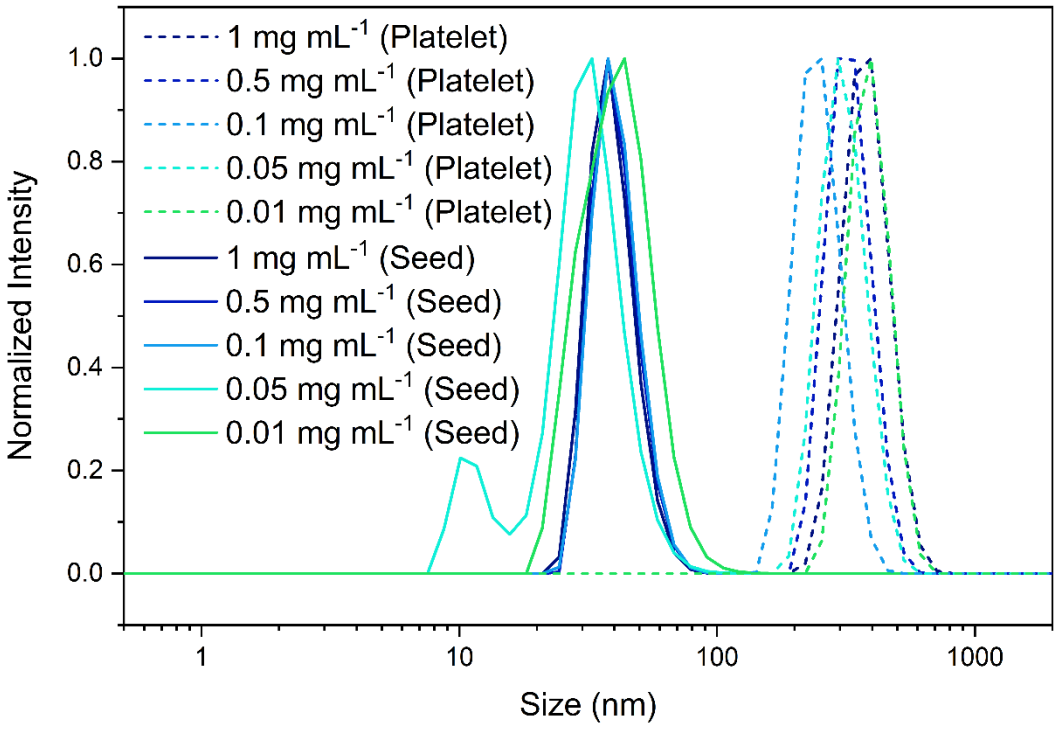

Figure S30. Comparison of DLS size distribution of flash-frozen seeds prepared at various concentrations and platelets prepared from these seed samples. The size is based on number distribution.

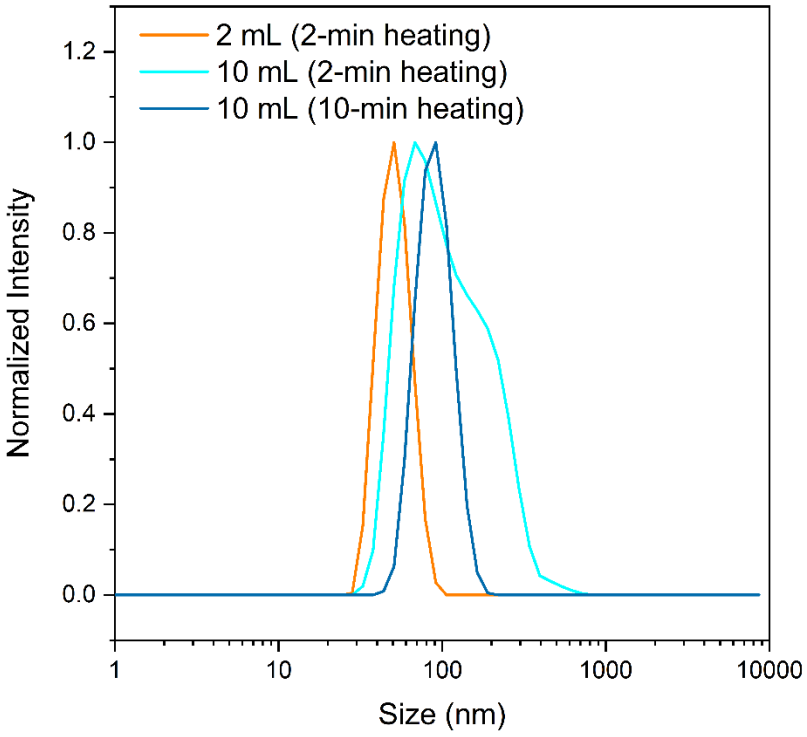

Figure S31. Comparison of flash-frozen seeds prepared at 2 mL scale (orange), 10-mL scale with 2-min heating (cyan), and 10-mL scale with 10-min heating (blue).

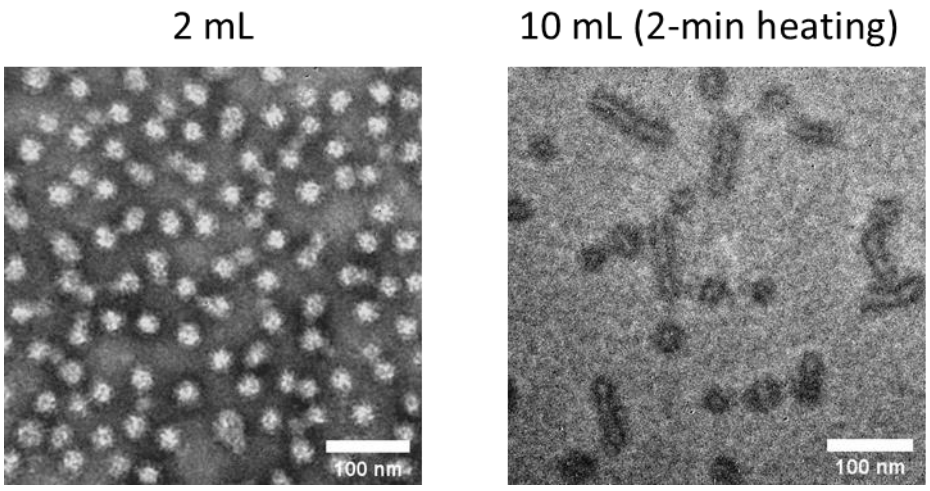

Figure S32. TEM images of flash-frozen seeds prepared at different scales. Scale bar = 100 nm. TEM samples were stained by uranyl acetate solution (1 wt%).

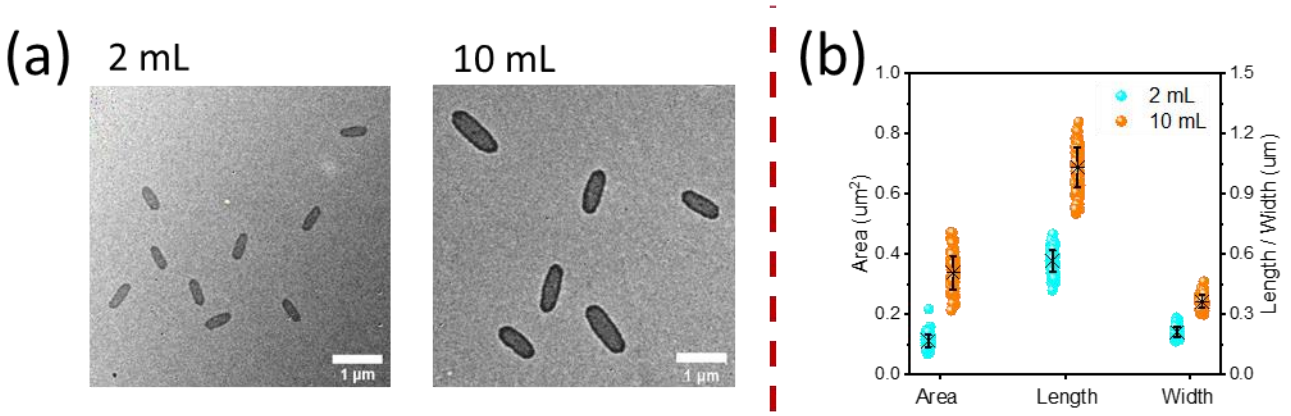

Figure S33. Living CDSA using flash-frozen seeds prepared at 2-mL and 10-mL scales: (a) TEM images of platelets, and (b) Statical sizes of obtained platelets. 100 platelets were measured. Data are presented as mean values +/- standard deviation. Scale bar = 1 µm.

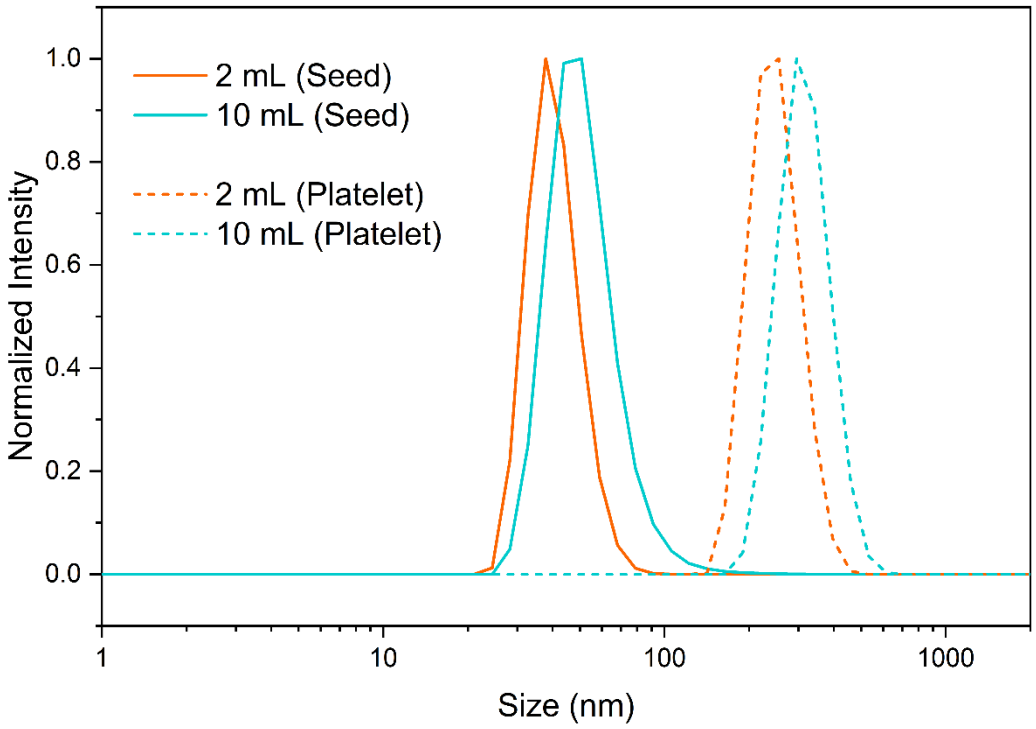

Figure S34. Comparison of DLS size distribution of flash-frozen seeds prepared on different scales and platelets prepared from these seed samples. The size is based on number distribution.

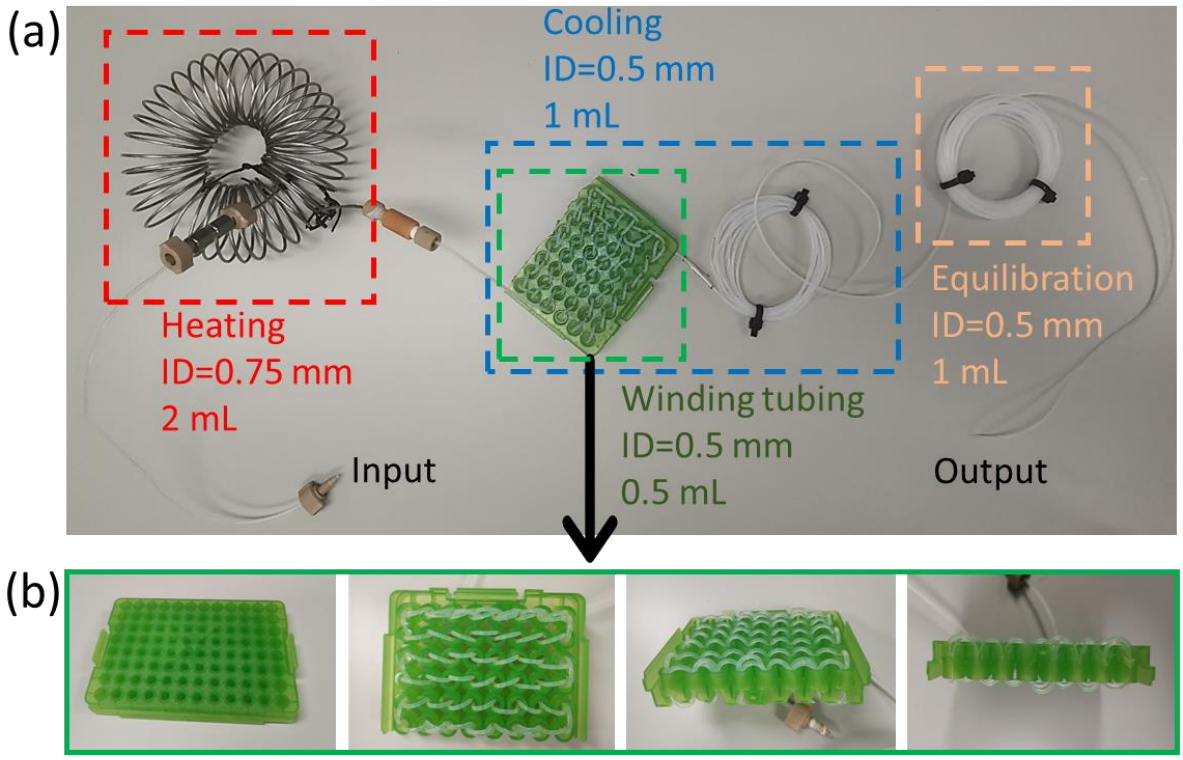

Figure S35. Photograph of flow setup to prepare flash-frozen seeds: (a) The integral flow setup, and (b) Detail photographs of self-designed winding tubing by winding PTFE tubing in an S-shape on the tip holder (SureOne^{TM} Pipet Tips, Fisher brand).

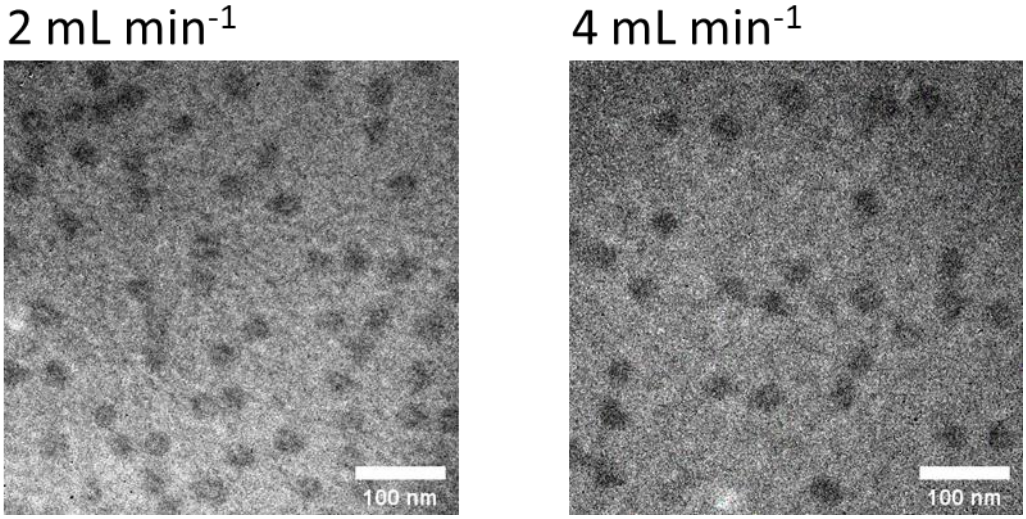

Figure S36. TEM images of seeds prepared at enhanced flow rates. Scale bar = 100 nm. TEM samples were stained by uranyl acetate solution (1 wt%).

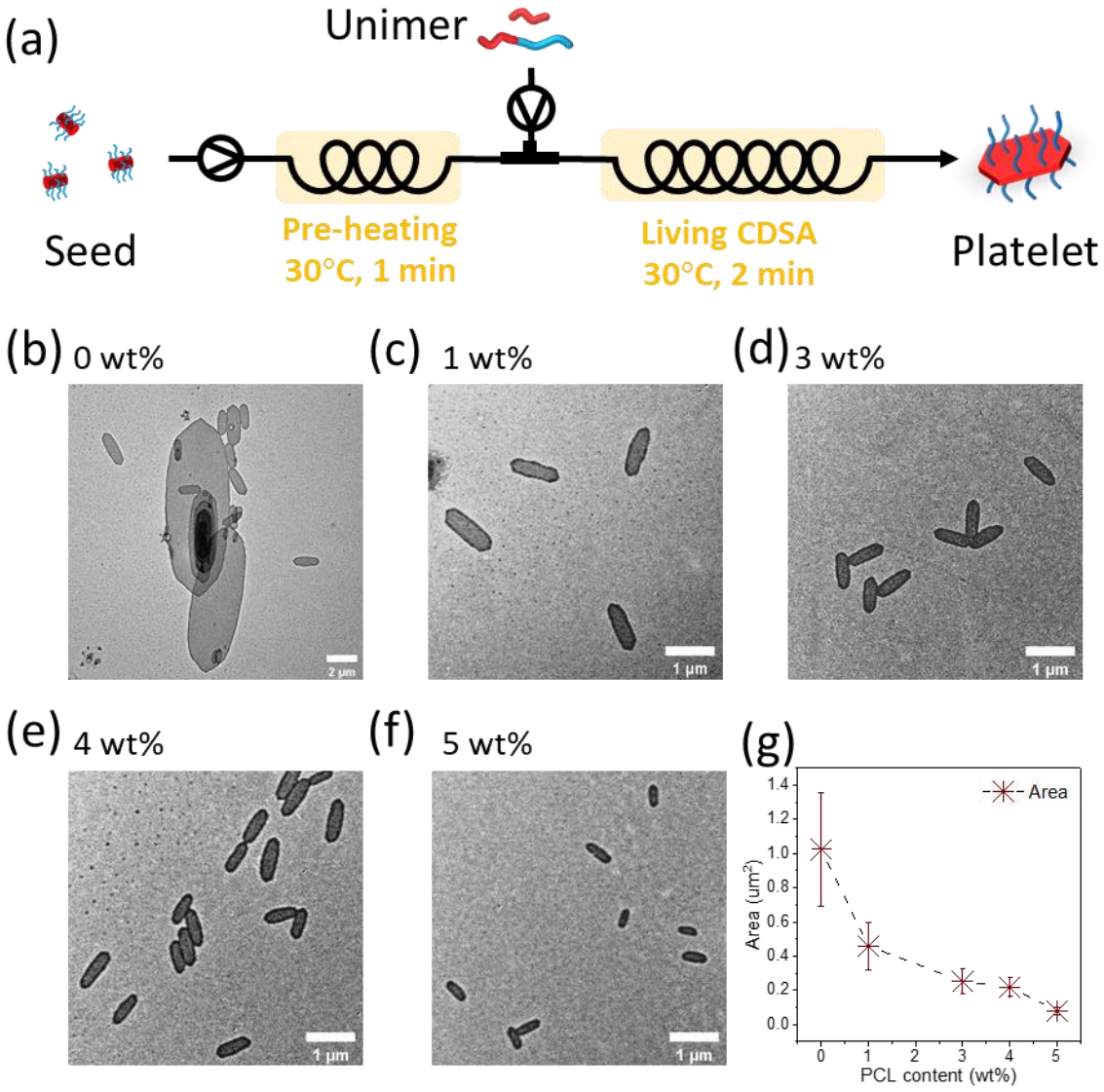

Figure S37. Flow living CDSA using seeds prepared with various PCL contents: (a) Scheme of flow living CDSA preparing platelets from seeds, (b)-(f) TEM images of platelets prepared form robust seeds with various PCL contents, and (g) Size trend of platelets against the PCL content added in seed preparation. 100 platelets were measured. Data are presented as mean values +/- standard deviation. Scale bar = 2 μm (b) and 1 μm (c)-(f).

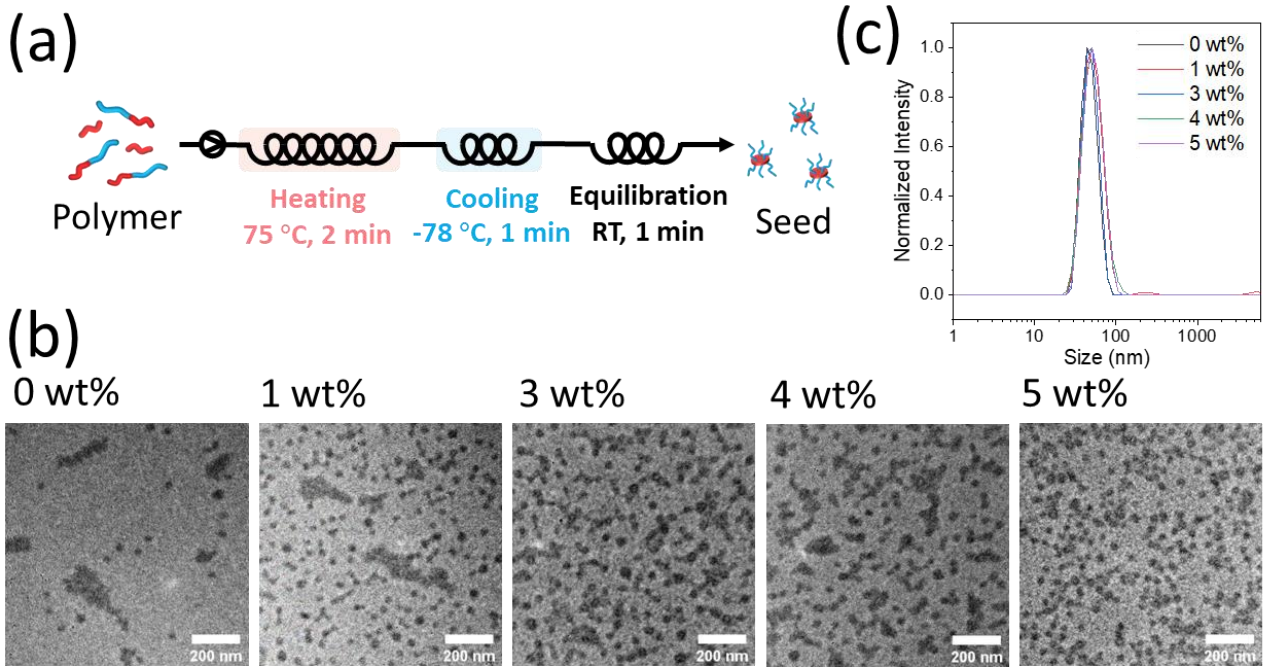

Figure S38. Seeds with various PCL contents prepared in flow without 30 °C annealing: (a) Preparation scheme, (b)TEM images of seeds with various PCL contents, and (c) Size distribution based on scattering intensity. Scale bar = 200 nm. TEM samples were stained by uranyl acetate solution (1 wt%).

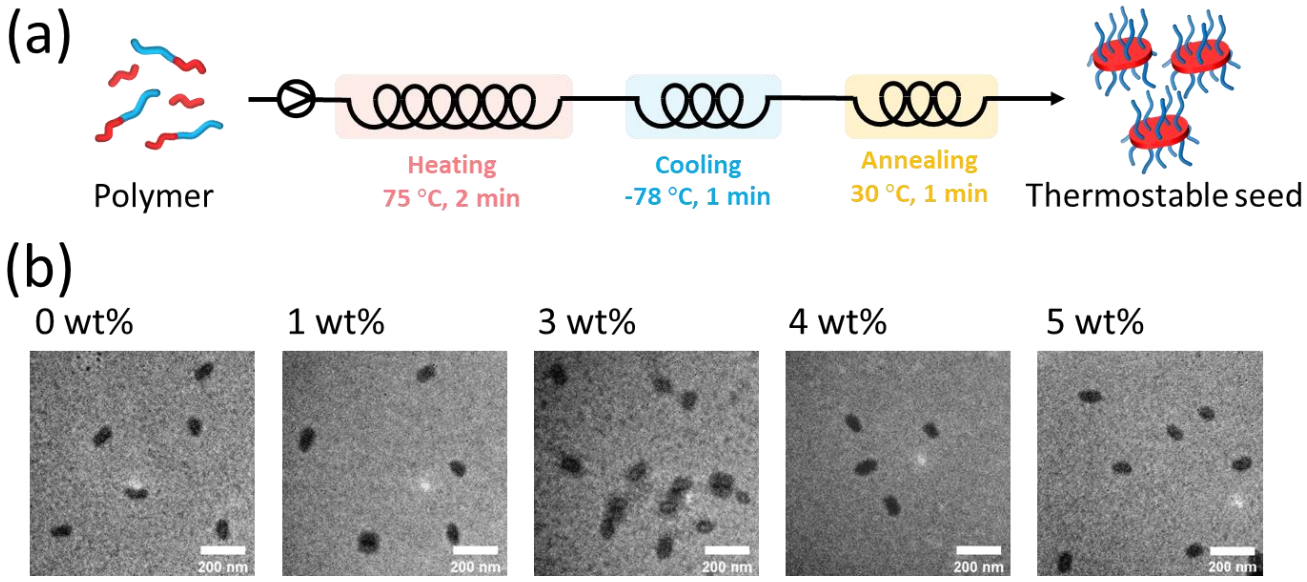

Figure S39. Thermostable seeds with various PCL contents prepared in flow with 30 °C annealing: (a) Preparation scheme, (b) TEM images of seeds prepared with various PCL contents characterized immediately after sample collection. Scale bar = 200 nm. TEM samples were stained by uranyl acetate solution (1 wt%).

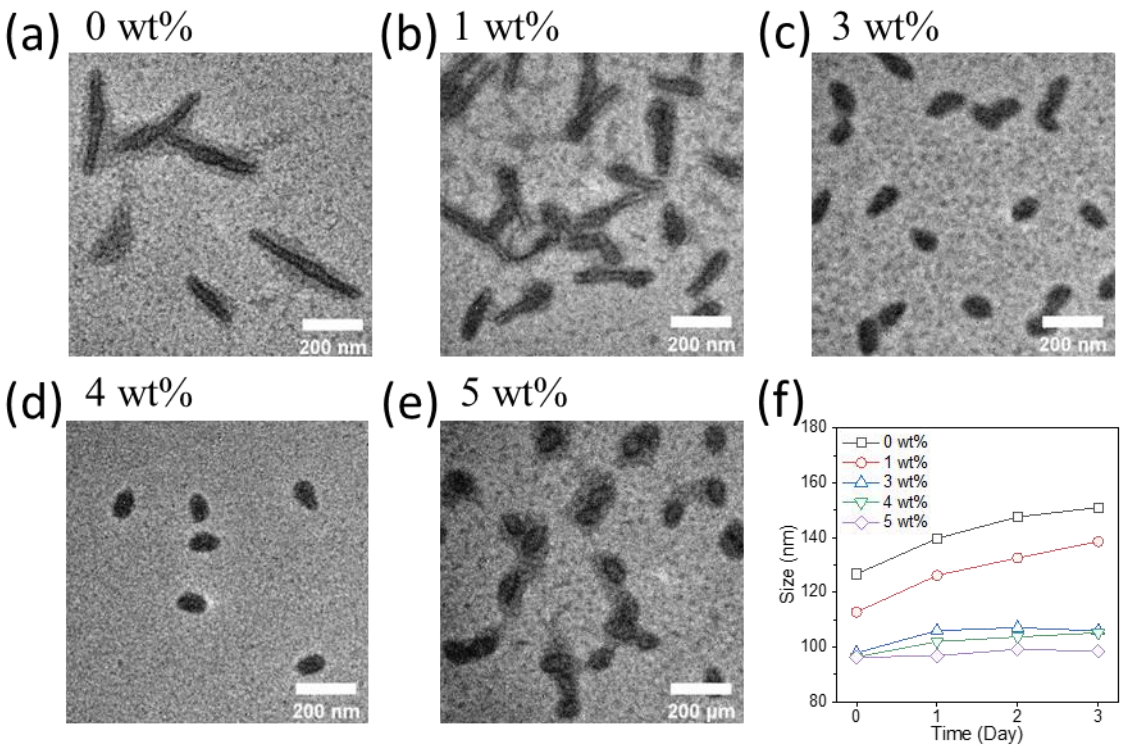

Figure S40. Robust seeds aged at room temperature: (a)-(e) TEM images of robust seeds prepared with various PCL contents characterized after a 3-day aging, (f) Trends of seed size over time for different PCL contents. Scale bar = 200 nm. TEM samples were stained by uranyl acetate solution (1 wt%).

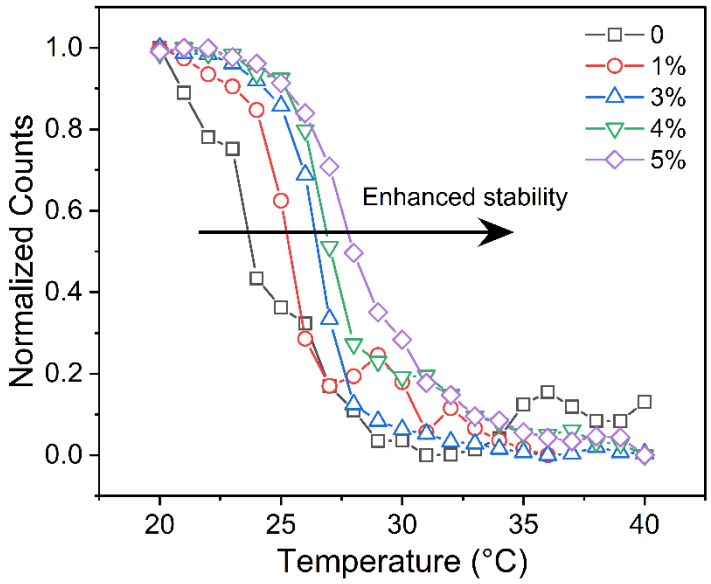

Figure S41. Size trends of seeds with various PCL contents as a function of temperature. Samples were characterized in the temperature range of 20-40 °C, with the heating rate of 1 °C min^{-1}. Samples were equilibrated for 2 min before testing at each new temperature.

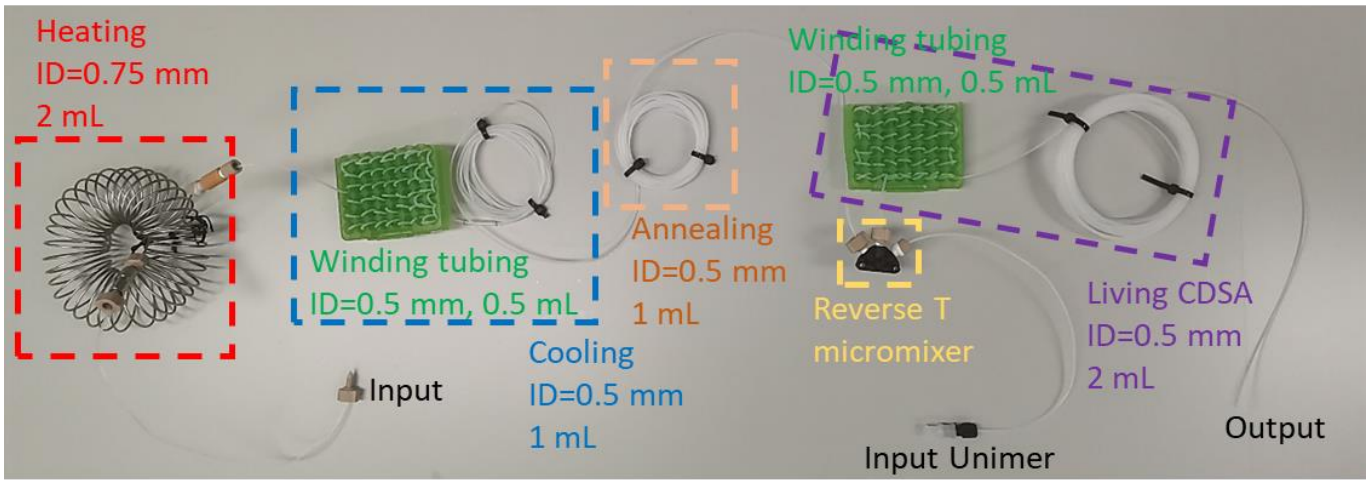

Figure S42. Photograph of the integral flow setup to prepare platelets from polymer.

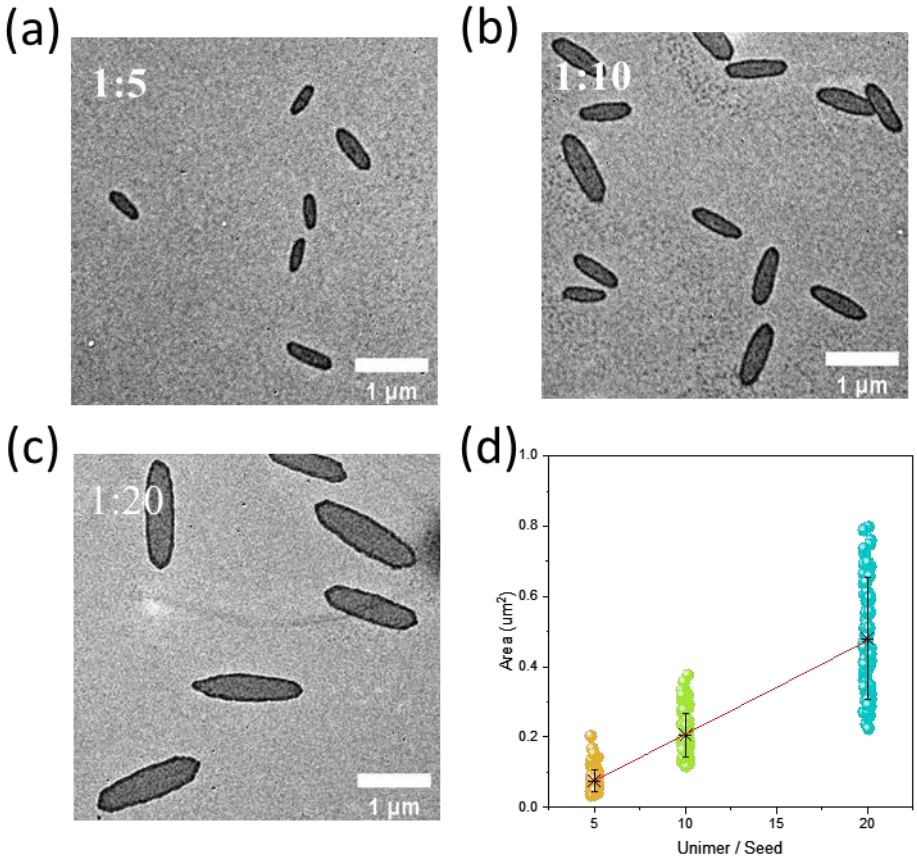

Figure S43. Platelets prepared from polymer directly using the integral flow cascade: (a)-(c) TEM images of platelets prepared at unimer-to-seed ratios, and (d) Linear fit of area upon different unimer-to-seed ratios. 100 platelets were measured. Data are presented as mean values +/- standard deviation. Scale bar = 1 µm.

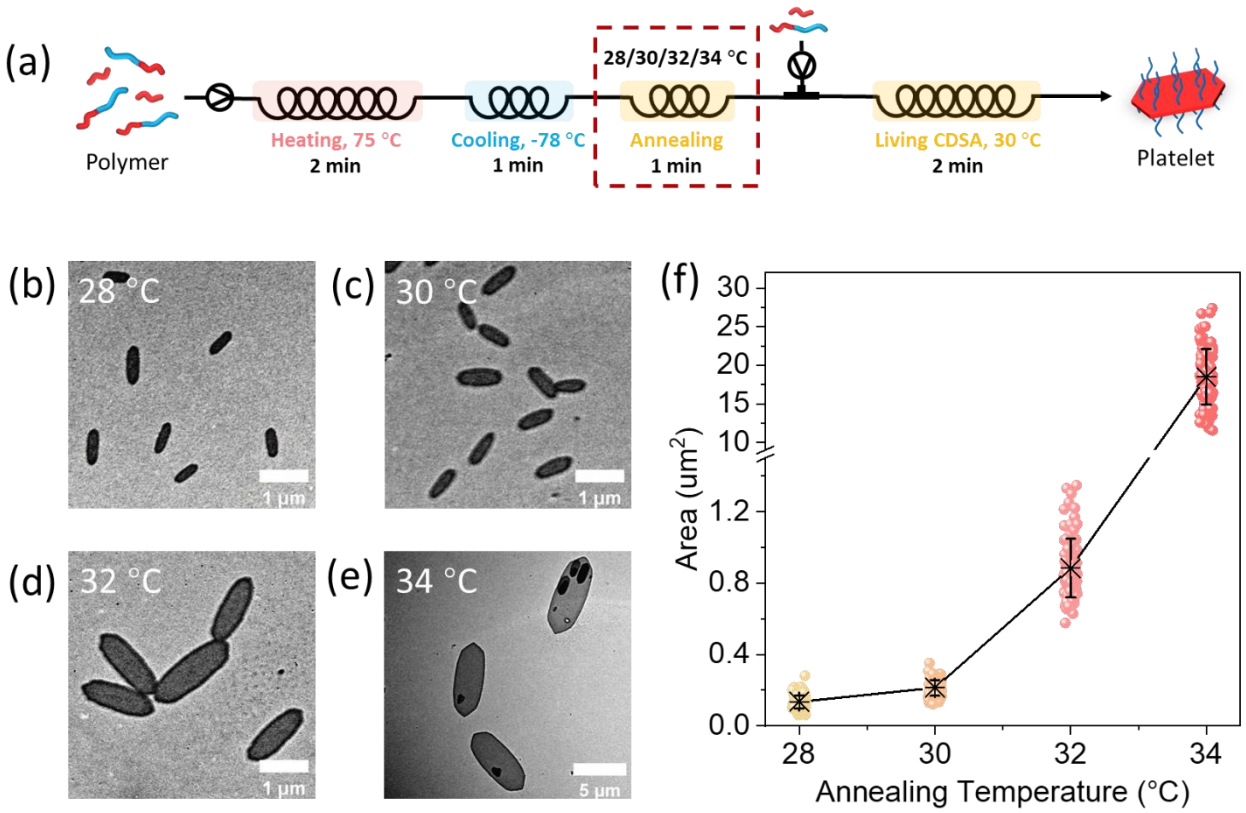

Figure S44. Self-seeding strategy for controlled preparation of platelets through integral flow cascade: (a) Preparation scheme, (b)-(e) TEM images of platelets prepared at various annealing temperatures, and (f) Size variation of platelets against annealing temperature. 100 platelets were measured. Data are presented as mean values +/- standard deviation. Scale bar = 1 μm (b)-(d) and 5 μm (e).

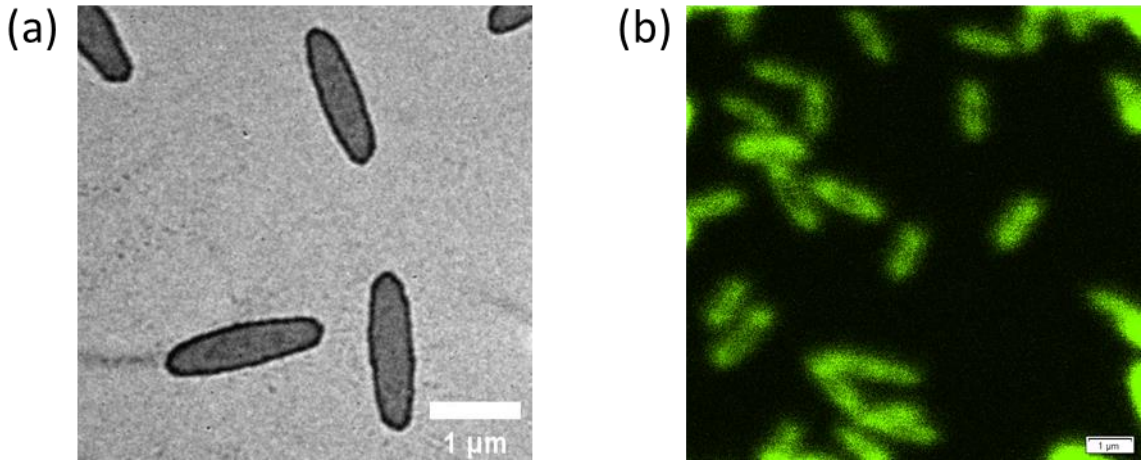

Figure S45. Double-layered platelets prepared from polymer directly using the integral flow cascade: (a) TEM image of platelets prepared at unimer-to-seed ratio of 20:1, and (b) Layered structure of platelets shown in the CLSM image. Scale bar = 1 µm.

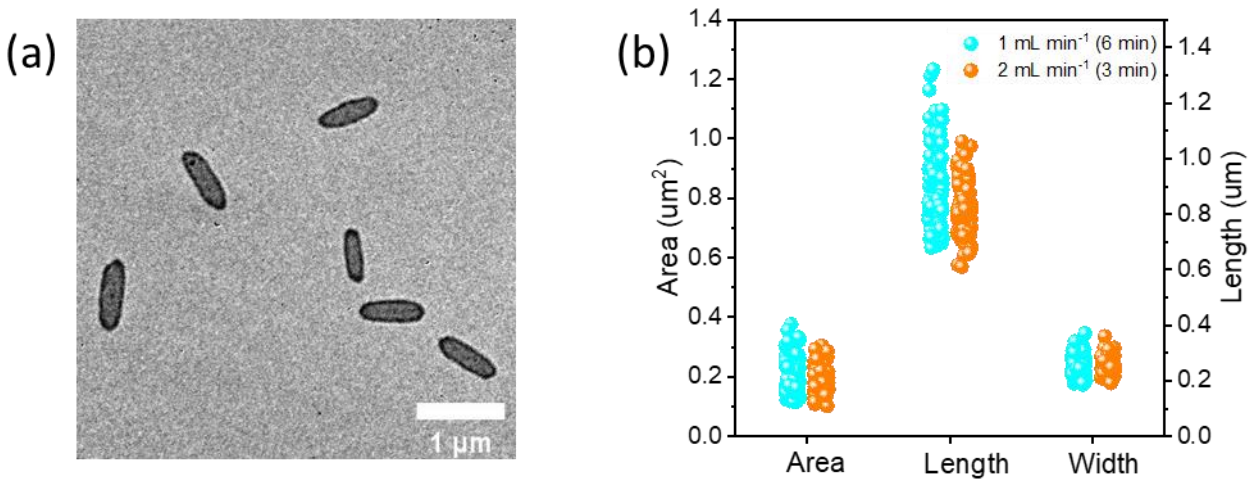

Figure S46. Platelets prepared in 3 min by increasing flow rate to 2 mL min^{-1}: (a) TEM image, and (b) Size comparison of platelets prepared at different flow rates.

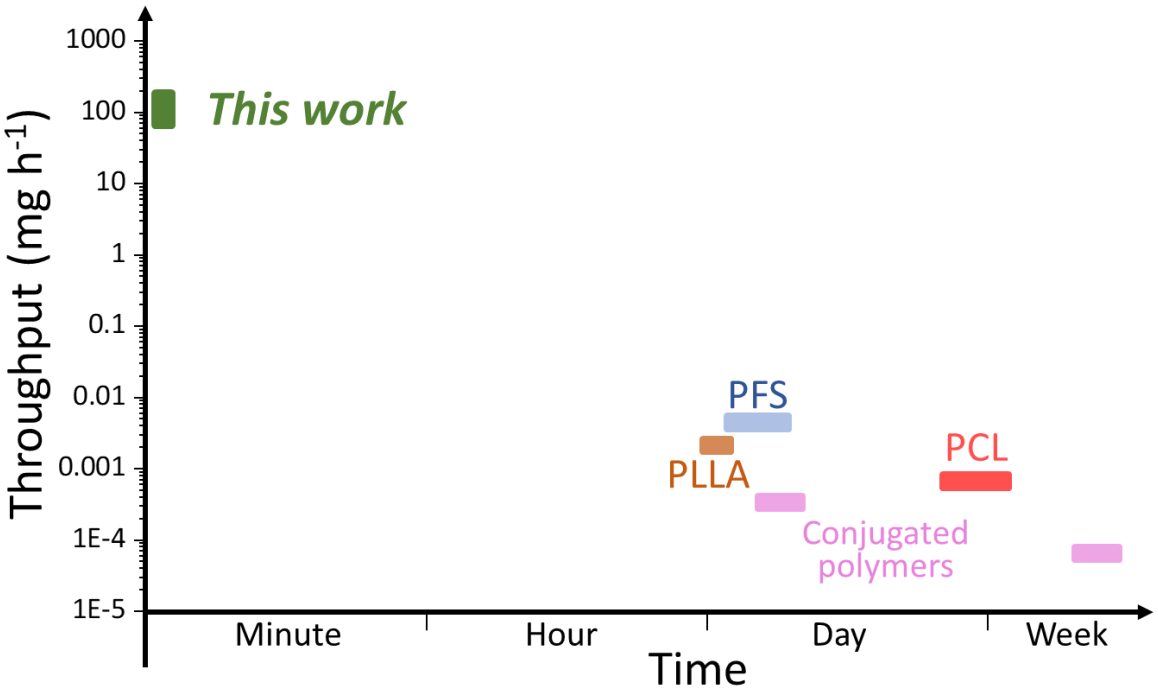

Figure S47. Comparison of processing time and throughput of reported 2D platelets of various core chemistries.

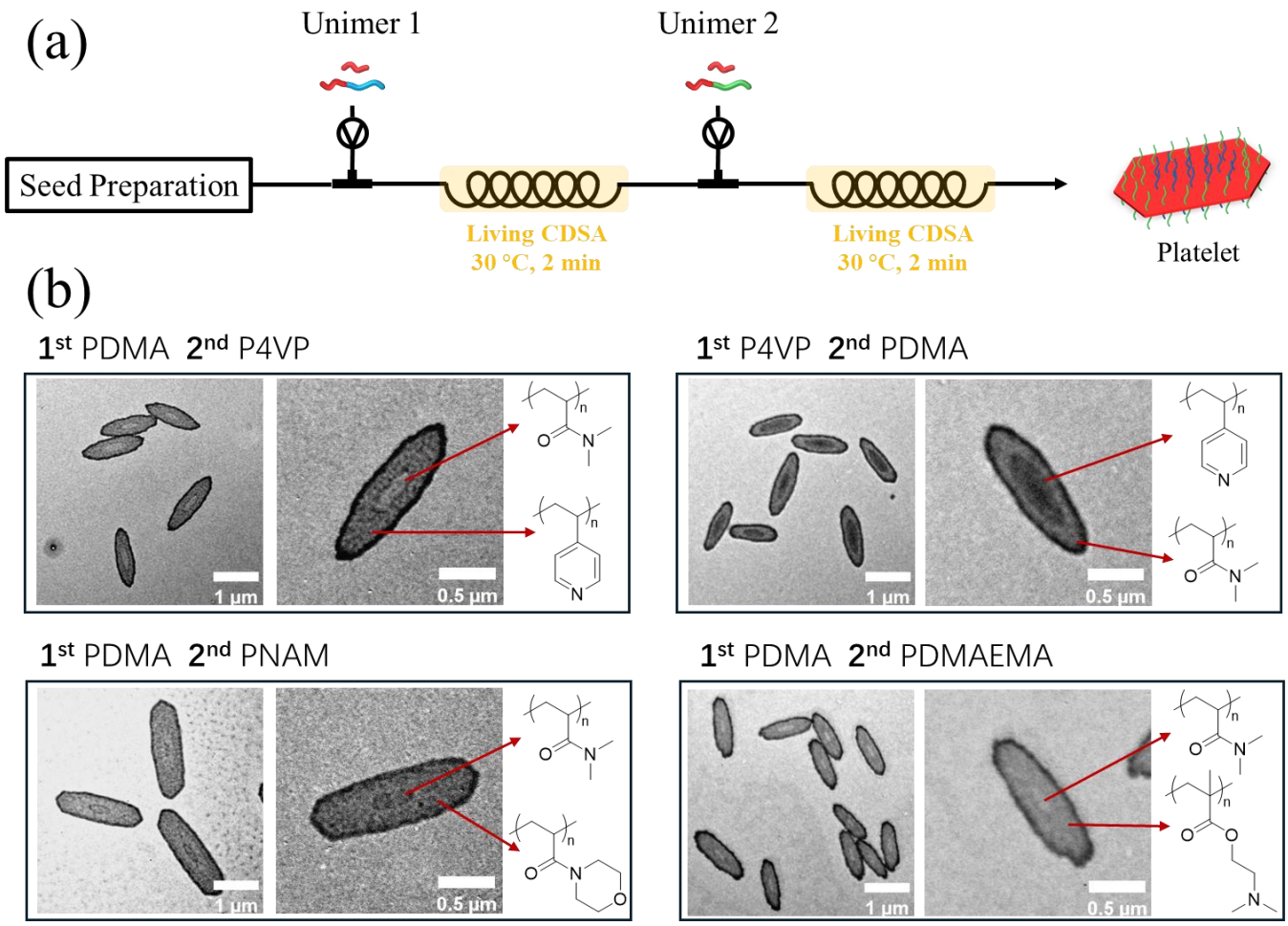

Figure S48. Double-layered platelets with heterogeneous corona chemistry prepared by the integral flow cascade: (a) Preparation scheme, and (b) TEM images of multiple platelets (Scale bar = 1 μm) and single platelets (Scale bar = 0.5 μm) of higher magnification. Samples were stained by 1 wt% uranyl acetate aqueous solution.

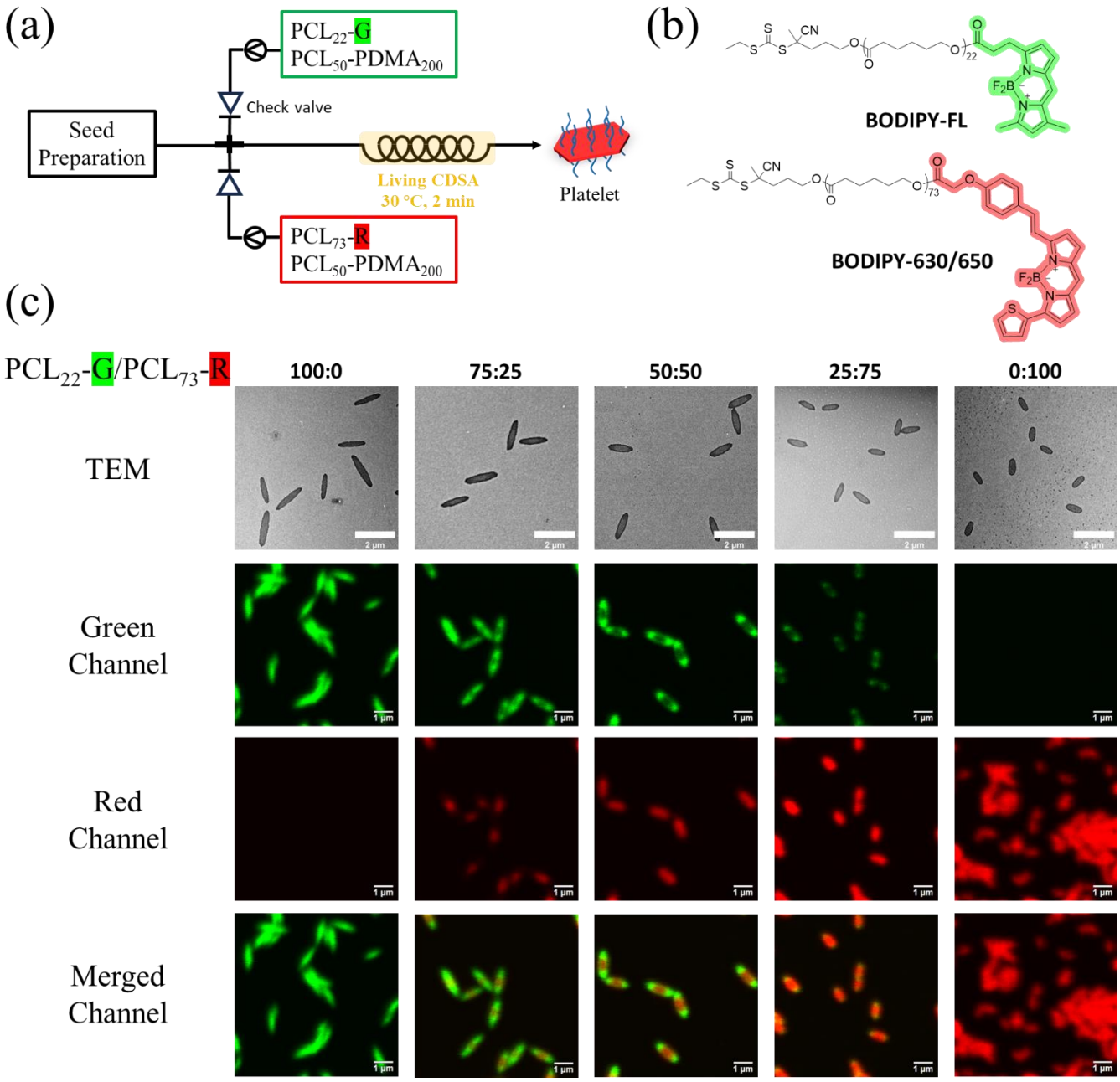

Figure S49. Platelets with tunable core chemistry prepared by the integral flow cascade: (a) Preparation scheme, (b) Chemical structures of fluorescent dye modified PCL homopolymers, and (c) Platelet samples imaged by TEM and CLSM of different channels. Scale bar = 2 μm (TEM) and 1 μm (CLSM).

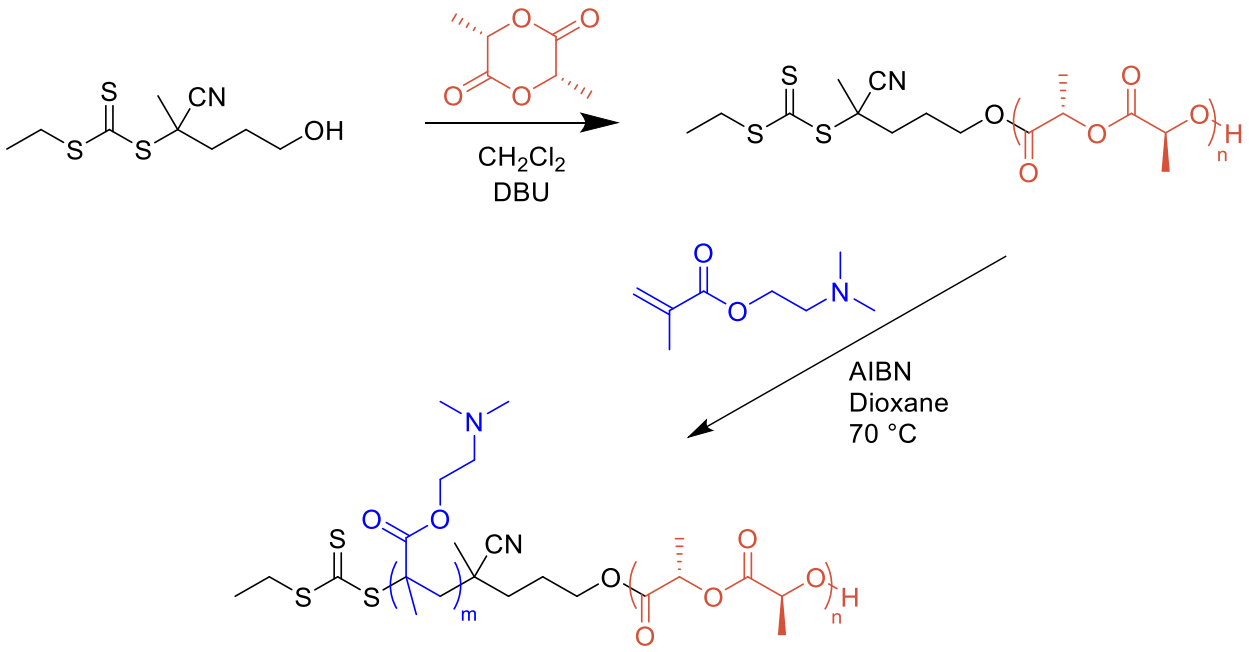

Figure S50. Synthetic routes of PLLA-based polymers.

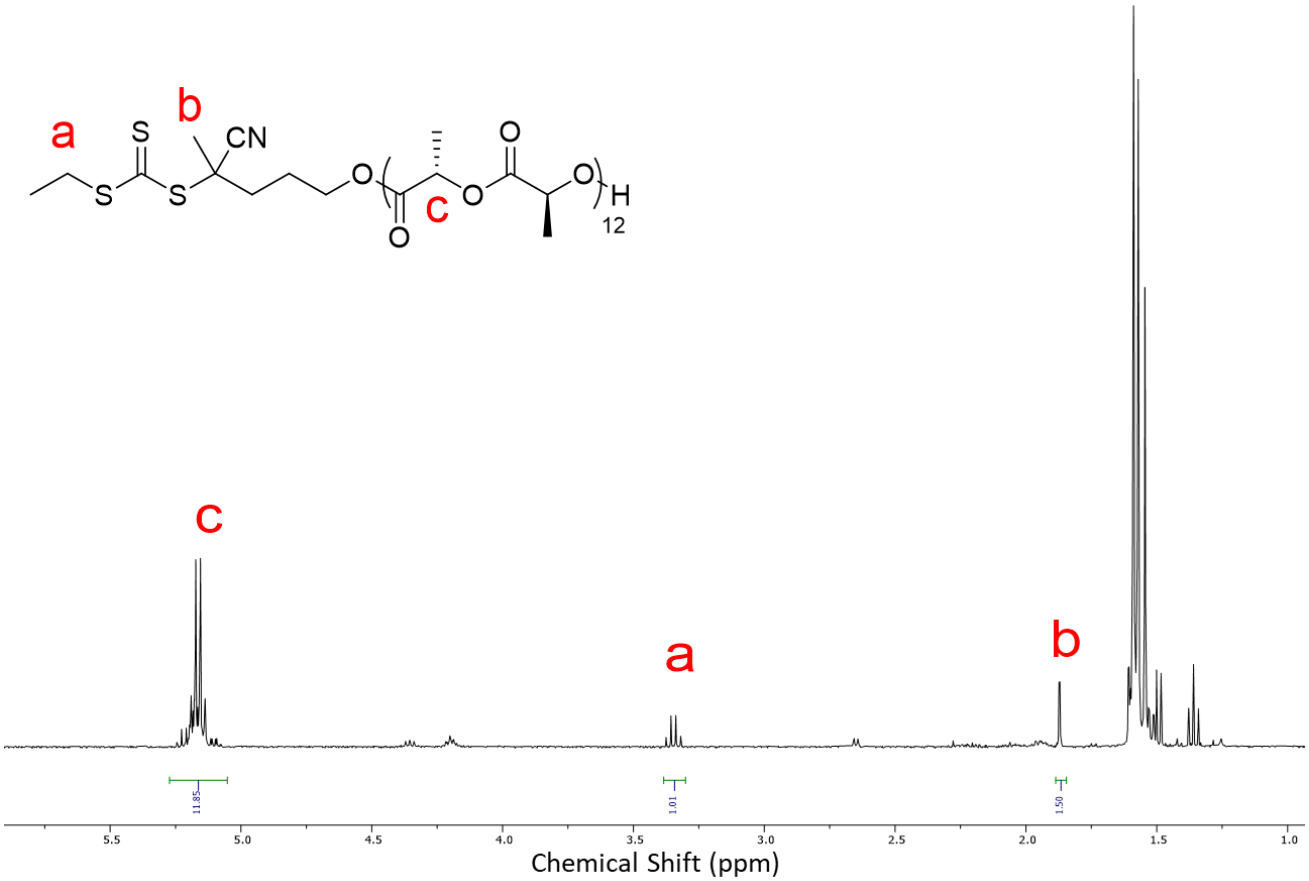

Figure S51. ^{1}H NMR spectra of PLLA.

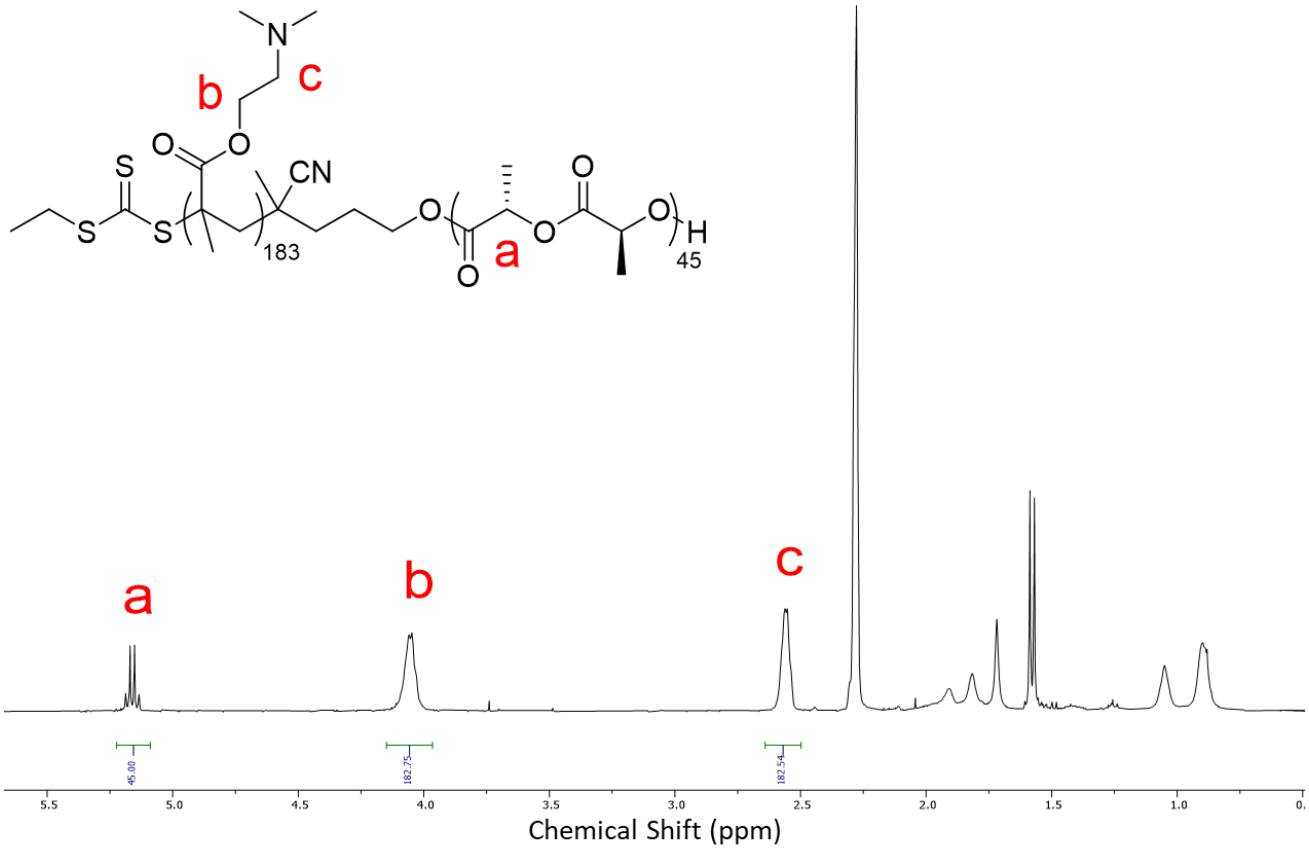

Figure S52. ^{1}H NMR spectra of PLLA-*b*-PDMAEMA.

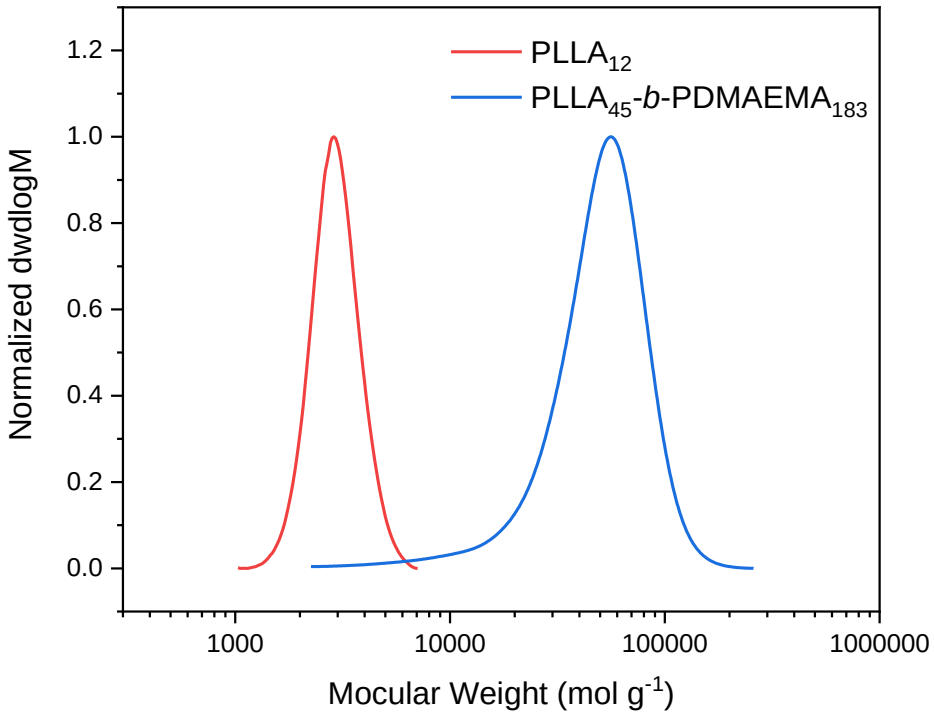

Figure S53. Normalized SEC curves of PLLA and PLLA-*b*-PDMAEMA.

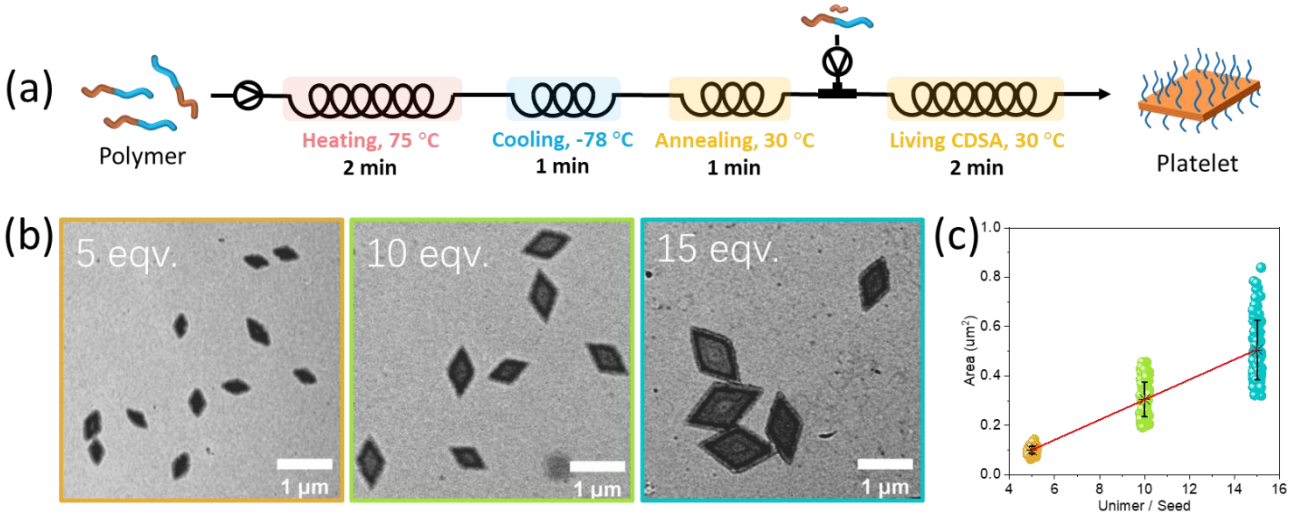

Figure S54. PLLA-based platelets prepared from polymer directly using the integral flow cascade: (a) Preparation scheme, (b) TEM images of platelets prepared at various unimer-to-seed ratios, and (c) Linear fit of area upon different unimer-to-seed ratios. 100 platelets were measured. Data are presented as mean values +/- standard deviation. TEM samples were stained by uranyl acetate solution (1wt%). Scale bar = 1 μm.

Reference

1. Xiao, L., Parkinson, S.J., Xia, T., Edge, P. & O'Reilly, R.K. Enhancing the Scalability of Crystallization-Driven Self-Assembly Using Flow Reactors. *ACS Macro Lett.* **12**, 1636-1641 (2023).
2. Arno, M.C. *et al.* Precision Epitaxy for Aqueous 1D and 2D Poly(epsilon-caprolactone) Assemblies. *J. Am. Chem. Soc.* **139**, 16980-16985 (2017).
3. Rajak, A. & Das, A. Crystallization-Driven Controlled Two-Dimensional (2D) Assemblies from Chromophore-Appended Poly(L-lactide)s: Highly Efficient Energy Transfer on a 2D Surface. *Angew. Chem. Int. Ed.* **61**, e202116572 (2022).
4. Xia, T. *et al.* Tuning the Functionality of Self-Assembled 2D Platelets in the Third Dimension. *J. Am. Chem. Soc.* **145**, 25274-25282 (2023).
5. Xia, T. *et al.* Control over Aspect Ratio and Polymer Spatial Distribution of 2D Platelets via Living Crystallization-Driven Self-Assembly. *Macromolecules* **57**, 11210–11220 (2024).

Chapter 4 - 3D Nanopatterning of Platelets via Temperature-Controlled Self-Sorting

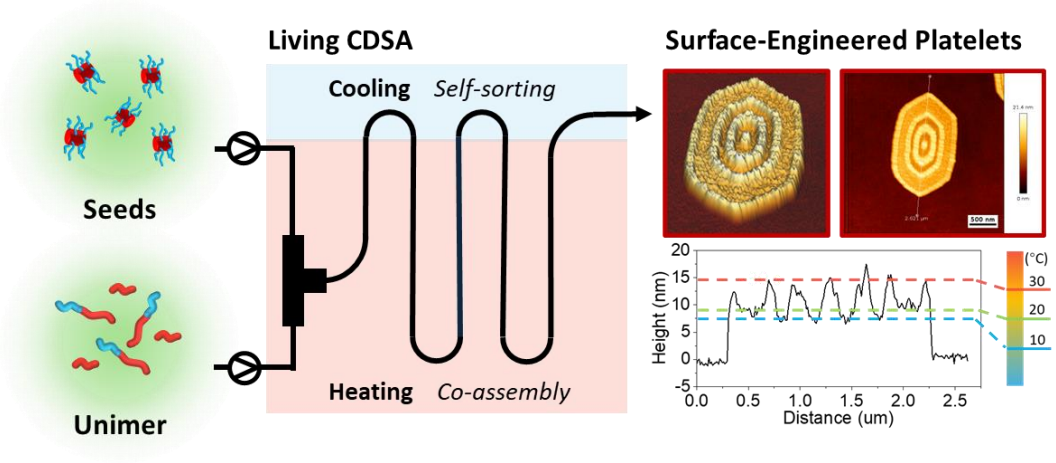

4.1 Publication Details and Overview

Title: 3D Nanopatterning of Platelets via Temperature-Controlled Self-Sorting

Authors: Laihui Xiao,[†] Tianlai Xia,[†] Calum T. J. Ferguson,[†] Andrew P. Dove,[†,*] Rachel K. O'Reilly[†,*]

Affiliation: [†]School of Chemistry, University of Birmingham, Edgbaston, Birmingham B15 2TT, UK

Manuscript Prepared

Coauthor Contributions:

Mr. Tianlai Xia assisted with confocal tests, kinetic simulations, characterization exploration, and progress discussions. Dr. Calum T. J. Ferguson contributed to progress discussions and manuscript revisions. Prof. Andrew P. Dove helped with proofreading and supervision. Prof. Rachel K. O'Reilly supervised the project, helped with ideation, progress discussions, funding acquisition, and reviewed the manuscript.

Overview:

This chapter presents a controlled method for fabricating 3D patterns on the surface of assembled platelets, demonstrating a bottom-up approach for the preparation of nanoparticles with fine structural details.

A temperature-responsive homo/diblock polymer system was initially developed, exhibiting distinct co-assembly behaviors when used as unimers for living CDSA. Specifically, the two polymers co-assemble at 30 °C, while self-sorting occurs at 10 °C, based on the differences in crystallization kinetics at these temperatures. Thus, the distribution of polymers on the platelets is controlled by temperature, allowing for the fabrication of various surface patterns formed by the corona. Furthermore, the height of these patterns can be precisely regulated by adjusting the polymer composition. Leveraging the superior heat transfer capabilities of flow reactors, living CDSA was conducted in a flow system to achieve precise control over the surface patterns. Remarkably, layered fine 3D patterns, which are challenging to obtain in batch processes, were efficiently produced by rapid temperature-switching in flow, resulting in nanopatterns with an accuracy comparable to lithographic structures.

Overall, this work demonstrates a novel strategy for simultaneously constructing a platelet base and intricate 3D nanopatterns, streamlining the entire production process. This novel method provides a highly efficient and precise approach for producing complex nanostructures, significantly advancing the capabilities of nanoparticle fabrication.

3D Nanopatterning of Platelets via Temperature-Controlled Self-Sorting

Laihui Xiao,[a] Tianlai Xia,[a] Calum T. J. Ferguson,[a] Andrew P. Dove,[a]* Rachel K. O'Reilly[a]*

[a] School of Chemistry, University of Birmingham, Edgbaston, Birmingham B15 2TT, UK

*Corresponding Author: r.oreilly@bham.ac.uk (ROR) and a.dove@bham.ac.uk (APD)

Abstract

Precise control of surface patterns in assembled nanostructures remains a significant challenge in material science. Here, we introduce a scalable bottom-up strategy utilizing living crystallization-driven self-assembly (CDSA) to fabricate tunable 3D surface patterns on polymer platelets. By leveraging polymer systems with temperature-dependent assembly mechanisms, we achieved diverse morphologies, including layered, concave, and convex patterns, through controlled co-assembly and self-sorting. A flow reactor with precise temperature modulation enabled rapid formation of multilayered structures, delivering a resolution of 100 nm in the 2D plane and 2 nm in the vertical dimension. Unlike traditional lithographic techniques, which offer limited control over vertical features, this approach provides high-resolution 3D patterning via a cost-effective, bottom-up process. These advancements address critical gaps in nanostructure precision and scalability, enabling transformative applications in fields like functional materials and nanotechnology.

Introduction

Crystallization-driven self-assembly (CDSA) has emerged as a powerful method for constructing well-defined anisotropic nanostructures.[1-4] Through this technique, polymers with crystalline blocks undergo directional crystallization, and the nanostructure size can be precisely tuned via a seeded growth process, known as "living" CDSA. Specifically, when preparing two-dimensional (2D) platelet structures, co-assembly of homopolymers and diblock copolymers is commonly employed to achieve complex, tunable architectures, where each polymer type brings unique structural and functional contributions to the final assembly.[5-7] Importantly, varying the polymer composition and processing conditions impacts key structural features, such as morphology, stability, and size, allowing precise engineering of functional nanostructures.[5, 8, 9]

Surface patterns of assembled nanostructure are crucial for nanomaterial functionality, but achieving precise control remains challenging.[10-12] Conventional top-down methods, like photolithography and etching, can create three-dimensional (3D) patterns on 2D substrates with high precision but offer limited control over the third dimension.[13] Additionally, these techniques are often complex, equipment-intensive, and challenging to apply directly to assembled nanostructures. Our previous work demonstrated a graft-from strategy to extend corona length in specific areas of CDSA platelets to form defined 3D patterns.[14] While effective, this method required laborious synthesis and post-processing. Alternatively, manipulating 3D patterns on platelets could be potentially achieved by controlling the spatial distribution of polymers. This is based on the previous reports that layered structures can be formed on platelets where homopolymers crystallize significantly faster than diblock polymers, and this kinetically controlled behavior leads to the spatial separation of the two polymers and formation of layered structures.[5]

This kind of behavior, where different polymers organize into distinct domains or patterns in multicomponent co-assembly systems, is called self-sorting, which facilitates spatial separation

within the same structure.[15, 16] This selective organization is widespread in natural systems, playing a central role in building highly organized cellular structures. By mimicking this process, self-sorting in synthetic assemblies enables spatial control over multiple components in a single nanostructure, offering an approach to design more sophisticated materials.[17] External stimuli such as temperature, pH, or solvent composition can influence or even induce self-sorting, providing an additional level of control over the co-assembly process.[18, 19] Although kinetically controlled self-sorting in CDSA nanostructures has been reported, achieving reliable control for precise patterning remains a significant challenge.[6, 20]

In this study, we investigated the co-assembly of polycaprolactone (PCL)-based homopolymers and diblock copolymers through living CDSA to create self-sorted, patterned platelets. Variations in polymer molecular weight and chemistry lead to distinct crystallization rates in response to temperature,[21, 22] enabling self-sorting behavior driven by kinetic differences. This process was precisely controlled in flow reactors, facilitated by the excellent temperature management they provide. In this manner, we aim to develop innovative strategies for controlling the 3D patterning on the surfaces of assembled nanostructures.

Results and discussion

Synthesis

Initially, PCL homo (PCL_{50}, the subscript refers to the number-average polymerization degree) and diblock (poly(ε-caprolactone)-*b*-poly(N,N-dimethylacrylamide), PCL_{136}-*b*-$PDMA_{200}$) polymers were prepared by the combined ring opening and reversible addition-fragmentation chain-transfer (RAFT) polymerization (Scheme S1).[23-26] The polymerization degree was confirmed by proton nuclear magnetic resonance (^{1}H NMR, Figures S1 and S2), and the molecular weight and dispersity were characterized using size exclusion chromatography (SEC, Figure S3 and Table S3). Different from our previous work,[5, 7, 14, 23, 26] a diblock polymer (PCL_{136}-*b*-$PDMA_{200}$) with a much longer PCL block was prepared to increase the crystallization capacity.

Living CDSA at Various Temperatures

Temperature is a readily tunable external stimulus and can significantly influence the crystallization behavior of polymers.[21] To explore this effect, living CDSA was conducted at various temperatures to control the dynamics of polymer growth. The same seed sample previously reported (Figures 1 and S4), with an average size of 25.2 nm, was used for this process.[23] Following the addition of unimer (PCL_{50} / PCL_{136}-*b*-$PDMA_{200}$, 1:1 weight ratio, 10 mg mL^{-1} in $CHCl_3$; Figure 1a), platelets with diverse morphologies were formed, as shown in the atomic force microscopy (AFM) images (Figures 1c and S5).

Previous results indicated that platelet patterns are formed by polymer coronas, representing the distribution of diblock polymers.[5, 14] Therefore, height profiles were recorded to map this distribution and characterize the 3D patterns. At 30 °C, the central region of the platelet (13.5 nm) was higher than the edge (11.1 nm), indicating that diblock polymers crystallized faster than homopolymers. When the temperature was reduced to 20 °C, the crystallization of homopolymers became faster than that of diblock polymers, resulting in a decreased central

height (9.9 nm) and accumulation of diblock polymers at the platelet edges (12.8 nm), consistent with previous observations.[5, 14, 27] At 10 °C, the crystallization disparity increased further, forming distinct layered platelets with a thin central region with a height of 7.8 nm—corresponding to the PCL single crystal—and a thicker edge (15.5 nm) contributed by diblock polymers.[28] To confirm that these temperature-dependent patterns were due to the increased crystallization tendency of the diblock polymer, control samples were prepared using PCL_{50} / PCL_{50}-*b*-$PDMA_{200}$ unimers (Figure S6). In these controls, regardless of preparation temperature, the platelet edge consistently remained higher than the centre.

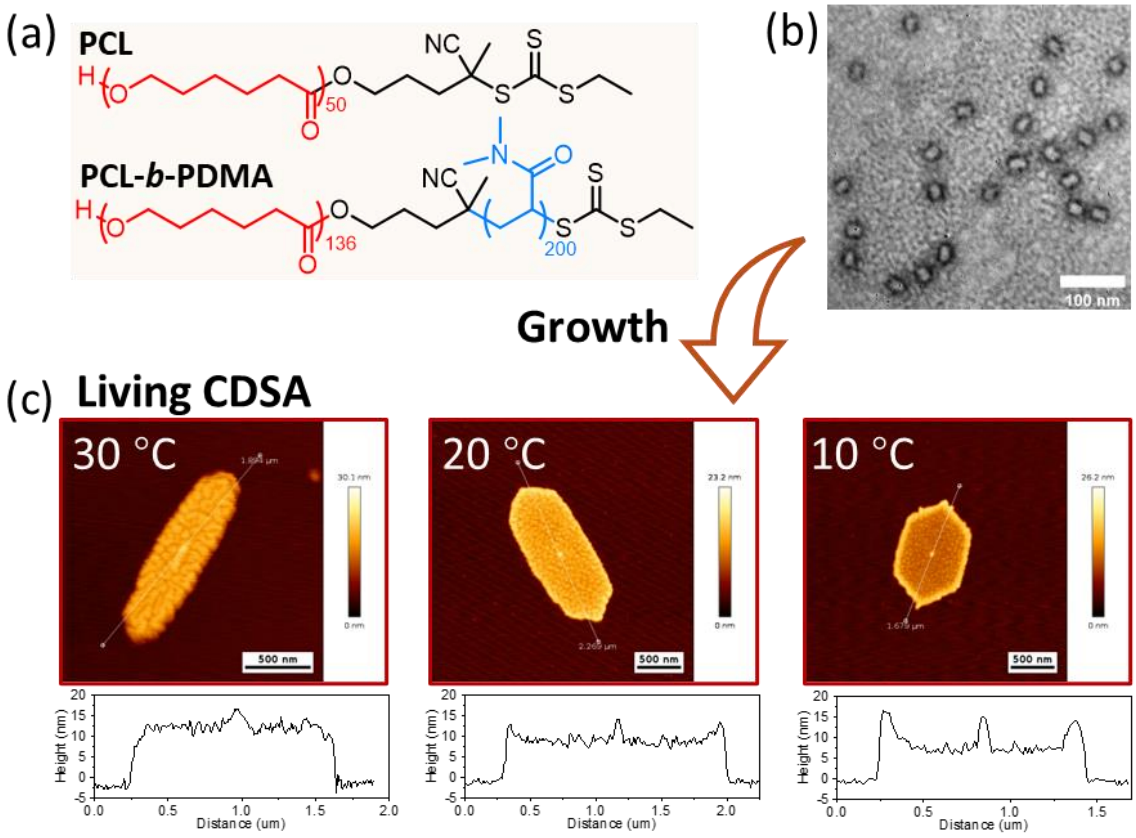

Figure 1. Living CDSA using 10 eqv. unimer at various temperatures: (a) Chemical structures of homo and diblock polymers, (b) TEM image of seeds, and (c) AFM images of platelets prepared at 30, 20, and 10 °C respectively. TEM sample was stained by uranyl acetate aqueous solution (1%). Scale bar = 100 nm (a) and 500 nm (c).

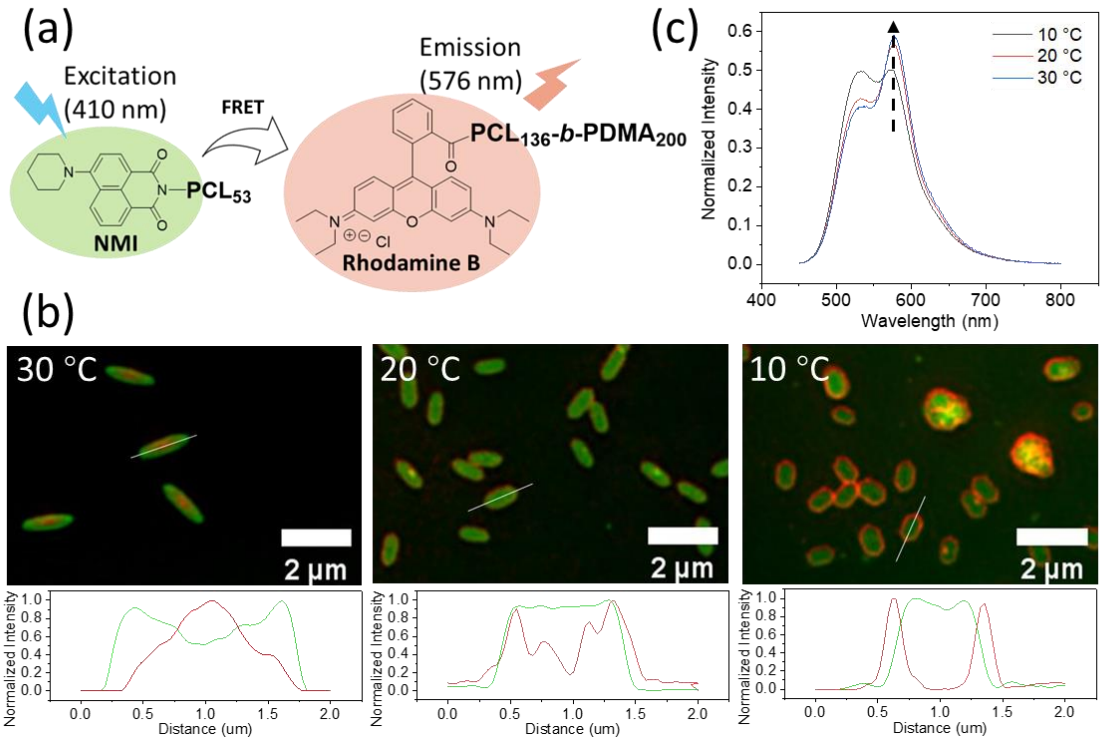

Figure 2. FRET on fluorescent dye-labelled platelets: (a) Schematic illustration of FRET between PCL_{53}-NMI (green) and PCL_{136}-*b*-$PDMA_{200}$-rhodamine B (red), (b) SIM images of fluorescent platelets prepared at various temperatures, and (c) Emission spectra of platelets excited at 410 nm, with peaks observed at 530 nm (NMI) and 575 nm (rhodamine B). Scale bar = 2 μm.

Fluorescent Mapping and FRET

Although AFM can map the distribution of diblock polymers by detecting the additional height from coronas, it cannot precisely determine the distribution of homopolymers. Therefore, fluorescence labelling was used as a complementary method to further investigate the distribution of polymers across platelets. Naphthalene monoamide (NMI, green) and rhodamine B (RB, red) were attached to the ends of homopolymers and diblock polymers (Figures 2a, S7 and S8),[29] respectively, and the same procedure was followed for living CDSA. As shown in the structured illumination microscopy (SIM) images (Figure 2b), the distribution of diblock polymers was consistent with the AFM results. At 30 °C, they concentrated at the center of the

platelet, gradually extending toward the edges as the temperature decreased to 20 °C. At 10 °C, diblock polymers predominantly accumulated at the edges, forming distinct layered structures. In contrast, PCL homopolymers were distributed on the whole platelets regardless of temperature and extensively overlapped with diblock polymers at 30 and 20 °C.

Next, we used Förster resonance energy transfer (FRET) to assess the degree of overlap between the two polymers on different platelet samples, as FRET occurs when the donor and acceptor are in close proximity, typically within 10 nm.[29-32] The fluorescent emission spectra were recorded upon excitation of the FRET donor at 410 nm. To facilitate comparison, the spectra were normalized by the total fluorescence intensity at 530 nm and 576 nm, corresponding to the maximum emission of the FRET donor and acceptor, respectively (Figure 2c). The results showed significant FRET in all samples, indicated by a prominent emission peak at 576 nm. As the temperature increased, the decreasing intensity of donor and the increasing intensity of acceptor suggested enhanced FRET efficiency and greater overlap between the polymers.[32] These findings, coupled with AFM results, indicate that self-sorting occurs at 10 °C, while co-crystallization takes place at 30 °C.

Mechanism Exploration

The different crystallization behaviours of homo and diblock polymers upon temperature variation were explored in terms of both thermodynamic and kinetic aspects (Figure 3). To get a better understanding of the thermodynamic properties, solution-based crystallization enthalpy was measured by nano DSC, which was then used to determine crystallinity (Figures 3a, S9, and S10, and Table S4).[33] Out of our expectation, even though the solution-based crystallization was conducted at various temperature, their crystallinities were stable (homopolymer: 80%, and diblock polymer: 92%) and much higher than those obtained from their bulk state (homopolymer: 56%, and diblock polymer: 42%). We reasoned that the enhanced diffusion and adjustability of polymers in the solution state promote to form perfect polymeric crystals. Thus, we focused on the crystallization kinetics instead, which was characterized using UV-Vis

spectroscopy.[34] The crystallization kinetics of the two polymers were tested separately to evaluate their temperature dependence (Figures 3b and S11). The homopolymer crystallized faster at lower temperatures due to increased supercooling, consistent with prior reports on crystallization in the bulk state.[21, 35] In contrast, the diblock polymer showed the opposite trend, with decreasing temperatures leading to slower crystallization kinetics. To compare the isothermal crystallization rates of the two polymers, rate constants were calculated (Figures 3c and S12). The rate constants for the diblock polymer at 20 and 10 °C (0.107 and 0.001) are significantly lower than those of the homopolymer (3.827 and 4.312), whereas at 30 °C, the rate constant for diblock polymer (0.633) exceeds that of the homopolymer (0.27), which corresponds to the polymer distribution observed in the platelets. We attribute these differing kinetic behaviors to hydrogen bonding between the PDMA corona and ethanol, which acts as a drag on molecular motion.[36, 37] This hindrance is reduced at higher temperatures, where hydrogen bonds are more readily disrupted.

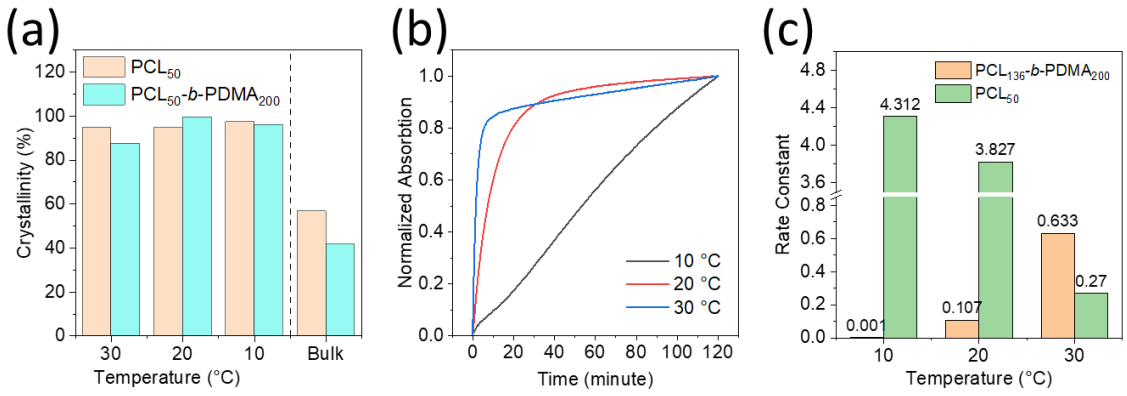

Figure 3. Mechanism study: (a) Comparison of crystallinities of homo and diblock polymers crystallized at various temperatures in ethanol (Nano DSC) and bulk states (DSC), (b) UV-Vis spectra for monitoring crystallization kinetics of diblock polymers by tracking signal intensity at 500 nm over time, and (c) Rate constant derived from UV-Vis analysis of crystallization kinetics.

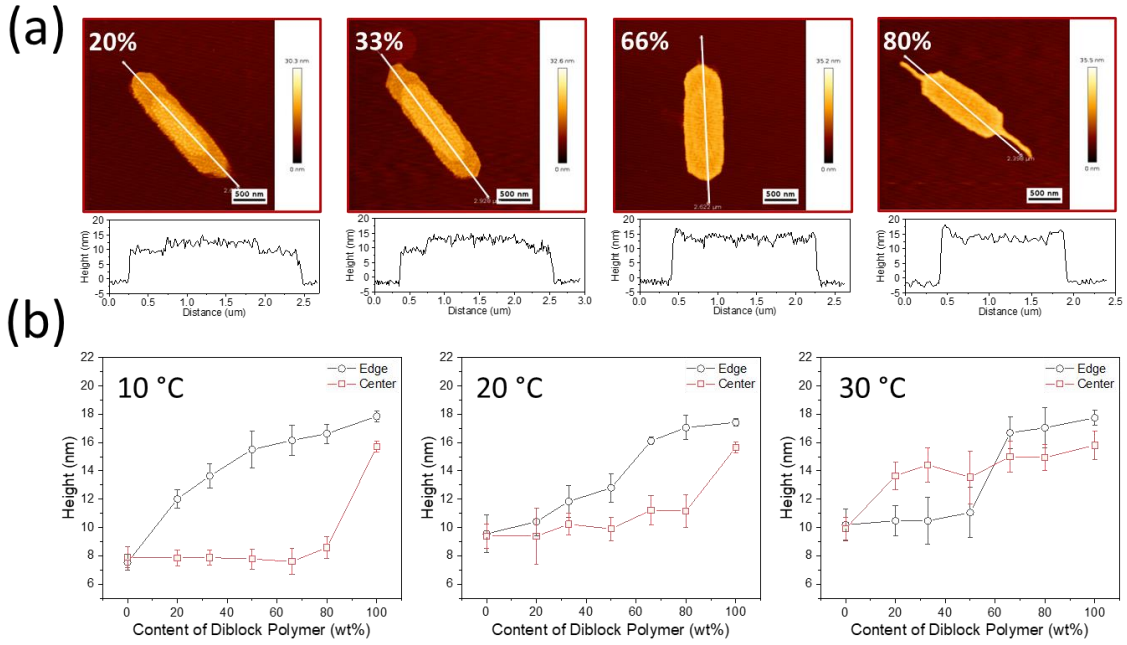

Figure 4. Living CDSA at varying temperatures using 10 eq. unimer with different diblock polymer contents: (a) AFM images and height profiles of platelets prepared at 30 °C, with percentages indicating diblock polymer content, and (b) Height variation at edge and center of platelets relative to diblock polymer content. Scale bar = 500 nm.

Extension of Control into the Third Dimension by Tuning Polymer Composition

Next, the homo-to-diblock ratios were tuned to expect more patterns on platelets, and adjust the height in the third dimension. This approach builds on previous findings that altering the unimer composition can modulate platelet patterns through the correlation between crystallization rate and concentration.[2, 6] However, while the surface patterns in prior studies were distinct, they lacked clarity and precision. Hence, the synergistic modulation of temperature and unimer composition is expected to yield more precise regulation of the pattern. The diblock polymer ratio was tuned between 0-100 wt%, and living CDSA was performed at 10, 20, and 30 °C respectively for each unimer composition (Figures 4a, S13 and S14). AFM studies were then

performed to quantify the variation in platelet center and edge height profiles across all assembly temperatures ((Figure S15 and Table S5)

At 10 °C, platelets maintained a concave surface when mixed unimers (homo and diblock) were used, with the edge height consistently surpassing that of the center and increasing with higher diblock polymer content (Figures 4b and S13). When diblock content reached 66 wt%, the platelet contour can no longer accommodate the excess diblock polymers due to the steric repulsion form coronas, leading to cylinder formation. The central height remained steady at approximately 7.8 nm, the height of the PCL single crystal, with only minor increases at 80 wt% diblock content. This behavior was attributed to the significant difference in crystallization kinetics between the two polymers at 10 °C, where higher diblock concentrations did not markedly enhance the relative crystallization rate. At 20 °C, the crystallization rate difference between the two polymers decreased, leading to partial co-assembly. As a result, both the edge and center heights increased with increasing diblock polymer content, while the edge height remained consistently greater when mixed unimers were used.

At 30 °C, platelets of a convex surface were obtained when the diblock polymer content was between 20-50 wt%, characterized by a significant shift as the central height surpassed the edge height, while the edge height remained constant at approximately 7.8 nm. This was because diblock polymers, which crystallized faster at this temperature, were consumed first. As the content of diblock polymer increased further, the central height initially rose but was eventually surpassed by the edge height due to the accumulation of excess diblock polymers at the edges. Similar trends were observed at 20 °C and 30 °C, where epitaxially grown cylinders appeared at high diblock polymer content (Figures S13 and S14), although this threshold was higher at these temperatures compared to lower temperatures, as more diblock polymers could still be accommodated in the platelet plane.

Overall, the synergistic regulation of temperature and unimer composition could be effective to precisely adjust the morphology of platelets. While temperature remained the primary factor governing self-sorting behavior and polymer spatial distribution, tuning unimer composition proved to be a practical strategy for adjusting pattern height in the third dimension and achieving specific structural characteristics (Figure S16).

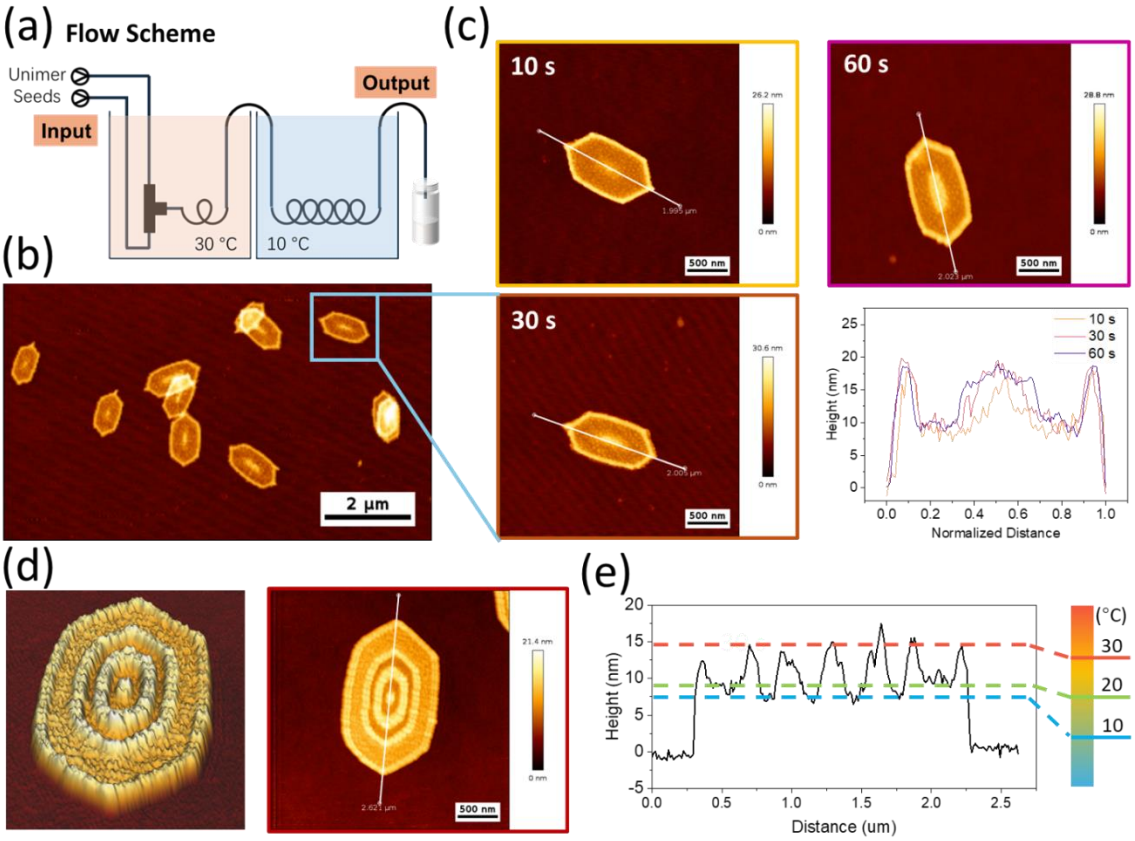

Figure 5. Flow living CDSA for layered platelet synthesis with single unimer addition: (a) Schematic of flow living CDSA, (b) 3-Layer platelets prepared by aging at 30 °C for 30 s, followed by 10 °C for 60 s, (c) Tunable inner-layer of 3-layer platelets prepared with 30 °C aging for 10, 30, and 60 s respectively, followed by 10 °C for 60 s, (d) 3D view of 7-layered platelets, and (e) Height profile of 7-layered platelets with corresponding preparation temperatures. Scale bar = 2 μm (b) and 500 nm (c) and (d).

Layered Platelets Prepared in Flow

To leverage temperature-controlled self-sorting, we aimed to precisely modulate 3D platelet patterns through a simplified method. Previously, creating layered patterns on platelets required multiple unimer additions, which was time-consuming and produced low-resolution patterns.[5, 14] Here, using precise temperature modulation, we aim to achieve well-defined layered structures with a single unimer addition, streamlining the process. The proof-of-concept living CDSA process was initiated at 30 °C and then cooled to 10 °C, resulting in 3-layer platelets (Figure S17). The first layer formed through the co-assembly of homopolymer and diblock polymer at 30 °C, followed by self-sorted layers at 10 °C, confirming the feasibility of this temperature-controlled approach for layered patterning.

To further refine the 3-layer structures described above, we addressed the challenge of achieving rapid temperature switching in batch processing, which led to blurred interfaces between layers due to insufficient temperature control (Figure S17). To overcome this, we adapted the CDSA process to a tubular flow reactor with modular temperature-controlled channels, based on our previous work (Figure 5a).[23] The high surface area-to-volume ratio of the flow reactor facilitated rapid heat transfer,[38-40] enabling precise temperature control and the consistent formation of uniform 3-layer platelets within 2 minutes (Figure 5b). By varying the residence time at specific temperatures, we could fine-tune the resulting patterns. For example, the size of the first layer could be adjusted by altering the residence time at 30 °C, as illustrated by AFM images and height profiles showing larger inner layers with increased residence time (Figure 5c).

To leverage rapid temperature-switching in flow for regulating self-assembly, we implemented multiple temperature cycles to achieve high-resolution patterns after a single unimer addition. The key challenge was enhancing the efficiency of temperature-switching to prevent blurring (Figure S18). To achieve this, we developed a dual flow system (Figure S19) using wide tubing with circulating 10 °C water positioned above a 30 °C water bath. The CDSA aging channel

alternated between heating and cooling, allowing temperature-switching within 0.5 seconds. This approach produced a distinct 7-layer pattern in just 2 minutes after three temperature-switching cycles (Figure 5d). The resulting structure resembles lithographed patterns but is achieved through a more efficient bottom-up strategy.[13] Unlike lithography, which is typically used to fabricate 2D structures with limited control over the third dimension, our method allows precise tuning of height in the third dimension, achieving a discernible height difference of 2 nm between layers prepared at 10 °C and 20 °C. Each layer's height encodes the specific temperature conditions during growth, akin to tree rings indicating their growth environment (Figure 5e), potentially paving the way for applications in data storage.[41-43] Increasing the number of temperature-switching cycles allowed the successful fabrication of 9-layer and 11-layer patterns (Figure S20). Although some variations in precision arose with more cycles, this method's scalability and ability to create increasingly complex structures demonstrates significant promise for advanced material applications requiring tunable architectures.

Conclusions

In conclusion, we developed a polymer combination capable of distinct CDSA behaviors at different temperatures and leveraged precise temperature control in flow reactors to fabricate tunable 3D patterns on the surface of platelets. Co-assembly of homopolymers and diblock polymers occurred at 30 °C due to similar crystallization kinetics, whereas lowering the temperature to 10 °C led to kinetically controlled self-sorted assembly. The resulting 3D patterns were formed by coronas, with their height effectively regulated by adjusting the unimer composition during living CDSA. By implementing a flow-based strategy, we achieved layered patterns on platelets with accuracy comparable to lithographic techniques. These results present a novel, scalable strategy for creating complex structures and advancing materials with tunable architectures for a range of applications.

Acknowledgments

The authors would like to thank the University of Birmingham and China Scholarship Council for funding and support.

Author contributions

L.X. performed the experiments with assistance from T.X. T.X. conducted the theoretical calculation of constant rates. L.X., T.X., C.T.J.F., A.P.D. and R.O.R. analyzed the data and prepared the manuscript. The project was supervised by A.P.D. and R.O.R.

Competing interests

Authors declare that they have no competing interests.

Additional information

All data are available in the manuscript or the supplementary materials.

References

(1) Jin, X.-H.; Price, M. B.; Finnegan, J. R.; Boott, C. E.; Richter, J. M.; Rao, A.; Menke, S. M.; Friend, R. H.; Whittell, G. R.; Manners, I. Long-range exciton transport in conjugated polymer nanofibers prepared by seeded growth. *Science* **2018**, *360*, 897-900.

(2) Qiu, H.; Gao, Y.; Boott, C. E.; Gould, O. E. C.; Harniman, R. L.; Miles, M. J.; Webb, S. E. D.; Winnik, M. A.; Manners, I. Uniform patchy and hollow rectangular platelet micelles from crystallizable polymer blends. *Science* **2016**, *352*, 697-701.

(3) Qiu, H.; Hudson, Z. M.; Winnik, M. A.; Manners, I. Multidimensional hierarchical self-assembly of amphiphilic cylindrical block comicelles. *Science* **2015**, *347*, 1329-1332.

(4) MacFarlane, L.; Zhao, C.; Cai, J.; Qiu, H.; Manners, I. Emerging applications for living crystallization-driven self-assembly. *Chem. Sci.* **2021**, *12*, 4661-4682.

(5) Tong, Z.; Xie, Y.; Arno, M. C.; Zhang, Y.; Manners, I.; O'Reilly, R. K.; Dove, A. P. Uniform segmented platelet micelles with compositionally distinct and selectively degradable cores. *Nat. Chem.* **2023**, *15*, 824-831.

(6) Deng, R.; Mao, X.; Pearce, S.; Tian, J.; Zhang, Y.; Manners, I. Role of Competitive Crystallization Kinetics in the Formation of 2D Platelets with Distinct Coronal Surface Patterns via Seeded Growth. *J. Am. Chem. Soc.* **2022**, *144*, 19051-19059.

(7) Xie, Y.; Tong, Z.; Xia, T.; Worch, J. C.; Rho, J. Y.; Dove, A. P.; O'Reilly, R. K. 2D Hierarchical Microbarcodes with Expanded Storage Capacity for Optical Multiplex and Information Encryption. *Adv. Mater.* **2023**, *36*, 2308154.

(8) Liu, L.; Ferguson, C. T. J.; Zhu, L.; Chen, S.; Wang, R.-Y.; Wang, S.; Dove, A. P.; O'Reilly, R. K.; Tong, Z. Synthesis of hollow platelet polymer particles by spontaneous precision fragmentation. *Nat. Synth.* **2024**, *3*, 903-912.

(9) Jiang, J.; Nikbin, E.; Liu, Y.; Lei, S.; Ye, G.; Howe, J. Y.; Manners, I.; Winnik, M. A. Defect-Induced Secondary Crystals Drive Two-Dimensional to Three-Dimensional Morphological Evolution in the Co-Self-Assembly of Polyferrocenylsilane Block Copolymer and Homopolymer. *J. Am. Chem. Soc.* **2023**, *145*, 28096-28110.

(10) Liao, C.; Gong, Y.; Che, Y.; Ji, H.; Liu, B.; Zang, L.; Che, Y.; Zhao, J. Concentric hollow multi-hexagonal platelets from a small molecule. *Nat. Commun.* **2024**, *15*, 5668.

(11) Shen, J.; Sun, W.; Liu, D.; Schaus, T.; Yin, P. Three-dimensional nanolithography guided by DNA modular epitaxy. *Nat. Mater.* **2021**, *20*, 683-690.

(12) Li, C.; Li, Q.; Kaneti, Y. V.; Hou, D.; Yamauchi, Y.; Mai, Y. Self-assembly of block copolymers towards mesoporous materials for energy storage and conversion systems. *Chem. Soc. Rev.* **2020**, *49*, 4681-4736.

(13) Liu, S.; Wang, J.; Shao, J.; Ouyang, D.; Zhang, W.; Liu, S.; Li, Y.; Zhai, T. Nanopatterning Technologies of 2D Materials for Integrated Electronic and Optoelectronic Devices. *Advanced Materials* **2022**, *34*, 2200734.

(14) Xia, T.; Tong, Z.; Xie, Y.; Arno, M. C.; Lei, S.; Xiao, L.; Rho, J. Y.; Ferguson, C. T. J.; Manners, I.; Dove, A. P.; et al. Tuning the Functionality of Self-Assembled 2D Platelets in the Third Dimension. *J. Am. Chem. Soc.* **2023**, *145*, 25274-25282.

(15) Safont-Sempere, M. M.; Fernández, G.; Würthner, F. Self-Sorting Phenomena in Complex Supramolecular Systems. *Chem. Rev.* **2011**, *111*, 5784-5814.

(16) He, Z.; Jiang, W.; Schalley, C. A. Integrative self-sorting: a versatile strategy for the construction of complex supramolecular architecture. *Chem. Soc. Rev.* **2015**, *44*, 779-789.

(17) Liu, Q.; Jin, B.; Li, Q.; Yang, H.; Luo, Y.; Li, X. Self-sorting assembly of artificial building blocks. *Soft Matter* **2022**, *18*, 2484-2499.

(18) Kanno, R.; Kono, H.; Ryoki, A.; Ouchi, M.; Terashima, T. Multicomponent Self-Assembly and Self-Sorting of Polymer Micelles in Water: Selective and Switchable Association by Kinetic or Thermodynamic Control. *J. Am. Chem. Soc.* **2024**.

(19) Morris, K. L.; Chen, L.; Raeburn, J.; Sellick, O. R.; Cotanda, P.; Paul, A.; Griffiths, P. C.; King, S. M.; O'Reilly, R. K.; Serpell, L. C.; et al. Chemically programmed self-sorting of gelator networks. *Nat. Commun.* **2013**, *4*, 1480.

(20) Xu, J.; Zhou, H.; Yu, Q.; Manners, I.; Winnik, M. A. Competitive Self-Assembly Kinetics as a Route To Control the Morphology of Core-Crystalline Cylindrical Micelles. *J. Am. Chem. Soc.* **2018**, *140*, 2619-2628.

(21) Caputo, M. R.; Olmos, A.; Li, B.; Olmedo-Martínez, J. L.; Malafronte, A.; De Rosa, C.; Sardon, H.; O'Reilly, R. K.; Dove, A. P.; Müller, A. J. Synthesis, Morphology, and Crystallization Kinetics of Polyheptalactone (PHL). *Biomacromolecules* **2023**, *24*, 3256-3267.

(22) Castillo, R. V.; Müller, A. J. Crystallization and morphology of biodegradable or biostable single and double crystalline block copolymers. *Prog. Polym. Sci.* **2009**, *34*, 516-560.

(23) Xiao, L.; Parkinson, S. J.; Xia, T.; Edge, P.; O'Reilly, R. K. Enhancing the Scalability of Crystallization-Driven Self-Assembly Using Flow Reactors. *ACS Macro Lett.* **2023**, *12*, 1636-1641.

(24) Arno, M. C.; Inam, M.; Coe, Z.; Cambridge, G.; Macdougall, L. J.; Keogh, R.; Dove, A. P.; O'Reilly, R. K. Precision Epitaxy for Aqueous 1D and 2D Poly(epsilon-caprolactone) Assemblies. *J. Am. Chem. Soc.* **2017**, *139*, 16980-16985.

(25) Zhang, X.; Chen, G.; Zheng, B.; Wan, Z.; Liu, L.; Zhu, L.; Xie, Y.; Tong, Z. Uniform Two-Dimensional Crystalline Platelets with Tailored Compositions for pH Stimulus-Responsive Drug Release. *Biomacromolecules* **2023**, *24*, 1032-1041.

(26) Tong, Z.; Su, Y.; Jiang, Y.; Xie, Y.; Chen, S.; O'Reilly, R. K. Spatially Restricted Templated Growth of Poly(ε-caprolactone) from Carbon Nanotubes by Crystallization-Driven Self-Assembly. *Macromolecules* **2021**, *54*, 2844-2851.

(27) Liu, L.; Zhu, L.; Chu, Z.; Tong, Z. Seeded Epitaxial Growth of Crystallizable Polymers Governed by Crystallization Temperatures. *Macromolecules* **2023**, *56*, 5984-5992.

(28) Zhang, H.; Liu, M.; Zhou, T.; Dong, B.; Li, C. Y. Stepwise assembly of a cross-linked free-standing nanoparticle sheet with controllable shape. *Nanoscale* **2015**, *7*, 11033-11039.

(29) Rajak, A.; Das, A. Crystallization-Driven Controlled Two-Dimensional (2D) Assemblies from Chromophore-Appended Poly(L-lactide)s: Highly Efficient Energy Transfer on a 2D Surface. *Angew. Chem. Int. Ed.* **2022**, *61*, e202116572.

(30) Wu, L.; Huang, C.; Emery, B. P.; Sedgwick, A. C.; Bull, S. D.; He, X.-P.; Tian, H.; Yoon, J.; Sessler, J. L.; James, T. D. Förster resonance energy transfer (FRET)-based small-molecule sensors and imaging agents. *Chem. Soc. Rev.* **2020**, *49*, 5110-5139.

(31) Varlas, S.; Keogh, R.; Xie, Y.; Horswell, S. L.; Foster, J. C.; O'Reilly, R. K. Polymerization-Induced Polymersome Fusion. *J. Am. Chem. Soc.* **2019**, *141*, 20234-20248.

(32) Chakraborty, C.; Rajak, A.; Das, A. Shape-tunable two-dimensional assemblies from chromophore-conjugated crystallizable poly(l-lactides) with chain-length-dependent photophysical properties. *Nanoscale* **2024**, *16*, 13019-13028.

(33) Clamor, C.; Dale, S. D.; Beament, J.; Mould, E.; O'Reilly, R. K.; Dove, A. P. Uniform Polyester-Based Nanoparticles Assembled via Living Crystallization-Driven Self-Assembly as Friction-Reducing Agents in Engine Oil. *Macromolecules* **2023**, *56*, 9821-9828.

(34) Hurst, P. J.; Rakowski, A. M.; Patterson, J. P. Ring-opening polymerization-induced crystallization-driven self-assembly of poly-L-lactide-block-polyethylene glycol block copolymers (ROPI-CDSA). *Nat. Commun.* **2020**, *11*, 4690.

(35) Gupta, S.; Yuan, X.; Chung, T. C. M.; Cakmak, M.; Weiss, R. A. Isothermal and non-isothermal crystallization kinetics of hydroxyl-functionalized polypropylene. *Polymer* **2014**, *55*, 924-935.

(36) Zhang, Q.; Weber, C.; Schubert, U. S.; Hoogenboom, R. Thermoresponsive polymers with lower critical solution temperature: from fundamental aspects and measuring techniques to recommended turbidimetry conditions. *Materials Horizons* **2017**, *4*, 109-116.

(37) Akar, I.; Foster, J. C.; Leng, X.; Pearce, A. K.; Mathers, R. T.; O'Reilly, R. K. Log Poct/SA Predicts the Thermoresponsive Behavior of P(DMA-co-RA) Statistical Copolymers. *ACS Macro Lett.* **2022**, 498-503.

(38) Knox, S. T.; Warren, N. J. Enabling technologies in polymer synthesis: accessing a new design space for advanced polymer materials. *Reac. Chem. Eng.* **2020**, *5*, 405-423.

(39) Zaquen, N.; Rubens, M.; Corrigan, N.; Xu, J.; Zetterlund, P. B.; Boyer, C.; Junkers, T. Polymer Synthesis in Continuous Flow Reactors. *Prog. Polym. Sci.* **2020**, *107*, 101256.

(40) Wong, C. K.; Lai, R. Y.; Stenzel, M. H. Dynamic metastable polymersomes enable continuous flow manufacturing. *Nat. Commun.* **2023**, *14*, 6237.

(41) Soete, M.; Mertens, C.; Aksakal, R.; Badi, N.; Du Prez, F. Sequence-Encoded Macromolecules with Increased Data Storage Capacity through a Thiol-Epoxy Reaction. *ACS Macro Lett.* **2021**, *10*, 616-622.

(42) Soete, M.; Mertens, C.; Badi, N.; Du Prez, F. E. Reading Information Stored in Synthetic Macromolecules. *J. Am. Chem. Soc.* **2022**, *144*, 22378-22390.

(43) Vrijsen, J. H.; Rubens, M.; Junkers, T. Simple and secure data encryption via molecular weight distribution fingerprints. *Polym. Chem.* **2020**, *11*, 6463-6470.

4.2 Supporting Information

Supporting Information

3D Nanopatterning of Platelets via Temperature-Controlled Self-Sorting

Laihui Xiao,[a] Tianlai Xia,[a] Calum T. J. Ferguson,[a] Andrew P. Dove,[a]* Rachel K. O'Reilly[a]*

[a] School of Chemistry, University of Birmingham, Edgbaston, Birmingham B15 2TT, UK

*Corresponding Author: r.oreilly@bham.ac.uk (ROR) and a.dove@bham.ac.uk (APD)

Summary of Content:

Number of pages: 33

Number of tables: 5

Number of figures: 20

Number of schemes: 1

Materials

The dual-functional chain transfer agent (CTA), 2-cyano-5-hydroxypentan-2-yl-ethyl carbonotrithioate (CHPET), was synthesized following our previous work.[1] Diphenyl phosphate (DPP, 99%, Sigma Aldrich) underwent drying with P_2O_5 and was stored in the glove box. ε-Caprolactone (99%, ACROS Organics) was dried with CaH_2, distilled, and then stored in a N_2-filled glovebox. The initiator, 2,2'-azobis(2-methylpropionitrile) (AIBN, 98%, Sigma Aldrich), was recrystallized in methanol and stored at 4 °C in the dark. 1,4-Dioxane (anhydrous, 99.8%, Fisher Scientific) and N, N-dimethyl acrylamide (DMA, 99%, Sigma Aldrich containing 500 ppm monomethyl ether hydroquinone as an inhibitor) were purified with basic alumina before each use. A hydroxy-functionalized naphthalene monoimide (NMI-OH) was synthesized following the literature.[2] Rhodamine B (≥95%, Sigma Aldrich), 4-(dimethylamino)pyridine (DMAP, Sigma Aldrich), N-Ethyl-N′-(3-dimethylaminopropyl)carbodiimide hydrochloride (EDAC, ≥98%, Sigma Aldrich), ethanol (anhydrous, ≥99.5%, Fisher Scientific), diethyl ether (anhydrous, ≥99.0%, Fisher Scientific), Dichloromethane (DCM, anhydrous, ≥99%, Sigma Aldrich) and chloroform ($CHCl_3$, anhydrous, ≥99%, Sigma Aldrich) were used as received.

Instrumentation

Nuclear magnetic resonance (NMR) spectra were acquired using a Bruker DPX-400 (400 MHz) spectrometer, with deuterated chloroform ($CDCl_3$) serving as the solvent. The data were analysed and processed using MestReNova x64 software. Size exclusion chromatography (SEC) was performed on Agilent 390-MDS equipment, employing PLgel Mixed-D type columns and detecting signals through refractive index (RI) and ultraviolet (UV) detectors. Chloroform with 0.5% NEt_3 was used as the eluent, and the flow rate was maintained at 1 $mL \cdot min^{-1}$. Number-average (M_n) and weight-average (M_w) molecular weights, along with dispersity ($Đ_M$), were calibrated against polystyrene (PS) standards utilizing Agilent SEC software. UV-Vis spectroscopy was carried out on an Agilent Cary 6300 UV-Vis Spectrometer, with a wavelength range of 250 – 800 nm. The seed solution (2 mL) was equilibrated at the set temperature for 2 minutes prior to initiating measurements after unimer addition. Fluorescence spectra were

recorded using an Edinburgh FS5 spectrofluorometer with a xenon light source and processed in Fluoracle software provided with the instrument. Differential scanning calorimetry (DSC) was conducted using a Mettler Toledo HP DSC827 instrument. Samples weighing 5-10 mg were subjected to heating and cooling cycles between -100 °C and 100 °C at 10 °C·min^{-1} under a nitrogen atmosphere. Three cycles were executed for each sample, and data from the second cycle were analysed. Nano differential scanning calorimetry (Nano DSC) was conducted on a TA NanoDSC with 300 μL samples (1 mg mL^{-1}), using a heating and cooling rate of 1 °C min^{-1} under a constant pressure of 3 atmospheres. Atomic force microscopy (AFM) was performed on a JPK Nanowizard 4 system fitted with Nanosensor PPP-NCHAuD tips. All samples were tested in the supplied acoustic enclosure and vibration isolation at 20 °C, and the results were analysed by Data Processing Software V.6.1.117 software. Samples were prepared by spin-coating 10 μL of solution on a freshly cleaved mica wafer, the spin model was 3000 rpm for 50 seconds and 5000 rpm for 10 seconds. Fluorescent samples were imaged by structured illumination microscopy (SIM) using COMPARE N-SIM S system coupled with 2x Hamamatsu Flash4.0 sCMOS camera. Image data were acquired by NIKON NIS Elements 5 software and analysed by NIS Elements 5 workstation, WXG92. Samples were prepared by spin-coating 10 μL of solution on cover glass, the spin model was 3000 rpm for 50 seconds and 5000 rpm for 10 seconds.

Synthesis

Polycaprolactone (PCL)

PCL_{50}, PCL_{53}-NMI and PCL_{136} were synthesized via ring-opening polymerization (ROP) in a nitrogen-filled glove box. Taking PCL_{136} as an example, caprolactone (7.33g, 64.26 mmol), diphenylphosphate (DPP, 80.4 mg, 0.32 mmol), and CHPET (80 mg, 0.32 mmol) were accurately weighed in vials and then transferred to a 50-mL round-bottom flask. Toluene (22.54 mL) was used as the reaction solvent. Polymerization occurred at room temperature, with ^{1}H NMR used for real-time monitoring. After approximately 24 hours, the reaction was quenched with Amberlyst, and the solution was removed from the glove box. The crude product

underwent precipitation in cold diethyl ether three times, and the collected solid was obtained after centrifugation. A yield of 4.62 g of light-yellow solid was obtained and subsequently dried in the vacuum oven.

^{1}H NMR (400 MHz, Chloroform-d, δ (ppm)): 4.12 (t, J = 6.2 Hz, 2H), 4.06 (t, J = 6.7 Hz, 272H), 3.35 (q, J = 7.4 Hz, 2H), 2.30 (t, J = 7.5 Hz, 272H), 1.88 (s, 3H), 1.71 – 1.59 (m, 544H), 1.44 – 1.31 (m, 272H).

Polycaprolactone-b-Polydimethylacetamide (PCL-*b*-PDMA) Synthesized by RAFT Polymerization

PCL_{136}-*b*-$PDMA_{200}$ was prepared by the chain extending using RAFT polymerization. As an example preparation for PCL_{136}-*b*-$PDMA_{200}$, macro-CTA (PCL_{136}, 100 mg, 0.00634 mmol), DMA (150.8 mg, 1.52 mmol), and AIBN (0.104 mg, 0.000634 mmol, 10 mg mL^{-1} in dioxane) were dissolved in dioxane (0.76 mL) and then transferred into an ampoule. The solution was freeze-pump-thawed three times before the ampoule was immersed in an oil bath set at 70 °C. After 2 hours, polymerization was quenched by immersing the ampoule in the liquid N_2. The crude product was precipitated into the cold diethyl ether once it reached room temperature and then collected by centrifugation, and this process was repeated three times. After drying in a vacuum oven for 3 days, 215.5 mg of a solid product was obtained.

^{1}H NMR (400 MHz, Chloroform-d, δ (ppm)): 4.06 (t, J = 6.7 Hz, 272H, $COOC\boldsymbol{H}_2$), 3.21 – 2.75 (m, 1200H, $CON(C\boldsymbol{H}_3)_2$), 2.30 (t, J = 7.5 Hz, 272H, $C\boldsymbol{H}_2COO$), 1.71 – 1.58 (m, 544H, $COOCH_2C\boldsymbol{H}_2CH_2C\boldsymbol{H}_2CH_2OH$), 1.44 – 1.32 (m, 272H, $(CH2)_2C\boldsymbol{H}_2(CH_2)_2$).

Red Dye-Modified PCL-PDMA (PCL-*b*-PDMA-RB)

Rhodamine B was grafted to PCL-PDMA by esterification reaction, which was catalyzed by DMAP and EDAC. In brief, PCL_{136}-*b*-$PDMA_{200}$ (100 mg, 0.00281 mmol), rhodamine B (6.73 mg, 0.014 mmol), EDAC (5.39 mg, 0.0281 mmol), DMAP (0.343 mg, 0.00281 mmol, 10 mg mL^{-1} in DCM), and DCM (2 mL) were added into a vial and stirred at room temperature for 2 days. After the reaction, the undissolved substance was removed by filtration, and the filtrate

was precipitated into the cold diethyl ether and then the precipitated polymer was collected after centrifugation. Another five precipitation and centrifugation processes were conducted, and the final product was dried in a vacuum oven overnight.

General procedure for Crystallization-Driven Self-Assembly (CDSA)

Seed Preparation

Seeds prepared and used in this work were the same as we previously reported.[1] The size and distribution are shown in Figure S4.

General Procedure to Prepare Platelets by Living CDSA

Living CDSA was performed in 2-mL vials. Briefly, seed solutions (1 mL, 0.01 mg mL^{-1} in ethanol) was equivalent for 2 minutes in water bath set at various temperatures (10, 20, and 30 °C), then unimer solution (10 µL, 10 mg mL^{-1} in $CHCl_3$) was added. After being vigorously stirred for 10 seconds, solutions were aged at the same temperature for another 2 minutes. After that, samples were prepared for microscopy test.

Flow Cascade to Prepare Three-layered Platelet with Single Heating-Cooling Cycle

Seed solution (0.01 mg mL^{-1} in ethanol, 100 µL min^{-1}) was injected into the flow cascade using a HPLC pump, and initially passed a pre-heating channel (100 µL) immersed in 30 °C water bath. Then in a reverse T micromixer, seed flow mixed with unimer flow (10 mg mL^{-1} in $CHCl_3$, 1 µL min^{-1}) that injected by syringe pump, and the ratio of unimer-to-seed was constant at 10. After that, epitaxial growth occurred in an aging channel (100-200 µL) with various heating and cooling (immersed in 10 °C water bath) periods. Samples were collected after passing 3 reactor volumes to make sure they reached the steady state. The detailed flow setups for different experiments were listed in Table S1.

Flow Cascade to Prepare Multi-Layered Platelet with Several Heating-Cooling Cycles

Seed solution (0.0025 mg mL^{-1} in ethanol, 100 µL min^{-1}) was injected into the flow cascade using a HPLC pump, and initially passed a pre-heating channel (100 µL) immersed in 30 °C water bath. Then in a reverse T micromixer, seed flow mixed with unimer flow (5 mg mL^{-1} in $CHCl_3$, 1 µL min^{-1}) that injected by syringe pump, and the ratio of unimer-to-seed was constant at 20. After that, epitaxial growth occurred in an aging channel (200 µL) with various heating and cooling periods. Samples were collected after passing 3 reactor volumes to make sure they reached the steady state. The detailed flow setups for different experiments were listed in Table S2.

Table S1. Flow setup to prepare three-layered platelets.

Sample	30 °C (s)	10 °C (s)
(1)	10	50
(2)	30	30
(3)	60	30

Note: Unimer-to-seed ratio was constant at 10, and flow rates of seeds and unimer were maintained at 100 and 1 µL·min^{-1} respectively.

Table S2. Flow setup to prepare multi layered platelets.

Layer	R_{seed} [a] (µL·min^{-1})	R_{unimer} [a] (µL·min^{-1})	30 °C (s)	0 °C (s)	30 °C (s)	0 °C (s)	30 °C (s)	0 °C (s)	30 °C (s)	0 °C (s)	20 °C (s)	0 °C (s)
7	100	2					10	1	10	1	10	88
9	100	2			10	1	10	1	10	1	10	77
11	100	2	10	1	10	1	10	1	10	1	10	66

[a] R_{seed} and R_{unimer} represent the flow rates of seeds and unimer respectively.

Note: Unimer-to-seed ratio was constant at 20, and flow rates of seeds and unimer were maintained at 100 and 1 µL·min^{-1} respectively.

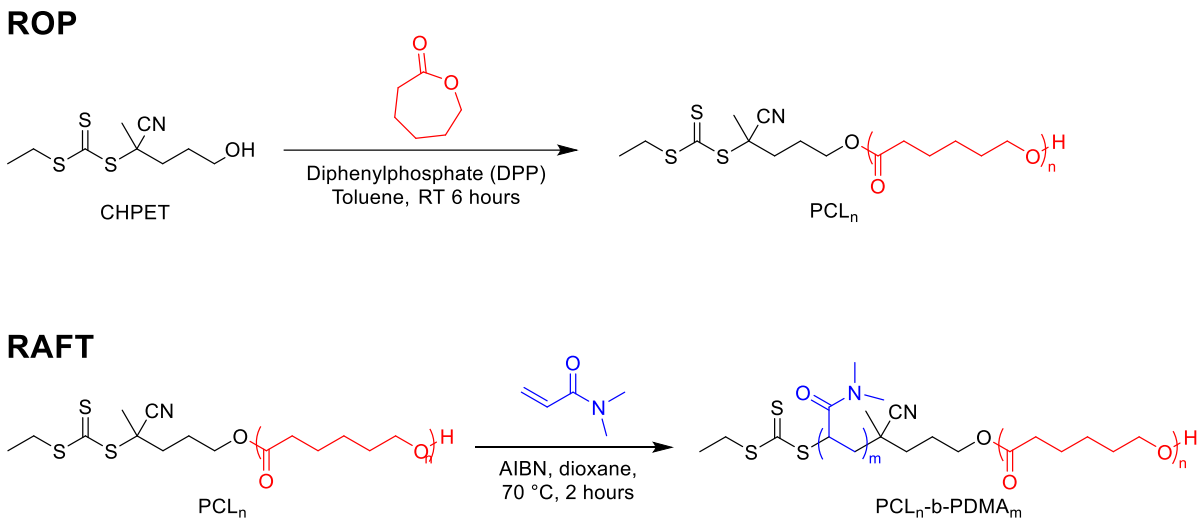

Scheme S1. Synthetic route of PCL and PCL-*b*-PDMA.

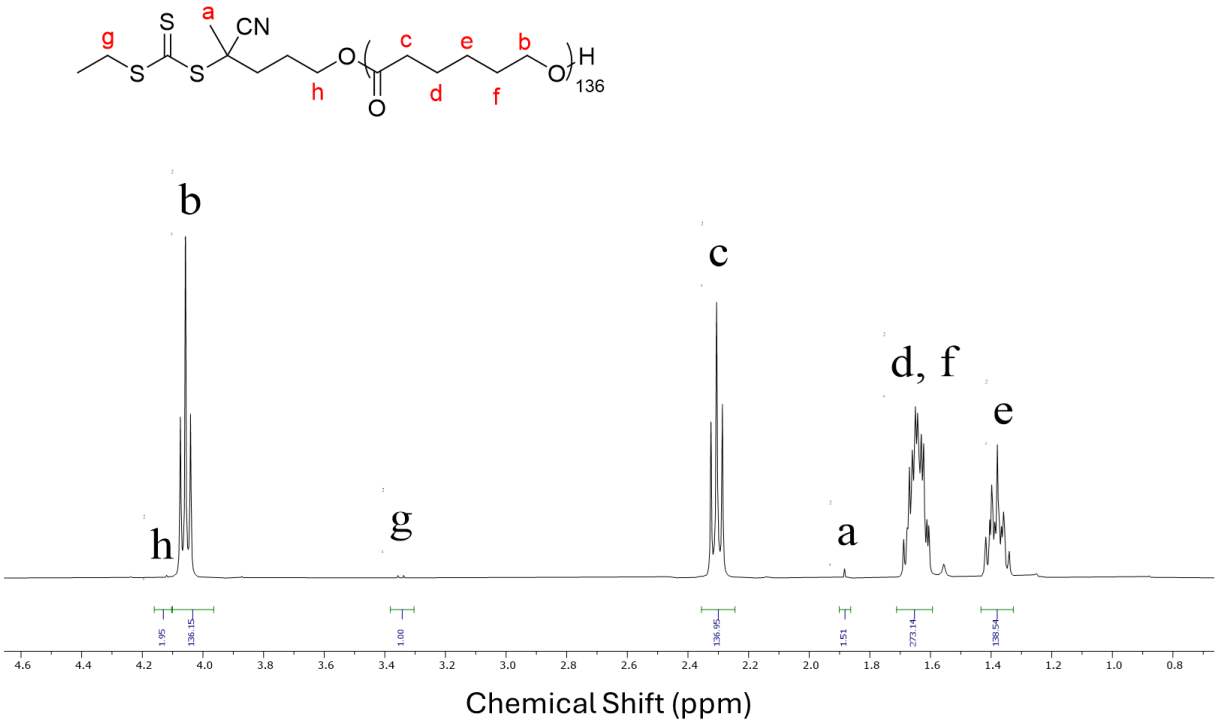

Figure S1. ^{1}H NMR spectra of PCL_{136} (400 MHz, in $CDCl_3$).

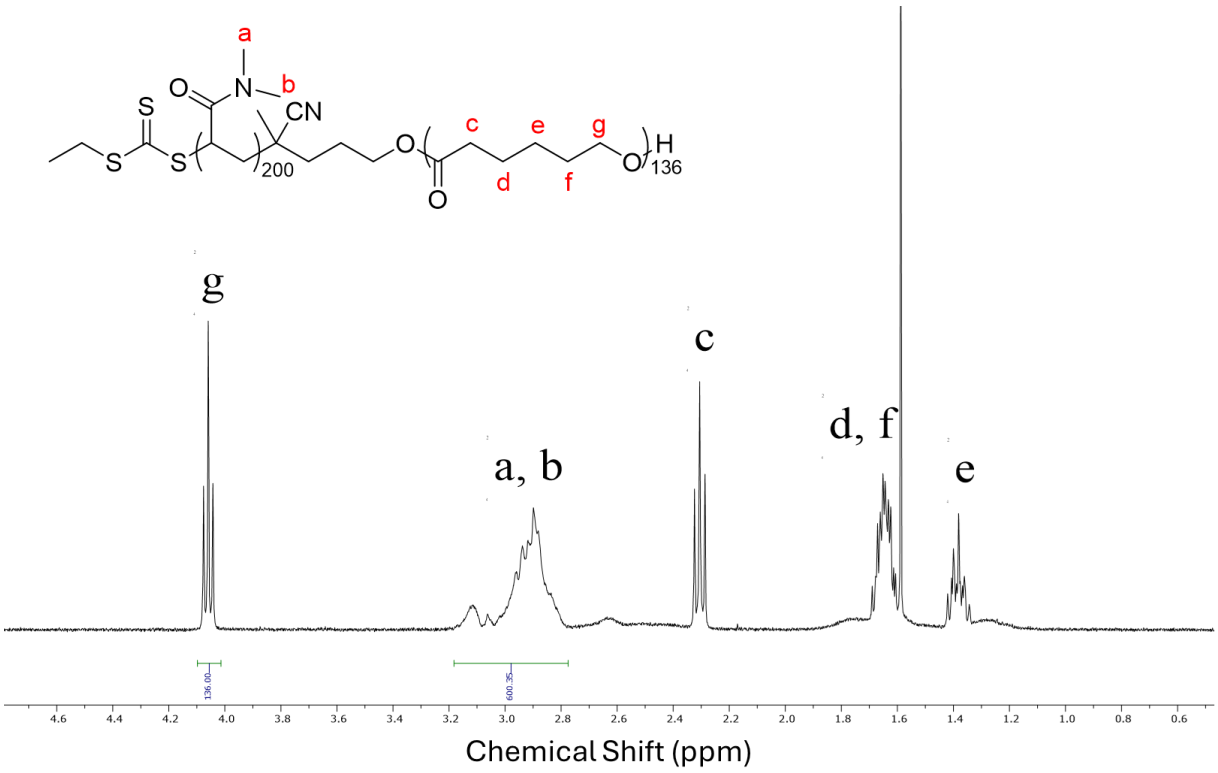

Figure S2. ^{1}H NMR spectra of PCL_{136}-*b*-$PDMA_{200}$ (400 MHz, in $CDCl_3$).

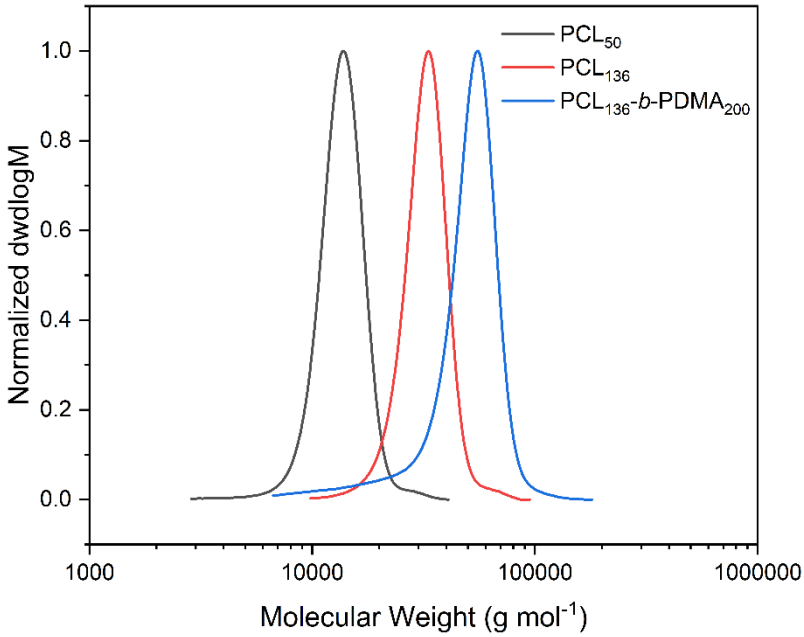

Figure S3. Normalized SEC curves of PCL_{50}, PCL_{136}, and PCL_{136}-*b*-$PDMA_{200}$.

Table S3. SEC results of polymers detected by RI.

Polymer	M_n (kg·mol^{-1})	M_w (kg·mol^{-1})	$Đ$
PCL_{50}*	13.3	14.2	1.06
NMI-PCL_{53}	13.6	14.5	1.07
PCL_{136}	31.0	32.9	1.06
PCL_{136}-*b*-$PDMA_{200}$	43.8	51.7	1.18

*This is the same polymer as we used before.[1]

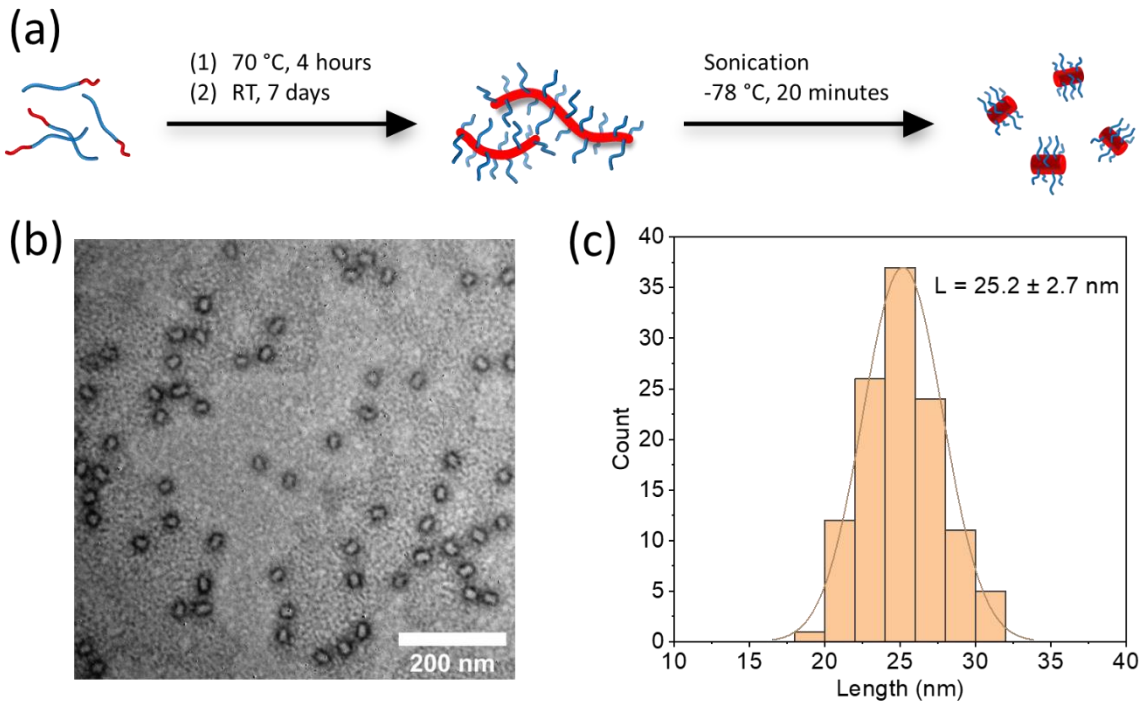

Figure S4. (a) Scheme to prepare seeds from PCL_{50}-$PDMA_{196}$. (b) TEM images of seeds. Uranyl acetate aqueous solution (1%) was used for stain. (c) Length distribution of seeds. At least 100 particles were analysed to obtain statistical results.

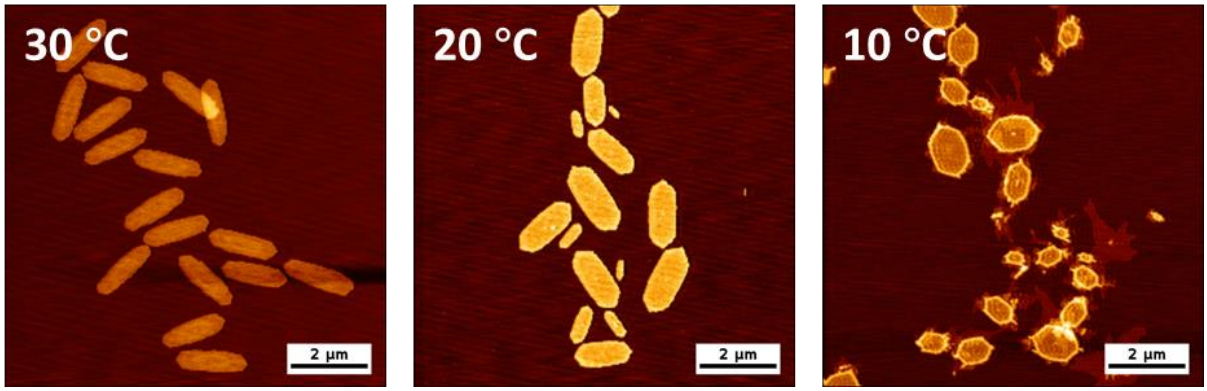

Figure S5. Overview of platelets prepared at various temperatures using 1:1 wt % PCL_{50}/PCL_{136}-$PDMA_{200}$ unimer.

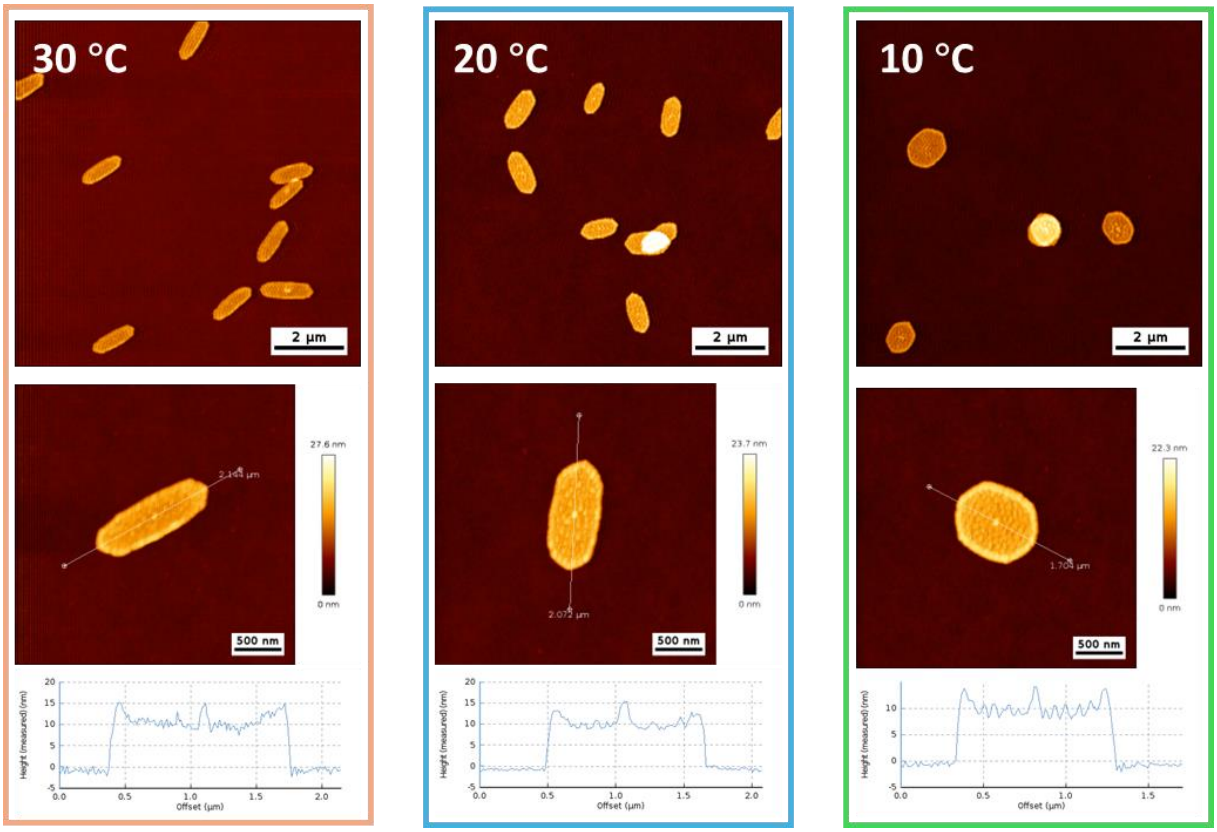

Figure S6. Platelets prepared at various temperatures using PCL_{50} / PCL_{50}-*b*-$PDMA_{200}$ unimer.

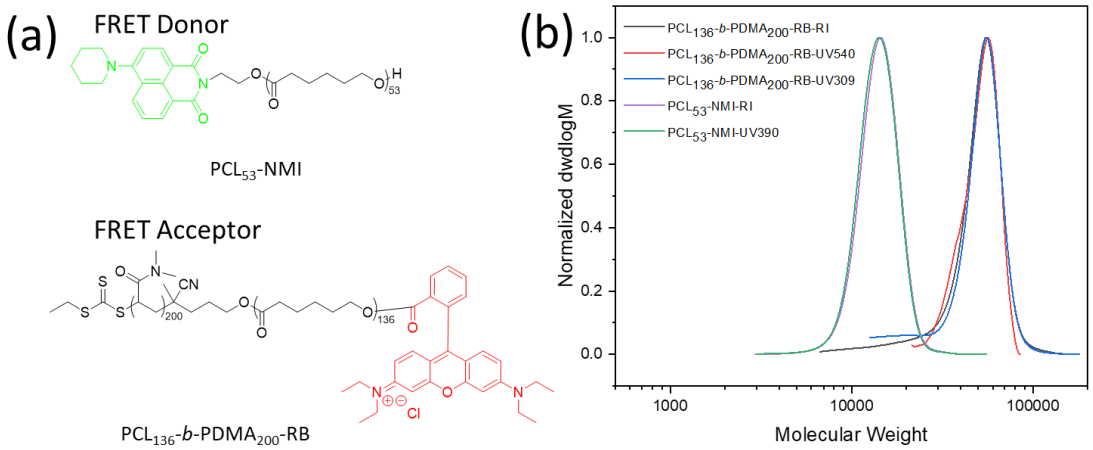

Figure S7. (a) Molecular structures of fluorescent dye-modified polymers, and (b) Normalized SEC curves of fluorescent dye-modified polymers detected by diffferent signals.

(a)

	Excitation (nm)	Emission (nm)
PCL_{53}-NMI	408	537
PCL_{53}-*b*-$PDMA_{200}$-RB	558	580

(b)

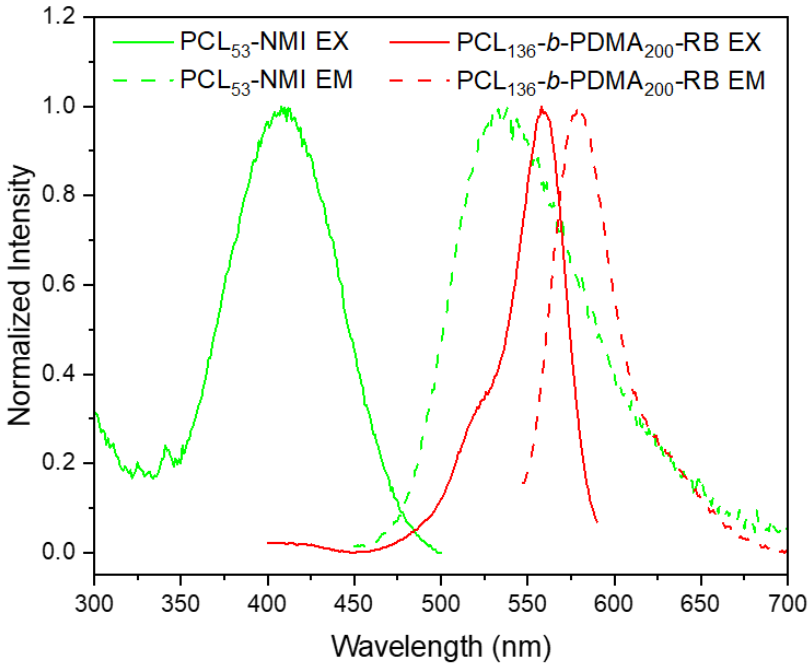

Figure S8. (a) Table of maximum excitation and emission wavelengths, and (b) Fluorescence spectra with solid lines for excitation and dashed lines for emission.

Table S4. Crystallinity of polymers in solution versus bulk state.

	Temperature (°C)	**Enthalpy (J/g)**	**Crystallinity* (X_c, %)**
PCL_{50}	30	112.16 ± 1.39	80.4 ± 1.0
	20	111.74 ± 1.58	80.1 ± 1.1
	10	110.89 ± 0.75	79.5 ± 0.5
	bulk	79.01 ± 0.34	56.6 ± 0.2
PCL_{136}-*b*-$PDMA_{200}$	30	123.69 ± 1.28	88.7 ± 0.9
	20	132.79 ± 3.11	94.8 ± 2.2
	10	129.92 ± 3.78	93.1 ± 2.7
	bulk	59.48 ± 1.02	42.6 ± 0.7

* The crystallinity (X_c) of PCL was calculated according to $X_c = (\Delta Hm)/(\Delta Hm0)$, where ΔHm is the measured mass crystallization/melting enthalpy and ΔHm0 is the mass crystallization/melting enthalpy of completely crystalline PCL (139.5 J/g).[3]

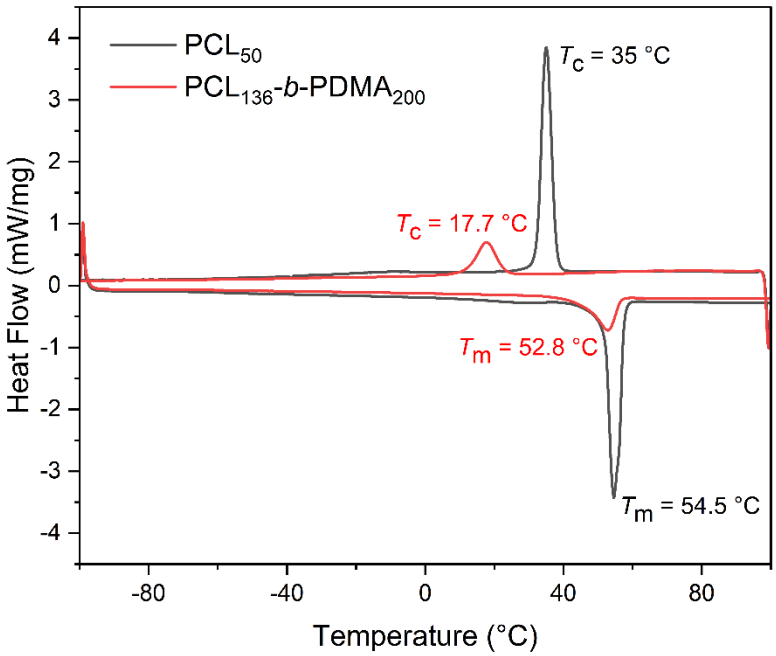

Figure S9. DSC thermograms of PCL_{50} and PCL_{136}-*b*-$PDMA_{200}$.

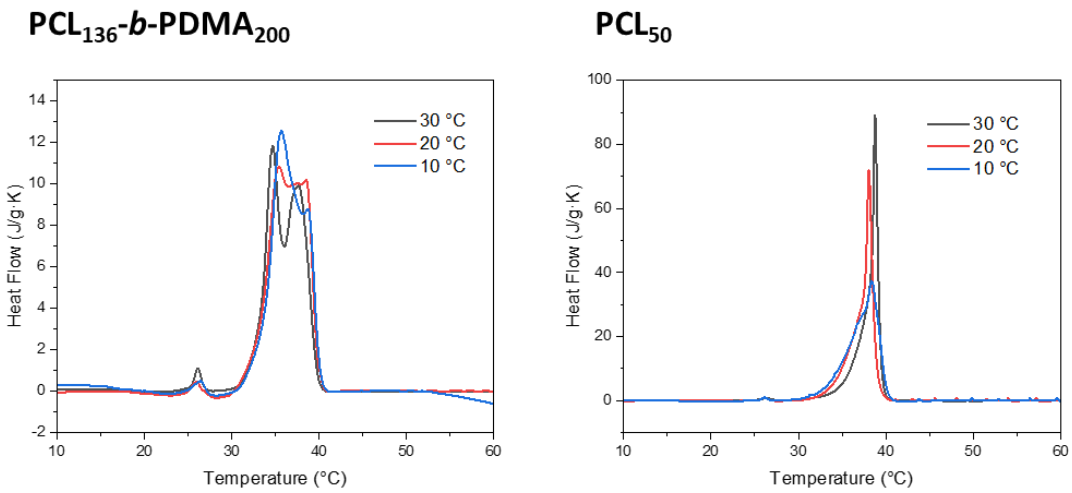

Figure S10. Nano DSC thermograms of solution-based PCL_{50} and PCL_{136}-*b*-$PDMA_{200}$.

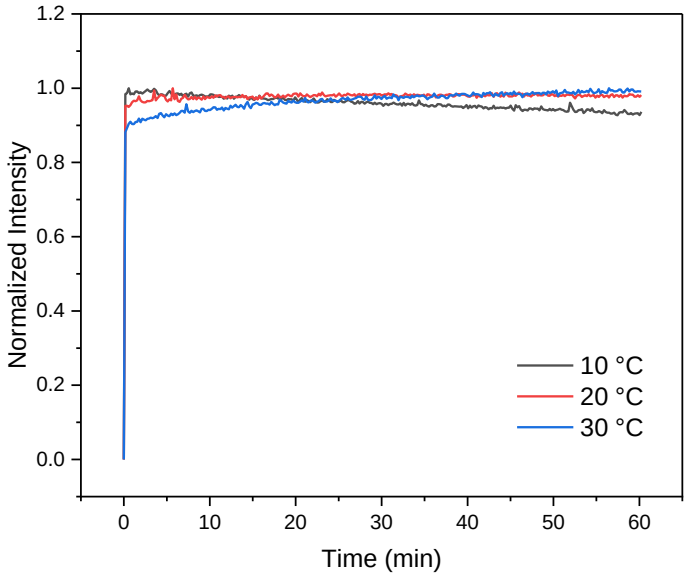

Figure S11. UV-Vis spectra for monitoring crystallization kinetics of homopolymer by tracking signal intensity at 500 nm over time.

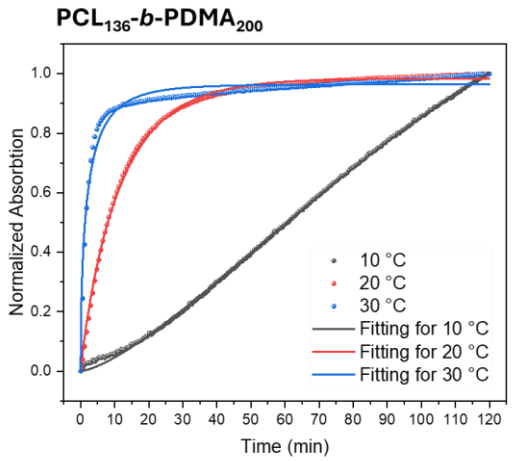

Model	UV-Vis Fitting Curve		
Equation	a*(1-exp(-b*x^c))		
Plot	Normalized Absorbtion	F	I
a	1.60957 ± 0.01664	0.98429 ± 5.73725E-4	0.96391 ± 0.0012
b	0.00112 ± 1.32721E-5	0.10652 ± 0.00115	0.63332 ± 0.01236
c	1.41553 ± 0.00538	0.9126 ± 0.00408	0.56965 ± 0.01101
Reduced Chi-Sqr	4.79304E-5	9.30584E-5	5.6544E-4
R-Square (COD)	0.9995	0.99753	0.94039
Adj. R-Square	0.9995	0.99752	0.94019

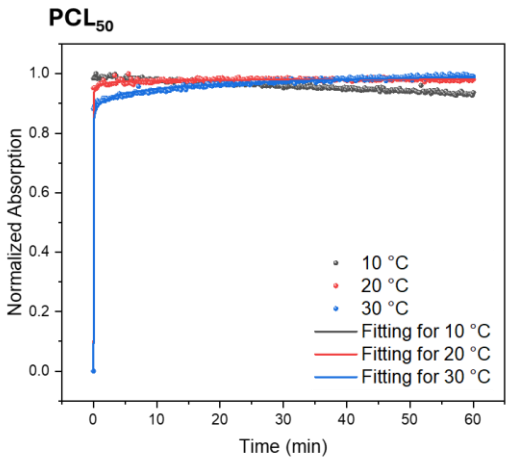

Model	UV-Vis Curve Fitting		
Equation	a*(1-exp(-b*x^c))		
Plot	Normalized Absorption	Normalized Absorption	Normalized Absorption
a	0.99166 ± 0.5375	0.98474 ± 0.02096	3.79467 ± 116.34402
b	4.31205 ± 160.23121	3.82741 ± 1.10208	0.26978 ± 9.49859
c	-0.58661 ± 144.23993	0.0994 ± 0.18031	0.02792 ± 0.15047
Reduced Chi-Sqr	0.3231	0.00301	0.00259
R-Square (COD)	-0.19101	0.05527	0.28207
Adj. R-Square	-0.98502	0.04904	0.27733

Figure S12. Fitted crystallization kinetics of PCL_{136}-*b*-$PDMA_{200}$ and PCL_{50} using Origin software. The detailed method is described below.

Kinetic Model

The overall area of platelets formed in living CDSA seeded growth experiments is proportional to the unimer-to-seed ratio. This is analogous to living covalent polymerizations in which the chain length is dependent on the ratio of monomer to initiator. It was therefore of interest to investigate whether this analogy also applied to the reaction kinetics. In a living covalent polymerization the reaction is first order in both monomer and initiator concentrations, and this would translate to the reaction being first order in both unimer, [*U*], and seed, [*S*], concentrations for living CDSA. As the latter remains constant during the course of the reaction and initiation occurs from edges of the seed, $[S]_0$, (the concentration at $t = 0$) in the differential form of the rate eq (eq 1).

$$\frac{d[U]}{dt} = -k[U][S]_0 \quad (1)$$

Integrating eq1 then affords an expression for the concentration of unimer as a function of time, $[U]_t$, in terms of the initial concentrations (eq 2).

$$[U]_t = [U]_0 e^{-k[S]_0 t} \quad (2)$$

Determining the concentrations of micelle and unimer in solution, however, is problematic. We therefore chose to monitor the reaction kinetics by determining the average area, *Area*(*t*), of the individual platelets formed, which could be measured microscopically. The total area grown over all platelets, $Area_{total}(t)$, is related to the concentrations of unimer, $[U]_t$ and $[U]_0$, the volume of solution, *V*, and the aggregation number (number of unimer molecules per unit area), $N_{agg/A}$ (eq 3). We have shown (*vide supra*) that the latter is constant with platelets area, under the growth conditions used.

$$[U]_t = [U]_0 - \frac{Area_{total}(t) N_{agg/A}}{N_A V} \quad (3)$$

$$Area_{total}(t) = \frac{N_A V}{N_{agg/A}} [U]_0 [1 - e^{-k[S]_0 t}] \quad (4)$$

Combining eq 2 and 3, rearranging to make $Area_{total}(t)$ the subject and dividing by the number of platelets, which for a living process equals the number of seeds, N_{seed}, then affords an expression for the area grown $Area_{grown}(t)$ for each platelets (eq 4, 5).

$$Area_{grown}(t) = \frac{1}{N_{seed}} \frac{N_A V}{N_{agg/A}} [U]_0 [1 - e^{-k[S]_0 t}] \quad (5)$$

N_{seed} is related to $[S]_0$ (eq 6), and this leads to eq7.

$$N_{seed} = [S]_0 N_A V \quad (6)$$

$$Area_{grown}(t) = \frac{1}{N_{agg/A}} \frac{[U]_0}{[S]_0} [1 - e^{-k[S]_0 t}] \quad (7)$$

The experimentally determined Area, *A*(*t*), also included that of the seed, A_{seed}, however, area of seed is tiny and can be neglected, and this does not need to be taken into account in the final model (eq 7).

From current understanding, the absorbance change during living CDSA process tracked by UV-Vis, which is shown a relatively linear relationship between absorbance intensity and platelets area. The $Absorbance_{grown}(t)$ should follow the change of the area grown $Area_{grown}(t)$, and assumed k' as a constant (eq 8).

$$Absorbance_{grown}(t) = k' Area_{grown}(t) \quad (8)$$

Also, the value of $Absorbance_{seed}$ is very low, which can be neglected. Combine eq 7 and 8 to get final model (eq 9).

$$Absorbance_{grown}(t) = k' \frac{1}{N_{agg/A}} \frac{[U]_0}{[S]_0} [1 - e^{-k[S]_0 t}] \quad (9)$$

Kinetic Data Fitting

Fitting of the kinetics data was performed using Origin (OriginLab) software. The fitting model was chosen according to the above proposed model and simplified as A(t)= a*(1-exp(-k*t^b)). The values were obtained when the fit converged and the chi-squared tolerance value of 1×10^{-9} was reached. See below for an example data set, note k is reported in min^{-1}.

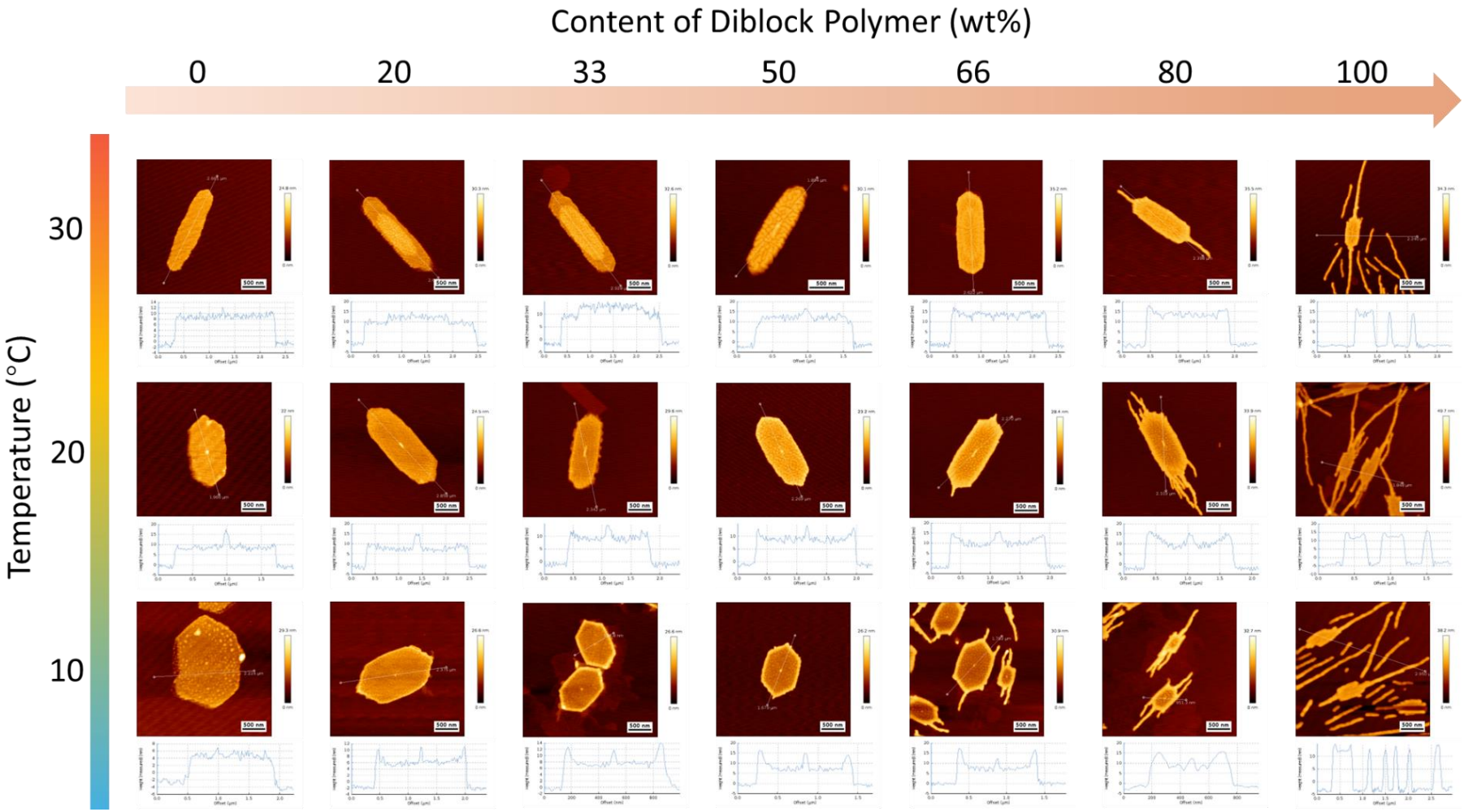

Figure S13. Images of a single platelet showing the morphological variation as a function of temperature and the content of diblock polymer.

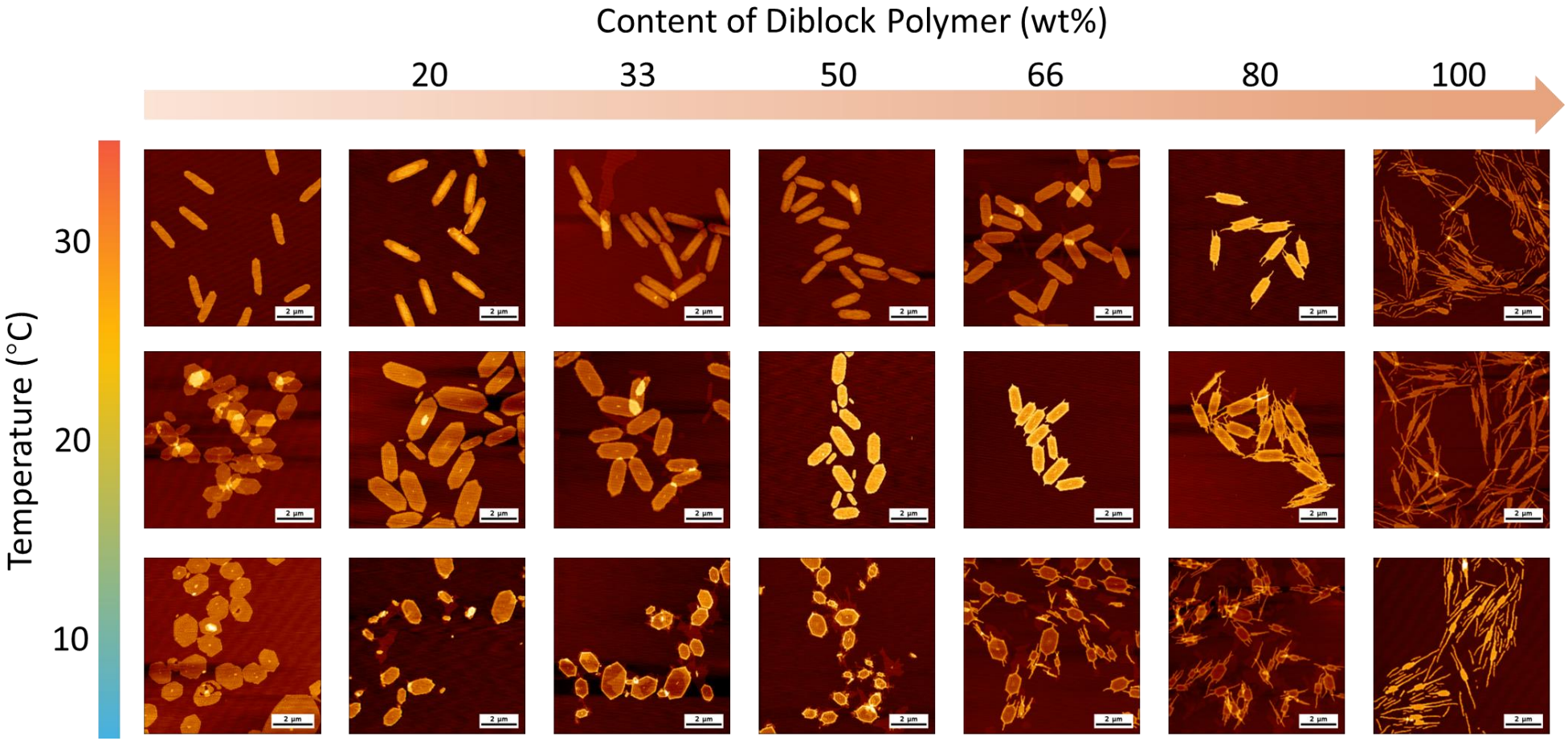

Figure S14. Overview images of a collection of platelets showing morphological variation as a function of temperature and the content of diblock polymer.

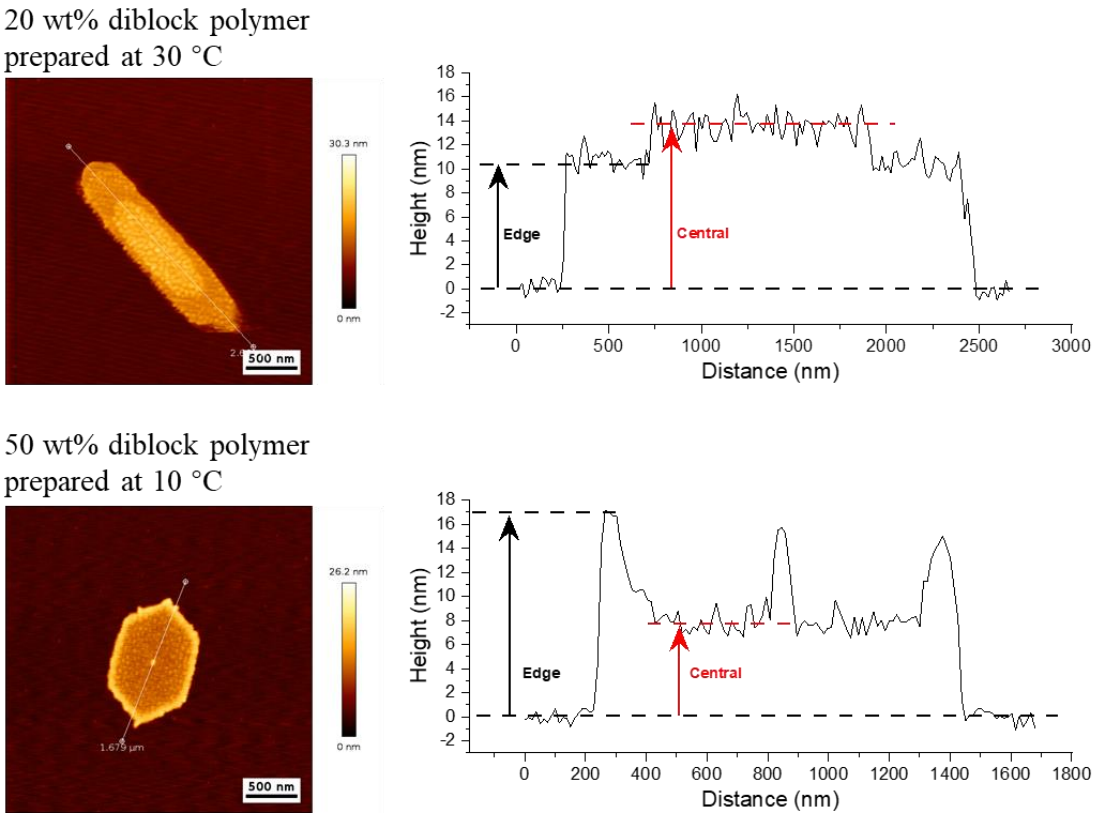

Figure S15. Illustrated examples for measuring the height at the center and edges of platelets.

Table S5. Statistical analysis of height profile.

Temperature (°C)	**30**		**20**		**10**	
Diblock content (wt%)	Edge (nm)	Central (nm)	Edge (nm)	Central (nm)	Edge (nm)	Central (nm)
0	10.2 ± 1.1	9.9 ± 0.8	9.6 ± 1.3	9.4 ± 0.9	7.5 ± 0.6	7.9 ± 0.7
20	10.5 ± 1.1	13.7 ± 1.0	10.4 ±1.0	9.4 ± 2.0	12.0 ± 0.7	7.8 ± 0.6
33	10.5 ± 1.6	14.4 ± 1.2	11.8 ± 1.1	10.2 ± 0.8	13.6 ± 0.9	7.9 ± 0.5
50	11.1 ± 1.8	13.5 ± 1.9	12.8 ± 1.0	9.9 ± 0.8	15.5 ± 1.3	7.8 ± 0.7
66	16.7 ± 1.1	15.0 ± 1.1	16.1 ± 0.3	11.2 ± 1.0	16.2 ± 1.1	7.6 ± 0.9
80	17.0 ± 1.4	14.9 ± 0.9	17.1 ± 0.8	11.1 ± 1.2	16.6 ± 0.7	8.6 ± 0.8
100	17.7 ± 0.5	15.8 ± 1.0	17.4 ± 0.3	15.7 ±0.4	17.9 ± 0.4	15.7 ± 0.4

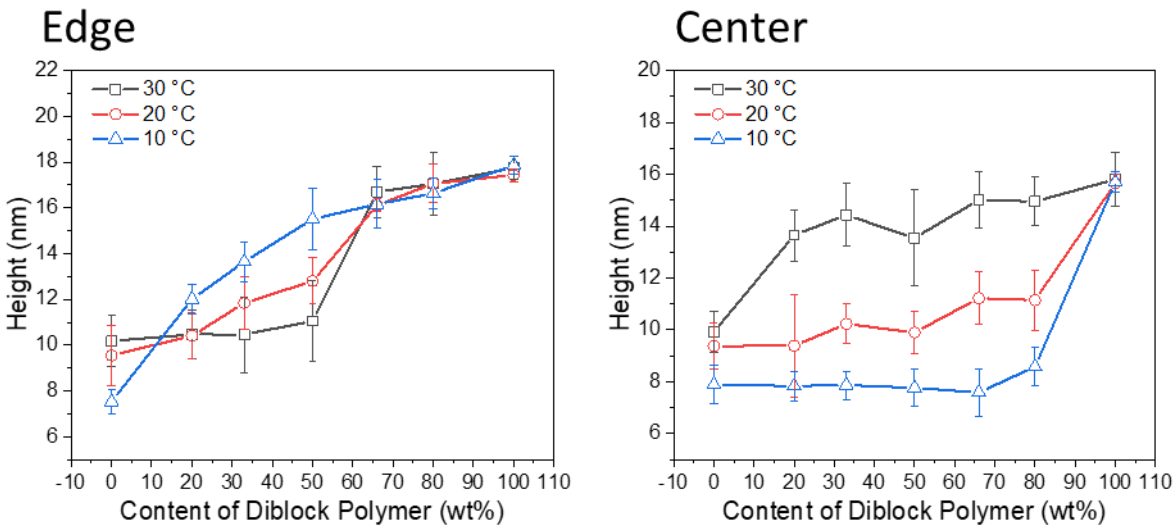

Figure S16. Variation in edge and central heights of platelets as a function of diblock polymer content at different temperatures.

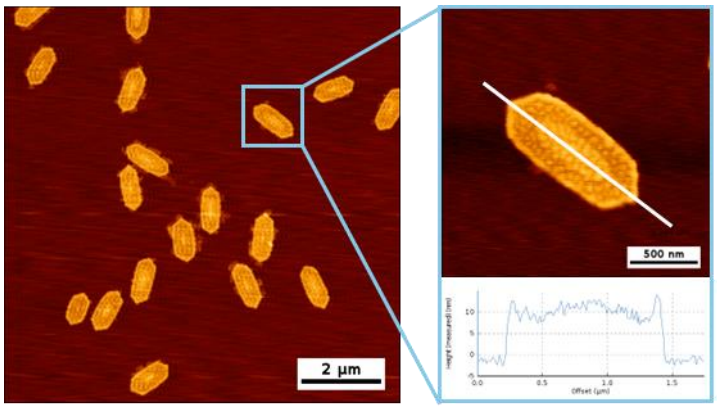

Figure S17. Platelets prepared in batch *via* rapid temperature switching. A 1 mL sample in a 2 mL glass vial was aged in a 30 °C water bath for 10 seconds, followed by 2 minutes in a 10 °C water bath.

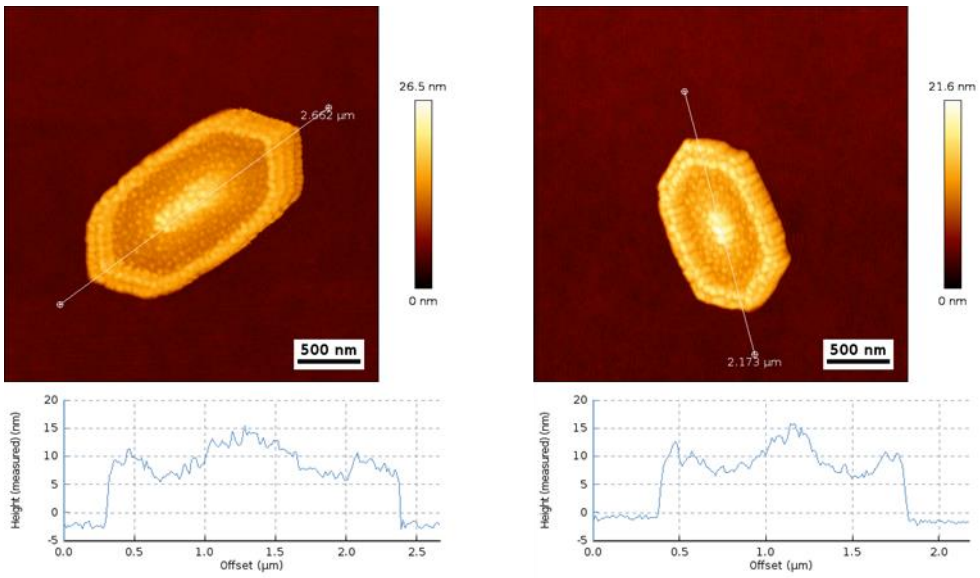

Figure S18. Layered platelets prepared under the conditions lack rapid temperature-switching capability.

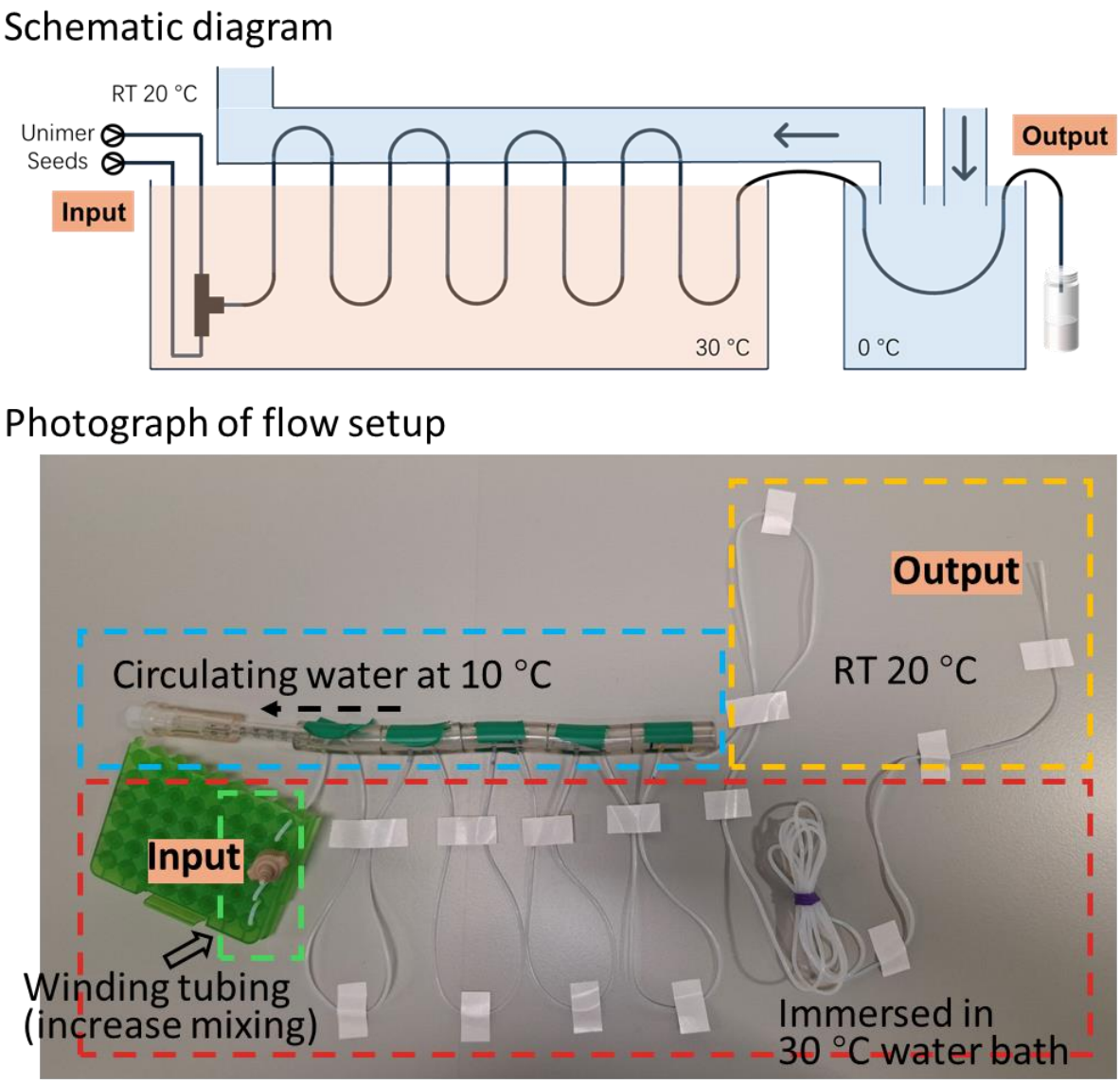

Figure S19. Schematic diagram (upper) and photograph of flow setup (lower) to prepare platelets with layered patterns by rapid temperature switching in flow.

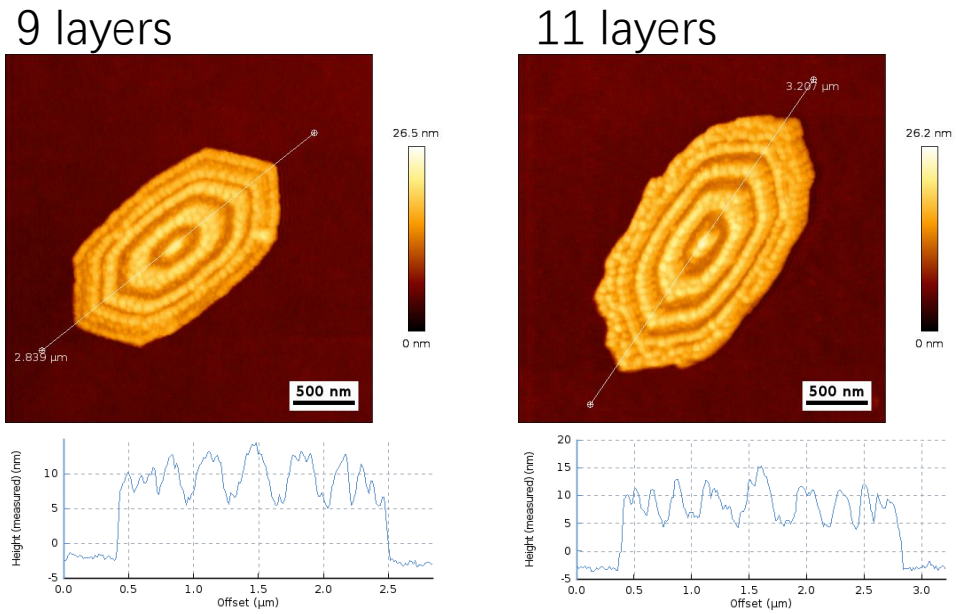

Figure S20. AFM images of 9-layer and 11-layer platelets.

Reference

(1) Xiao, L.; Parkinson, S. J.; Xia, T.; Edge, P.; O'Reilly, R. K. Enhancing the Scalability of Crystallization-Driven Self-Assembly Using Flow Reactors. *ACS Macro Lett.* **2023**, *12*, 1636-1641.

(2) Rajak, A.; Das, A. Crystallization-Driven Controlled Two-Dimensional (2D) Assemblies from Chromophore-Appended Poly(L-lactide)s: Highly Efficient Energy Transfer on a 2D Surface. *Angew. Chem. Int. Ed.* **2022**, *61*, e202116572.

(3) Fernández-Tena, A.; Pérez-Camargo, R. A.; Coulembier, O.; Sangroniz, L.; Aranburu, N.; Guerrica-Echevarria, G.; Liu, G.; Wang, D.; Cavallo, D.; Müller, A. J. Effect of Molecular Weight on the Crystallization and Melt Memory of Poly(ε-caprolactone) (PCL). *Macromolecules* **2023**, *56*, 4602-4620.

Chapter 5 - Conclusions and Outlook

Conclusions

CDSA is an effective method for preparing anisotropic nanostructures; however, it faces challenges in scalability and structural complexity. This thesis introduces flow chemistry to CDSA for the first time, successfully scaling up platelet preparation and leveraging enhanced heat-transfer capabilities to produce more complex and refined nanostructures.

Due to the fact that transforming polymers into platelets involves multiple steps and several morphological changes, a reverse strategy was adopted to adapt these processes for the flow system, with the goal of scaling up the entire production streamline from polymer to final platelets. Initially, living CDSA, preparing platelets from seeds, was conducted in flow (Chapter 2). This section presents the first combination of CDSA with flow, where flow conditions were explored in detail, and challenges such as poor mixing and self-nucleation were addressed. The enhanced scalability and reproducibility demonstrated in this work motivated the expansion of these efforts.

Traditional seed formation involves long aging times and sonicating cylinders, which poses challenges for flow integration. Therefore, the next phase of work focused on addressing the challenge of seed preparation in flow (Chapter 3). Based on an understanding of crystal nucleation-growth theory, a flash-freezing strategy was introduced to regulate direct CDSA during the nucleation step, significantly enhancing seed formation efficiency. Using this method, seed preparation time was reduced from one week to just three minutes. This timeframe can be

further minimized when transferring seed preparation to the flow reactor. Following this, an integrated flow system was developed by connecting channels for both seed preparation and living CDSA, achieving the highest reported throughput for preparing size-controllable PCL-based platelets.

After establishing a scalable platelet preparation, the focus shifted to increasing the structural complexity and refinement of platelets (Chapter 4). In this section, a temperature-responsive unimer system was developed in which, at high temperatures, homopolymers and diblock polymers co-assemble simultaneously, while self-sorted assembly occurs at lower temperatures. Leveraging precise temperature control, which is easily achieved in flow, living CDSA regulated by temperature-switching was conducted. This novel approach yielded platelets with tunable, fine 3D surface patterns comparable to lithographic structures.

Although this thesis primarily demonstrated the preparation of platelets, the methodologies developed here hold broader potential, especially considering the growing interest in nanoparticles. The techniques used in this work could serve as a foundation for further advances in scaling up nanoparticle synthesis, as well as enhancing structural complexity and functional properties.

Challenges

Like most research projects, my PhD was a continuous process of encountering challenges and systematically addressing them. At the start of my PhD, I focused on batch experiments to reproduce previous work on CDSA conducted by our group. However, I encountered significant reproducibility issues and poor control over living CDSA, primarily due to the fast kinetics of the process. By systematically comparing platelets from various batches, I identified temperature as a key parameter for controlling living CDSA, which led me to explore flow living CDSA at elevated temperatures. This approach ultimately resulted in the successful work described in Chapter 2.

In my second year, I faced challenges with sonicating cylinders in flow. The process was inefficient, and long cylinders persisted even after extended sonication. This led me to explore alternative methods for seed preparation. Through systematic investigation, I found that the cooling rate played a crucial role in direct CDSA. Fast cooling resulted in short cylinders, while slow cooling produced longer ones. This realization made me think about an extreme case where an extremely fast cooling rate could drive the polymer solution to low temperatures. This idea became the basis for the flash-freezing strategy described in Chapter 3, which enabled instant seed preparation in flow.

Following this, I encountered a new challenge with the instability of flash-frozen seeds. These seeds had low crystallinity, making them unable to withstand elevated temperatures and shear

forces in flow. Drawing from my engineering background, I adopted an industry-proven approach of introducing additives to enhance stability. Specifically, I incorporated homopolymer for seed preparation, which proved to be an effective and straightforward solution.

Another major challenge was increasing mixing efficiency in flow. This issue became even more pronounced in all-flow CDSA, where platelets were prepared directly from polymers at higher concentrations. The increased concentration led to faster kinetics, making rapid and efficient mixing even more critical for achieving homogeneity. To overcome this, I designed a winding channel by folding tubing with a disposable tip holder. This design took advantage of fluid flow through curved geometries, which helps disrupt laminar regimes and improves mixing.

In my third year, I developed an advanced flow setup, detailed in Chapter 4, to achieve efficient heat transfer for controlling the epitaxial growth of platelets and fine-tuning their surface patterns. Due to the fast crystallization kinetics, it was critical to minimize the channel pathway between heating and cooling baths. To resolve this, I replaced the traditional cooling bath with a cooling flow channel positioned just above the heating bath. This allowed the CDSA tubing to shift seamlessly between them, effectively eliminating unnecessary pathway distances while maintaining precise temperature control. This modification significantly improved the process.

Throughout my PhD, I tackled significant research challenges with innovative approaches, which not only enhanced the novelty of my work but also contributed to the broader impact in the field. This experience further honed my ability to conduct independent research and make meaningful advancements on my own.

Outlook

Flow synthesis presents a powerful strategy for bridging the gap between academic research and industrial applications. Its inherent scalability makes it well-suited for translating cutting-edge scientific discoveries into industrial production. Furthermore, automation is a key trend in current development, and integrating AI-assisted flow synthesis represents a promising research direction. Such an approach could significantly enhance the development and screening of functional nanoparticles, accelerating discovery and optimization processes while potentially leading to innovations that dramatically improve quality of life.

Building on the findings of this PhD, the following research opportunities are proposed:

(1) Building on our initial demonstration, further research is required to scale up the process for practical commercial applications. This can be achieved by integrating larger flow reactors into the system. However, optimizing mixing efficiency remains critical, as larger reactor volumes can lead to mass transfer limitations, uneven reactant distribution, and reduced reaction uniformity. To address this challenge, a collaborative effort between engineers and chemists is

necessary to design advanced mixing strategies that ensure uniform reactant distribution and reaction kinetics at larger scales. Alternatively, process intensification can be pursued by implementing a flow cascade system with multiple parallel reactor lines. While this approach enhances throughput and maintains process control, it also increases capital and operational costs, which must be carefully evaluated to ensure economic feasibility.

(2) Integrating in-line analysis techniques (e.g., SAXS, NMR, and DLS) along with automation into the flow system will enable real-time monitoring and precise synthesis control. Advances in characterization technology, including high-resolution and miniaturized desktop devices, have enhanced their applicability in continuous processes. Unlike batch reactions, where a specific reaction state corresponds to a fixed time point, and once the reaction progresses, the system is no longer in the previous state, in tubular flow reactors, different reaction states exist simultaneously along the reactor length, allowing for continuous monitoring and targeted observation of reaction kinetics over time. This characteristic, combined with the modularity of flow systems, allows for targeted observation of specific reaction conditions over extended periods. Consequently, real-time data acquisition provides more accurate and reliable insights, which can be instantly fed back into the control system. This feedback loop facilitates precise, automated production, improving process efficiency and reproducibility.

(3) Exploring the applications of CDSA nanoparticles is crucial, as their practical utilization drives innovation and justifies further research efforts. Despite extensive studies, only a small fraction of CDSA nanoparticles have been implemented in real-world applications. One

potential barrier is the inefficiency of traditional batch production, which limits large-scale synthesis and, in turn, hinders application development. Without efficient production methods, translating research into practical use remains challenging. Therefore, prioritizing application-driven research will not only reveal new opportunities but also create demand for improved fabrication techniques, ultimately accelerating progress in the field.